

# **The Pressure Resistance of hollow Glass Fibers at internal Pressure Load**

## **Dissertation**

zur Erlangung des akademischen Grades

**Doktoringenieur**

**(Dr.-Ing.)**

von Dipl.-Ing. Ronald Meyer-Scherf

geb. am 21. Oktober 1981 in Königs Wusterhausen

genehmigt durch die Fakultät für Maschinenbau

der Otto-von-Guericke-Universität Magdeburg

Gutachter: Prof. Dr.-Ing. habil. Thomas Böllinghaus

Prof. Dan Eliezer

Dr. rer. nat. Kai Holtappels

Promotionskolloquium am 15. Dezember 2015



---

## Abstract

Glass has different outstanding material-specific properties which offer theoretically the application of thin-walled hollow fibers in the field of high pressure gas storage. Especially the storage of hydrogen as renewable and environmental friendly energy carrier is possible.

Glass is an amorphous material which is characterized by a theoretical tensile strength much higher than this of other materials. However, in practice the tensile strength is decreased significantly by defects on the glass surface or in the material and its network structure. As part of this thesis the burst pressures of hollow glass fibers were determined. The burst pressure correlates very well with the tensile strength of hollow glass fibers. By using the Weibull statistic the results of different test series were evaluated in respect to failure probabilities and compared to each other. Thereby the influence of various parameters on the pressure resistance was investigated. Beside the influence of the chemical composition of the material the aging by environmental and their effect on the pressure resistance was investigated. Additionally hollow glass fibers were loaded dynamically and statically with different gases. Afterwards the burst pressure was determined and the effect of used gas on the pressure resistance could be determined as well as the impact of method and duration of loading. A further influence of the dimension of hollow glass fibers on their resistance against inner pressure load is the ratio between wall thickness and inner diameter which was investigated as well as the combination of different glasses and the utilization of their disparate coefficient of thermal expansion which lead to prestressing of the hollow glass fiber. Finally, the impact of the variation of several production parameters on the pressure resistance was determined experimentally as like as the influence of surface coatings. These shall protect the glass surface from subsequently procured defects and, hence, increase the pressure resistance.

As essential part of current thesis the defect analysis of test samples of various series was done whereby the differentiation between material and production dependent defects was important. Not only a light microscope but a scanning electron microscope was used for the investigation, as well. Beside volume defects like bubbles or inclusions surface defects in the form of scratches or spalling can be detected and observed.

A calculation of the failure-causing defect size from measured burst pressure is possible. Dependent on the dimension and determined burst pressure value of each single fiber defect sizes of less than one micron were calculated. Particularly the geometry of the test samples inappropriate for many examination methods and the fact that the

---

calculated defect size occurs only under loaded conditions at actual burst pressure the local detection of corresponding defect rendered impossible.

In the end, the present thesis shows the pressure resistance of hollow glass fibers and their potential to store safely gases under high pressure.

## Zusammenfassung

Glas besitzt einige herausragende materialspezifische Eigenschaften, die theoretisch den Einsatz von dünnwandigen Hohlfasern zur Hochdruckspeicherung von Gasen zulassen. Besonders die Speicherung von Wasserstoff als regenerativer Energieträger ist denkbar.

Glas ist ein amorphes Material, welches sich durch eine theoretische Zugfestigkeit auszeichnet, die mehrfach höher ist als anderer Materialien. Jedoch wird die Zugfestigkeit in der Praxis durch Defekte auf der Glasoberfläche oder im Material und dessen Netzwerk deutlich herabgesetzt. In dieser Arbeit wurde der Berstdruck von hohlen Glasfasern ermittelt, wobei der Berstdruck sehr gut mit der Zugfestigkeit von Gläsern korreliert. Unter Verwendung der Weibull Statistik wurden die Ergebnisse der verschiedenen Versuchsreihen hinsichtlich möglicher Ausfallwahrscheinlichkeiten ausgewertet und miteinander verglichen. Der Einfluss verschiedener Parameter wurde untersucht. Neben der chemischen Materialzusammensetzung wurde auch die Alterung durch Umwelteinflüsse und deren Wirkung auf die Druckfestigkeit gegen innere Belastung untersucht. Zusätzlich wurden die Hohlglasfasern unter Verwendung verschiedener Prüfgase zyklisch und statisch vor der Berstdruckbestimmung belastet, um die Wirkung des verwendeten Gases als auch der Art und Dauer der Belastung auf das Material zu bestimmen. Ein weiterer Einfluss auf die Druckfestigkeit von Hohlglasfasern ist das Wandstärken-Innendurchmesser-Verhältnis, welcher ebenso untersucht wurde wie die Kombination verschiedener Gläser mit unterschiedlichen thermischen Ausdehnungskoeffizienten, die zu Vorspannungen in den Glasfasern führen. Abschließend wurde die Auswirkung von Variationen verschiedener Produktionsparameter auf die Druckresistenz ebenso experimentell bestimmt wie der Einfluss von Beschichtungen, die die Glasoberflächen vor nachträglich beigebrachten Defekten schützen und die Druckfestigkeit bei innerer Belastung erhöhen sollen.

Wichtiger Bestandteil der Arbeit ist die Defektanalyse von Prüfmustern einzelner Testreihen. Es muss zwischen material- und produktionsbedingten Defekten unterschieden werden. Neben der Untersuchung von Hohlglasfasern mittels Lichtmikroskop wurde auch ein Rasterelektronenmikroskop verwendet. Sowohl Volumendefekte, wie Blasen und Steinchen, als auch Oberflächendefekte, in Form von Kratzern oder Ablagerungen, konnten als produktionsbedingte Defekte beobachtet werden. Materialbedingte Fehler wie Fehlstellen im Netzwerk konnten mit den verwendeten Untersuchungsmöglichkeiten nicht ermittelt werden.

---

Aus den ermittelten Berstdücken von Hohlglasfasern lassen sich die zum Versagen führenden Defektgrößen errechnen. Abhängig von Dimension der Faser und erreichtem Berstdruck ergeben sich Defektgrößen kleiner als ein Mikrometer. Insbesondere durch die für viele Untersuchungsmethoden ungünstige Geometrie der Prüfmuster sowie die Tatsache, dass die errechneten Defektgrößen nur unter Spannung beim vorliegenden Berstdruck auftreten, war eine örtliche Bestimmung des entsprechenden Defekts bzw. die Zuordnung zu ermittelten Defekten nicht möglich.

Letztlich zeigt die vorliegende Arbeit, dass Hohlglasfasern unter bestimmten Voraussetzungen die erforderliche Druckfestigkeit aufweisen, um Gase unter Druck sicher speichern zu können.

---

## Acknowledgement

As part of my work as research scientist at the BAM Federal Institute for Materials Research and Testing in the divisions “Gases, Gas Plants” and “Constructive Fire and Explosion Safety Gases” this thesis arose.

My thank goes to C.En Ltd which supported this thesis and the research project “Characterization of glass capillaries with respect to the storage of gases at high pressures”.

I would like to thank Prof. Thomas Böllinghaus, my supervisor at the Otto von Guericke University Magdeburg, who took the academic responsibility. His advice and technical suggestions helped me as well as his support in organizational questions and were essential for the success of this thesis. I would also like to express my appreciation to Prof. Dan Eliezer, my external supervisor from Ben Gurion University of the Negev, not only for the academic responsibility but as well for the numerous discussions and conceptions which lead to the successful graduation.

A special thank goes to my supervisor and head of the project Dr. Kai Holtappels for the interesting research topic. His never-ending help and feedback in different questions supported my ideas and work a lot. I am grateful for his guidance and dedications over the last years.

I want to acknowledge the help and assistance of all my colleagues at BAM. A very big thanks goes to Dr. Alida Nooke, Dennis Grasse, Emilio Balcazar Pust, Dr. Martin Kluge, Dr. Enis Askar and Dr. Rico Tschirschwitz for any aid in work-related and private questions.

Especially I want to thank my colleagues of the research project Andreas Krause, Kai Dame and Marco Steinhübel for the great teamwork and successful progression of our research work. Of course, I want to appreciate in a special way Miriam Grüneberg and Christian Gröschl for their support and great help during all tests carried out for this thesis and for all advising discussions and motivating conversations. Your helpfulness and motivation was irreplaceable. Thank you for being such a great team!

I would also want to thank my parents, my sister and my whole family for their extended support, their advice in any situation and their trust in me.

Last but not least I would like to thank my son Eleazar for any distraction, any laugh and all the fun he brought me. Furthermore, I thank my wife Solveig for all her love, patience and support she gave me during that time. You are my biggest backing.

---

## Table of Contents

<b>Abstract</b> .....	<b>I</b>
<b>Zusammenfassung</b> .....	<b>III</b>
<b>Acknowledgement</b> .....	<b>V</b>
<b>Table of Contents</b> .....	<b>VI</b>
<b>Index of Abbreviations</b> .....	<b>IX</b>
<b>List of Figures</b> .....	<b>XIII</b>
<b>List of Tables</b> .....	<b>XX</b>
<b>1 Introduction</b> .....	<b>1</b>
<b>2 Objectives</b> .....	<b>2</b>
<b>3 Hydrogen Storage</b> .....	<b>3</b>
3.1 Compressed Hydrogen Storage .....	4
3.2 Liquefied Hydrogen Storage .....	6
3.3 Hydrogen Storage in Metal Hydrides .....	8
3.4 Chemical Storage in Liquid Stage.....	11
3.5 Metal-Organic Frameworks (MOF) .....	13
3.6 Activated Carbon and Carbon Nanotubes as Hydrogen Storage Systems.....	15
3.7 Glass Microspheres .....	17
3.8 Hollow Glass Fibers.....	18
<b>4 Fundamentals</b> .....	<b>20</b>
4.1 The Material Glass .....	20
4.1.1 Definition and Structure of Glass.....	20
4.1.2 Chemical Composition and Physical Characteristics of Glass.....	23
4.1.3 Chemical Resistance .....	27
4.1.4 Mechanical Characteristics .....	29
4.2 Griffith Fracture Theory.....	32
4.3 Defects in Glass .....	34
4.3.1 Formation and Definition of Defects .....	34
4.3.2 Detection of Defects.....	40
4.4 Prevention and Removing of Defects in Glass .....	42
4.4.1 Thermal Treatment of Glass .....	42
4.4.2 Chemical Treatment.....	47



---

4.4.3 Coating of Surfaces .....	48
4.5 Weibull Distribution .....	51
<b>5 Experimental .....</b>	<b>55</b>
5.1 Experimental Setup .....	55
5.2 Test Sample Preparation .....	58
5.3 Experimental Execution .....	60
5.3.1 Determination of Burst Pressure .....	60
5.3.2 Burst Pressure after Storage in Different Air Humidity.....	61
5.3.3 Influence of Cyclic and Static Pressure Load .....	62
<b>6 Results and Discussion .....</b>	<b>63</b>
6.1 Different Types of Glass .....	63
6.1.1 Pre-Tests in Prior Stage.....	64
6.1.2 Repetition of Prior Test Series with Higher Number of Test Samples.....	66
6.2 Influence of Aging by Environmental Conditions .....	75
6.2.1 Aging under Constant Temperature Conditions .....	75
6.2.2 Aging under Constant Air Humidity Conditions.....	83
6.3 Pressure Resistance at Cyclic and Static Pressure Load.....	89
6.3.1 Cyclic Pressure Load.....	90
6.3.2 Static Pressure Load.....	97
6.4 Impact of Dimension Variations on the Pressure Resistance .....	104
6.4.1 Fixed Ratio of Outer to Inner Diameter .....	104
6.4.2 Different Wall Thicknesses at Fixed Inner Diameter.....	112
6.5 Comparison of different Borosilicate Glasses.....	122
6.6 Pre-stressed Glass Fibers .....	129
6.7 Aluminosilicate Glasses.....	141
6.8 Influence of Variation of Production Parameter on the Pressure Resistance .....	148
6.8.1 Increase of Residence Time .....	149
6.8.2 Increase of Drawing Stress .....	155
6.8.3 Increase of Drawing Temperature.....	158
6.9 Investigation of the Effect of Surface Coating on Hollow Glass Fibers .....	165
6.9.1 ALD-Coated Hollow Borosilicate Glass Fibers .....	166
6.9.2 Hollow Quartz Glass Fibers with different Coatings .....	179
6.10 Investigation on Defects .....	185
6.10.1 Volume Defects .....	185
6.10.2 Surface Defects.....	191
6.10.3 Investigation of Glass Fiber Surface by SEM and EDS.....	198

---

6.11 Calculation of Defect Sizes .....	204
6.12 Influence of Defects on Pressure Resistance of Hollow Glass Fibers .....	210
6.12.1 Material-dependent Defects.....	210
6.12.2 Production-dependent Defects .....	211
<b>7 Conclusions and Perspectives .....</b>	<b>214</b>
7.1 Conclusions.....	214
7.2 Perspectives.....	218
<b>8 List of references.....</b>	<b>221</b>
<b>Curriculum Vitae .....</b>	<b>237</b>

## Index of Abbreviations

A/D	Analogue / Digital
AFM	Atomic force microscopy
ALD	Atomic layer deposition
CTE	Coefficient of thermal expansion
CVD	Chemical vapor deposition
EDS	Energy dispersive X-ray spectroscopy
HDPE	High density polyethylene
LH2	Liquefied hydrogen
MOF	Metal Organic Framework
PVD	Physical vapor deposition
SEM	Scanning electron microscope
UV	Ultra violet

## Chemical Formulas

$\text{Al}_2\text{O}_3$	Aluminum oxide
$\text{As}_2\text{O}_3$	Arsenic trioxide
$\text{As}_2\text{O}_5$	Arsenic pentoxide
$\text{B}_2\text{O}_3$	Boron trioxide
BaO	Barium oxide
$\text{CaCO}_3$	Calcium carbonate
CaO	Calcium oxide
$\text{CsO}_2$	Cesium oxide
$\text{GeO}_2$	Germanium oxide
$\text{H}_2$	Hydrogen
HF	Hydrofluoric acid
$\text{K}_2\text{O}$	Potassium oxide
$\text{Li}_2\text{O}$	Lithium oxide
MgCl	Magnesium chloride
$\text{N}_2$	Nitrogen

NaCl	Sodium chloride
Na <sub>2</sub> CO <sub>3</sub>	Sodium carbonate
Na <sub>2</sub> O	Sodium oxide
OH-	Hydroxide ion
P <sub>2</sub> O <sub>5</sub>	Phosphorus oxide
PbO	Lead monoxide
Rb <sub>2</sub> O	Rubidium oxide
Si-OH	Silanol group
SiO <sub>2</sub>	Silicon dioxide
SiO <sub>4</sub>	Silicon dioxide tetrahedron as part of glass structure
Zn <sub>4</sub> O	Zinc oxide

### Formula Symbols

A <sub>i</sub>	mm <sup>2</sup>	Open area of hollow tube
b		Form parameter
C	μm	Critical crack diameter
c <sub>0</sub>	μm	Critical defect radius
D	m <sup>2</sup> s <sup>-1</sup>	Coefficient of diffusion
D <sub>o</sub>	mm	Outer diameter of glass raw material
d	μm	Diameter
d <sub>i</sub>	μm	Inner diameter
d <sub>o</sub>	μm	Outer diameter
E	MPa	Young's modulus
F	N	force
F(t)	%	Failure probability dependent on time
F <sub>B</sub>	%	Probability of bursting
F <sub>i</sub>	%	Estimated failure probability
FS	%	Free space; Ratio of open area
gsc	kWh kg <sup>-1</sup> resp. wt.%	Gravimetric storage capacity
i		Individual number of test in a test series
l	mm	Length of tested hollow glass fiber

---

$l_0$	m	Atomic distance
$l_{\min}$	mm	Minimum length of adhesive bonding
N		Total number of tests in a test series
$n_c$		Number of cyclic pressure loads
P	MPa	Characteristic pressure (Weibull parameter)
p	MPa	Pressure
$\Delta p$	MPa	Change of pressure
$p_0$	MPa	Threshold pressure to first failure
$p_{\text{average}}$	MPa	Average burst pressure of a test series
$p_B$	MPa	Burst pressure
$p_{\text{cyclic}}$	MPa	Pressure of cyclic load applications
$p_m$	MPa	Measurable pressure
$p_{\max}$	MPa	Maximum burst pressure of a test series
$p_{\min}$	MPa	Minimum burst pressure of a test series
$p_{\text{storage}}$	MPa	Storage pressure
$p_{\text{static}}$	MPa	Pressure of static load applications
$p_{\text{system}}$	MPa	Maximum inner pressure of test plant
s	$\mu\text{m}$	Wall thickness
T	s	Characteristic time (Weibull parameter)
T	$^{\circ}\text{C}$	Temperature
$\Delta T$	K	Temperature difference
$T_g$	$^{\circ}\text{C}$	Transformation temperature
$T_H$	$^{\circ}\text{C}$	Hardening temperature
$T_m$	$^{\circ}\text{C}$	Melting temperature
$T_S$	$^{\circ}\text{C}$	Operating temperature
$T_{\text{storage}}$	$^{\circ}\text{C}$	Storage temperature
$T_{\text{test}}$	$^{\circ}\text{C}$	Test temperature
t	s	time
$t_0$	s	Threshold time to first failure
$t_H$	s	Hardening time
$t_s$	s	Time period of static pressure load

---

U	V	Electrical voltage
U	J	Energy
U <sub>A</sub>	J	Potential energy
U <sub>E</sub>	J	Elastic stored energy in crack region
U <sub>M</sub>	J	Mechanical energy
U <sub>S</sub>	J	Surface energy
V	m <sup>3</sup>	Volume
vsc	kWh l <sup>-1</sup> resp. gH <sub>2</sub> l <sup>-1</sup>	Volumetric storage capacity

### Greek Symbols

$\alpha$	K <sup>-1</sup>	Coefficient of thermal expansion
$\gamma$	N m <sup>-1</sup>	Normalized surface energy
E		Strain
$\eta$	%	Efficiency
$\eta$	dPa s	Kinematic viscosity
$\rho_g$	MJ kg <sup>-1</sup>	Gravimetric energy density
$\rho_v$	MJ m <sup>-3</sup>	Volumetric energy density
$\sigma$	MPa	Acting stress
$\sigma_c$	MPa	Critical stress
$\sigma_{comp}$	MPa	Compression stress
$\sigma_p$	MPa	Practical tensile strength
$\sigma_t$	MPa	Tangential stress
$\sigma_{th}$	MPa	Theoretical tensile strength
T <sub>max</sub>	N mm <sup>-2</sup>	Maximum shear stress
$\varphi$	%	Relative air humidity

---

## List of Figures

Figure 1:	Gas cylinder type III with aluminum liner and carbon fiber wrap [19]	5
Figure 2:	Polymer liner (left) and complete wrapped gas cylinder type IV [19]	5
Figure 3:	Liquefied hydrogen tank [24]	7
Figure 4:	Absorption (left) and desorption (right) kinetics of pure magnesium dependent on milling time at 300 °C [33]	10
Figure 5:	Adsorption (left) and desorption (right) kinetics of nanocrystalline magnesium mixed with 0.2 mol % of Cr <sub>2</sub> O <sub>3</sub> respectively Nb <sub>2</sub> O <sub>5</sub> at 300 °C and 0.84 MPa hydrogen pressure [35]	11
Figure 6:	(a) SBU from Zn <sub>4</sub> O; the carboxylic acid used in the synthesis of (b) MOF-5 and (c) MOF-177; the structure of (d) MOF-5 and (e) MOF-177 [40]	13
Figure 7:	Hydrogen adsorption of MOF-5 dependent on pressure at T = -195 °C (78 K) (left) and at T = 20 °C (298 K) [44]	14
Figure 8:	Different MOFs shows the development of pore size and surface in the material; with increasing inner surface consequently the amount of absorbed gas is increasing [39]	14
Figure 9:	Comparison of gravimetric storage capacities of activated carbon and MWCN at different temperature and pressure regimes [47]	16
Figure 10:	Highest gravimetric storage capacity for the different hydrogen storage techniques	19
Figure 11:	Dependence of the specific glass volume on temperature during melting (red curve) and cooling (blue curve) [77]	20
Figure 12:	Ordered tetrahedron structure of crystal silicon dioxide, like quartz, (left) and less ordered structure of glass with defects in molecular level (right) [12]	22
Figure 13:	Reaction of Na <sub>2</sub> O as representative of modifiers: Splitting up the network and forming a point of disconnection [78]	22
Figure 14:	Reaction of Al <sub>2</sub> O <sub>3</sub> to point of disconnection: Network is closed and stabilized [78]	23
Figure 15:	Displacement and load data from a tensile test of solid glass fibers [99]	30
Figure 16:	Tensile strength of glass fibers dependent on diameter [8]	33

---

Figure 17: Stones of different sizes in glass: Decreasing sizes of stones from top left to bottom right due to the influence of heat [114]	34
Figure 18: Knot formed in glass as a result of potter's earth, clear distinction to defect free glass, optical variations and formation of schlieren surrounding the knot are detectable; emphasized by corrugated card board [114]	35
Figure 19: Schlieren in glass as result of inhomogeneous zones, the upper series of pictures displays them around knots of different origins, the lower series represents schlieren in glass formed from inhomogeneous zones in melting [114]	36
Figure 20: Movement of gas bubbles through schlieren in molten mass, the schlieren should be eliminated by that movement [114]	37
Figure 21: Gas bubbles in solidified material as result of remaining gas in molten glass [114]	37
Figure 22: Schematic progress of stress in a tempered glass (according to [6])	45
Figure 23: Load acting on tempered glass causing bending and movement of different zones of stress by interaction with bending force (according to [6])	46
Figure 24: Typical fracture appearance of tempered glass [131]	46
Figure 25: Schematic illustration of ALD coated glass, the surface of glass (bright region) is covered by nanoscale defects, ALD coating (dark region) fills the cracks completely or partially [136]	50
Figure 26: Constructed Weibull diagram for one species of hollow borosilicate 3.3 fibers; ( $d_o = 400 \mu\text{m}$ , $d_i = 300 \mu\text{m}$ ; $s = 50 \mu\text{m}$ ), definable form parameter $b = 5.1$	53
Figure 27: Developing of failure probability of borosilicate 3.3 fibers ( $d_o = 400 \mu\text{m}$ , $d_i = 300 \mu\text{m}$ ; $s = 50 \mu\text{m}$ ), characteristic pressure $P = 89.4 \text{ MPa}$ ; step function represents ideal case of failure of all samples at one test pressure	54
Figure 28: Schematic figure of test setup	56
Figure 29: Complete test setup with four measuring stations surrounded by acrylic glass box (left picture); one measuring station in enlargement, single hollow glass fiber connected to test setup and surrounded by heating jacket (right picture)	58
Figure 30: Finished connection after hardening of glue	59



---

Figure 31: Weibull diagram of hollow glass fibers made of different types of glass with the dimensions $d_o = 340 \mu\text{m}$ , $d_i = 300 \mu\text{m}$ , $s = 20 \mu\text{m}$	68
Figure 32: Failure probability curves of hollow fibers made of different glass types with the dimensions $d_o = 340 \mu\text{m}$ , $d_i = 300 \mu\text{m}$ , $s = 20 \mu\text{m}$	70
Figure 33: Weibull diagram of glass fibers made of different types of glass with the dimensions $d_o = 400 \mu\text{m}$ , $d_i = 300 \mu\text{m}$ , $s = 50 \mu\text{m}$	71
Figure 34: Failure probability curves of hollow fibers made of four different glass types with the dimensions $d_o = 400 \mu\text{m}$ , $d_i = 300 \mu\text{m}$ , $s = 50 \mu\text{m}$	72
Figure 35: Failure probability curves of fibers made of four different glass types with the dimensions $d_o = 340 \mu\text{m}$ , $d_i = 300 \mu\text{m}$ , $s = 20 \mu\text{m}$ aged one year under controlled temperature conditions	77
Figure 36: Failure probability curves of hollow fibers made of four different glass types with the dimensions $d_o = 400 \mu\text{m}$ , $d_i = 300 \mu\text{m}$ , $s = 50 \mu\text{m}$ aged one year under controlled temperature conditions	78
Figure 37: Influence of aging under different humidity on failure probability and pressure resistance of borosilicate 3.3 (DURAN) fibers with the dimensions $d_o = 400 \mu\text{m}$ , $d_i = 300 \mu\text{m}$ , $s = 50 \mu\text{m}$	85
Figure 38: Influence of different humidity on failure probability and pressure resistance of hollow quartz glass fibers with the dimensions $d_o = 400 \mu\text{m}$ , $d_i = 300 \mu\text{m}$ , $s = 50 \mu\text{m}$	86
Figure 39: Characteristic pressures of hollow quartz respective borosilicate fibers (both $d_o = 400 \mu\text{m}$ , $d_i = 300 \mu\text{m}$ , $s = 50 \mu\text{m}$ ) after cyclic treatment of $p_{\text{cyclic}} = 50 \text{ MPa}$ with the test gases nitrogen and hydrogen	94
Figure 40: Characteristic pressures $P$ of fibers made of borosilicate glass ( $d_o = 400 \mu\text{m}$ , $d_i = 300 \mu\text{m}$ , $s = 50 \mu\text{m}$ ) plotted against time period of static pressure load with $p_{\text{static}} = 50 \text{ MPa}$ and test gases hydrogen and nitrogen	101
Figure 41: Characteristic pressure $P$ for hollow borosilicate fibers with different fixed diameter ratios plotted against the corresponding wall thickness $s$	109
Figure 42: Failure curves against burst pressure of fibers with selected wall thicknesses and a fixed diameter ratio of $d_o / d_i = 1.25$	110
Figure 43: Weibull diagram of hollow borosilicate fibers with inner diameter of about $d_i = 150 \mu\text{m}$ and different wall thicknesses, double logarithmic function of estimated failure probability $F_i$ plotted against logarithmic burst pressure $p_B$	116

- 
- Figure 44: Defined defects of different populations on beverage bottle surface caused distinctions in burst pressures, according graphs in Weibull diagram exhibited different slopes and distributions [97] 117
- Figure 45: Failure probability  $F_B$  plotted against burst pressure  $p_B$  for hollow borosilicate fibers of inner diameter of about  $d_i = 150 \mu\text{m}$  118
- Figure 46: Characteristic pressure of hollow fibers with different fixed inner diameter plotted against wall thickness, the encircled values are valid for hollow glass fibers with similar free spaces but different inner diameter 119
- Figure 47: Failure probability of hollow fibers with comparable free space of about  $FS = 63\%$  but decreasing wall thickness and inner diameter plotted against related burst pressure values 120
- Figure 48: Failure probability of hollow fibers made of different types of borosilicate glass with similar outer diameter but different wall thickness ( $d_o = 488 \mu\text{m}$ ,  $d_i = 441 \mu\text{m}$ ,  $s = 23 \mu\text{m}$  respectively  $d_o = 478 \mu\text{m}$ ,  $d_i = 400 \mu\text{m}$ ,  $s = 39 \mu\text{m}$ ) 126
- Figure 49: Failure probability of pre-stressed hollow fibers with comparable dimensions ( $d_o \approx 210 \mu\text{m}$ ,  $d_i \approx 170 \mu\text{m}$ ,  $s \approx 20 \mu\text{m}$ ), pre-stressed condition reached by combination of glasses with different CTE 133
- Figure 50: Failure probability of pre-stressed hollow fibers with comparable dimensions ( $d_o \approx 320 \mu\text{m}$ ,  $d_i \approx 250 \mu\text{m}$ ,  $s \approx 35 \mu\text{m}$ ), pre-stressed condition reached by combination of glasses with different CTE 134
- Figure 51: Failure probability of pre-stressed hollow fibers with comparable dimensions ( $d_o \approx 400 \mu\text{m}$ ,  $d_i \approx 320 \mu\text{m}$ ,  $s \approx 40 \mu\text{m}$ ), pre-stressed condition reached by combination of glasses with different CTE 135
- Figure 52: Microscopic view of C5-C1S combined fiber ( $d_o \approx 400 \mu\text{m}$ ,  $d_i \approx 320 \mu\text{m}$ ,  $s \approx 40 \mu\text{m}$ ) with clear boundary of inner and outer layer, magnified 400 times 137
- Figure 53: Microscopic picture of C1S-C5 fiber ( $d_o \approx 400 \mu\text{m}$ ,  $d_i \approx 320 \mu\text{m}$ ,  $s \approx 40 \mu\text{m}$ ) with clear borderline between inner C5 layer and outer C1S layer 139
- Figure 54: Comparison of the failure probability of hollow aluminosilicate glass fibers with similar dimensions in the range of  $d_o \approx 320 \mu\text{m}$ ,  $d_i \approx 250 \mu\text{m}$  and  $s \approx 30 \mu\text{m}$  but different glass mixture, as comparison value the test results of borosilicate C5 fibers were plotted 144

- 
- Figure 55: Comparison of the failure probability of hollow aluminosilicate glass fibers with similar dimensions in the range of  $d_o \approx 400 \mu\text{m}$ ,  $d_i \approx 300 \mu\text{m}$  and  $s \approx 50 \mu\text{m}$  but different glass mixture, as reference value the results of borosilicate C5 fibers was taken 145
- Figure 56: Influence of increased residence time during drawing process on failure probability of hollow DURAN fibers with  $d_o \approx 490 \mu\text{m}$ ,  $d_i \approx 420 \mu\text{m}$  and  $s \approx 35 \mu\text{m}$  152
- Figure 57: Surface defects of hollow DURAN fiber of series A with  $d_o \approx 490 \mu\text{m}$ ,  $d_i \approx 420 \mu\text{m}$  and  $s \approx 35 \mu\text{m}$  (magnified 100 times), test samples act as reference in investigation of the effect of product parameter on pressure resistance 153
- Figure 58: Surface defects of Duran fiber of series B with  $d_o \approx 490 \mu\text{m}$ ,  $d_i \approx 420 \mu\text{m}$  and  $s \approx 35 \mu\text{m}$  (magnified 100 times) produced at increased residence time 154
- Figure 59: Influence of increased drawing stress on the failure probability of DURAN fibers, increasing the drawing speed led to increased drawing stress 157
- Figure 60: Surface defects of Duran fiber of series C with  $d_o \approx 270 \mu\text{m}$ ,  $d_i \approx 240 \mu\text{m}$  and  $s \approx 15 \mu\text{m}$  produced at increased drawing stress (magnified 100 times) 158
- Figure 61: Effect of increased drawing temperature and residence time on failure probability of DURAN fibers with dimensions of  $d_o \approx 490 \mu\text{m}$ ,  $d_i \approx 420 \mu\text{m}$  and  $s \approx 35 \mu\text{m}$  compared to reference series A 161
- Figure 62: Surface defects on hollow DURAN fiber of series D with dimensions of  $d_o \approx 490 \mu\text{m}$ ,  $d_i \approx 420 \mu\text{m}$  and  $s \approx 35 \mu\text{m}$  (magnified 100 times), fibers were produced at increased drawing temperature compared to reference, both pictures show same fiber but rotated by  $90^\circ$  on lower picture 162
- Figure 63: Surface of DURAN fiber of series E with dimensions of  $d_o \approx 490 \mu\text{m}$ ,  $d_i \approx 420 \mu\text{m}$  and  $s \approx 35 \mu\text{m}$  (magnified 100 times) 163
- Figure 64: Transport system for coated single fibers consists of stainless steel box (left picture) and the stainless steel brackets (right picture) 166
- Figure 65: Failure probability of hollow borosilicate C5 fibers covered with ALD-coating of different thicknesses at  $T = 300 \text{ }^\circ\text{C}$ , the reference series was carried out without coating and temperature treatment 169
- Figure 66: Failure probability of hollow borosilicate C5 fibers with the dimensions of  $d_o \approx 500 \mu\text{m}$ ,  $d_i \approx 465 \mu\text{m}$  and  $s \approx 17.5 \mu\text{m}$  covered with an aluminum ALD-

---

coating of different thicknesses at $T = 500\text{ }^{\circ}\text{C}$ , the reference series was carried out with samples without coating and temperature treatment	171
Figure 67: Comparison failure probability of uncoated hollow fibers but different thermal history	173
Figure 68: Surface defects of uncoated borosilicate C5 fibers with dimensions of $d_o \approx 500\text{ }\mu\text{m}$ , $d_i \approx 465\text{ }\mu\text{m}$ and $s \approx 17.5\text{ }\mu\text{m}$	175
Figure 69: Damages of ALD-coating of different thicknesses applied at $T = 300\text{ }^{\circ}\text{C}$ on borosilicate C5 fibers, the layer thickness increases from upper left to bottom right ( $s_c = (50, 100, 200, 500)\text{ nm}$ )	176
Figure 70: Imperfections of ALD-coating of different thicknesses applied at $T = 500\text{ }^{\circ}\text{C}$ on borosilicate C5 fibers, layer thickness increases from upper left to bottom right ( $s_c = (50, 100, 200, 500)\text{ nm}$ )	177
Figure 71: Volume defects inside the wall of single quartz fiber with the dimensions $d_o = 400\text{ }\mu\text{m}$ , $d_i = 300\text{ }\mu\text{m}$ , $s = 50\text{ }\mu\text{m}$	186
Figure 72: Cross section of borosilicate fiber with the dimensions $d_o = 400\text{ }\mu\text{m}$ , $d_i = 300\text{ }\mu\text{m}$ , $s = 50\text{ }\mu\text{m}$ , the enclosures of gas bubbles are detectable, rough inner surface caused by grinding during the preparation	187
Figure 73: Sealed end of a single borosilicate fiber with dimensions $d_o = 310\text{ }\mu\text{m}$ , $d_i = 270\text{ }\mu\text{m}$ , $s = 20\text{ }\mu\text{m}$ , magnified 200 times, wire visible passing through the glass pellet, generation of a sharp peak at bottom	188
Figure 74: Sealed end of a single borosilicate fiber with dimensions $d_o = 150\text{ }\mu\text{m}$ , $d_i = 100\text{ }\mu\text{m}$ , $s = 15\text{ }\mu\text{m}$ , magnified 100 times (left) and 400 times (right), detection of sharp peak	189
Figure 75: Uncomplete sealed end of single borosilicate fiber with $d_o = 700\text{ }\mu\text{m}$ , $d_i = 460\text{ }\mu\text{m}$ , $s = 120\text{ }\mu\text{m}$ , magnified 100 times, open channel visible at the end resulting in gas leakage	190
Figure 76: Surface of a hollow aluminosilicate fiber, detection of flatting or spalling on the surface was done under light microscope	192
Figure 77: Quartz fiber surface under the microscope, straight lines detectable which could be caused during drawing process	192
Figure 78: Hollow fiber surface with scratches, potential results transportation damages	193
Figure 79: Borosilicate fiber with enclosures which are located at the surface	194

---

Figure 80: Open end of a borosilicate glass fiber with $d_o = 570\mu\text{m}$ , $d_i = 460\mu\text{m}$ , $s = 50\mu\text{m}$ , magnified 100 times, taped in different levels	195
Figure 81: Open end of a borosilicate glass fiber with $d_o = 180\mu\text{m}$ , $d_i = 160\mu\text{m}$ , $s = 10\mu\text{m}$ , magnified 200 times, taped in different levels	196
Figure 82: Open end of two different borosilicate fibers with $d_o = 540\mu\text{m}$ , $d_i = 360\mu\text{m}$ , $s = 50\mu\text{m}$ , magnified 100 times	196
Figure 83: Typical surface defect on borosilicate glass fibers with dimensions of $d_o \approx 490\mu\text{m}$ , $d_i \approx 420\mu\text{m}$ and $s \approx 35\mu\text{m}$ , magnified 400 times	198
Figure 84: Surface defects on borosilicate DURAN fibers with dimensions of $d_o \approx 490\mu\text{m}$ , $d_i \approx 420\mu\text{m}$ and $s \approx 35\mu\text{m}$ , four different measuring points are marked and the chemical elements were investigated	199
Figure 85: EDS-spectrum of measuring point no. 1 defined in Figure 84, significant peaks for the elements Na, K, and Cl are detectable	200
Figure 86: EDS-spectrum of cubic shaped particle on DURAN fiber surface	201
Figure 87: EDS spectrum of measuring point no. 4 with elevated crystal structures on fibers' surface	202
Figure 88: EDS spectrum of measuring point no. 3 of a defect free area of the DURAN fiber surface	203
Figure 89: Characteristic pressure of hollow borosilicate fibers against wall thickness, theoretical calculation in comparison to experimental results	206
Figure 90: Tangential stress plotted against wall thickness for borosilicate fibers with free space of $FS = 63\%$ ; development of related critical crack size $C$ in micrometer is given as well	209

---

## List of Tables

Table 1:	Compilation of weight of gas storage cylinders of different types with same operating pressure of 20 MPa and 100 l inner volume [19]	6
Table 2:	Gravimetric storage capacities of selected metal hydrides [28]	9
Table 3:	Substances classified as network former, network modifier and stabilizer, which can act as network former and modifier	23
Table 4:	Viscosities of different characteristic points during manufacturing process of glass [78]	24
Table 5:	Summary of components of technical most relevant glasses	25
Table 6:	Classification of glass by type of applications and manufacture	27
Table 7:	Classification of defects dependent on size and corresponding option of detection without optical tool according to [6]	39
Table 8:	Shear stress of UHU PLUS ENDFEST 300 dependent on hardening temperature and time [145]	60
Table 9:	Literature and measured values of relative air humidity above confectioned saline solutions	61
Table 10:	Chemical compositions of tested hollow glass fibers given in mass-%	64
Table 11:	Data of average, maximum and minimum burst pressures of hollow glass fibers of different types of glass and different dimensions [10]	65
Table 12:	Measured burst pressure values in ascending order of tested fibers made of quartz, borosilicate 3.3, soda-lime and aluminosilicate with the dimensions $d_o = 340 \mu\text{m}$ , $d_i = 300 \mu\text{m}$ , $s = 20 \mu\text{m}$	67
Table 13:	Form parameters $b$ and corresponding characteristic pressures $p_o$ of tested hollow fibers with the dimensions $d_o = 340 \mu\text{m}$ , $d_i = 300 \mu\text{m}$ , $s = 20 \mu\text{m}$	69
Table 14:	Form parameters $b$ and corresponding characteristic pressures $P$ of tested fibers with the dimensions $d_o = 400 \mu\text{m}$ , $d_i = 300 \mu\text{m}$ , $s = 50 \mu\text{m}$	72
Table 15:	Young's modulus and corresponding theoretical tensile strength estimated by equation (3.4) [5]	73
Table 16:	Minimum and maximum burst pressures with correlating form parameter $b$ and characteristic pressure $P$ of tested fibers made of different glasses and	

dimensions; the hollow fibers were stored for one year under controlled temperature conditions	76
Table 17: Characteristic values of hollow borosilicate and aluminosilicate fibers with different dimensions and ages	79
Table 18: Characteristic values of hollow quartz fibers with different dimensions and ages	80
Table 19: Characteristic data of soda-lime fibers with different dimensions and age	81
Table 20: Development of burst pressure resistance of glass fibers after aging one year compared new tested fibers by reference to the characteristic pressure P	83
Table 21: Characteristic test data of borosilicate 3.3 fibers at different air humidity with the dimension $d_o = 400 \mu\text{m}$ , $d_i = 300 \mu\text{m}$ , $s = 50 \mu\text{m}$	84
Table 22: Characteristic test data of hollow quartz fibers stored at different air humidity with the dimensions $d_o = 400 \mu\text{m}$ , $d_i = 300 \mu\text{m}$ , $s = 50 \mu\text{m}$	86
Table 23: Pressure resistance development of glass fibers aged under the influence of different defined air humidity compared new tested fibers by reference to the characteristic pressure P	89
Table 24: Characteristic results of hollow borosilicate fibers ( $d_o = 400 \mu\text{m}$ , $d_i = 300 \mu\text{m}$ , $s = 50 \mu\text{m}$ ) loaded with nitrogen with different numbers of cycles with $p_{\text{cyclic}} = 50 \text{ MPa}$	91
Table 25: Test results of borosilicate fibers ( $d_o = 400 \mu\text{m}$ , $d_i = 300 \mu\text{m}$ , $s = 50 \mu\text{m}$ ) loaded with hydrogen with different numbers of cycles with $p_{\text{cyclic}} = 50 \text{ MPa}$	92
Table 26: Significant results of quartz fibers ( $d_o = 400 \mu\text{m}$ , $d_i = 300 \mu\text{m}$ , $s = 50 \mu\text{m}$ ) tested with nitrogen with different numbers of cyclic pressure load of $p_{\text{cyclic}} = 50 \text{ MPa}$	93
Table 27: Distinct test data of quartz fibers ( $d_o = 400 \mu\text{m}$ , $d_i = 300 \mu\text{m}$ , $s = 50 \mu\text{m}$ ) tested with hydrogen and different numbers of pressure load cycles	93
Table 28: Distinct test results of borosilicate fibers ( $d_o = 400 \mu\text{m}$ , $d_i = 300 \mu\text{m}$ , $s = 50 \mu\text{m}$ ) loaded with static pressure of $p_{\text{static}} = 50 \text{ MPa}$ with nitrogen for different time periods before determining the burst pressures	98
Table 29: Distinct test results of borosilicate fibers ( $d_o = 400 \mu\text{m}$ , $d_i = 300 \mu\text{m}$ , $s = 50 \mu\text{m}$ ) loaded with static pressure of $p_{\text{static}} = 50 \text{ MPa}$ with hydrogen for different time periods before determining the burst pressures	99

---

Table 30: Distinct test results of borosilicate fibers ( $d_o = 400 \mu\text{m}$ , $d_i = 300 \mu\text{m}$ , $s = 50 \mu\text{m}$ ) loaded up with static pressure of $p_{\text{static}} = 50 \text{ MPa}$ with nitrogen for different time periods; burst pressures were determined by using hydrogen	100
Table 31: Specifications of tested borosilicate hollow fibers with respect to $d_o / d_i$ ratio, each series has a consecutive number independent on diameter ratio	105
Table 32: Distinctive test results of borosilicate fibers with different wall thicknesses and fixed diameter ratio of $d_o / d_i = 1.33$	106
Table 33: Distinctive test results of borosilicate fibers with different wall thicknesses and fixed diameter ratio of $d_o / d_i = 1.25$	107
Table 34: Distinctive test results of borosilicate fibers with different wall thicknesses and fixed diameter ratio of $d_o / d_i = 1.15$	108
Table 35: Specifications (real and desired) for hollow borosilicate fibers with fixed inner diameter $d_i$ , but different wall thicknesses $s$ (desired values given in brackets)	113
Table 36: Test results of hollow borosilicate fibers with similar inner diameter but varied wall thicknesses	115
Table 37: Chemical main components of tested borosilicate glass fibers, as determined in chemical analysis	123
Table 38: Physical properties of tested borosilicate glasses	124
Table 39: Characteristic test results of hollow glass fibers made of three different borosilicate glasses and different dimensions	125
Table 40: Development of pressure resistance of different borosilicate fibers compared to a borosilicate C5 fiber	128
Table 41: Thermal properties of tested borosilicate glasses C5 and C1S	130
Table 42: Characteristic test results of pre-stressed hollow glass fibers with different dimensions, whereby the fibers were combined from two borosilicate tubes with different coefficient of thermal expansion (CTE)	132
Table 43: Development of pressure resistance of combined fibers compared to a borosilicate C5 fiber (uncombined)	140
Table 44: Chemical main components of tested aluminosilicate glass fibers given in technical data sheets of the manufacturer	142



---

Table 45:	Characteristic test results of hollow aluminosilicate fibers with different dimensions, the fibers were made of two types of aluminosilicate glass with different composition, borosilicate C5 fibers conduce as reference	142
Table 46:	Development of pressure resistance of aluminosilicate fibers compared to a borosilicate C5 fiber	148
Table 47:	Process parameters of hollow DURAN glass fibers with different residence time but similar dimensions of $d_o \approx 490 \mu\text{m}$ , $d_i \approx 420 \mu\text{m}$ and $s \approx 35 \mu\text{m}$ , whereby series A represents the reference series	151
Table 48:	Distinct test results of borosilicate DURAN glass fibers with comparable dimensions, series B produced with increased residence time but same drawing temperature	151
Table 49:	Process parameters of hollow DURAN glass fibers with increased drawing stress and dimensions of $d_o \approx 490 \mu\text{m}$ , $d_i \approx 420 \mu\text{m}$ and $s \approx 35 \mu\text{m}$ (series A) and $d_o \approx 270 \mu\text{m}$ , $d_i \approx 240 \mu\text{m}$ and $s \approx 15 \mu\text{m}$ (series C)	155
Table 50:	Characteristic test results of DURAN glass fibers at inner pressure load, the fibers were produced at different drawing speed and stress	156
Table 51:	Process parameters of hollow DURAN glass fibers with different drawing temperature and residence time and similar dimensions of $d_o \approx 490 \mu\text{m}$ , $d_i \approx 420 \mu\text{m}$ and $s \approx 35 \mu\text{m}$	159
Table 52:	Distinct test results of DURAN fibers of similar dimensions with different drawing temperatures and residence times	160
Table 53:	Characteristic test results of fibers covered with different coating thickness at a temperature of $T = 300 \text{ }^\circ\text{C}$ , all fibers exhibit dimensions of $d_o \approx 500 \mu\text{m}$ , $d_i \approx 465 \mu\text{m}$ and $s \approx 17.5 \mu\text{m}$	167
Table 54:	Characteristic test results of fibers covered with different coating thickness at a temperature of $T = 500 \text{ }^\circ\text{C}$ , all fibers exhibit dimensions of $d_o \approx 500 \mu\text{m}$ , $d_i \approx 465 \mu\text{m}$ and $s \approx 17.5 \mu\text{m}$	170
Table 55:	Characteristic test results of uncoated fibers with dimensions $d_o \approx 500 \mu\text{m}$ , $d_i \approx 465 \mu\text{m}$ and $s \approx 17.5 \mu\text{m}$ annealed at different temperatures	173
Table 56:	Properties of different coated hollow silica fibers	180
Table 57:	Characteristic test results of coated silica fibers with different dimensions	182

---

Table 58: Calculated maximum burst pressures $p_{max}$ of coated silica fibers, $p_{max}$ was not determinable up to the limit of experimental limit, as $\sigma_{t\ max}$ the value of PM 530/660 was taken	183
Table 59: Characteristic data and calculated critical crack size of hollow borosilicate fibers with similar free spaces	208

## 1 Introduction

The material glass is present in many applications in daily life. Mostly it is used as plate glass in windows and mirrors or as containment glass for a multitude of liquids. Here, as most known characteristic, the high transmission of light is utilized.

Nevertheless, the existence of a multitude of chemical mixtures of glass each with different properties leads to wide fields of applications with special requirements in industry and engineering [1], [2]. The outstanding properties of the individual glass types and consequent advantages are adjusted to specific usages.

Quartz glass is used for optical applications with highest requirements because of its high translucence and pureness [3], [4]. Furthermore, the high temperature resistance predestines that glass for the usage as sight glass in high thermal claimed areas of facilities as well. Another glass type is e.g. borosilicate glass which stands out due to its high chemical resistance and high reliability against changes of temperature. The main advantage compared to quartz glass is the lower melting temperature and therefore a more economical manufacturing process.

Beside the named properties the enormous theoretical tensile strength is impressive but decreases many times by different outer influences [5], [6]. Here, solid bars or plates were investigated by using the three-point-bending-test to understand and verify the mechanisms. However, the size and the test method of a test sample made from glass have a major influence on the tensile strength. By decreasing the size of the test sample the determined tensile strength increases significantly [7], [8].

A possible field of application by utilization of the high mechanical resistance is the storage of highly compressed gases in thin walled hollow fibers made from glass. The target is the development of a lightweight storage system which realizes high gravimetric and volumetric storage capacities [9]. Thereby a high number of single hollow fibers could be bundled and combined to complex structures to reach a competitive amount of stored hydrogen. Consequently, depending on the application the number of fibers is changeable and the size and shape is adaptable to the required shape and volume. Each hollow fiber represents an individual pressure vessel able to withstand high pressures. Preceding test series showed high pressure resistance as a result of the outstanding tensile strength of the material and the high mechanical solidity of the component and demonstrated the high potential of hollow glass fibers [10], [11].

---

## 2 Objectives

The pressure resistance of hollow glass fibers should be tested as well the influences of tests methods and outer effects on the pressure resistance with the objective of evaluation of failure distribution and reliability.

Not only various hollow fibers made from different types of glass shall be tested, but different dimensions and the effect of aging under varied air humidity will be also investigated. Impacts of gases stored inside the hollow glass fibers were determined in the past [12]. To extend and prove the results different dynamic and static load cycles again with different test gases will be carried out. Once again the impact of outer influences should be observed under stressed conditions. The investigation on possible defects and the theoretical reflection and calculation of these are issues as well.

The main objective of the thesis is the determination of influences on the pressure resistance of hollow glass fibers and the effects caused by those. The evaluation of test results by using the Weibull distribution as statistical instrument gives the possibility to point out not only the pressure resistance but also on the failure probability at inner pressure load.

### 3 Hydrogen Storage

The production of hydrogen from fossil fuels but also from renewable energies is already technologically feasible; the storage and transportation of hydrogen are serious challenges for mobile and stationary applications. At this stage numerous approaches exist and different opinions are held regarding that topic.

The contained energy content of a storage or energy system is one of the most important characteristics. This general information of capacity is not only used for hydrogen or gas tanks but also for batteries. So, an opportunity is given to compare energy storage systems of different types of construction or storage technology. Thereby, the storage capacity can be given as gravimetric as well as volumetric capacity. The capacity of a system per weight is defined as gravimetric storage capacity (gsc). Here the ratio of stored energy to weight of the storage system is given in different units. The most common units are kWh kg<sup>-1</sup>, gH<sub>2</sub> kg<sup>-1</sup> or wt.%.

The volumetric storage capacity is defined as the ratio of stored energy to outer volume of the storage system and is given in kilowatt-hours per liter system volume (kWh l<sup>-1</sup>) or otherwise as ratio between mass of hydrogen and outer volume of the storage system, which is given in grams hydrogen per liter system volume (gH<sub>2</sub> l<sup>-1</sup>).

A special advantage compared with fossil fuels is the high gravimetric energy density  $\rho_g$  of molecular hydrogen per mass ( $\rho_g = 142 \text{ MJ kg}^{-1}$ ), which is three times higher than of liquid carbon hydrides [13]. The production of hydrogen from renewable energies like water power, sun or wind power plants with the help of electrolysis do not cause any emission of greenhouse gases as well as the transformation in electricity via fuel cells.

Nevertheless, hydrogen shows a deficit in volumetric energy density  $\rho_v$  which is in the range of  $\rho_v = 11 \text{ kJ l}^{-1}$  [14] in gaseous state and ambient pressure. Liquid carbon hydrides feature volumetric energy densities in the range between  $\rho_v = 32 \text{ MJ l}^{-1}$  and  $\rho_v = 38 \text{ MJ l}^{-1}$  [15] which is significantly higher. Therefore, the increase of storage capacity can be reached by compression, liquefaction or the application of chemical or physical bond to a substrate.

The required infrastructure to distribute the hydrogen has to be built up and developed. Here the buildup of hydrogen fueling station for mobile sector had already started especially cars and buses. The distribution of hydrogen for smaller mobile application is much more complex. Here the constitution of a distribution network with stations for changing the storage systems is possible [16]. These will be re-charged in a central fueling station and circulated for next use. Due to usual comfort of available energy

sources at home also the delivery of hydrogen directly to the customer by pipelines is discussed as well as a portable system of electrolysis for home-recharging of storage systems [16].

Numerous technologies to store hydrogen in acceptable costs, efforts and amounts were researched in the past and still are developed for improving the storage capacities. The technologies include:

1. Compressed Hydrogen Storage
2. Liquefied Hydrogen Storage
3. Hydrogen Storage in Metal Hydrides
4. Chemical Hydrogen Storage in suitable Liquids
5. Metal Organic Frameworks (MOFs)
6. Activated Carbon and Carbon Nanotubes as Hydrogen Storage Systems
7. Glass Microspheres
8. Hollow Glass Fibers

In following the features and storage principles of the mentioned technologies are explained and discussed in detail

### **3.1 Compressed Hydrogen Storage**

Storing hydrogen as compressed gas is a conventional and well known storage technology. Standardized is the storage in metal cylinders, mostly made of steel or aluminum, with a maximum storage pressure of  $p_{\text{storage}} = 20 \text{ MPa}$ . Due to the advantages in developing storage cylinders for compressed hydrogen and to differentiate between the types of cylinder, the metal cylinders without any supporting jacket are defined as cylinder type I [17].

Enhancements of these containments are cylinders wrapped partly with glass fiber composite material, called cylinder type II [18]. Only the lateral surface but not the neck of the gas cylinder is encapsulated. The material of the inner layer is still a metal, mostly steel or aluminum. The composite jacket takes 50 % of stress caused by internal pressurization so the wall thickness of the metal cylinder can be reduced at the same internal working pressure.

The next generation of development is cylinder type III, generally an aluminum liner with full composite overwrap and shown in Figure 1.



Figure 1: Gas cylinder type III with aluminum liner and carbon fiber wrap [19]

The composite material is carbon fiber reinforced plastic or a mixture of carbon fiber and glass fiber reinforced plastics [19]. The liner takes only a small amount of pressure stress but has to meet completely the demands of gas tightness.

The demand of increase gravimetric storage capacity leads to gas cylinder type IV, which is again a complete carbon fiber reinforced plastic cylinder. The most exiting difference and improvement is the use of a polymer liner as opposed to the metal liner used in cylinder type I to III. The polymer liner is made from a high density polyethylene (HDPE) [18], which features absolute gas tightness and a low permeation rate of hydrogen. The composite jacket material carries the complete structural loads affects by the inner pressure up to 70 MPa. A third layer formed as caps and placed at the ends of the cylinder serve as protection of the cylinder against outer influences and forceful impacts [20]. The left picture of Figure 2 presents an inner liner and in contrast the right picture shows a complete cylinder type IV.



Figure 2: Polymer liner (left) and complete wrapped gas cylinder type IV [19]

The basic principle of construction of all cylindrical tanks is the same, but every stage of development with different enhancements of design leads to a decrease of weight at same internal pressure and volume, which is shown in Table 1. The total weight of a pressurized gas storage system could be reduced by the factor four by comparison of type I to type IV.

Table 1: Compilation of weight of gas storage cylinders of different types with same operating pressure of 20 MPa and 100 l inner volume [19]

Cylinder type	Empty weight [kg]
Type I	110
Type II	80
Type III	33
Type IV	31

The reinforcement of the cylinder with composite material has not only an effect on the weight but also an effect to the pressure resistance. The operating pressure could be increased from  $p_{\text{storage}} = 20$  MPa of cylinder type I to  $p_{\text{storage}} = 35$  MPa or actually  $p_{\text{storage}} = 70$  MPa for cylinder of type III and type IV. This constructional arrangement leads to the increase of the gravimetric as well as the volumetric capacity of compressed hydrogen storage systems.

### 3.2 Liquefied Hydrogen Storage

The storage of liquid hydrogen is an established technology [21] with a high volumetric ( $v_{\text{sc}} = 33 \text{ gH}_2 \text{ l}^{-1}$  [22]) and gravimetric storage capacity ( $g_{\text{sc}} = 7 \text{ wt.}\%$  with periphery). Several steps of compression and irreversible decompression with concomitant refrigeration are necessary to cool down hydrogen to  $T_{\text{storage}} = -253$  °C and reach liquefaction. The accompanying volume decrease leads to a higher energy density and an economical type of storage at moderate pressures with an energy density which is two times higher than this of compressed hydrogen [16].

However, the high energy demand of liquefaction decreases the efficiency  $\eta$  of stored hydrogen to only  $\eta = 64 \%$  [20], [23]. Additionally the very low temperature necessitates a thermal multi-layer insulation of the storage system to avoid boil off losses, which are



nonetheless 9 % per day [20] and have to blow off by a safety valve. A schematic assembly of a liquid hydrogen storage system is given in Figure 3.

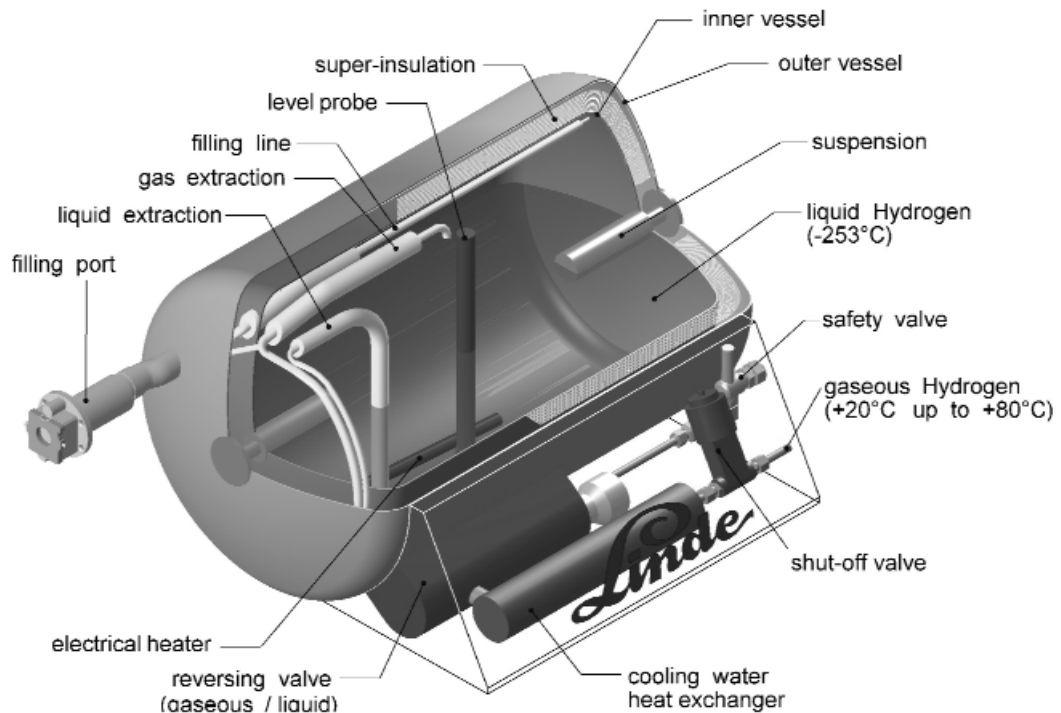


Figure 3: Liquefied hydrogen tank [24]

Further developments of the insulation material and the temperature management leads to a decrease of boil off losses and is today on a level between 1 % per day and 1.5 % per day [13], [20], [23]. Due to the liquid stage and the moderate pressures the tanks are scalable to different applications and affords in space and shape. But, the smaller the tank, the bigger is the surface to volume ratio which directly is an influence parameter of the loss of hydrogen [13]. Therefore smaller tanks, e.g. for vehicles, will have higher loss rates due to the appealing environmental temperature, even if the insulation material is improved. So the application for portable devices is less suitable [16].

Empty liquefied hydrogen tanks mostly have assimilated ambient temperature. Therefore, the fueling with liquid hydrogen requires a specific boil off for cooling down to storage temperature. The vaporized hydrogen has to be vented to guaranty a low pressure inside the tank [25]. Only after that, the fueled liquid hydrogen will remain inside the tank. For the release of gaseous hydrogen, the liquid state has to be heated up to ensure the volume flow rate required for the specific application, what requires an additional heater inside the tank. Hence, the boil off for cooling the tank and the input energy again leads to further decrease of the efficiency.

A significant reduction of the boil off losses can be reached by using cryo-compressed hydrogen storage, whereby the pressure inside the system is increased to  $p_{\text{storage}} = 30 \text{ MPa}$  [26] and  $p_{\text{storage}} = 35 \text{ MPa}$  [25], respectively. The temperature is kept at the same low level as for liquid hydrogen. That storage system features the opportunity to store both, liquid hydrogen at  $T_{\text{storage}} = -253 \text{ }^\circ\text{C}$  (20 K) or cold compressed hydrogen [25].

In case of storing liquid hydrogen the boil off can be stored in gaseous state due to the high pressure resistance of the storage tank. A safety valve is still installed but did not open until  $p_{\text{storage}} = 35 \text{ MPa}$  is reached. The refueling is done in the same way as like as in pure liquefied hydrogen tanks. The liquid hydrogen is filled in the tank, whereby at first the tank is cooled down. The boil off, which is formed due to the ambient temperature of the tank, is released until the temperature has reached the storage temperature of  $T_{\text{storage}} = -253 \text{ }^\circ\text{C}$  (20 K). After that the liquid hydrogen will stay in the tank during fueling process.

If cooled compressed hydrogen is stored in a cryo-compressed hydrogen tank, the storage pressure  $p_{\text{storage}} = 35 \text{ MPa}$  is reached at a storage temperature of  $T_{\text{storage}} = -210 \text{ }^\circ\text{C}$  (63 K). Thereby, hydrogen is in the state of a super-critical fluid, which changes over in gaseous state at pressure decrease at release. Hence, a re-heater is installed inside of the cryo-compressed storage tank, but is not necessary to use, when cold compressed hydrogen is stored.

Thus, it is the only hydrogen storage system which meets the DOE targets for 2015 [27], which are in the range of  $g_{\text{sc}} = 5 \text{ wt.}\%$  gravimetric and  $v_{\text{sc}} = 40 \text{ g l}^{-1}$  volumetric storage capacity.

### 3.3 Hydrogen Storage in Metal Hydrides

The chemical storage of hydrogen gives the opportunity to combine hydrogen as energy carrier with the physical properties of the storage medium. The best known and researched type of chemical storage is the application of metal-hydride systems as storage system for hydrogen. Thereby, hydrogen is first adsorbed at the surface of the metal and in second step integrated in the crystal lattice, whereby the metal hydride is formed in an exothermal chemical reaction [13].

When the fueling process is started the storage system has to be cooled, due to the exothermal reaction. Beside the chemical also physical bond can occur so the metal hydride provides the opportunity of bonding hydrogen by van der Waals forces and increases the stored amount of hydrogen many times [13]. The release of hydrogen

requires the reheating of the system to crack the chemical bonds and form back the pure metal. So a quick and intelligent heat management is essential at the application of metal hydride storage systems.

Numerous metals and alloys were investigated about their ability of storing hydrogen. Each of them features a different storage temperature and pressure at which the charging can be executed successful. Therefore the systems are classified in low-temperature and high-temperature metal hydrides. Here the main advantage of the low-temperature hydrides is the low energy for heating the system at initial time of charging and during the release of hydrogen. However, such hydrides feature gravimetric storage capacities of not more than 2 wt.% at a storage pressure of  $p_{\text{storage}} = 0.6 \text{ MPa}$  [28], [29].

On the contrary, high temperature hydrides exhibit gravimetric storage capacities up to 7.6 wt.% [28], [30], [31] but require much more energy to reach the high temperatures. Additionally the heat management has to be much more complex, as well. In Table 2 selected metal hydrides are listed with their gravimetric storage capacity.

Table 2: Gravimetric storage capacities of selected metal hydrides [28]

Material	Gravimetric storage capacity [wt.%]
$\text{LaNi}_5\text{H}_{6.7}$	1.37
$\text{ZrMn}_2\text{H}_{3.6}$	1.75
$\text{FeTiH}_{1.95}$	1.89
$\text{VH}_2$	2.1
$\text{Mg}_2\text{NiH}_4$	3.6
$\text{MgH}_2$	7.6

The most promising material is magnesium with a maximum gravimetric storage capacity of 7.6 wt.%. Nevertheless, it also features a big disadvantage of very slow reaction kinetic [32]. Hence, the upload but as well the release of hydrogen will take up to some hours depending on the size of the tank. Different ways of improving the surface kinetics of magnesium were investigated in the past with positive results.

The surface is the most important factor of the hydrogen kinetics [28]. Milling magnesium to nanocrystalline powder leads to a significant increase of surface and hydrogen kinetics, as well [28], [33]. Pure unmilled magnesium needs 3 hours to be charged with 6 wt.% of hydrogen, whereby the temperature has to be kept at a level of 300 °C [33].

Milled magnesium without any alloying material needs only about 5 minutes to be charged to the same content at same temperature [33]. Desorption of hydrogen is accelerated as well. So the complete desorption out of unmilled magnesium will take several hours as well as the hydrogen uptake. The complete dehydrogenation of milled magnesium will only take 30 to 90 minutes dependent on the milling duration [33]. A comparison of hydrogenation/dehydrogenation of milled and unmilled magnesium is shown in Figure 4

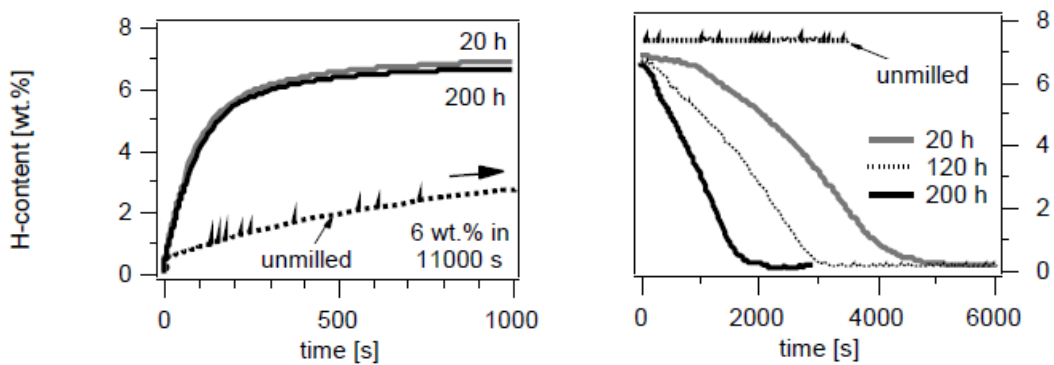


Figure 4: Absorption (left) and desorption (right) kinetics of pure magnesium dependent on milling time at 300 °C [33]

Nevertheless, the high temperature necessary to charge and discharge the storage system has an effect on the storage material magnesium. As nanocrystalline powder the heat effects the growing of the crystallites [34]. After 1000 loading and unloading cycles the single powder crystallites grew up from 20 nm up to 200 nm at different temperatures in the range of 300 °C to 400 °C [34]. Hence, the reaction rate is slowed down due to growing grains.

Alloying magnesium with different other metals has also a positive factor on the hydrogen kinetics and leads to a lower working temperature as secondary effect [28]. However, most alloys feature a lower gravimetric capacity which has decreased from 7.6 wt.% for pure magnesium to about 3.1 wt.% for an alloy of magnesium, nickel and copper ( $\text{Mg}_2\text{Ni}_{0.5}\text{Cu}_{0.5}$ ) [33]. However, the sorption temperature can be reduced to 200 °C instead of 300 °C [33] and 400 °C [28], respectively.

The increase of the reaction rate of hydrogenation and dehydrogenation by using milled nanocrystalline magnesium is already improved [33]. Using a catalyst is another way to improve the reaction of uptake and release of hydrogen again without alloying the

material with other metals. Here, different materials were investigated on their effect on the hydrogen kinetics. A promising material was  $\text{Cr}_2\text{O}_3$  which accelerated the already faster kinetics of hydrogen in milled magnesium again. So with the application of this catalyst in the amount of 0.2 mol % the first 95% of the full capacity is already reached after 30 seconds at 300 °C and 0.84 MPa hydrogen pressure. The full capacity can be reached after 5 minutes. Desorption kinetic is accelerated, as well. However, an enhancement of the amount of catalyst has a negative effect on the reaction rate.

$\text{Nb}_2\text{O}_5$  were found to have also a positive effect on the kinetics [32], [34], [35]. Mixing the nanocrystalline Mg with 0.2 mol % of  $\text{Nb}_2\text{O}_5$  leads to an accelerated reaction kinetics, even faster than that with  $\text{Cr}_2\text{O}_3$ . So, 6.9 wt.% of hydrogen are absorbed in about 60 seconds, which is 1 wt.% more than with  $\text{Cr}_2\text{O}_3$  [35]. The absorption and desorption kinetics of both  $\text{Cr}_2\text{O}_3$  and  $\text{Nb}_2\text{O}_5$  are displayed in Figure 5.

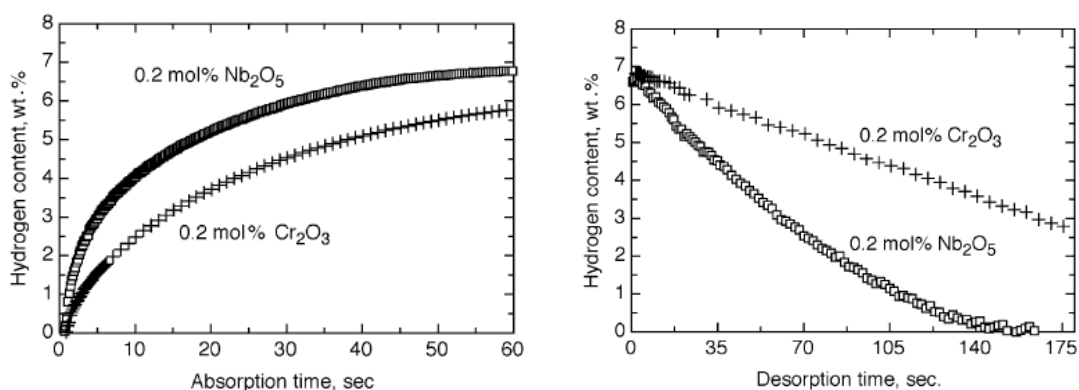


Figure 5: Adsorption (left) and desorption (right) kinetics of nanocrystalline magnesium mixed with 0.2 mol % of  $\text{Cr}_2\text{O}_3$  respectively  $\text{Nb}_2\text{O}_5$  at 300 °C and 0.84 MPa hydrogen pressure [35]

A big advantage of mixing nanocrystalline magnesium with catalysts is the opportunity to decrease the adsorption and desorption temperature [33], whereby the reaction kinetics is decelerated again. Hence, the absorption is possible at 40 °C [33].

### 3.4 Chemical Storage in Liquid Stage

Not only metals or their alloys can be used for chemical hydrogen storage but also liquids are possible storage media. Storing hydrogen chemical in liquids offers different advantages over solid storage [36]. The liquids can be pumped in pipelines or be distributed in fuel tankers in accustomed manner. The refueling of storage systems, not only in a vehicle but also in other applications, is much easier and works without any

heating or cooling device. The dehydrogenation process is simplified as well in comparison to solid chemical storage systems like metal hydrides. So not the whole system is heated up but only a small part of the liquid is transported to a heating chamber for heating [36]. The off-loaded material could be replaced at a fueling station with fresh H<sub>2</sub>-loaded liquid. Transported by tanker or pipelines the off-loaded liquid could be returned to a central recharging station. To prevent the mixing of fresh, H<sub>2</sub>-loaded liquid with off loaded material not only during refueling but also during normal operation, a second tank is necessary [36]. However, that second tank represents a disadvantage of liquid chemical hydrogen storage materials. That fact requires more space in the possible application and has to be considered during design and construction.

Possible materials for liquid chemical hydrogen storage are common liquids like methanol or gasoline which can be used in high temperature fuel cells to generate energy as pure hydrogen in a low temperature fuel cell [37]. An upstream reformer which cracks the fossil fuels and generates hydrogen enables also the use of low temperature fuel cells like PEMFC for the operation with gasoline or diesel. Different other materials, e.g. carbazole [38], are investigated as carrier liquid and used in above mentioned way. Therefore a reformer which solve the hydrogen at temperatures of about  $T = 100\text{ }^{\circ}\text{C}$  out of the liquid phase is necessary as well. However, the opportunities are given but do not solve the problems of air pollution and ongoing scarcity of fossil fuels.

Therefore, the storage of hydrogen in aromatic heterocycles can be a promising way in liquid chemical hydrogen storage because of a high possible gravimetric storage capacity of 11.7 wt.% [36]. Different variations, like five-membered or six-membered rings, were investigated. Here, a positive effect on the thermodynamics of hydrogen release could be identified by the introduction of nitrogen into the aromatic rings [36].

Nevertheless, the hydrogenation temperature of such aromatic rings is up to 160 °C by using a catalyst, which improves the chemical reaction. The dehydrogenation can be realized at temperatures between 50 °C to about 200 °C, as well with the application of a catalyst. However, a degradation of the hydrogen storage material could be detected after 5 cycles of hydrogenation and dehydrogenation [36].

For further progress of liquid storage materials the development of suitable catalysts is necessary as well the research and development of heterocycles. Due to the simpler scalability and heat management [36] they offer a big advantage in comparison to solid chemical storage materials.

### 3.5 Metal-Organic Frameworks (MOF)

Physisorption as storage method contains the adsorption of different substances on the surface or the micropores of a material. This storage method is applied in metal hydrides as secondary storage method when chemical storage is finished and further hydrogen is adsorbed on the surface of formed metal hydrides due to Van-der-Waals forces. Metal organic frameworks are compounded crystalline materials which providing robustness, due to strong bonding, and a geometrically well-defined structure [39]. Thereby, MOF consist of metal clusters, which are defined as secondary building units (SBU) and represents the inorganic compounds of the network [39]. The SBUs are affiliated via organic aromatic anions, called linkers. The assembly process of MOF is comparable to organic polymerization process [39]. The schematic composition is shown in Figure 6.

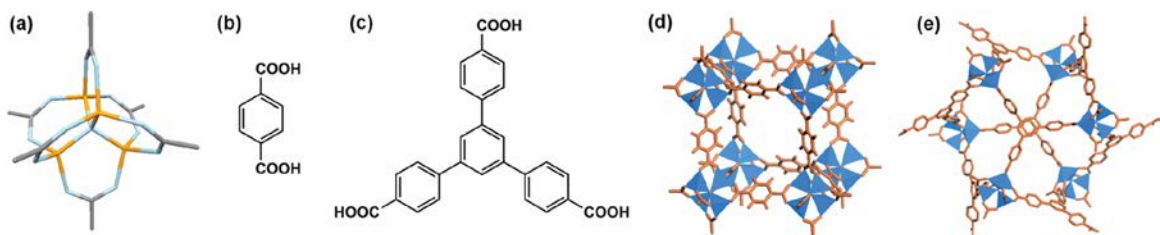


Figure 6: (a) SBU from  $Zn_4O$ ; the carboxylic acid used in the synthesis of (b) MOF-5 and (c) MOF-177; the structure of (d) MOF-5 and (e) MOF-177 [40]

During fueling process, hydrogen diffuses into the pores and is adsorbed at the surface of the metal cluster only by physisorption without any chemical reaction. Due to the increased pressure, existing mostly during fueling process, hydrogen is stored as compressed gas in the pores of the framework as well. Hence, the complete hydrogen content, which is affiliated by MOFs, includes both surface-adsorbed hydrogen and compressed hydrogen in the pores [41].

At low storage temperatures ( $T_{\text{storage}} = -196\text{ }^{\circ}\text{C}$ ) and pressures up to  $p_{\text{storage}} = 10\text{ MPa}$  gravimetric storage capacities up to  $g_{\text{sc}} = 10\text{ wt.}\%$  can be realized with  $Zn_4O$  as carrier material [41], [42]. The gravimetric capacity depends strongly on storage temperature and pressure. The same material features  $g_{\text{sc}} = 1.5\text{ wt.}\%$  at  $T_{\text{storage}} = -196\text{ }^{\circ}\text{C}$  and  $p_{\text{storage}} = 0.1\text{ MPa}$  or  $g_{\text{sc}} = 2\text{ wt.}\%$  at room temperature and  $p_{\text{storage}} = 1\text{ MPa}$  [43]. In Figure 7 the storage capacity of a MOF is displayed dependent on the temperature and storage pressure. Here the significant dependency on the temperature becomes clear.

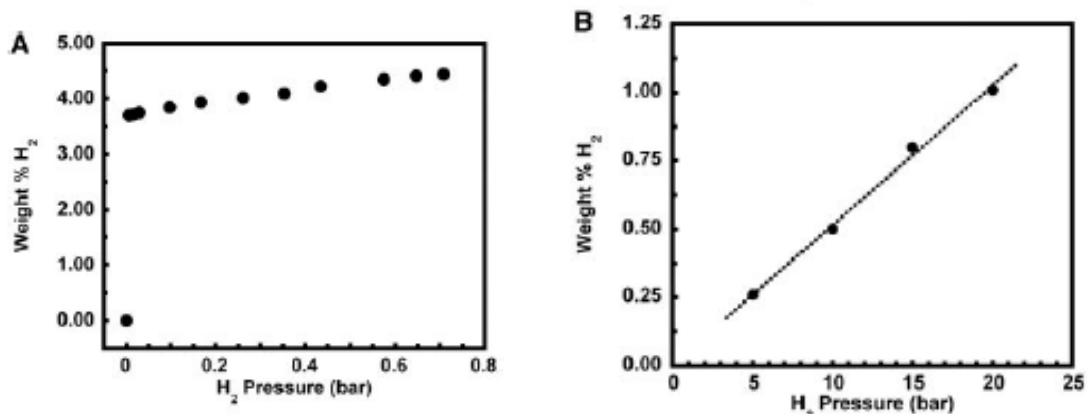


Figure 7: Hydrogen adsorption of MOF-5 dependent on pressure at T = -195 °C (78 K) (left) and at T = 20 °C (298 K) [44]

Like metal hydrides also MOF need to be heated during release of stored hydrogen. The storage capacity can be increased by using different metal clusters and linkers, so the pore size and the amount of stored hydrogen are variable. Thereby, the conditions for optimization of storage can be changed as well. Figure 8 shows the development of pore size and surface and therefore the increasing amount of hydrogen stored in MOFs.

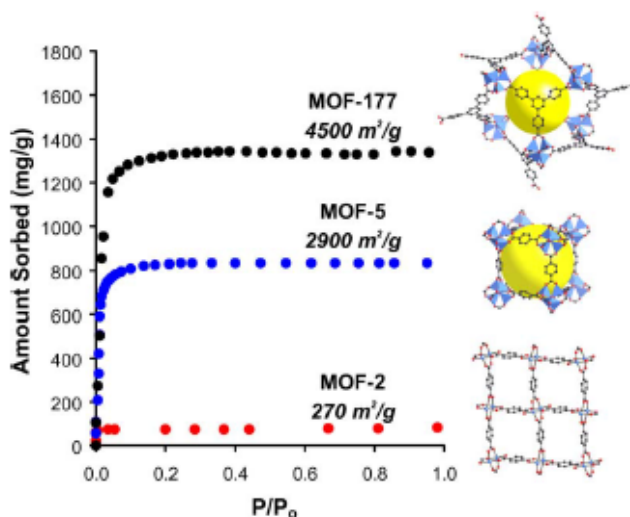


Figure 8: Different MOFs shows the development of pore size and surface in the material; with increasing inner surface consequently the amount of absorbed gas is increasing [39]



### 3.6 Activated Carbon and Carbon Nanotubes as Hydrogen Storage Systems

A comparable storage principle like in MOFs is adapted to carbon adsorbents [45]. Thereby, the first adsorption of hydrogen to carbon with a high surface area was reported already in 1960's [46]. Hydrogen was stored at cryogenic temperatures of liquid nitrogen  $T_{\text{storage}} = -196\text{ }^{\circ}\text{C}$  and pressures up to  $p = 2.5\text{ MPa}$  on activated carbon with a maximum gravimetric storage capacity of about 2 wt.% [46]. Different researchers investigated this technology but weren't able to improve the storage capacity above 4.8 wt.% at  $T_{\text{storage}} = -186\text{ }^{\circ}\text{C}$  and a pressure of  $p = 5.9\text{ MPa}$ .

Further developments of carbon based hydrogen storage systems are carbon nanofibers, single wall carbon nanotubes (SWCN) or multi wall carbon nanotubes (MWCN).

Carbon nanofibers with a typically diameter from 5 nm to 500 nm were reported with gravimetric storage capacities of up to 10 wt.%. Thereby, the samples were stored in a suitable vessel and loaded up with pressure of  $p = 11.2\text{ MPa}$  at ambient temperature. Over 24 hours a decrease of the pressure could be recorded what from the storage capacity was calculated [46]. Hence, the hydrogen kinetics in carbon fibers is very slow and could be accelerated by reducing the layer thickness.

That reduction was tried by using MWCN, which consists of different numbers of layers of nested cylinders of graphite with hollow centers [46]. The number of shells lies in a range between two up to 50 layers. Thereby, the MWCN have inner diameters between 2 nm to 10 nm and outer diameters 15 nm to 30 nm. The length of each individual tube can vary and reaches lengths of about 2 mm [46]. The catalytic decomposition of acetylene is used to produce MWCN, whereby the reaction product has to be cleaned with an acid treatment to remove the catalyst [46]. Enormous gravimetric capacities of 14 wt.% at room temperature and 20 wt.% at  $T_{\text{storage}} = 380\text{ }^{\circ}\text{C}$  were reported, whereby the MWCN were doped by potassium and lithium, respectively [46]. However, other researcher found out that the gravimetric capacity of MWCN being not doped by any substances are not that high and reaches only half the capacity of activated carbon at ambient and elevated temperatures [47]. A corresponding diagram is given in Figure 9.

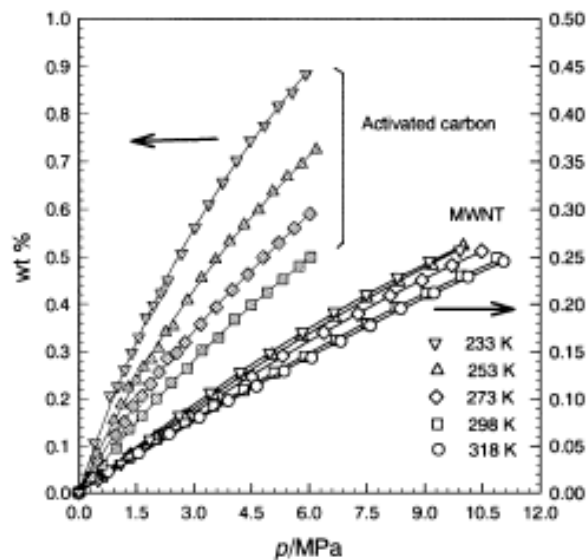


Figure 9: Comparison of gravimetric storage capacities of activated carbon and MWCN at different temperature and pressure regimes [47]

Thereby, clearly to observe is the very low capacity of both activated carbon and MWCN of below 1 wt.%. Nevertheless, the storage capacities could be doubled by using activated carbon instead of MWCN.

The performance of conventional physisorption based on adsorption can be maximized by using porous solids with pores of very small diameters, not larger than a few molecular diameters [46], [48]. Therefore the application of SWNC at the hydrogen storage promised larger and faster adsorption, even at ambient temperature. Single walled carbon nanotubes features diameters in the range of 10 Å to 15 Å and are bundled to larger structures. The estimated storage capacities for such structures are about 10 wt.% [46]. However, the measured results show a wide spread. So for SWCN at room temperature are very low, but measurable. At cryogenic temperatures not more than 1 wt.% is detectable [49]. Other researcher were able to reach gravimetric storage capacities of 4.2 wt.% at  $p = 10\text{MPa}$  [50]. Here the SMCN were pretreated by HCl and temperature and only 80 % of adsorbed hydrogen could be released in different tests. The maximum reached storage capacity is about 7 wt.% [46], whereby temperatures up to  $T = 580\text{ °C}$  are necessary.

Although this storage technology promise large storage capacities, a wide spread of results exists and different data of one researcher could not be proven by another.

### 3.7 Glass Microspheres

Beside the described storage technologies and materials a complete new material could be used in different ways. The material glass is common in optical or structural application of daily use and life. But to use such a brittle material as storage material for hydrogen seems to be complete incredible.

Although glass is a brittle material, it has some outstanding properties which qualify this material for the storage of hydrogen. Not only has a very high pressure resistance in small sizes distinguished this material for the described use but also a very low permeation rate of hydrogen in glass.

Glass microspheres as hydrogen storage material were investigated by different researchers and offer the opportunity of high pressure storage with competitive capacities [51], [52], [53]. Small balloons made of glass with diameters of  $d_o = 25 \mu\text{m}$  to  $d_o = 500 \mu\text{m}$  and wall thicknesses between  $s = 0.5 \mu\text{m}$  to  $s = 10 \mu\text{m}$  [54], [55], [56] were filled with hydrogen. Thereby, gravimetric storage capacities of  $\text{gsc} = 2.2 \text{ wt.}\%$  at operating pressure of  $p = 34.5 \text{ MPa}$  were reached [57] with the option of doubling the operating pressure in future.

Other researchers were able to reach a gravimetric storage capacity of  $\text{gsc} = 10 \%$  and volumetric storage capacity of  $\text{vsc} = 20 \text{ g/l}$  at internal pressure of  $p = 62 \text{ MPa}$  [56]. Further research leads to the increase of gravimetric storage capacity up to  $\text{gsc} = 17 \%$  at  $p = 25 \text{ MPa}$  by using microspheres with a large ratio of diameter to wall thickness [55]. Thereby the impact of different production and preparation parameters were tested [58], [59].

The filling process of such glass spheres can be realized by utilizing the temperature dependence of permeability of glass [60] - [65]. So at elevated temperature the permeability of glass is increased and a charging with pressurized hydrogen is possible. Hence, different filling times dependent on the application and the used glass are feasible by changing the temperature. Using quartz glass the filling time at  $T = 200 \text{ }^\circ\text{C}$  is  $t = 16760 \text{ s}$  (4.6 hours). Increasing the temperature to  $T = 350 \text{ }^\circ\text{C}$  leads to a decrease of filling time to  $t = 1440 \text{ s}$ . At ambient temperatures the permeability and therefore the loss as well is negligible small.

The release of stored hydrogen again requires heating energy to increase the permeability. However, to reach faster release of hydrogen the illumination of filled microspheres with near-infrared light was researched and found [66], [67] as well as the application of a laser [68]. Nevertheless, the required energy to achieve the elevated

temperature needed for filling and release of hydrogen decreases the efficiency of that kind of storage system.

### 3.8 Hollow Glass Fibers

Using a high number of thin hollow glass fibers for the built-up of a hydrogen storage system instead of glass microspheres will offer different advantages. Significantly higher volumetric storage capacities of  $vsc = 45 \text{ g l}^{-1}$  [69] up to  $vsc = 48.3 \text{ g l}^{-1}$  [70] are achievable. The better packing ratio has to be emphasized as main advantage because of less unused space [70]. The gravimetric storage capacity is given with up to  $gsc = 10 \%$  at a storage pressure of  $p = 168.5 \text{ MPa}$  [70]. Loading and release of such hydrogen storage system can be realized in different ways.

One opportunity is a loading and release process based on permeation at elevated temperatures comparable to glass microspheres [69], which entails both ends of the thin glass fibers closed by melting. That time-consuming method can be replaced by using a special stopper alloy. Thereby, only one end of the glass fiber is sealed. After charging the structure with hydrogen the open end is closed by applying heat to a low melting alloy. In a specialized procedure the alloy is pressed in the open end and after cooling it forms a gas-proof plug [70], [71]. But the required heating energy will decrease the efficiency of the storage system as well. In order to increase the efficiency by avoid the need of heating energy for permeation or stopper alloy a connection of glass fibers to a micro valve is feasible [72], [73].

Since the pressure resistance can be increased significantly at cryogenic temperatures [74] the storage capacities can be increased by storing compressed hydrogen in hollow glass fibers at such temperatures. Under those conditions capillaries with a wall thickness of  $s = 43 \mu\text{m}$  were able to withstand internal pressures of  $p = 184 \text{ MPa}$  [74] whereby the capillaries were immersed in liquid nitrogen and pressurized with gaseous hydrogen. The corresponding storage capacities came to  $gsc = 9 \text{ wt.}\%$  respectively  $vsc = 32 \text{ g l}^{-1}$ , which is below the values of pure compressed storage. Additionally the challenges of cooling and insulation have to be solved.

Each storage technology features unique advantages outstanding for specific advantages. A storage system made of thin hollow glass fiber thereby combines the common technique of storing hydrogen in compressed gas state with freedom in shape and volume due to the modular assembling of the storage system. Therefore the storage of hydrogen in hollow glass fibers is a promising technology which shall be investigated as part of this thesis.

As summary and comparison the following diagram gives the highest values of the gravimetric capacity of each hydrogen storage technique given in literature. It can be seen that hollow glass fibers as hydrogen storage system are a promising technology. It does not have the highest gravimetric storage capacity of all listed techniques but requires no special equipment. Commercial available parts as used for composite tanks can be applied. Furthermore, no heat has to be applied when storing or releasing hydrogen.

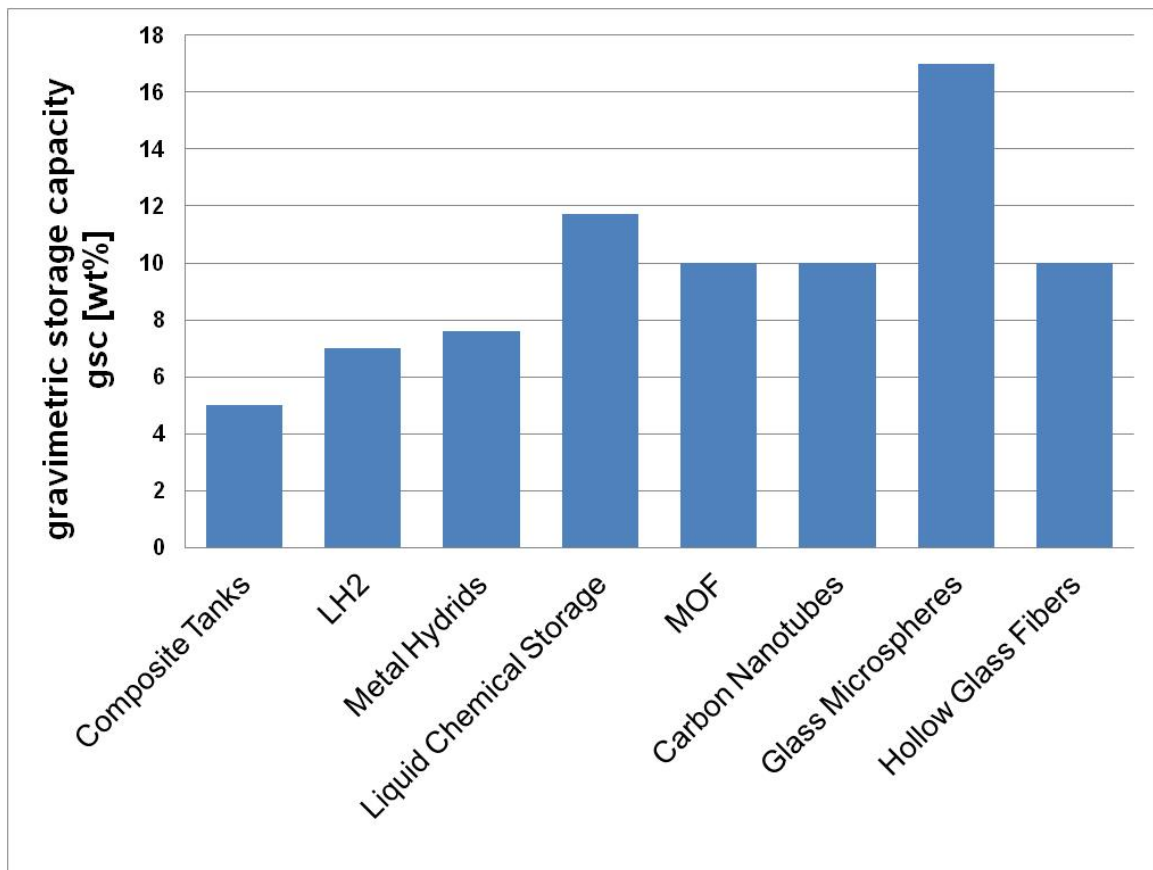


Figure 10: Highest gravimetric storage capacity for the different hydrogen storage techniques

## 4 Fundamentals

### 4.1 The Material Glass

Glass is a well-known material used in wide fields of applications. The characteristics can be modified by employing different chemical compositions or physical treatments of the material. The following chapters will present an overview of glass properties and their dependencies on various influences.

#### 4.1.1 Definition and Structure of Glass

Glass is defined as an amorphous and “inorganic liquefied material that solidifies without crystallization” [75]. This special feature arises clearly by plotting the specific volume against temperature during the manufacturing process as shown in Figure 11.

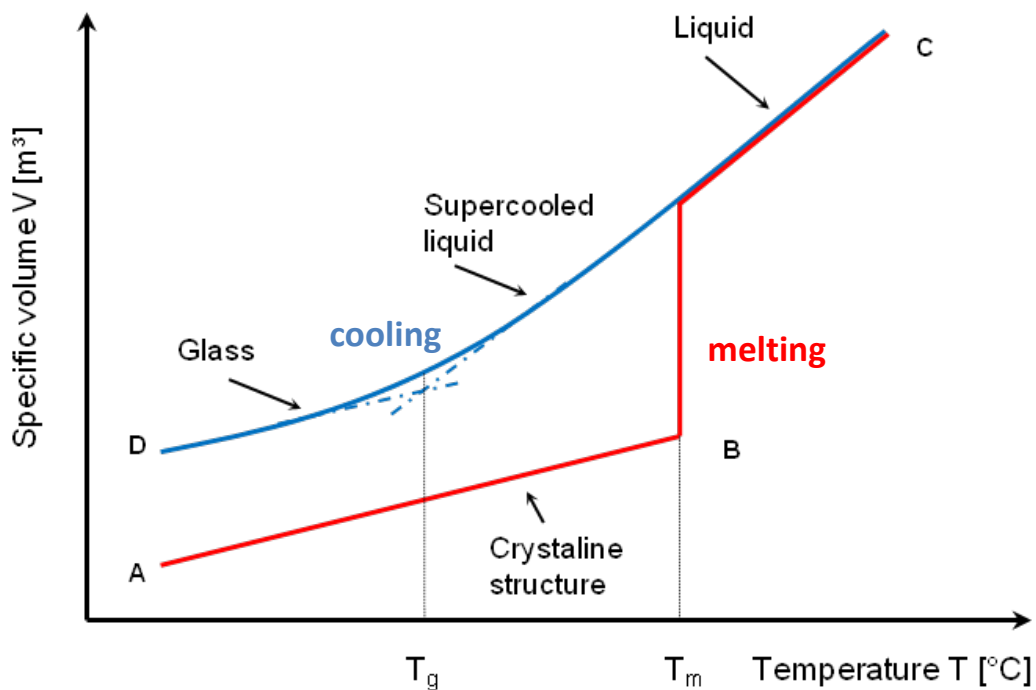


Figure 11: Dependence of the specific glass volume on temperature during melting (red curve) and cooling (blue curve) [77]

Silicon oxide ( $\text{SiO}_2$ ) as main component of glass is probably one of the most occurring minerals and forms ordered crystal structure of  $\text{SiO}_4$  tetrahedrons in solid state. At the production process of glass silicon oxide in the form of quartz sand is first molten

(point A), which is represented by the red line. Reaching the melting temperature  $T_m$  at point B the volume increases significantly and the crystal structure is opened. Further heating to point C is necessary to ensure a continuous and homogeneous liquid phase. During the cooling process (blue curve) the decrease of volume is a continuous process and no crystallization occurs. The liquid material crosses over to a super cooled liquid. Thus, the thermodynamic state of the liquid glass changes from a stable equilibrium to a meta-stable one. The cooling procedure induces not only the decrease in volume of the liquid glass but also the increase of its viscosity. The molten and still liquid glass passes through the range of transition in which the increase of viscosity reaches a specific value of  $\eta = 10^{13}$  dPa s [1]. For viscosities higher than this value the material is glass by definition. The mass does not flow and the meta-stable equilibrium ceases to change. The corresponding temperature is defined as transformation temperature  $T_g$ . Because of the continuous process and smooth transition that temperature is not clearly identifiable by measurements. A tool for determination is the extension of the different slopes of the blue curve. The point of intersection of the extensions describes the transition temperature. The basic raw material crystal silica exhibits a long range order at molecular level which is shown in Figure 12 (left picture). Hence, the complete material presents the same ordered structure of  $\text{SiO}_4$  tetrahedrons independent from point of inspection. Due to absent crystallization a long range order is missing; solely a short range order in the adjustment at molecular level can be found. Only in small ranges, ordered structures of  $\text{SiO}_4$  tetrahedrons can be detected. For larger ranges of inspection, less ordered structures are observable. That is why glass is integrated in the group of amorphous materials and even in solid state is considered a liquid.

The structure of glass arises from the network theory of Zachariasen [76], which signifies that the difference in the lattice energy is only very small for glass and crystal of the same composition. The conclusion was made that glass must have the same structural elements like quartz crystals. The liquid material changes over to solid state with formation of a disordered  $\text{SiO}_4$  tetrahedron structure which shows defects in the molecular level, as displayed in Figure 12 (right picture). Because of that behavior, silicon dioxide ( $\text{SiO}_2$ ) is classified as a network former. Glass forming acid oxides can act as a network former as well.  $\text{B}_2\text{O}_3$ ,  $\text{P}_2\text{O}_5$ ,  $\text{GeO}_2$ ,  $\text{As}_2\text{O}_3$  and  $\text{As}_2\text{O}_5$  belong to that group of materials [3].

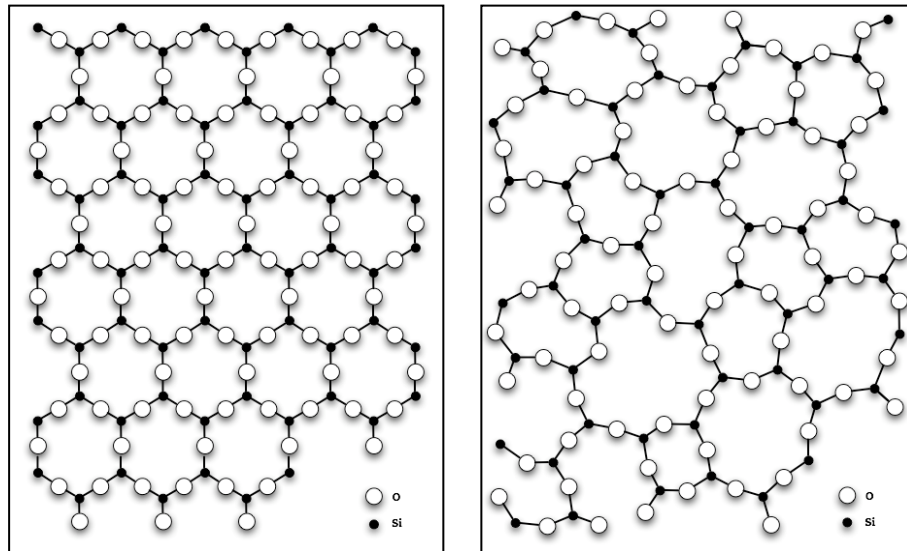


Figure 12: Ordered tetrahedron structure of crystal silicon dioxide, like quartz, (left) and less ordered structure of glass with defects in molecular level (right) [12]

The network can be changed by network modifiers which are mostly alkaline or alkaline earth oxides [3]. These crack the bonds between silicon dioxide and oxygen and form a point of disconnection in the network. The chemical reaction is displayed in the following figure.

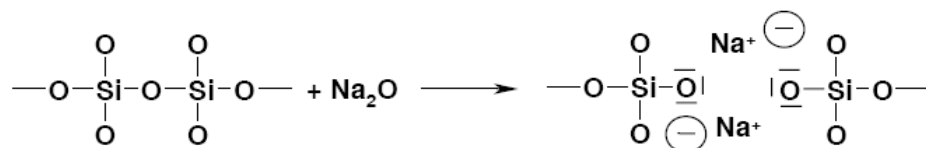


Figure 13: Reaction of  $\text{Na}_2\text{O}$  as representative of modifiers: Splitting up the network and forming a point of disconnection [78]

Network modifiers have the task of a fluxing agent in molten material and decrease the melting temperature of the glass. Furthermore, the coefficient of thermal expansion increases and the chemical durability decreases while the higher the concentration of the network modifier.

Another group of substances can act as both, as network former and as network modifier, depending on their concentration in the mixture. These substances are classified as a stabilizer [3], [79]. As long as the concentration of the stabilizer is lower than the network modifier the stabilizer acts as a network former. One example is presented in Figure 14, where aluminum oxide  $\text{Al}_2\text{O}_3$  forms a covalent bond at the point



of disconnection caused by sodium oxide. Due to this reaction the network is closed and stabilized.

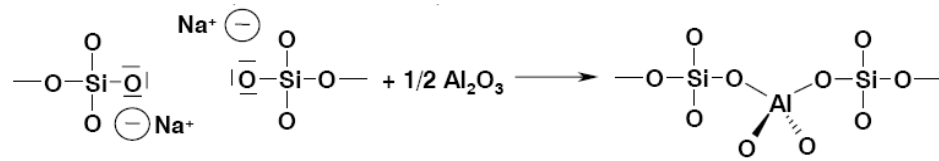


Figure 14: Reaction of  $\text{Al}_2\text{O}_3$  to point of disconnection: Network is closed and stabilized [78]

In the case that the concentration of  $\text{Al}_2\text{O}_3$  is higher than the concentration of the modifier the points of disconnection will be formed as well (see also Figure 13).

A compilation of the different substances and their network functions is displayed in Table 3.

Table 3: Substances classified as network former, network modifier and stabilizer, which can act as network former and modifier

Network former [3]	Network modifier [3], [78]	Stabilizer [78]
$\text{SiO}_2$	$\text{CaO}$	$\text{Al}_2\text{O}_3$
$\text{B}_2\text{O}_3$	$\text{K}_2\text{O}$	$\text{B}_2\text{O}_3$
$\text{P}_2\text{O}_5$	$\text{PbO}$	
$\text{GeO}_2$	$\text{Na}_2\text{O}$	
$\text{As}_2\text{O}_3$	$\text{Li}_2\text{O}$	
$\text{As}_2\text{O}_5$	$\text{Rb}_2\text{O}$	
$\text{Al}_2\text{O}_3$	$\text{CsO}_2$	
	$\text{BaO}$	

#### 4.1.2 Chemical Composition and Physical Characteristics of Glass

Dependent on the field of application, the characteristics of glass are varied by different mixtures of network former, modifier and stabilizer. Pure quartz glass has a very high melting temperature of around  $T_m = 2000 \text{ }^\circ\text{C}$  [1], [4]. The addition of different

components leads to a lower melting temperature and usually to advantages during the following processing since lower temperature levels are required. A reduction of energy demand is the consequence during all production steps.

A large variety of substances which can be added to quartz and a high number of possible resulting mixtures exists. Each mixture with its specific composition has its specific properties. The melting temperature  $T_m$ , the transformation temperature  $T_g$  and other temperatures, different for each glass mixture and important for the manufacturing and forming process, are some of those properties. With regard to the manufacturing process, a unification based on the viscosity was correlated to defined characteristic points respective of temperatures. The viscosity was chosen because that property has the same value at the characteristic points for every single glass composition while changing temperatures. The determination of the viscosimetric fixed points is standardized in different procedures [80], [86]. A summary of the characteristic points is given in Table 4.

Table 4: Viscosities of different characteristic points during manufacturing process of glass [78]

Viscosity $\eta$ [dPa s]	Characteristic points
$10^{2.0}$	Melting temperature to reach a homogeneous molten mass
$10^{4.0}$	Working point
$10^{7.6}$	Softening point
$10^{13.0}$	Annealing point
$10^{14.5}$	Strain point

The technical most relevant glasses are quartz glass, soda-lime glass, borosilicate glass and aluminosilicate glass. Table 5 gives the composition of the main substances of these glasses.

Each of those four glass types is classified as silicate glass due to the fact that the essential element is  $\text{SiO}_2$ . The opportunity of variation the percentage of components leads to different chemical compositions and glasses with different characteristics and properties even in those four types. The result is a multitude of glasses which can be classified in one of the mentioned glass types.

Table 5: Summary of components of technical most relevant glasses

Component	Percentage [mass-%]			
	Quartz glass [1]	Soda-lime glass [1]	Borosilicate glass [1], [87]	Aluminosilicate glass [4], [88]
SiO <sub>2</sub>	≥ 99	69 - 74	70 - 87	53 - 60
CaO		5 - 12	-	0 - 7
B <sub>2</sub> O <sub>3</sub>		-	7 - 15	0 - 8
Na <sub>2</sub> O		12 - 16	0 - 9	0 - 1
K <sub>2</sub> O		12 - 16	0 - 9	≤ 0.5
MgO		0 - 6	-	0 - 3
Al <sub>2</sub> O <sub>3</sub>		0 - 3	0 - 8	14 - 18
BaO		0 - 2	0 - 3	0 - 19

Pure quartz glass is mostly used as refractory material, because of the high melting temperature. The very low coefficient of thermal expansion is one of the main advantages of using glass. It has a very high chemical resistance [4], low electrical conductivity and a high UV transparency. The high costs of manufacturing, a result of the high pureness and the necessity of high temperature, limits the use of quartz glass mostly to astronomical, optical or high temperature applications with maximal operating temperature of  $T_s \sim 1000 \text{ °C}$  [4].

Soda-lime glass is the most used type of commercial glasses. The mixture of that glass leads to a decrease of the melting temperature in a range of  $T_m = 1400 \text{ °C}$  to  $T_m = 1500 \text{ °C}$  and results in large scale continuous melting and high-speed production compared to other glasses. Substances used in the mixture are low cost products, like Na<sub>2</sub>CO<sub>3</sub> or CaCO<sub>3</sub>, so the price of soda-lime can be kept low as well. The main use is in window glasses, beverage containers or even as thermal insulation wool [4]. Soda-lime shows a good chemical durability, but the high coefficient of thermal expansion (CTE) and the resulting possibility of thermal shock make this a bad option for a wide range of applications.

Characterized by high durability against aggressive chemicals, in addition to low CTE, borosilicate is an excellent glass for laboratory and pharmaceutical glassware. Other applications of that glass are kitchen implements or headlamps in the automotive sector.

The hazard of failure caused by thermal shock is very small, as a result of a low CTE. Temperature differences create only small displacements and stresses and do not lead to breakage. Moreover the  $B_2O_3$  acts as a network former in concentrations existing in borosilicate glass. The network is stabilized and the chemical resistance is increased. The manufacturing process is comparable to soda-lime, but the differences in mixture of basic materials leads to higher melting temperatures in the range of  $T_m = 1550\text{ °C}$  to  $T_m = 1600\text{ °C}$  [4].

The special feature of aluminum oxide as a component of glass allows it to act as both a network former and a network modifier. This along with a low amount of alkalis leads to the effect of very high chemical resistance while the coefficient of thermal expansion ranges between soda-lime glass and borosilicate. Aluminosilicate manufactured as glass fibers is used as a component in fiber reinforced plastics, especially E-glass and S-glass. E-glass is a representative of a mixed type of glasses - the alumo-borosilicate glass. This results from the percentage of aluminum oxide of 12 mass-percent to 15 mass-percent and the percentage of boron oxide between 5 mass-percent to 8 mass-percent [88]. S-glass is a special development for the application as a reinforcing material and features a higher fraction of aluminum oxide compared to E-glass and is free of alkaline or boron components [88]. The density is decreased while the hardness and tensile strength of the material are increased. In addition to the application in composite materials, aluminosilicate is also used as flat glass sheet for multimedia displays. The chemical composition gives the potential of hardening the surface and resulting in higher resistance against scratches.

The described types of glasses were used in tests in the context of that thesis and represent the most used and manufactured glasses of industrial interest.

Corresponding to the individual use, glass can be classified as one of three types depending on the application and manufacturing process. This classification is given in Table 6 with possible fields of applications. The most common type is flat glass, resulting in its use as architectural material for windows or glazing of buildings. In the past the float process came to be the most important in manufacturing flat glass. The molten mass is lead over a molten bath of tin. Because of lower density the glass floats on the surface of the tin bath. Smoother surfaces and thinner glass thicknesses can be realized with this manufacturing process. Older production techniques are the milling or the stretching and drawing of molten glass. These are still applied but features lower production capacities and rougher surfaces of the glass. Furthermore, irregularities in thickness can occur.

Table 6: Classification of glass by type of applications and manufacture

Glass type	Application
Flat glass	Windows; architectural glass, automotive applications; mirrors; heat protection
Container glass and glass tubes	Laboratory glassware; pharmaceuticals; lighting technology;
Optical glass	Lenses; prism; mirrors;

Containment glass is mostly produced from molten mass by glassblowing process. A special species of that type of glass are glass tubes, which were formed in a manufacturing process by drawing tubes from the melting in horizontal or vertical direction dependent on procedure used [89] - [91]. The melting flows through a circular slot and is blown up by compressed air to prevent the collapse of round shape of drawn tube [91], [92]. The flow of material and drawing speed defines the wall thickness and the diameter of the glass tube. Due to the production from glass tubes thin glass fibers can be classified as containment glass as well. Containment glass has to comply with special requirements which are contrasted to flat glass or optical glass. So the resistance against internal pressure and axial strain is more important than optical criterions.

Optical glass may have the same chemical composition as flat glass or containment glass. An important characteristic of optical glass is the index of refraction, whose change depending on the temperature and the machinability of the glass. Lenses or prisms are mostly formed from other shapes like round slices or blocks of glass by grinding and cutting.

#### 4.1.3 Chemical Resistance

The high chemical resistance of glass is one of its most outstanding characteristics. Different compositions of glass and interaction of water, acids or bases lead to various chemical reactions on surface, which can modify or destroy the surface or complete glass material. This process is called glass corrosion. Three types of chemical attack are normally differentiated: acid reaction, alkali reaction and hydrolytic reaction.

### Acid Reaction

The exposure of most acids to the surface of glass leads to the separation of alkali or alkali earth ions from the network, insofar as they are solvent in the surrounding acid. The vacant position in network is restocked by hydrogen ions from the acid. These are forming hydroxyl groups at the end of the  $\text{SiO}_2$  network. As a result a gel coat with two phases is formed on the surface. The first phase near the surface consists of leached out glass network with Si-OH groups and water, whereby the second phase is composed mostly from a hydrous solution [93]. The thickness of that coat is in a range of 1 nanometer up to 1 micrometer [94]. The growth of gel coat decelerates chemical reactions due to increased diffusion path and required time.

Two acid solutions are able to dissolve the  $\text{SiO}_2$  network and can destroy glass. These are at first hydrofluoric acid in all concentrations independent from temperature and second phosphoric acid in concentrated form at high temperatures.

### Alkali Reaction

For pH-value  $> 10$  [95] a chemical reaction on the glass surface leads to the destruction of the glass independent of the type and mixture. The present  $\text{OH}^-$  ions are able to crack the Si-O-Si bonds and remove the glass. Also bonds of other network formers like boron or phosphor and even the bonds of network modifier and stabilizer like sodium or aluminum will be destroyed. The complete network is exposed to destruction and is a linear and steady process. Due to the impact of alkali reactions on glass the aging can be accelerated many times. Especially in the case of thin glass fibers this reaction has a clear influence on the time to mechanical resistance [96]. Thus initial failures could occur.

### Hydrolytic Reaction

Hydrolytic reaction on glass surface due to water features the same reaction processes as with acid reaction. The ions of alkali and earth alkali are dissolved from the surface and a gel coat is formed. Different scenarios can arise dependent on the water concentration. If excess water is available the dissolved ions are solved in water, forming alkaline compounds and afterward flushed away to the bulk of the liquid. If water in small amounts is available alkaline compounds will enrich the present water and the pH-value will be increased. In that case an alkaline reaction will begin [97]. Hydrolytic reaction is not limited to only water in larger amounts. Even due to air moisture, a thin water film is formed on the surface of glass. Therefore, the first step is the physical adsorption of

water by the glass surface without any chemical reaction. In the second phase the reaction with alkali ions will occur and a local increase of pH-value is possible which can lead to alkali reaction. That behavior is forced by enhanced air moisture or air moisture which changes often.

Glass corrosion is defined as a reaction between glass and water or acid solutions. Because of dissolving alkali ions the resistance of glass against corrosion can be increased by decreasing the percentage of alkali or alkali earth in the composition of the glass mixture [98]. If that is not possible, the addition of several additives to the composition is possible but in every case these additives have side effects which change the characteristics of the glass in other ways. A safe and easy way is the coating of glass surface to prevent the contact with any water or moisture. The details of different coating processes are described in chapter 4.4.3.

#### 4.1.4 Mechanical Characteristics

An acting load leads to strain in a material. As reaction stress occurs in the material. Thereby different progressions of the stress against the strain can be detected. Ductile materials like most metals and polymer or elastomeric material pass through an elastic range, which is followed by an area of plastic deformation.

Glass as amorphous material shows no plastic deformation. When stress acts on glass it will pass through an elastic range up to the rupture limit [6]. Displacements in that range will return to their original shape. When rupture limit is reached, failure of the material will occur without any plastic deformation.

A typical diagram of a tensile test of solid glass fibers is plotted in Figure 15. In the diagram a linear behavior in elastic range is shown. In that case the displacement is proportional to the acting load. The absence of a plastic range is a typical attribute of brittle material which glass belongs to. Without the supply of heat no plastic deformation is possible. The point of highest acting stress is defined as the tensile strength of glass. Thereby the force is measured and divided by the original cross sectional area. For calculation of resulting strain the measured displacement is divided by the original length.

The elastic range is linear and follows the Hook's law whereby the slope of stress-strain curve indicates the value of Young's modulus  $E$  and can be calculated by formula (3.1). Consequently Young's modulus  $E$  constitutes an absolute term:

$$E = \frac{\sigma}{\varepsilon} \quad (3.1),$$

where  $\sigma$  is the acting stress and  $\varepsilon$  stands for the resulting strain.

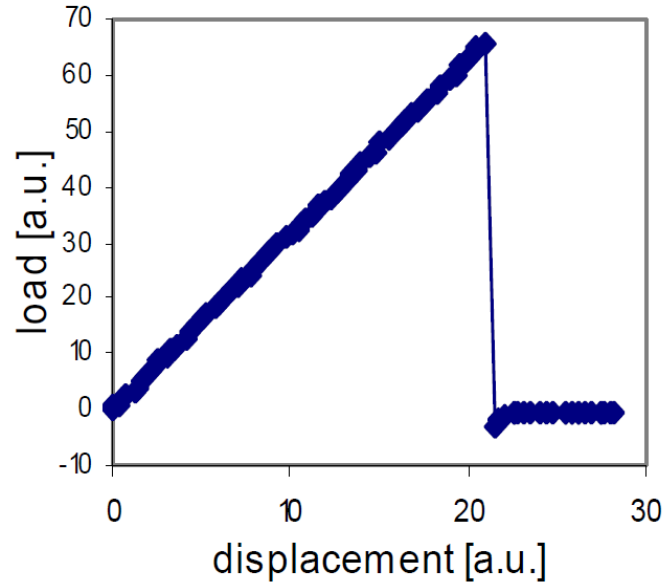


Figure 15: Displacement and load data from a tensile test of solid glass fibers [99]

The theoretical tensile strength of glass can be calculated by equation (3.2) [3], which is a modified form of Griffith criteria:

$$\sigma_{th} = \sqrt{\frac{4 E \gamma}{\pi l_0}} \quad (3.2),$$

where  $\gamma$  = surface energy (fracture energy per surface unit),  $E$  = Young's Modulus,  $l_0$  = atomic distance. Hereby, it is expected that a crack forms new surface with a specific surface energy and the chemical bonds between the atoms has to be fractured. Therefore, the required energy, attached by acting stress, has to be higher than the energy of the chemical bonds. Calculated with averaged values, given in [3]:

$$E = 70000 \text{ MPa}$$

$$\gamma = 0.3 \text{ N m}^{-1}$$

$$l_0 = 1.6 \times 10^{-10} \text{ m}$$



the theoretical tensile strength of glass is about

$$\sigma_{th} \approx 12,900 \text{ MPa.}$$

VARNER followed the same approach that the chemical bonds have to be broken for the formation of new surface [5]. The curve of the acting load is adopted as sinus-shaped. With the assumption of only small strain of the chemical bonds and the validness of HOOK's law the theoretical tensile strength is calculable with equation (3.3) [5]:

$$\sigma_{th} = \sqrt{\frac{E \gamma}{l_0}} \quad (3.3).$$

Thereby,  $l_0$  is defined as atomic distance in equilibrium. With the practical values of  $\gamma$  and  $l_0$  the theoretical tensile strength can be estimated by equation (3.4) [5]:

$$\sigma_{th} \approx \frac{E}{10} \quad (3.4).$$

Hence, the theoretical strength of quartz glass calculated by (3.4) by use of above-named value for Young's modulus should be in the range

$$\sigma_{th} \approx 7,000 \text{ MPa.}$$

Other researchers number the theoretical tensile strength in a range of even about

$$\sigma_{th} \approx 100,000 \text{ MPa [78].}$$

However, the measured values of the tensile strength depend on shape and chemical composition of the tested glass. In most cases a standardized three or four point bending test procedure is carried out as describes e.g. in DIN EN ISO 1288-1 [100] whereby the test samples are standardized as well. The test sample is a small bar which is loaded with an increasing force. The acting force and resulting deformation is measured and the calculated tensile strength is given in literature in the range of

$$\sigma_p = 30 \text{ MPa to } 200 \text{ MPa [3], [78], [101], [102].}$$

An explanation why the measured tensile strength is considerably lower than the theoretical is the existence of microscopic defects on the surface. Such defects originate local stresses inside the component and lead to lower mechanical resistance. An increasing of the mechanical resistance of a component made from glass can be reached by thermal or chemical treatment or downsizing the dimensions of the sample. Tensile tests with solid glass fibers with diameters in the range of  $d_0 = 10 \text{ nm}$  to  $d_0 = 20 \text{ nm}$  resulted in a tensile strength in the range of

$$\sigma_p = 1,000 \text{ MPa to } 5,000 \text{ MPa [78], [88], [103].}$$

The wide range of measured values can be ascribed not only to the different types of glass which are tested but also to different test methods. The tensile strength of optical glass fibers can be determined by adopting the tensile or the bending method. Thereby massive differences can arise in the evaluation of measured data because of the different length of the fiber which is loaded during test [104]. Not only influences of the several test methods but also test conditions can have a massive impact on the tensile strength of glass fibers. Under the influence of liquid nitrogen and a temperature of  $T = -190\text{ }^{\circ}\text{C}$  ( $83\text{ K}$ ) glass fibers are able to withstand stresses up to  $\sigma_p = 8270\text{ MPa}$  [103]. An explanation for that behavior is the absence of air humidity. No dissolving of alkali or alkali earth oxides occurs and corrosion cannot weaken the test sample. Hence, extraordinary high tensile strength can be reached. It can be summarized that only a standardized test procedure will lead to comparable values of the tensile strength of glass fibers. Thereby, the diameter and the length of the test sample as well as the test atmosphere have to be defined.

## 4.2 Griffith Fracture Theory

In 1920 Griffith used glass as model material for the investigation of the influence of surface conditions on materials tensile strength [7]. Tests were done with rods and fibers made from glass and resulted in a strong diameter dependent tensile strength. Also the age of test samples had an influence on the result of the tests. Griffith supposed the decrease of the tensile strength by defects of the surface wherefore stress concentrations can arise directly at crack tips. His fracture theory was based on the statistical principle of minimum potential energy [99]. The following was hypothesized: Energy equilibrium at a crack tip between surface energy and mechanical energy, results from applied stress and strain energy inside the material. If the deformation energy is higher than the energy required for formation of new surfaces the crack will grow and the strain energy will be transformed into fracture energy. Griffith disposed a relationship of critical external stress  $\sigma_c$  to radius of an existing crack  $c_0$ ; the resulting equation is given in (3.5) [7], with  $E$  = Young`s modulus,  $\gamma$  = surface energy and  $c_0$  = the radius of existing defect.

$$\sigma_c = \sqrt{\frac{2 E \gamma}{\pi c_0}} \quad (3.5)$$

For every stress  $\sigma_c$  the radius of the critical fracture dimension  $c_0$  can be calculated and the same in reverse direction. The occurring defects can be formed by aging of samples, whereby the process of aging comprehends handling, transport and storing of glass or

can be resulted by manufacturing process. By decreasing the diameter of samples the statistical probability of defects per defined volume unit will be decreased also. That leads to an increase of measured tensile stress. Furthermore, Griffith supposed a special orientation of surface molecules due to drawing process but was not able to test his theory because no techniques were available at that time.

Later investigations by other researchers demonstrated many different results, yet at the same time, confirmed Griffith's theory. The diagram illustrated in Figure 16 by Rexer [8] confirmed the theory and reflects Griffith's results. Glass fibers with different diameters were tested and their tensile strength increased with decreasing diameter.

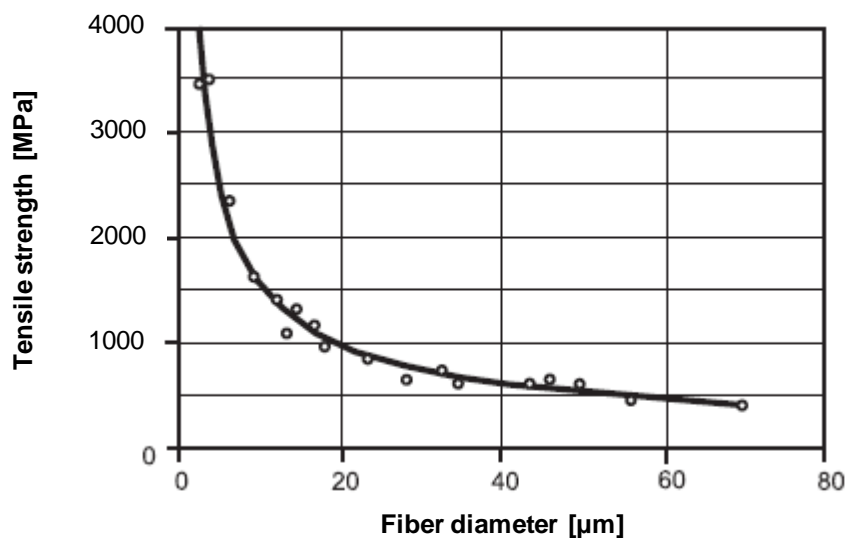


Figure 16: Tensile strength of glass fibers dependent on diameter [8]

Several researchers came to comparable results and conclusions and supported Griffith's theory of dependence between fiber diameter and tensile strength as well as the theory of orientation of surface molecules [105] - [108].

In contrast to them, Otto showed in 1955 that careful and constant production conditions of glass fibers leads to constant tensile strength of test samples, independent on the diameter [109]. He investigated the dependence of drawing temperature and speed on the tensile strength of thin fibers. As result he demonstrated that with higher drawing temperature the tensile strength of solid fibers of the same diameter would be increased. Further tests with the same formation temperature and drawing speed but different diameters showed only small variations of tensile strength of all fibers. Comparable conclusions were done by Stockhorst and Bruckner [110]. Otto argues against the theory

of oriented surface molecules as well [111]. Consequently, the conclusion was drawn that thermal and mechanical history of the material is the influencing factor of material strength [109], [110], [112].

### 4.3 Defects in Glass

The significant reduction of the global strength of the material glass is ascribed to defects [3], [6], [7]. A clear classification of the defects has to be done whereby the formation and the location are regarded as well as the size.

#### 4.3.1 Formation and Definition of Defects

The first opportunity of formation of defects in material is the manufacturing process itself. Faults caused by different influences on molten mass can occur in flat glass as well as in optical or container glass. These faults appear in glass volume and prejudice the surface only in rare cases.

The molten mass of glass is a composition of different raw materials, which are molten at temperatures above  $T_m = 1400$  °C. Variations from desired composition caused by impurities of raw materials can modify the molten mass and produce inhomogeneous zones [113]. Alkaline and earth alkaline materials pit the high melting components and a primary phase is formed by low melting materials followed by liquefying the high melting components. An excessive concentration of high melting materials like chromite, quartzite or corundum could remain as solid particles because of missing time for complete melting in a continuous melting process. Those can form stones and knots as a form of defects in glass. Figure 17 displays examples of stones in different sizes.

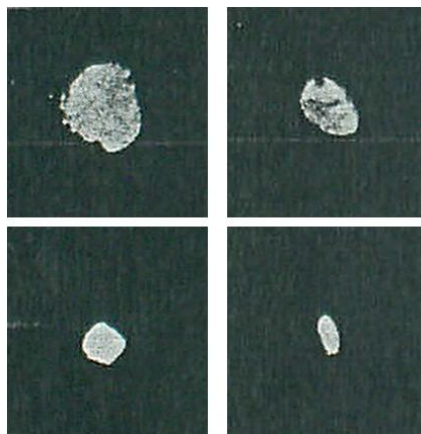


Figure 17: Stones of different sizes in glass: Decreasing sizes of stones from top left to bottom right due to the influence of heat [114]

All solid enclosures in glass are defined as stones independent on their origin. Therefore stones can be enclosures of foreign materials or not liquefied portions of raw materials in small areas, where crystallization of glass batches takes place. A longer time under the effect of heat can decrease the size of the high melting material as displayed in Figure 17. Knots are defined as regional corrosion signs or decompositions in glass [113] which form in most cases round structures with characteristics completely different to the bulk of the glass. In most cases knots are glassy enclosures which feature similar properties than the surrounding glass material. But the viscosity of knots is many times higher than of the glass. Knots originate from stones which decompose due to the influence of alkaline glass components. However, the stones are decomposed the arising area is not mixed completely with surrounding glass [114]. An example is shown in Figure 18. A clear distinction to the defect free area is detectable. Furthermore, variations in optical behavior can be seen as a result of surrounding schlieren. The described types of defects are accompanied by occurring stresses in surrounding glass. The optical and structural requirements cannot be achieved or reduced.

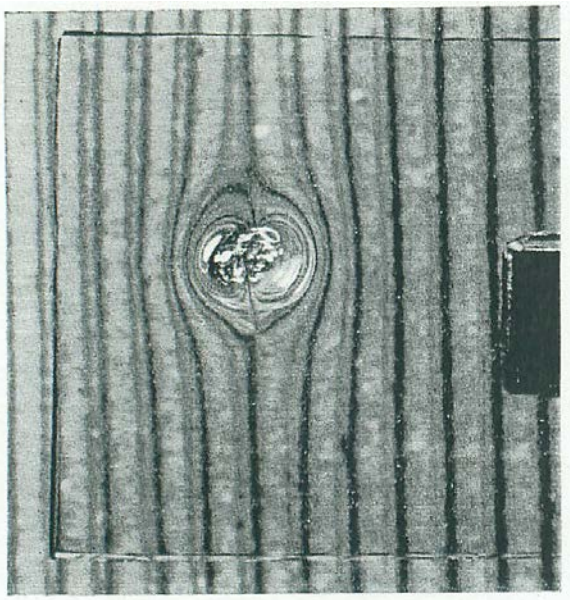


Figure 18: Knot formed in glass as a result of potter's earth, clear distinction to defect free glass, optical variations and formation of schlieren surrounding the knot are detectable; emphasized by corrugated card board [114]

Another type of fault resulting from inhomogeneity of molten mass is defined as schlieren. Thereby, insufficient mixing of the melting is the reason for that type of defect. Stones and knots are mostly surrounded by schlieren which are clearly visible. An

example for the typical appearance of this type of defect is given in Figure 19. The upper series of pictures shows a knot surrounded by schlieren from different angles. The lined paper in the background of picture 2) and 3) eases the visualization. The lower picture series displays schlieren formed directly by inhomogeneous mixed zones of molten mass. Again the same fault is shown from different angles and in picture 5) and 6) lined paper is used to simplify the visualization. Inadequate temperatures, variations of grain of raw materials and undersized concentrations of components producing gas bubbles for mixing the melting are reasons for occurring inhomogeneous zones which lead to schlieren during formation process.

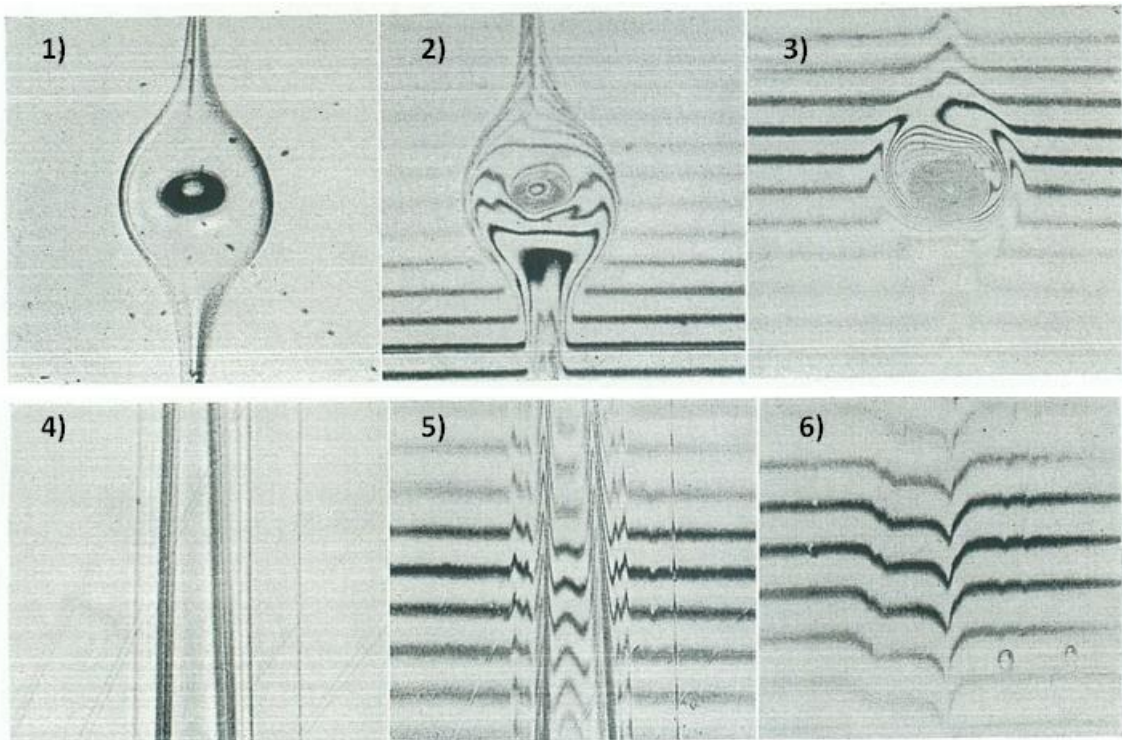


Figure 19: Schlieren in glass as result of inhomogeneous zones, the upper series of pictures displays them around knots of different origins, the lower series represents schlieren in glass formed from inhomogeneous zones in melting [114]

The existence of low concentrations of gas producing components increases the possibility of formation and enclosure of gas bubble in the bulk of glass [113]. The produced gas is necessary to mix the molten mass in an adequate way. That production step is defined as plaining. Mixing by stirrers is not feasible due to very high temperatures. The movement of gas bubbles can be seen in Figure 20. Each picture



displays another gas bubble in a glass sample with different impact on the flow. The resulting flow is detectable by the schlieren. The movement of bubbles should reduce or eliminate such schlieren inside the glass. If the amount of gas, forming bubbles, is too low, the uplift will not be high enough to release all gas from the molten mass.

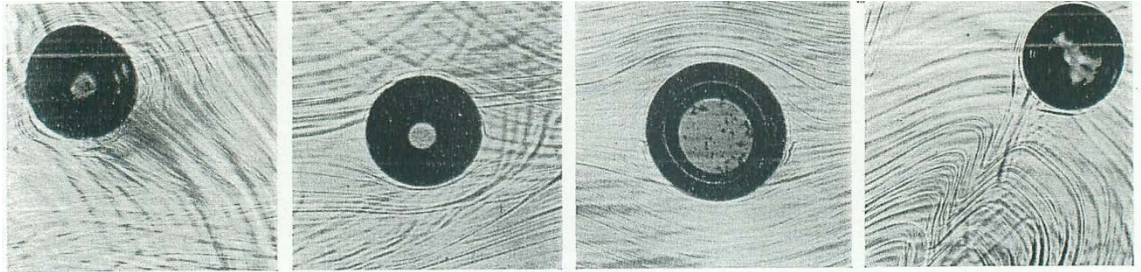


Figure 20: Movement of gas bubbles through schlieren in molten mass, the schlieren should be eliminated by that movement [114]

If the conglomeration of small gas bubbles to bigger ones is hampered with and gas remains in the molten mass. As a result, gas bubbles in frozen material are formed, as demonstrated in Figure 21. This represents flaws in the material, which can only be optical defects but additionally can reduce the durability and mechanical resistance.

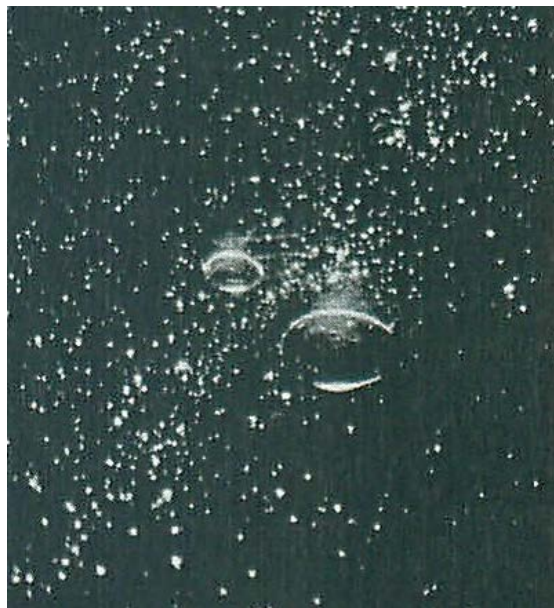


Figure 21: Gas bubbles in solidified material as result of remaining gas in molten glass [114]

Inhomogeneous zones are not only generated by impurities of raw materials or insufficient mixing. The recycling process of glass encourages the insertion of foreign substances like iron, silica or porcelain. The resulting enclosures create different stress levels in glass and can lead to structural failure of the material.

Refractory material used in melting pots is exposed to very high temperatures and small parts of it can detach. On account of the high temperature resistance of these materials the fragments do not liquefy in melting and are able to form enclosures like high melting materials. They are comparable to stones shown in Figure 17. As a general rule, the resulting stress around the enclosures exhibit high values [113] and degrade the mechanical resistance of the material.

Previously described flaws are volume specific defects formed during production process in all types of glass, independent of composition and type of application. Due to the enhancements in quality management and measurement engineering these defects can be minimized but not eliminated. Reasons for structural failures and breakages of glass are not only volume defects but also injuries of surface [97], [115]. Due to the fragility of glass products, especially against bending stress acting on surface defects, the mechanical resilience is decreased significantly by those flaws.

Surface damages can be found on every type of glass and are mostly formed during handling, which comprehends formation process after melting like blow forming, drawing, cutting as well as packing and transportation. The high temperatures of production process during melting and drawing glass ensure that the surface can be described as nearly defect free. Small defects are created during cutting of glass in manageable pieces or in finished shaping. The most executed form of cutting is the marking out with a diamond added plate. At this mark the glass can be broken easily. This technique does not cause a smooth breaking edge. Instead, it creates small defects like cracks and a rough breakage surface. In addition, it creates stresses inside of the edge and can generate breakouts at the breaking edge. A possible consequence can be the decrease of pressure resistance of containment glass or glass tubes at internal pressure load. Also small scratches or hacks in different sizes caused by contact with metal or other glass surfaces are added to that group of defects. Therefore, the smallest defects are not visible to the naked eye.

In general such defects are classified as microscopic and macroscopic defects. Microscopic defects are not visible and detectable without any optical tool. Visualization can be realized by light microscope or scanning electron microscope (SEM). Macroscopic defects can be detected without optical tools but in some cases a dark



background is necessary [6]. A classification in five different classes is given in Table 7 whereby no concrete sizing is given in literature.

Table 7: Classification of defects dependent on size and corresponding option of detection without optical tool according to [6]

Type of defect	Option of detection
extreme fine scratches	undetectable with naked eye and daylight, not noticeable by hand
fine scratches	detectable against a dark background with naked eye
slightly scars	against a dark background clearly detectable without any tool, noticeable by hand
severe scars	detectable from every perspective, also without dark background
areal damages	flock of scars of slight up to severe scratches, thus whitish discoloration

At crack tip, acting stress can rise to a multiple peak. Consequently, stress arises at that point. The result can be a mechanical collapse at pressure load. The reason for the decrease in mechanical resistance is not only the induced stress or stress peaks at crack tips but also stress corrosion generated by air moisture. Especially on new surfaces or in cracks and scratches, glass corrosion leads to further structural degradation. If stress is added and a scratch is increased, the corrosion supports the advance of the breakage. Under non-load conditions glass corrosion leads to a rounding of the crack tip and is able to decrease the mechanical sensibility at this point [97] by acting alkaline reaction: therefore the crack has to be big enough that water can intrude which leads to a hydrolytic reaction. Local increase of pH-value leads to alkaline reactions. The precise characterization of mechanism of water attack on glass surface is described in chapter 4.1.3.

Defects and flaws in the bulk of the glass lead to strains and stresses inside of the material. Due to the enhancements in production the probability of such big scaled defects has decreased a lot. However, the existence of small sized volume defects cannot be excluded. Obviously the prevention of surface defects is technically more

complex. Hence, the mechanical resilience of the material glass is a surface property [97].

Not only micro scratches but also cracks on the surface or in the walls of the hollow fibers can decrease the pressure resistance of small hollow glass fibers, especially with the aspect of their use as pressure vessel. Form errors are able to induce stress peaks in the material as well. The preferred form for pressure vessels is a round shape without any edges which is necessary to reach highest pressure resistance. Therefore deviations from that form, even a small displacement to an elliptical form caused by undesired forces during the manufacturing process, can decrease the resistance by forming irregular distribution of stress with higher stresses at one point. The changeover from wall to bottom is vitally important too. Here sharp edges or tips have to be avoided as in the wall because of possible stress peaks.

#### **4.3.2 Detection of Defects**

The detection of defects and flaws is dependent on the size (microscopic or macroscopic class of defects).

Macroscopic defects can be detected by the naked eye. Form and location are able to be determined in this way. The interaction of macroscopic flaws in the bulk of the glass or on the glass surface to surrounding material becomes more visible under light microscope.

Detection of microscopic defects in the bulk or on surface is more difficult and requires optical tools. The first determination can be done by light microscope with magnifications of up to 100 times. Use of transmitted-light or reflected light microscope is possible. The use of polarized light or an immersion liquid can be helpful to visualize stresses or schlieren inside the glass. For smaller defects the use of examination methods with higher resolution are necessary. Established procedures are the scanning electron microscopy (SEM) or the atomic force microscopy (AFM).

The SEM uses a focused electron ray to determine the surface of a test sample. This ray is generated at a hot cathode or a field emission gun and accelerated in an electric field. The surface of the sample is sensed in form of a raster scan with a wideness of the focus in the range of 1 nm to 20 nm [116]. Line by line the sample is scanned and the interactions between electron ray and atoms of surface are evaluated. The maximal magnification is thereby limited at one million times [117].

The AFM applies a sharp tip to determine the surface of a sample. Thereby the forces acting on the surface of the specimen are used to create a figure of it [118]. The tip is fixed at the end of a very small flat spring, the cantilever. Similar to the SEM the surface is scanned in a raster, whereby the flat spring is bent in different intensities dependent on the consistency of the sample [118]. These displacements are detected by optical sensors and reproduce the interaction between the tip and the sample surface. Here different methods of measurements can be applied. The first is the contact method, where the tip is in direct contact with the sample. The second method is the non-contact mode, where the spring is stimulated to swing by piezo elements, so that the spring is swinging in resonance frequency. Interactions and forces between tip and surface change the frequency and its difference is measured and evaluated. The detection of defects of thin hollow glass fibers as subject of this work posed different problems wherefore that method of detection discovered as not suitable for thin hollow glass fibers. The tip slipped off the sample at contact scanning method due to the roundness and no interactions between tip and surface are measurable because of too high distance between tip and surface. A definable rotation of the sample necessary to scan the whole surface was difficult because of the small size of samples.

The usage of SEM to determine the structure is more feasible. A big advantage of SEM against AFM is not only the possibility of optical investigations of the determined surface. Also chemical analysis can be done by using the energy dispersive X-ray spectroscopy (EDS). This method makes use of the electron beam emitted by the SEM. The test sample is bombarded by electrons, which separates electrons from the inner atomic shell. The arising void is restocked by an electron of the outer shells. Energy differences are emitted in form of x-rays which is characteristic for every element and can be detected. In principle, a high number of elements can be localized [119]. Scanning the surface in a raster creates an image with local element distributions. The bombardment with electrons produces characteristic X-ray spectra with characteristic peaks for every element.

In addition to the characteristic peaks a continuous spectrum is also created and defined as background. The intensity of the background decreases by increasing the X-ray energy. A qualitative analysis can be easily done. By identification of different peaks characteristic of every element, a statement about the composition can be realized. Though, the results of EDS determinations are fast possibilities for first estimations of composition. More precise determinations are considerably more time-consuming.

#### 4.4 Prevention and Removing of Defects in Glass

The presence of defects and flaws in the material and on its surface can have certain kinds of effects on the strength of the material and, finally, on the mechanical resistance of the hollow glass fibers. The flaws in the material create local stress because of inhomogeneous stress distribution. Origins of such flaws can be inhomogeneous parts of the melting and can be prevented by continuous enhanced measurement engineering. When flaws are detected in the glass, knowledge of numerous determinations gives information about the reasons and origins. Thus, changes in mixture or prevention of impurities by e.g. control of raw materials can reduce those flaws to a minimum. But also stress, caused by a high cooling rate after manufacturing, is able to form peaks and irregular stress distribution in glass and is a reason for failures as well. This stress can be reduced by thermal treatments of the glass and will be discussed in detail.

The surface of glass not only controls the chemical durability and the optical quality of the glass but also the tensile strength of the material [129]. The preventing or removing of defects on the surface consequently is matter of special importance. Especially in the field of optical glasses, mechanical methods of surface treatment are common. Since a smooth surface is necessary to reduce possible refraction and diffusion of light, the surface can be treated in three steps with different rates of removing material. A distinction is made between grinding, lapping and polishing; every step with a lower rate of material removing. The application of this method on thin hollow glass fibers is not possible because even polishing with the finest rate of material removing and equalization of the surface, leaves microscopic scratches on the surface which can be opened at pressure load and leads to an initial break of the hollow fiber. Accordingly, these methods are not advanced below. Instead, the attention is focused on thermal, chemical and coating processes of surface treatment.

##### 4.4.1 Thermal Treatment of Glass

###### Flame Polishing

Flame-polished surfaces of glass are juvenile. Thus, freshly formed surfaces after heating up the material above transformation temperature  $T_g$  and frozen in that state [94] can be seen as defects free. But directly after forming chemical reactions on the surface of glass with components of air and moisture take place. Fire-polishing is used to improve the quality of glass surfaces after a step of manufacturing like forming or cutting. The formation of glass can be done by pressing or blowing. During forming the contact

with a form tool like plunger leads to different cooling rates of the surface and the volume of the formed glass article. Due to that contact, different surface defects can be caused not only by thermal terms but also by the roughness of form tools. The damaged surface has to be treated in an adequate way to get an optical and mechanical perfect surface. A new selective heating above  $T_g$  leads to a melting of the outer layer of glass and removal of surface defects. An important factor is a minimum of inserted heat to avoid the softening and deformation of the whole item. In that case sustainable damaging or destruction is possible.

Cutting of glass creates not only a straight scratch where the glass can be broken easily but also small cracks as described above. The breakage edges can be treated with flame polishing as well. Defects are molten off and coalesce to a smooth surface. Sharp edges are avoided but mean an additional amount of work. An alternative method of cutting is use of a laser. Glasses cut in that way feature bending strength increased up to 2.5 times [6]. Mechanical breakage after scratching is no longer necessary by using that method. The laser inserts energy to the glass which is absorbed by surface layer. The originating heat leads to compressive stress and material fatigue. The following cooling of material by ambient air or applied cooling solvent forms tensile stress and leads to an initial break along the line of the laser. The formed cutting edges are smooth and free of defects. This cutting method requires different types of laser for the different types of glass. Thus, the implementation in manufacturing processes is confined.

Flame polishing of hollow glass fibers holds problems in usage. Determinations with light microscope show obvious defects and rough breakages at the open end of the single hollow fiber. Flame polishing of even breakouts and micro cracks would increase the pressure resistance. Also micro defects on the nanoscale on outer surface due to the contact with other fibers or drawing tools could be treated and minimized. Due to the small wall thicknesses the inserting of a small amount of heat only to melt up the surface layer is very difficult. The conduction of heat in that small size is fast enough to heat the complete material. As a result of continuous heating and occurring capillary effect the thin tube collapses.

### **Annealing**

The manufacture of different materials needs high temperature. At this juncture the heat dissipation after final forming plays an important role for mechanical properties of the item. False cooling rate entails stress inside the material. Inhomogeneous stress distribution on application of force is able to form stress peaks and initiate a breakage in

the material. Especially in amorphous and brittle materials like glass thermo-mechanical stresses are dangerous and reduces the resistance against force effects. The observance of the right cooling rate is very important and differs dependent on composition of the glass. Here the critical temperature range is around the transition temperature  $T_g$  and has to be passed through slowly to avoid stress in glass. This process used for glass is called annealing. Glass which is not annealed can break at relatively small mechanical impacts or thermal changes. However, stress is formed in glass because of too high cooling rate and annealing is a possible treatment to remove the stress. Therefore, the item has to be heated up to the annealing point which is defined as temperature where glass reaches a viscosity of  $\eta = 10^{13}$  dPa s. That critical value of viscosity is also defined as transition point between super cooled liquid and glass. The material is softened enough to relax thermal caused stress but still features a sufficient solid to resist any deformations. The period of time necessary to remove all stress depends on the composition and thickness of the treated glass. Then, the glass is slowly cooled down with predefined rate below the strain point, defined as temperature where the glass features a viscosity of  $\eta = 10^{14.5}$  dPa s. Further cooling to room temperature can be done faster and secure from formation of stress. The relaxing at annealing point is done in several minutes, nevertheless, an overriding of this temperature for a longer time can lead to slight deformations; at strain point annealing can be performed as well and the danger of deformation is much less but it will take several hours [130]. Hence, the annealing is often done at temperatures between strain and annealing point to minimize the hazard of deformation and shorten the time period necessary. Annealed glass will break into large, sharp shards when failure occurs.

### **Tempering**

Annealing glasses eliminate thermal stresses in glasses and leads to higher mechanical resistance but surface defects still remain. The tempering of glass, also called toughening, is also a thermal treatment and quite similar to annealing in first steps. Glass is quickly and uniformly heated up to temperatures above the annealing point but below the softening point [6] to eliminate any thermal stress inside the glass. In contrast to annealing, inner thermal stress has to dissipate as fast as possible, so temperatures are chosen where a viscosity of  $\eta = 10^9$  dPa s [95] is reached in glass. Due to short time and still high enough viscosity stresses are annealed very quickly and deformations are avoided. At this juncture, an override of the annealing point is acceptable to reach fast relaxing of the glass because after relaxing a fast cooling with cold air will generate a

solidification of the outer layer of the glass before any deformations can occur. The delayed cooling of the core leads to characteristic stress distribution, whereby the outer layer interferes with the contraction of the core during cooling. Consequently, tempering is a thermal treatment, where at first unwanted thermal stresses are eliminated and afterwards a specific progress of stress is formed in glass, as shown in Figure 22.

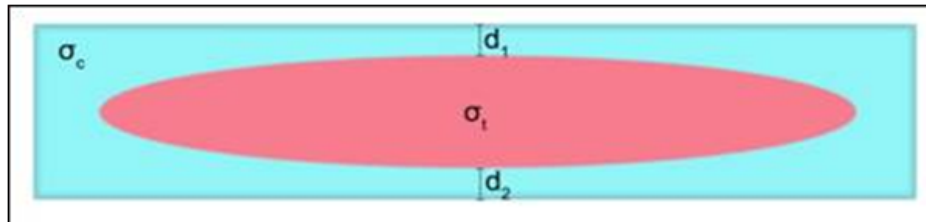


Figure 22: Schematic progress of stress in a tempered glass (according to [6])

The outer layer is forced by compressive stress  $\sigma_c$  with a specific layer thickness  $d = d_1 = d_2$  and the inner layer by tensile stress  $\sigma_t$ . The compression of outer layer leads to grouting under pressure of potential surface defects. Zones of stress are evenly distributed over the whole thickness. Thus, with increasing thickness of glass the thickness of zone of compressive stress increases as well. Without any acting load on the compression zone features the same thickness on each side of the glass. If a load is acting on the glass, the zone of tensile stress moves in direction of force to surface. A schematic illustration of that process is given in Figure 23.

The movement of zone of tensile stress leads to a changing of the layer thicknesses of the compression zone. If the acting load is high enough and the layer thickness  $d_2$  reaches  $d_2 = 0$  the failure of the glass will be the consequence. Tensile stress is applied to the surface and will open defects on it. Stress peaks can be formed and the break is initiated. Thereby, a breakage in small, not sharp-edged pieces will eventuate caused by the high acting stresses, as shown in Figure 24. For that reason tempered glass is used for applications where thermal resistance and high solidity is required, such as side windows in automobiles, architectural glasses with structural load, frameless glass doors or kitchen utensils.

The process of tempering is not applicable to glass of every thickness. Glasses with a thickness less than 3 millimeter [6] are tempered by chemical treatment for that reason.

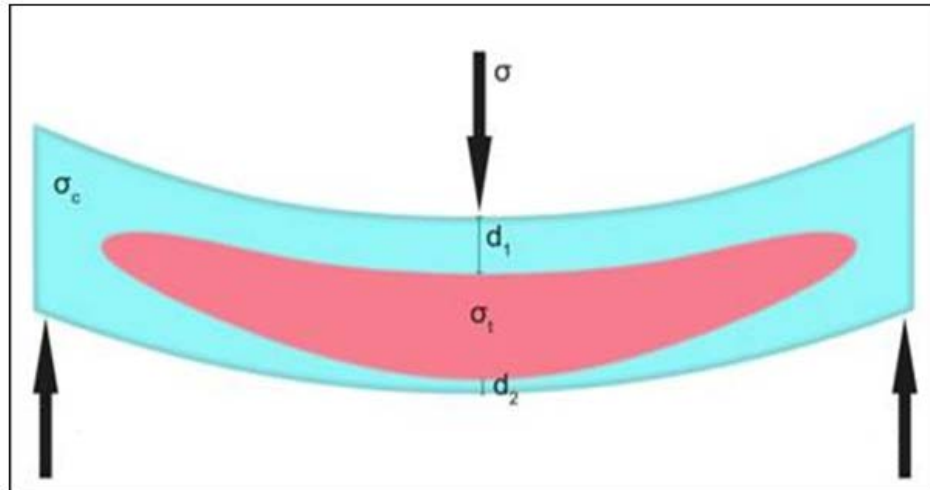


Figure 23: Load acting on tempered glass causing bending and movement of different zones of stress by interaction with bending force (according to [6])



Figure 24: Typical fracture appearance of tempered glass [131]

With regard for thin hollow glass fibers with wall thicknesses in the range of  $s = 10 \mu\text{m}$  to  $s = 100 \mu\text{m}$  thermal tempering can be suspended as adequate method for increase of the mechanical properties. The need of high percentages of sodium in glass for chemical tempering, set small limits for that method and is only adaptable satisfactory to soda lime glass [95]. A different thermal method can be established at manufacturing process of fibers. The advantage of different properties of each type of glass is taken and tubes of different CTE stick into each other and are fused in the drawing process. During cooling



the different shrinking of the materials leads to compressive or tensile stress of inner and outer surface. If the inner material has lower CTE than the outer material, then the inner surface of hollow fiber will be forced by compressive stress while outer surface is forced by tensile stress. If the placement of the materials is done in an opposite way the initial load of the surfaces will also be reversed. The use of three layer fibers produced from three tubes sticking into each other will lead to an initial load of outer and inner surface when inner and outer material has lower CTE than the material in the middle. Thus, a grouting under pressure of surface defects at the nanoscale on inner and outer surface can be reached and may lead to an increasing of pressure resistance. The measurement of CTE is a standardized procedure [132]; hence, even small differences are able to impact the result of this method.

#### 4.4.2 Chemical Treatment

##### Chemical Tempering

Chemical toughening benefits better results and advantages against the thermal toughening process by having glass of thicknesses less than 3 millimeter [6]. As against thermal tempering, the compression stress is created by changing the composition of the surface layer. During the process an exchange of sodium ions against potassium ions takes place, whereby the glass is immersed in a bath of molten potassium nitrate with temperatures of about  $\Delta T = 100 \text{ K}$  below  $T_g$ . Due to the bigger size of 30 % [95] of potassium ions the required space is higher and compression stress is formed in the diffusion layer. Chemical tempering is able to create compression stresses in the field of  $\sigma_{\text{comp}} = 400 \text{ MPa}$  to  $\sigma_{\text{comp}} = 500 \text{ MPa}$ , which has been demonstrated by technical tests [95]. This method of increasing the mechanical resilience of glass surfaces is applied for chemical glasses, break-proofed spectacle-lenses or lightweight glasses in aircraft production. That method is also adapted to glass of complex shapes [133], but the success is critical if glass with only a small percentage of sodium is treated with the above-mentioned method.

##### Etching

The damage of the surfaces reduces the tensile strength of glass by a multiple, whereby pristine glass without any fault exhibits a very high strength [130]. Beside thermal treatments like flame polishing the creation of such surfaces is possible by using the method of etching. Damaged surfaces are etched with hydrofluoric acid (HF) to remove the defects. HF has the unique characteristic in the class of acids that attacks the  $\text{SiO}_2$

network. The influence of other acid leads to an exchange of alkali ions from the glass with hydrogen ions from the acid. A gel coat is formed with hydroxyl groups comparable to the influence of water. By the attack of the  $\text{SiO}_2$  network by HF the damaged outer layer of the surface is completely removed from the glass and leads to a juvenile surface. The hazard of etched surfaces is the high sensitivity to new damages by handling.

#### 4.4.3 Coating of Surfaces

Coating of glass can be done in different ways. A differentiation between optical or mechanical reasons has to be done. Optical coatings are applied for antireflection, heat insulation or UV protection. These coatings are relevant to increase the pressure resistance of thin hollow glass fibers.

The protection of the surface from defects and lubrication are the primary purposes of coatings. The application of a cover on the surface also can be used to heal existing defects and to change the surface properties [134]. An effective way of coating is to spray a dispersion of organic components in water directly after drawing process on the surface of the fibers, whereby the organic component can be e.g. polyacrylate. The heat of the glass leads to vaporization of the water and an organic coat forms on the surface. Especially in the case of glass fibers and yarns the process of applying a coating has to be done almost immediately after the formation because of their abrasiveness [135].

The deposition of inorganic non-metallic layers on the glass surface improves mechanical characteristics as well as optical and chemical characteristics, which is called the sol-gel process. A dispersion of organic and inorganic materials is deposited on the glass surface to create a homogeneous phase. Afterward the hardening by heating up to temperatures between  $T_H = 400\text{ °C}$  and  $T_H = 550\text{ °C}$  is initiated. This forms a thin layer with a thickness of up to 1 micrometer by using inorganic brine as dispersion [94]. A usage of hybrid polymer as dispersion features the advantages of lower hardening temperatures of only about  $T_H = 150\text{ °C}$  or UV-light but leads to thicker layer up to 20 micrometer [94]. The adaption of CTE of substrate material (glass) and layer has to be considered. Thickness of layer affects the time of hardening and can lead to thermal stresses in material. Experimental tests showed that even a very thin layer of 0.2 micrometer increases the mechanical resistance of glass [95].

Another feasible method of glass coating is the chemical vapor deposition process (CVD-process). Selected coatings with highest pureness are manageable. So called precursors in gaseous phase flow over the surface of a substrate by dint of inert carrier

gas; near or directly on the surface, chemical reactions at specific temperatures take place. As a result of that reaction, the final product is formed and creates a thin layer on the surface of substrate. The creation of gaseous phase requires a heating of the precursors, thus the whole process setup has to be heated up to avoid condensation of them on colder parts.

The process can be divided into several single steps [95]:

1. Creating a gaseous phase of precursors;
2. Transport to substrate surface by carrier gas;
3. Adsorption;
4. Chemical reaction and decomposition of adsorbed components;
5. Formation of layer and desorption of unwanted reaction products;
6. Cooling.

Coating with CVD-process is deployed e.g. in hot end coating of containment glass, the formed layer fills up micro cracks and increases the resistance and solidity of glass components.

The atomic layer deposition process (ALD) as modifies CVD-method can be used to form coatings on glass surfaces as well. Contrary to the conventional CVD, in this connection precursors are lead separately into the heated reaction chamber. Between the single precursors, either a purging by inert gas or evacuating of reaction chamber ensures the outlet of non-reacted gases. Thus, the single reaction steps are separated from each other. A two-component process can be summarized as followed:

1. Discharge of the first precursor and limited chemical reaction;
2. Purging with inert gas or evacuation to remove non reacted components from step 1;
3. Discharge of second precursor with limited chemical reaction;
4. Purging with inert gas or evacuation to remove not reacted components from step 3.

The result of these steps is one process cycle which can be repeated several times. Dependent on the number of process cycles, the thickness of coating layer varies. That method produces accurate and conformal layer even at nanoscale [136]. The thin layer film covers the surface of the treated glass and cracks are partially or completely filled up. A schematic illustration is given in the next figure.



Figure 25: Schematic illustration of ALD coated glass, the surface of glass (bright region) is covered by nanoscale defects, ALD coating (dark region) fills the cracks completely or partially [136]

Since optical perfect surface features invisible micro defects, which decreases the mechanical resistance, with the coating jacket the crack tip will be smoothed and the radius is decreased. Additionally, the potential of formation of local stress peaks is decreased. Experimental tests were carried out and showed increase of tensile strength between 45.7 % up to 89.3 % [136], [137] by coating with ALD before cutting. If glass is cut first before coating, then the tensile strength can be increased again about 9 % [137]. In that case the ALD film not only heals the surface flaws but also heals the cracks caused by cutting in a conventional manner.

The described methods and processes of coating surfaces are feasible to form coating layers on different shapes and with different consequences to the material characteristics. These methods are feasible not only for flat glass but also for round or complex shapes. In view of pressure resistance of hollow glass fibers, the increase of mechanical resistance caused by reducing or preventing surface defects is the main advantage. Also layers with sun protective or heat insulating effects are feasible, which are not described as precisely.

Further coating processes are classified as physical vapor deposition. The layer material is also vaporized and is comparable to CVD, but on the surface no reaction takes place. The vaporized material forms a homogeneous layer caused by condensation. That process is adaptable to flat glass; in contrast the coating of complex or round shapes is not possible. That is why the PVD is not adaptive to glass fibers.

#### 4.5 Weibull Distribution

The knowledge about defects and their effects on glass is very important insofar as the former leads to a minimization of the latter. Nevertheless, defects can occur in glass or on its surface and determinations have to be evaluated in an adequate way. The Weibull distribution has proven to be the most suitable method of evaluation and is the standard tool in the glass manufacturing industry in statistical analysis.

The Weibull distribution is a statistical instrument which can be used for description of failure frequency of technical components. Especially in case of a wide spread of measured results due to different defect sizes and distribution in the test samples it is a meaningful evaluation. For different investigations the parameters can be changed, e.g. in case of durability of lamps the time  $t$  can be the main parameter. Thus, the general form of Weibull distribution function is given in equation (3.6) [99], [138]:

$$F(t) = 1 - e^{-\left(\frac{t-t_0}{T-t_0}\right)^b} \quad (3.6).$$

With  $F(t)$  as failure probability dependent on time  $t$ ,  $t_0$  as the threshold time, which is the minimum time below no failure occurs, and the characteristic time  $T$  with a failure probability of 63.2 %.

The pressure, during internal pressure load, when the structural failure of one hollow glass fiber takes place, is the main parameter and represents the property of the component which has to be determined for the evaluation. The resulting form of the Weibull function is given in equation (3.7).

$$F_B = 1 - e^{-\left(\frac{p-p_0}{P-p_0}\right)^b} \quad (3.7)$$

Here  $F_B$  is the probability of bursting (failure probability),  $p$  is the individual pressure at bursting and  $p_0$  is again the threshold parameter. The characteristic pressure with a probability of bursting of 63.2 % is given by  $P$ . The form parameter  $b$  is a dimension of the spreading of measured burst pressures and for the form of the failure density [139].

The function given in equation (3.6) and (3.7) are called the three-parametrical Weibull distribution. The complexity of determination of the single parameters from the measured values is the mainly shortcoming. A simplification of the function where the threshold parameter adjusts to zero is often used. In case of burst pressures it means that  $p_0 = 0$  which is acceptable when fibers with pressures of failure break before testing [140], [141]. The resulting two-parametrical Weibull function is given in equation (3.8) [138]:

$$F_B = 1 - e^{-\left(\frac{p}{P}\right)^b} \quad (3.8).$$

The usage of the two-parametrical Weibull distribution simplifies the related probability density function given in (3.9) [138]:

$$f(p) = b \frac{p^{b-1}}{P^b} e^{-\left(\frac{p}{P}\right)^b} \quad (3.9).$$

The form of graphic representation of the probability density function calculated with formula (3.9) against the pressure is dependent on the form parameter and the number of tested samples. With a sample size of  $N \geq 30$  the calculated density function tend to Gaussian distribution [139].

Taking the logarithms of (3.8) twice and rearrange the result in the form of equation (3.10) the Weibull diagram can be constructed.

$$\ln\left(\ln\left(\frac{1}{1-F_B}\right)\right) = b \ln p - b \ln P \quad (3.10)$$

In Weibull diagram the double logarithmic function  $\ln(\ln(1/(1-F_B)))$  is the value of the ordinate and the value of the abscissa is given by  $\ln p$ . The resulting graph in the diagram describes approximately a straight line with a slope of  $b$ . From here, a dependency between the parameters is apparent and an estimation of one parameter has to be done. Hence, an empiric formula was proposed to calculate the cumulative failure probability of the  $i$  th burst pressure. That means the measured values of the single burst pressures have to be sorted ascending and the failure probability for every single value can be calculated as a first approximation by equation (3.11) [99], [142].

$$F_i = \frac{i-0.5}{N} \quad (3.11)$$

$F_i$  is the failure probability from every single burst pressure,  $i$  stands for the individual number of the single pressure values sorted ascending and  $N$  is the total number of all tests in the determined series. At this juncture, equation 3.8 can be used for sample amounts of  $N \leq 50$ . The resulting Weibull diagram for one random species of fibers is given in Figure 26.

A double logarithmic function of the failure probability is plotted against the logarithmic burst pressures measured for the investigated series. The logarithmic functions of the axes were used to smooth the graph into a straight line. The form parameter, definable from slope of the straight line in Figure 26, can be used to calculate the failure probability  $F$  with equation (3.8) and the illustration of the developing of failure probability can be plotted. An example is given in Figure 27 according to Weibull diagram given in Figure 26.

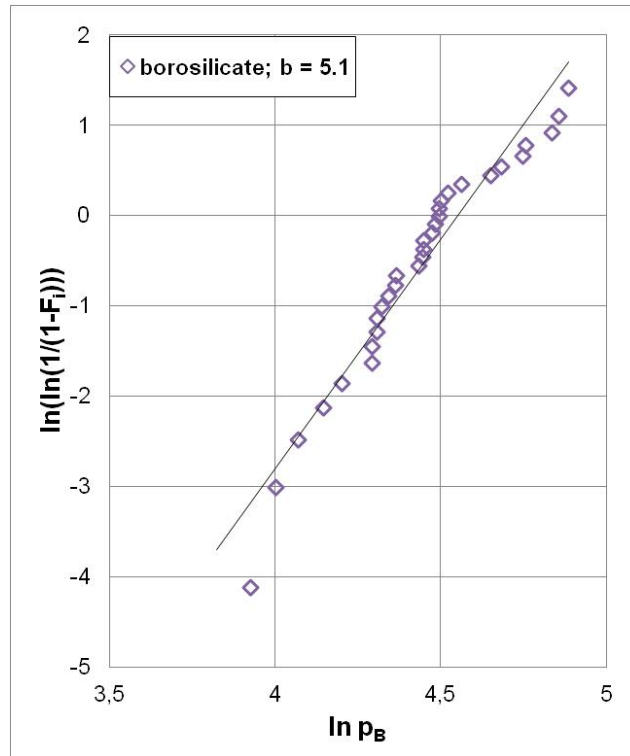


Figure 26: Constructed Weibull diagram for one species of hollow borosilicate 3.3 fibers; ( $d_o = 400 \mu\text{m}$ ,  $d_i = 300 \mu\text{m}$ ;  $s = 50 \mu\text{m}$ ), definable form parameter  $b = 5.1$

The value of the characteristic pressure  $P = 89.4 \text{ MPa}$  given in the diagram represents the pressure at a failure probability of  $F = 63.2 \%$ . It represents the inflection point of the curve of failure probability. The additionally plotted step function illustrates the ideal case, where every test sample fails at internal pressure  $p = P$  and the value of form parameter  $b$  would be infinite.

The minimum number of test samples is not required. Due to the fact of the convergence to the Gaussian distribution a minimum number of  $N \geq 30$  was defined for the investigations in the context of this thesis. However, a smaller sample size is possible as well the precision of the distribution increases with increasing number of samples.

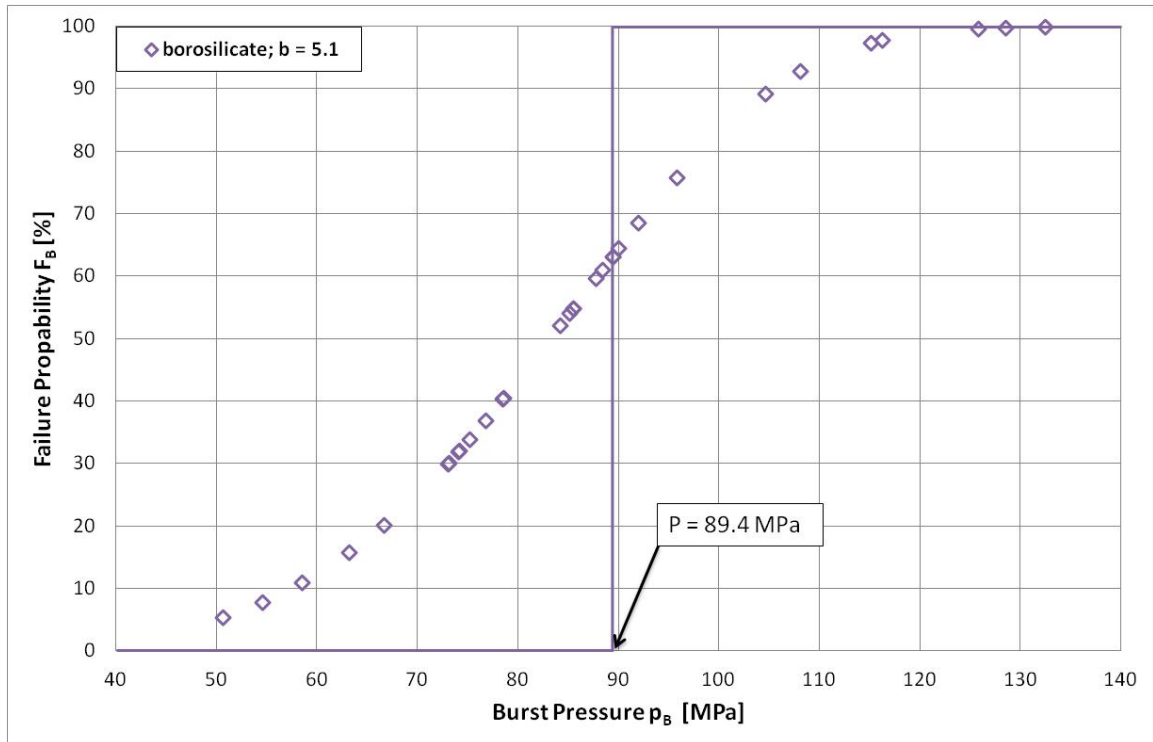


Figure 27: Developing of failure probability of borosilicate 3.3 fibers ( $d_o = 400 \mu\text{m}$ ,  $d_i = 300 \mu\text{m}$ ;  $s = 50 \mu\text{m}$ ), characteristic pressure  $P = 89.4$  MPa; step function represents ideal case of failure of all samples at one test pressure



## 5 Experimental

Test series of single hollow glass fibers were carried out to determine the influences of different glass materials and geometric parameters on the burst pressure. The burst pressure represents the most important property of hollow glass fibers concerning the investigation and evaluation of the pressure resistance. A quality check of the test samples before testing showed the existence of defects of different sizes and origins. Consequently, the analysis of measured data with Weibull statistics was done.

### 5.1 Experimental Setup

The tests were carried out in a laboratory at the Federal Institute for Materials Research and Testing (BAM) in Berlin, Germany, where special facilities for safe testing and handling of flammable gases are located.

The investigation of pressure resistance of containment glass is regulated by DIN 52320 [97], [143] and DIN EN ISO 7458 [144]. Test samples are first pressurized with water in a non-destructive procedure up to a pre-defined internal pressure with specified ratio of pressure increase. At a pre-defined internal pressure a dwell time of one minute is required. The number of samples which fail before the end of the test procedure is recorded. A second destructive test is required to fulfill the standards. The internal pressure is increased in steps of  $\Delta p = 0.1$  MPa until a failure of test sample eventuates. A dwell time of one minute is linked to every step of pressure increase.

These test procedures are not adaptable directly to thin hollow fibers made from glass because of the use of water as pressurizing medium. After non-destructive tests, water would remain in the hollow fibers; further tests with gases would be complicated or impossible. Hence, the test procedures were varied and a setup, suitable to carry out tests of resistance against internal pressure of hollow glass fibers with gases, was developed and installed.

The setup was located in a safety room, which achieves specific requirements for safe handling of compressed and flammable gases and was separated from the control room with a flame and explosion resistant door. Both rooms were equipped with gas sensors connected to a gas alert system which activates the alert and an automatic ventilation system, if a hydrogen concentration of 20 % of the lower explosion limit is measured. During the performance of the tests the entrance was permitted. The operating board was located in bordering control room and contained pilot valves, operating elements, control systems and measurement instruments. Gas cylinders with different gases were

located in a safety cupboard in the control room as well. A schematic figure of test setup is shown in Figure 28.

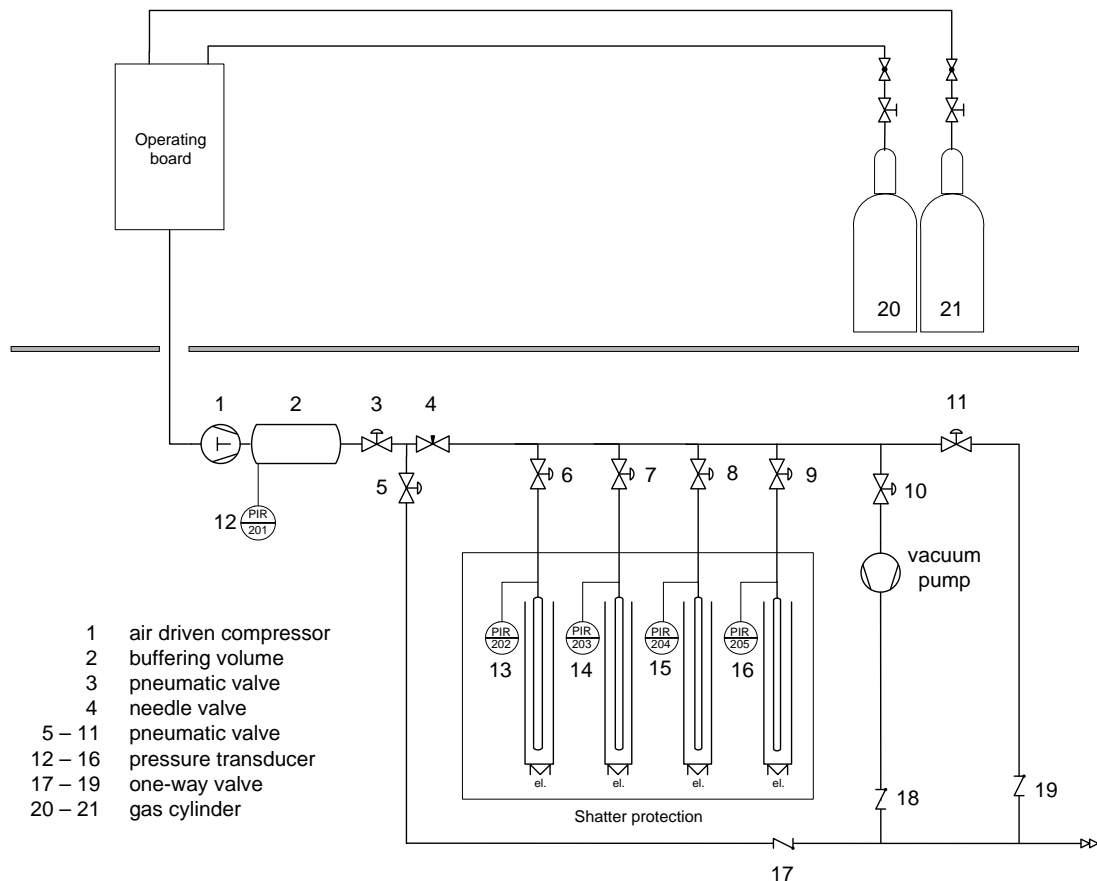


Figure 28: Schematic figure of test setup

The test set-up was built up with components able to withstand pressures of up to  $p = 310$  MPa. A compressor, driven and also cooled by pressurized air to avoid any ignition sources, was installed and able to realize test pressures of a maximum of  $p = 150$  MPa. Between compressor and test sample, a buffering volume was located to compensate the pulsation of compressor outlet and appease the gas flow. Three 1.4571 stainless steel vessels, engineered and manufactured at BAM, each with a maximum working pressure of  $p = 200$  MPa were installed. The buffering volume and following supply line were separated during filling process of buffering volume by a remote controlled pneumatic valve so a constant starting pressure in buffer for every test could be guaranteed. An additional needle valve was integrated to give the possibility of different constant gas flows from buffering volume to test samples. Four measuring stations for test samples were installed, each able to seal off with remote controlled pneumatic valves. In order to evacuate the test setup and operating board to avoid the

presence of air, a vacuum pump was connected to the supply line. Two exhausts, one per buffer volume and supply line including test samples, were installed for the safe release of compressed gases after testing or in case of a dysfunction.

Piezoresistive pressure transducers with an effective range of  $p_m = 100$  MPa were installed to detect the pressure in the buffer volume, the supply line and every single test station. The transducers were used for the precise determination of the pressure and pressure-time histories inside the complete experimental setup. All pressure transducers were calibrated by use of a digital pressure controller, type CPG 2500, WIKA Alexander Wiegand SE & Co. KG. The error of the pressure transducers was smaller than 0.5 % FS. Empirical data and manufacturer specifications allowed the use of described pressure transducer, up to an overload value of 50 % of maximum operating pressure. The transducers were connected to an A/D-converter (company Jet Systemtechnik GmbH, type MCL-USB, 16 channels 16 Bit A/D, sampling frequency 500 kHz) and a computer. All pressure-time histories in the setup and the single tested hollow glass fibers were measured and stored digitally. By using a special application the highest value of the pressure-time curve (burst pressure  $p_B$ ) was calculated, displayed and stored.

During testing the samples were surrounded by heating devices to ensure a constant temperature of  $T_{\text{test}} = 40$  °C of the glass structures. This equipment was also connected to a computer through the mentioned A/D-converter, so that all temperature-time histories could be measured and stored digitally.

Tests showed massive pollution with glass powder originated during bursting of hollow glass fibers. To satisfy the regulations of worker protection and to minimize the dangers for health a box, made from acrylic glass, was installed around the test samples. The glass powder was kept in that box during burst pressure tests and could be removed by using a vacuum cleaner. In order to avoid the formation of explosive gas mixtures after bursting of fibers filled with hydrogen, a fan and ventilation flaps were installed. Thus, an air stream was created that was high enough to avoid hazardous concentrations of hydrogen in the air. Nevertheless, no one was allowed to enter the safety room when tests were carried out or parts of the setup were under pressure. A picture of the complete test setup and enlargement of one measuring station is shown in Figure 29.

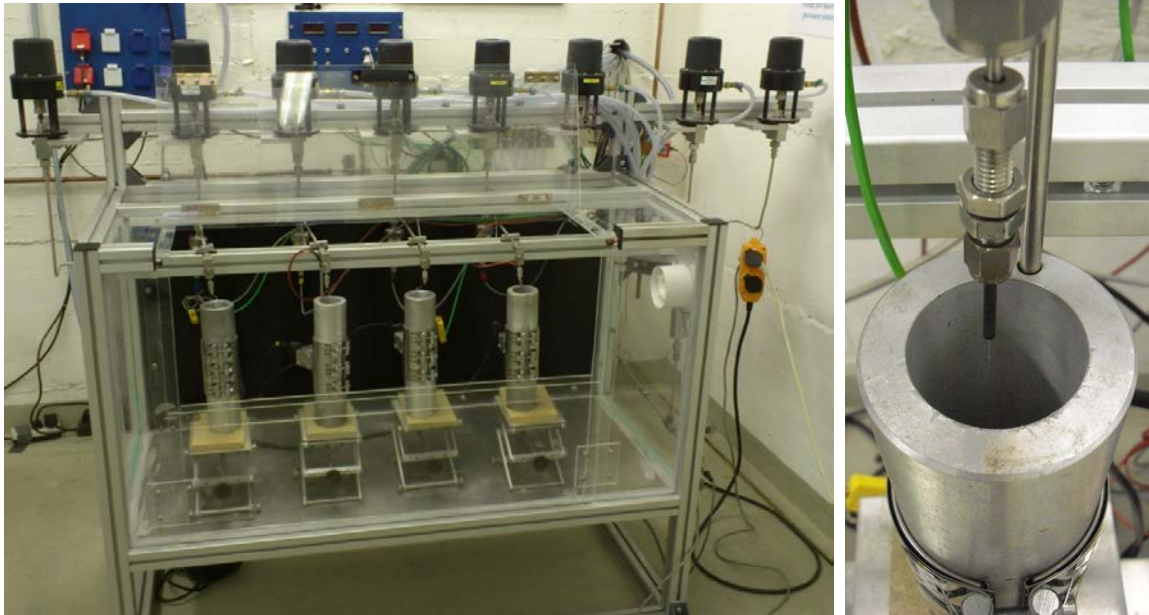


Figure 29: Complete test setup with four measuring stations surrounded by acrylic glass box (left picture); one measuring station in enlargement, single hollow glass fiber connected to test setup and surrounded by heating jacket (right picture)

## 5.2 Test Sample Preparation

After delivery the test samples were checked for macroscopic damage and stored in a dry box at constant temperature of  $T = 35\text{ }^{\circ}\text{C}$  until preparation. Thus, the influence of variations of temperature was avoided. Directly before preparation the fibers were checked a second time for macroscopic defects by the naked eye and randomly for microscopic defects under light microscope. If any defects were detected the relevant test sample was discarded and determined more exactly at a subsequent date.

The test setup was mainly built up with parts made from stainless steel wherefore a connection of the test samples had to ensure no damage or destruction of the sample and especially gas sealing. The test samples therefore were cleaned to ensure a fat-free surface and afterwards glued in thin stainless steel tubes with an outer diameter of 1/16 inch. The open end of the single hollow fiber was wetted with glue and stuck into the steel tube.

The 1/16 inch steel tube were glued again in stainless steel tubes of 1/8 inch outer diameter which were prepared for direct connection to the setup. The result of the described connection is displayed in Figure 30. As demonstrated the glued length between the two stainless steel tubes could be different.

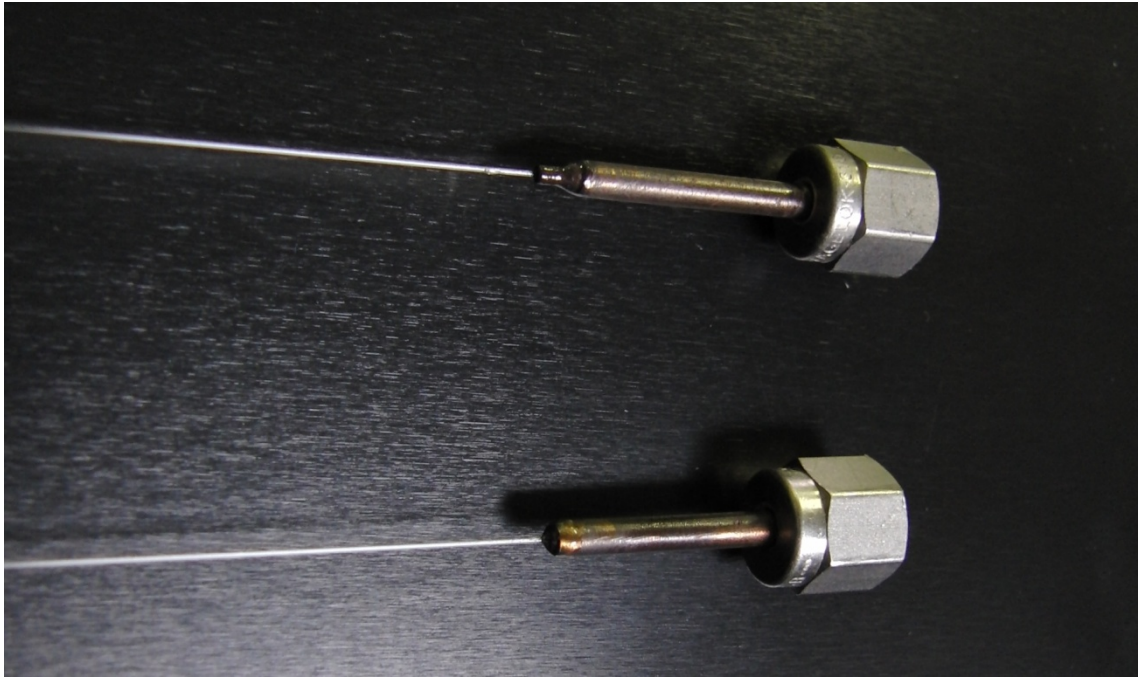


Figure 30: Finished connection after hardening of glue

For the adhesive connection between glass fibers and stainless steel tubes UHU PLUS ENDFEST 300 glue was used, which is based on epoxy resin and consists of two components. A chemical reaction began when both components came into contact for the first time and lead to the hardening of the glue. Dependent on hardening temperature the maximum reachable shear stress and hardening time varied; as listed in Table 8. The maximum service temperature of used glue was defined to  $T_s = 200 \text{ }^\circ\text{C}$  [145].

The big advantage of such kind of glue that is hardening without oxygen. Therefore homogeneous layer of glue with constant specifications over the total distance is guaranteed especially inside the stainless steel pipes.

Steel, glass and glue feature different coefficients of thermal expansion (CTE). Due to this phenomenon hardening was performed at test temperature. That method was introduced to avoid any leakages caused by different shrinkage during cooling down from hardening temperature to testing temperature.

Table 8: Shear stress of UHU PLUS ENDFEST 300 dependent on hardening temperature and time [145]

Hardening temperature $T_H$ [°C]	Hardening time $t_H$ [s]	Approximately maximum shear stress $\tau_{max}$ [N/mm <sup>2</sup> ]
20	43,200 (12 h)	12
40	10,800 (3 h)	18
70	2,700	20
100	600	25
180	300	30

### 5.3 Experimental Execution

The preparation of test setup was done in the same way for every single test series. After build-up a leak test was done to avoid any leakages at the tests setup. That test had to be repeated after every modification, regeneration or maintenance of test setup. A daily inspection of the setup was done after startup to ensure the functionality of all parts. Afterward, the heating devices were switched on and the test temperature of  $T = 40$  °C was adjusted. The evacuation of the whole setup was necessary to avoid any influences of air resided in setup and the formation of explosive atmospheres when hydrogen is discharged.

#### 5.3.1 Determination of Burst Pressure

The investigation of pressure resistance of hollow fibers made from different glass compositions with different ratios of diameter to wall thickness comprehended the determination of the burst pressure of tested single fibers.

The surface of prepared single hollow fibers was investigated for obvious defects and afterwards connected to the setup. Hereafter the test sample had to be evacuated. When connecting and evacuation were finished the buffer volume was charged with gas by keeping the valve between buffer and supply line closed. At a specific inner pressure the pneumatic valve was opened as well as the pneumatic valve to the first test sample. At the point of collapse of the fiber, the gas flow had to be interrupted immediately. Consequentially, the procedure had to be repeated for each single of the four connected test samples. When all four burst pressure tests were carried out, the pressure in the complete setup was released.

The maximum pressure of the test set-up was  $p = 150$  MPa, limited by the compressor. A constant pressure increase in the test samples was able to be controlled by a needle valve up to a pressure of about  $p = 100$  MPa. From that pressure, a compensation of the pulsation of the compressor outlet and an appeasing of the gas flow was not realizable even with the enlargement of buffer volume. In that case, the pressure increased stepwise due to compressor strokes to burst pressure.

### 5.3.2 Burst Pressure after Storage in Different Air Humidity

The knowledge regarding glass corrosion including interaction with air moisture led to the investigation of the influence of different air humidity on pressure resistance of hollow glass fibers. The prepared single fibers were stored for seven weeks at controlled conditions in atmospheres with different air humidity. Therefore, two different saturated saline solutions were confected and filled in two separate closed containers. Due to the saturation of the solution, in the atmosphere above the saline solution of a closed system defined constant air moisture ensues dependent on temperature and dissolved salt. Here the vapor pressure of the solvent is decreased as well as the relative air humidity above solution [155], [156]. Thus, two separate solutions, first of magnesium chloride ( $\text{MgCl}_2$ ) and second of sodium chloride ( $\text{NaCl}$ ) in water, were confected. The relative air moisture adjusted above the liquid phase is given in Table 9 for a storage temperature  $T_{\text{storage}} = 35$  °C.

Table 9: Literature and measured values of relative air humidity above confected saline solutions

Salt dissolved in water	Literature value of relative air humidity $\varphi$ [%]	Measured relative air humidity $\varphi$ [%]
$\text{MgCl}_2$	32.05 [157]	30.9
$\text{NaCl}$	74.87 [157]	75.8

The hollow fibers hung free in the atmosphere without any contact to the other fibers completely surrounded by the humid air. After finishing the storage time the burst pressure of the single glass fibers were determined in the final stage. Thereby, the tests were carried out with the same procedure described in chapter 5.3.1.

### 5.3.3 Influence of Cyclic and Static Pressure Load

#### Cyclic Pressure Load

After preparation of the test samples as described in chapter 5.2 the single fibers were connected to the test setup. The test samples were evacuated and the buffer volume filled with pressurized gas. In the case of the cyclic pressure procedure, all four fibers were loaded at the same time up to a predefined pressure of  $p_{\text{cyclic}} = 50$  MPa. When pressure was reached the buffer volume was separated from the supply line and refilled with gas. The pressure inside the hollow fibers was released to the exhaust and fibers were relaxed. Thereafter, the exhaust was closed and the hollow fibers filled again with gas up to  $p_{\text{cyclic}} = 50$  MPa. That procedure was repeated up to a pre-defined number. The different numbers of cycles  $n_c$  were  $n_c = (10; 30; 50; 100)$  and valid for all test series. After reaching the number of cycles the pressure was increased till the collapse eventuated and the burst pressure was reached. That was done for every test sample particular to ensure the correct measurement of burst pressure.

#### Static Pressure Load

After connecting the test samples to the setup the test plant was evacuated. The buffer volume was filled with gas and afterwards gas was piped to test samples. All connected fibers were loaded with pressure of  $p_{\text{static}} = 50$  MPa. The pressure load was continuously held on that pressure for a pre-defined period  $t_{\text{static}}$  and were  $t_{\text{static}} = (300; 1800; 3600)$  s. At the end of the specified time, the pressure inside the hollow fibers was increased up to burst pressure. The single hollow fibers had no time to relax first. Again, it was done for every single fiber particular to ensure the measuring of the correct pressure value at the point of collapse.



## 6 Results and Discussion

The experimental tests were carried out to determine the burst pressures of single test samples. Thereby, a single hollow glass fiber was loaded with increasing inner pressure until a collapse of the hollow fiber eventuated. This pressure value of every single fiber was defined as burst pressure. The information of the pressure resistance is a safety-related substance data, an important component property and a mechanical characteristic for glass structures. Pre-tests were carried out to investigate the influence of different glass types on the pressure resistance of the hollow glass fibers. Based on the data, hollow glass fibers with the highest pressure resistance were chosen to determine the effect on the burst pressure of several parameters, such as air humidity, different diameter and wall thicknesses, cyclic and static pressure load as well as the effect of coatings. The test results were evaluated by using the Weibull distribution as the statistical instrument.

### 6.1 Different Types of Glass

The existence of a multitude of glass types, each with different mechanical properties, led to the necessity of testing hollow fibers made from different glasses. The influence of the used glass on the pressure resistance of the single hollow fibers should be investigated and evaluated. Thereby, four technical relevant glass types were selected and tested as part of a diploma thesis [10]. Since the characteristics can be different even within one type of glass the choice was limited to one member per types of glass:

1. Fused Silica (Quartz glass);
2. Duran®/Borosilicate 3.3 (Borosilicate glass);
3. AR-Glass® (Soda-lime glass);
4. Schott glass 8252 (Aluminosilicate glass).

The chemical compositions of these glasses are given by manufacturer or required standards and listed in Table 10.

Table 10: Chemical compositions of tested hollow glass fibers given in mass-%

Components [ma-%]	Glass type			
	Fused silica [149]	Duran® [102], [148]	AR-glass® [147]	Schott 8252 [150], [153]
SiO <sub>2</sub>	99.99	81	69	60
Na <sub>2</sub> O		4	13	<0.02
Al <sub>2</sub> O <sub>3</sub>		2	4	14
K <sub>2</sub> O		4	3	
B <sub>2</sub> O <sub>3</sub>		13	1	4.5
BaO			2	9
CaO			5	10
MgO			3	2.5

### 6.1.1 Pre-Tests in Prior Stage

The determination comprehends hollow fibers made from different materials as well as different dimensions. The inner diameter ( $d_i$ ) was fixed to  $d_i = 300 \mu\text{m}$  and the outer diameter ( $d_o$ ) was changed. Moreover, two different wall thicknesses ( $s$ ) were produced, one series of each type of glass with  $s = 50 \mu\text{m}$  and with  $d_o = 400 \mu\text{m}$  and a second series with  $s = 20 \mu\text{m}$  and  $d_o = 340 \mu\text{m}$ . The tests, carried out with eight to ten tests samples per series, had shown different burst pressures for each dimension and each type of glass. The minimum, maximum and average burst pressures of these test series are listed in Table 11. The highest burst pressure of  $p_{\text{max}} = 124.2 \text{ MPa}$  was reached by a single hollow fiber made of borosilicate glass with  $d_o = 400 \mu\text{m}$  and  $s = 50 \mu\text{m}$ . Also fibers made from soda-lime, respectively, quartz with the same dimensions were able to withstand pressures above  $p = 100 \text{ MPa}$ . However, the spread of measured pressure values between maximum and minimum is much higher. Especially in the case of soda-lime glass with a  $d_o = 400 \mu\text{m}$  and  $d_i = 300 \mu\text{m}$ , the spread amounts to  $\Delta p = 89.7 \text{ MPa}$  in the range from  $p_{\text{min}} = 25 \text{ MPa}$  as minimum burst pressure to  $p_{\text{max}} = 114.7 \text{ MPa}$  as maximum burst pressure.

It can be seen that the difference of the pressure ranges for different dimensions. The average burst pressure of quartz and soda-lime glass is nearly doubled by having higher

wall thickness yet with the same inner diameter. Borosilicate glass even exhibits an increase of the average burst pressure by the factor of three. An exception of that behavior is aluminosilicate glass which shows nearly the same pressure ranges for both dimensions  $d_o = 400$  mm and  $d_o = 340$  mm.

Table 11: Data of average, maximum and minimum burst pressures of hollow glass fibers of different types of glass and different dimensions [10]

Material	Length [mm]	Outer diameter $d_o$ [ $\mu\text{m}$ ]	Inner diameter $d_i$ [ $\mu\text{m}$ ]	Min. burst pressure $p_{\text{min}}$ [MPa]	Max. burst pressure $p_{\text{max}}$ [MPa]	Average burst pressure $p_{\text{average}}$ [MPa]
Quartz	200	340	300	14.6	56.2	38.2
Borosilicate	200	340	300	22.3	40.1	29.3
Soda-lime	100	340	300	34.1	54.3	44.1
Aluminosilicate	200	340	300	32.6	62.7	44.3
Quartz	200	400	300	39.4	109.1	89.0
Borosilicate	200	400	300	73.7	124.2	100.2
Soda-lime	100	400	300	25.0	114.7	82.7
Aluminosilicate	200	400	300	42.1	53.5	46.0

This summary of test series, carried out as a part of a diploma thesis, serves as an overview about the outstanding pressure resistance able to be reached with hollow fibers made of glass. The tested glass types were chosen because of their technical relevance and therefore their availability without supply difficulties. The test results exhibit different pressure levels for both tested wall thicknesses.

Due to the highest value of the average and the maximum burst pressures fibers made of borosilicate and quartz glass were defined as test samples with the highest pressure resistance and chosen for further test series. A meaningful and concrete explanation of the test results could not be given at this stage of the research project. The tests were carried out to determine the burst pressures of single hollow glass fibers. The high spread of the value was recognized but the presence of defects and their possible influence on the pressure resistance became more important in the course of the project.

### 6.1.2 Repetition of Prior Test Series with Higher Number of Test Samples

Because of the low number of tests carried out [10], a reliable statistical analysis of the test results was not possible. Admittedly, the description of average, maximum and minimum burst pressure provides information about a range of pressure resistance of different glass types and the single fiber made from them. Nevertheless, an accurate statistical analysis with exact information about the distribution of failure probability, which has to be expected in use, requires a higher number of test values. In order to fulfill that requirement, hollow fibers made from the same four described glass materials and also the same dimensions were tested again. In the European standard DIN EN ISO 7458:2004 [143] the test methods for internal pressure resistance of glass containers with a minimum sample size of  $N \geq 20$  are defined as described in chapter 5.1. Although the tests methods were not suitable for testing hollow glass fibers the minimum sample size were taken as a first reference. Due to the fact that the Weibull distribution converge to the Gaussian distribution when testing a sample size of  $N \geq 30$  that number was defined as the minimum sample size for each series. Hence, both requirements mentioned above were fulfilled. Moreover, new hollow fibers were manufactured for these test series to preclude any influence of aging. Additionally, the test samples of each series were taken from the same batch to preclude influences of production parameters or basic raw material. Each burst pressure of each sample was considered without examination of the average burst pressure. In Table 12 all measured pressure values for test samples with the dimensions  $d_o = 400 \mu\text{m}$  and  $d_o = 340 \mu\text{m}$  are listed in ascending order. That order is not the chronology of test implementation. The table is given as example of the wealth of tests carried out per series.

Conspicuous is the lowest minimum burst pressure  $p_{\min} = 11.7 \text{ MPa}$  of quartz glass as well as the lowest maximum burst pressure  $p_{\max} = 33.8 \text{ MPa}$  of all tested glasses. Soda-lime glass shows a similar low minimum burst pressure of  $p_{\min} = 14.4 \text{ MPa}$  but explicitly higher maximum burst pressure. The calculation of the failure probability is significantly aggravated due to the wide range of burst pressures, which is an indicator for different defect species and sizes. Borosilicate 3.3 and aluminosilicate glass exhibit higher minimum burst pressure values but the maximum burst pressures are only slightly higher than that of soda-lime. Yet, the measured test results show a more narrow distribution. The summarized test values show a comparable pressure range of failure as the pre-tests, whereby the maximum burst pressures are lower. Notwithstanding, the difference between the individual measured test values is much smaller and therefore the distribution is more precise.

Table 12: Measured burst pressure values in ascending order of tested fibers made of quartz, borosilicate 3.3, soda-lime and aluminosilicate with the dimensions  $d_o = 340 \mu\text{m}$ ,  $d_i = 300 \mu\text{m}$ ,  $s = 20 \mu\text{m}$

<b>Burst pressure <math>p_B</math> [MPa]</b>				
<b>Individual test number</b>	<b>Quartz</b>	<b>Borosilicate 3.3</b>	<b>Soda-lime</b>	<b>Aluminosilicate</b>
1	11.7	21.9	14.4	20.7
2	19.4	22.6	15.1	26.2
3	19.6	23.7	16.0	28.1
4	19.6	25.2	18.7	28.1
5	20.9	26.0	20.1	28.4
6	21.9	28.7	22.6	28.9
7	22.0	29.2	23.5	30.1
8	22.6	29.9	27.1	30.6
9	22.9	30.9	28.7	31.4
10	23.1	31.5	28.7	31.7
11	23.6	32.0	30.4	31.9
12	25.3	32.9	31.0	32.2
13	26.0	34.3	31.1	32.5
14	26.5	34.4	31.4	33.0
15	27.2	35.1	31.9	33.5
16	27.7	35.3	31.9	36.0
17	27.7	36.5	32.1	36.4
18	27.8	36.5	32.8	36.8
19	27.8	36.8	33.5	37.1
20	28.1	36.9	33.7	37.9
21	28.4	37.0	33.9	38.1
22	28.4	37.1	34.1	38.7
23	28.5	38.1	34.6	38.8
24	29.2	38.1	35.9	39.1
25	29.6	38.3	36.8	40.0
26	30.3	38.7	37.2	40.3
27	30.7	38.7	37.3	40.3
28	32.0	39.0	38.4	40.5
29	33.1	43.1	40.2	41.3
30	33.5	43.9	40.8	44.2
31	33.6	46.3	41.0	44.3
32	33.8		42.8	44.9

The analysis of measured burst pressure values and their distribution was done by using the Weibull distribution described in chapter 4.5. In Figure 31 the Weibull diagram of the tested hollow fibers made of four different glasses with  $d_o = 340 \mu\text{m}$  and  $d_i = 300 \mu\text{m}$  is plotted.

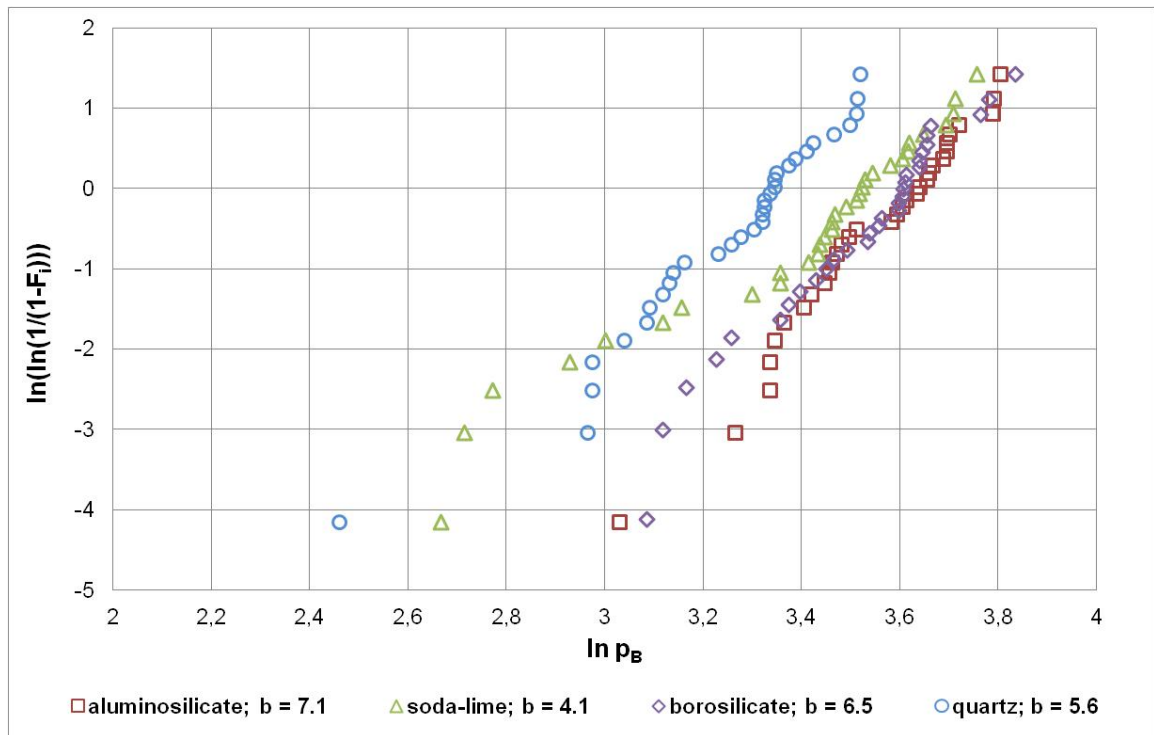


Figure 31: Weibull diagram of hollow glass fibers made of different types of glass with the dimensions  $d_o = 340 \mu\text{m}$ ,  $d_i = 300 \mu\text{m}$ ,  $s = 20 \mu\text{m}$

A double logarithmic function of the estimated failure probability  $F_i$  is plotted against the logarithmic burst pressures  $p_B$ . Obviously the graphs lie close together in the same region of the diagram. Hence, the pressure resistance of the tested glasses seems to be nearly the same and comparable. At this juncture, a more detailed evaluation of form parameter  $b$  and the characteristic pressure  $P$  is necessary. The form parameter  $b$  is given by the slope of each graph, whereby it provides information about the failure density and the spread of the measured pressure values. With higher value of the form parameter  $b$  the distribution of measured values and the range between minimum and maximum burst pressure are smaller. Consequently, the distribution of failure probability is much closer for a high value of the form parameter  $b$ . The characteristic pressure  $P$  is the measured pressure value at which 63.2 % of all tested samples fail. Table 13 summarizes the essential values of the tested samples.

Table 13: Form parameters  $b$  and corresponding characteristic pressures  $p_0$  of tested hollow fibers with the dimensions  $d_o = 340 \mu\text{m}$ ,  $d_i = 300 \mu\text{m}$ ,  $s = 20 \mu\text{m}$

<b>Glass material</b>	<b>Min. burst pressure <math>p_{\min}</math> [MPa]</b>	<b>Max. burst pressure <math>p_{\max}</math> [MPa]</b>	<b>Form parameter <math>b</math></b>	<b>Characteristic pressure <math>P</math> [MPa]</b>
Quartz glass	11.7	33.8	5.6	28.3
Borosilicate 3.3	21.9	46.3	6.5	36.9
Soda-lime	14.4	42.8	4.1	33.8
Aluminosilicate	20.7	44.9	7.1	38.0

Comparable developments of the graphs are recognizable for hollow fibers from borosilicate and aluminosilicate glass. The correspondent form parameters  $b$  and characteristic pressures only differs slightly from each other. Also, the curve of soda-lime test samples approximates the development of borosilicate and aluminosilicate fibers, which results in a comparable characteristic pressure. However, the graph differs significantly in the lower development. The reason for that behavior is the minimum burst pressure of soda-lime which is smaller by the factor 1.5. Hence, the spread of the distribution is much wider as of borosilicate or aluminosilicate and entails the low form parameter of  $b = 4.1$ . Quartz glass constitutes on average a form parameter of  $b = 5.6$ . The minimum burst pressure is similar to that of soda-lime but due to the lower maximum pressure value the spread is smaller.

With the knowledge of form parameter  $b$  and the characteristic pressure  $P$ , the distribution of failure probability  $F_B$  can be calculated by equation 3.6 and plotted as cumulated Weibull diagram which is displayed in Figure 32.

The failure probabilities of the different glass types are plotted as S-curves. Comparable to Figure 31 the diagram shows a concentration in certain regions. The graphs of aluminosilicate and borosilicate 3.3 describe a similar development. Due to the lowest pressure values, the curve of quartz glass is shifted to the left but the development and the form of the graph is comparable to alumino- or borosilicate. This is a clear evidence of analogues failure reasons or populations.

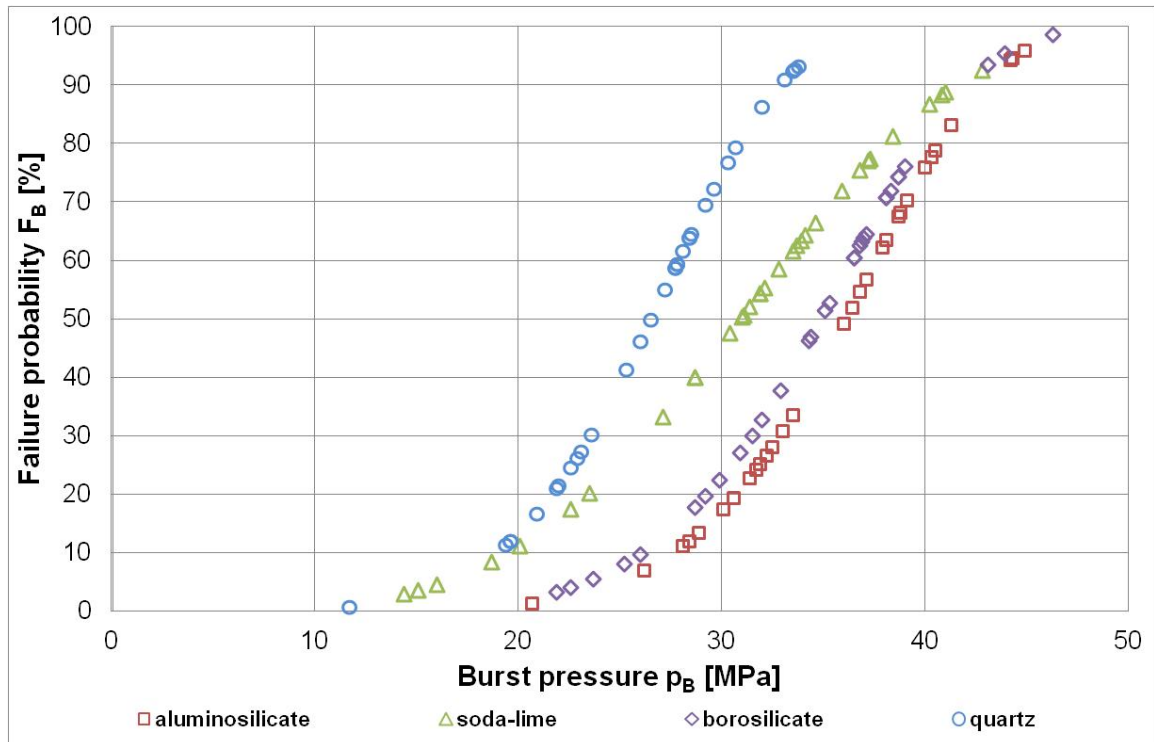


Figure 32: Failure probability curves of hollow fibers made of different glass types with the dimensions  $d_o = 340 \mu\text{m}$ ,  $d_i = 300 \mu\text{m}$ ,  $s = 20 \mu\text{m}$

The graph of soda-lime glass shows an obvious deviation in development compared to the other. This is a consequence of the high spread of measured burst pressure values and the resulting low value of the form parameter  $b = 4.1$ .

Also, the fibers with the dimensions  $d_o = 400 \mu\text{m}$  and  $d_o = 300 \mu\text{m}$  were tested again with a minimum of 30 test samples per test series. The resulting Weibull diagram is displayed in Figure 33. For better comparability, the same range of values of the axis as in Figure 31 is used.

The graphs of quartz glass, borosilicate glass and soda-lime glass are close together and have similar developments. All curves slid to the right in the diagram in comparison to the curves of samples with the dimensions  $d_o = 340 \mu\text{m}$ ,  $d_i = 300 \mu\text{m}$ ,  $s = 20 \mu\text{m}$  in Figure 31, which is an indicator for higher pressure resistance.



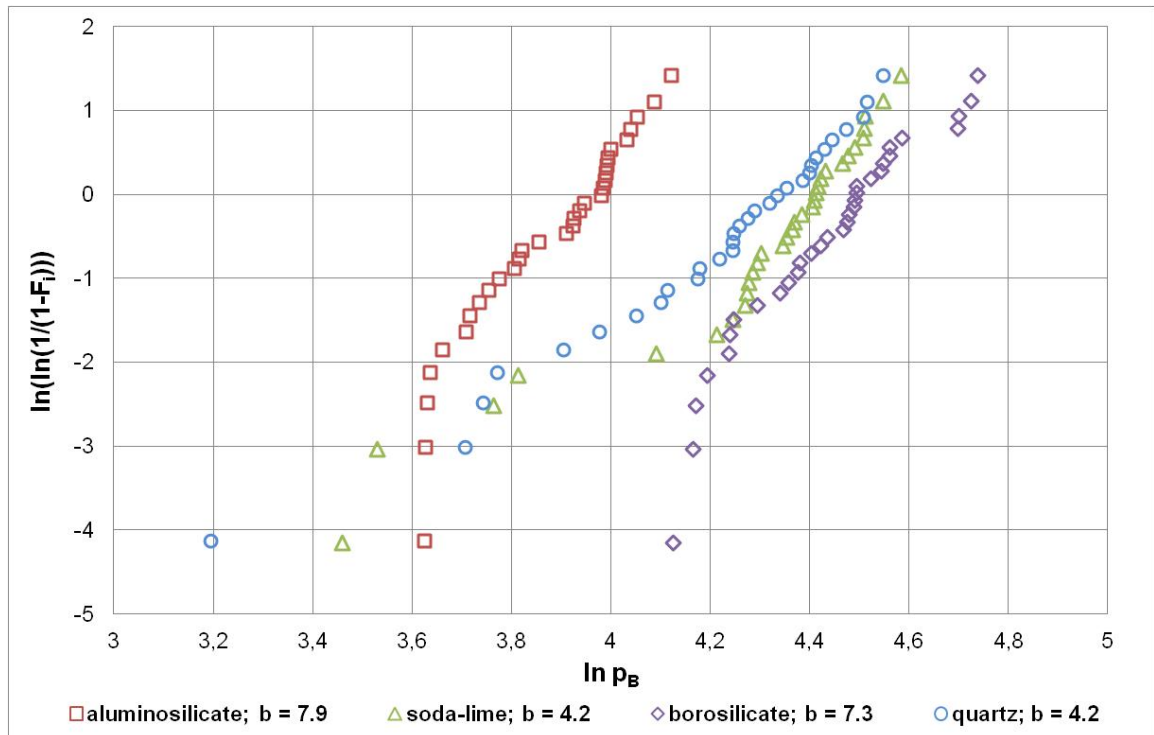


Figure 33: Weibull diagram of glass fibers made of different types of glass with the dimensions  $d_o = 400 \mu\text{m}$ ,  $d_i = 300 \mu\text{m}$ ,  $s = 50 \mu\text{m}$

The form and the development of the curves of quartz glass and soda-lime glass are similar. The determined form-parameters have the value of  $b = 4.2$ . The curve of borosilicate exhibits higher minimum pressure values but approaches in upper development to the curves of soda-lime and quartz glass, which is a result of the similar maximum pressure values. The lower spread of the measured values leads to a higher form parameter of  $b = 7.3$ . The characteristic pressure of soda-lime, quartz and borosilicate fibers are in a similar range between  $p = 76 \text{ MPa}$  and  $p = 89 \text{ MPa}$ , which are given in Table 14. The reason is the analogous development of the three graphs at higher burst pressures.

One exception is the curve of aluminosilicate glass. An outstanding feature is the deviation when compared to the other graphs. In form and development the curve is similar to those of borosilicate; yet again this curve slide distinctly to the left in diagram which is an indicator for higher burst pressure results during testing.

Although the initial point described by the minimum burst pressure is comparable to those of soda-lime glass, the slope of the curve of aluminosilicate is higher. Consequently, the resulting form parameter of  $b = 7.9$  is similar to borosilicate glass but the characteristic pressure of  $P = 53.5 \text{ MPa}$  is considerably smaller.

Table 14: Form parameters  $b$  and corresponding characteristic pressures  $P$  of tested fibers with the dimensions  $d_o = 400 \mu\text{m}$ ,  $d_i = 300 \mu\text{m}$ ,  $s = 50 \mu\text{m}$

Glass material	Min. burst pressure $p_{\min}$ [MPa]	Max. burst pressure $p_{\max}$ [MPa]	Form parameter $b$	Characteristic pressure $P$ [MPa]
Quartz glass	24.4	94.4	4.2	76.6
Borosilicate 3.3	61.9	114.2	7.3	89.3
Soda-lime	31.8	97.8	4.2	82.3
Aluminosilicate	37.5	61.6	7.9	53.5

The distribution of the calculated failure probability is significantly wider as a result of the higher spread of burst pressure values of tested fibers which features the higher wall thickness. The behavior and development of corresponding S-curves of failure probability against pressure values in Figure 34 is clearly different from these in Figure 32.

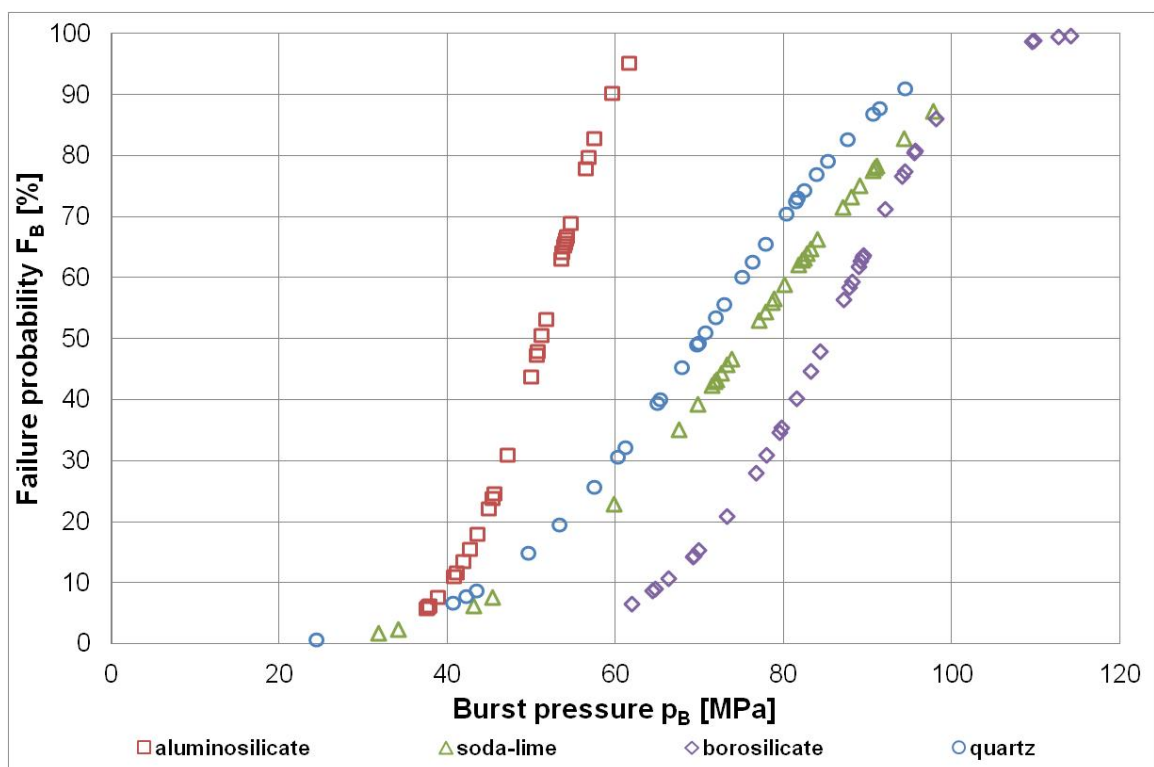


Figure 34: Failure probability curves of hollow fibers made of four different glass types with the dimensions  $d_o = 400 \mu\text{m}$ ,  $d_i = 300 \mu\text{m}$ ,  $s = 50 \mu\text{m}$

The difference between the graph of aluminosilicate and the other glasses is obvious. The slope of the curve is much steeper and a clearer approximation of an ideal step function is recognizable. Minimum and maximum burst pressures of this test series are closer together. Quartz, borosilicate and soda-lime exhibit maximum burst pressure, higher by the factor 2. Yet, the smaller form parameter  $b$  leads to flat slopes of the graphs. Obviously, the distribution of failure probabilities is much wider than those of aluminosilicate.

On examination of the different dimensions, no consistent trend of pressure resistance of hollow glass fibers can be seen. Clear to see are the deviating pressure developments of fibers of the same material by comparison of smaller dimension to bigger dimension.

The theoretical tensile strength of glass can be estimated with equation (3.4) [5]

$$\sigma_{th} \approx \frac{E}{10} \quad (3.4).$$

Therefore, the tensile strength is dependent on the Young's modulus of the corresponding glass. The values resulting are summarized in Table 15.

Table 15: Young's modulus and corresponding theoretical tensile strength estimated by equation (3.4) [5]

<b>Glass material</b>	<b>Young's modulus E [MPa]</b>	<b>Estimated theoretical tensile strength <math>\sigma_{th}</math> [MPa]</b>
Fused silica	75,000 [149]	7,500
Borosilicate 3.3	63,000 [154]	6,300
Soda-lime	73,000 [147]	7,300
Aluminosilicate	81,000 [150]	8,100

The applied formula is based on the theory of creating new surfaces during fracture. These surfaces are created by breaking the chemical bonds between atoms or ions in the material and so only the average inter-atomic distance is considered. Any defects or flaws are neglected. These could exist on the surface or in the bulk of the material and decrease the tensile strength by a multiple. Estimated theoretical strength can only be used as a rough evaluation of the resulting trend of pressure resistance of the different hollow glass fibers.

Therefore, hollow fibers made from aluminosilicate should exhibit the highest burst pressures. This behavior is detectable for hollow fibers of a wall thickness of  $s = 20 \mu\text{m}$ . Here, aluminosilicate fibers exhibit the highest parameters of the form parameter  $b$  as well as the characteristic pressure  $P$ . The results of fibers made from other glasses depart from the estimated trend. Thus quartz glass fibers but not borosilicate fibers showed the lowest pressure resistance.

Tested hollow fibers with higher wall thickness of  $s = 50 \mu\text{m}$  should exhibit the same trend in pressure resistance as the thinner fibers. At this point, massive deviations are recognizable. Having the higher wall thickness aluminosilicate fibers again have the highest form parameter  $b$  but show the lowest burst pressures. Borosilicate samples have the highest pressure resistance combined with a narrow distribution due to the high form parameter  $b$ . Test samples of quartz glass and soda-lime glass show high characteristic pressures  $P$  but as well a wide range of burst pressures.

As result from this study it can be summarized that:

- Test series with fibers made of four different glass materials and two different dimensions were carried out and showed different behaviors. Significant deviations from theoretical trend were detected.
- At small dimension, all test series exhibited similar pressure resistance with only slight deviations. The test results showed different behaviors of the fibers dependent on the type of glass. Hollow glass fibers made of aluminosilicate with dimensions of  $d_o = 340 \mu\text{m}$ ,  $d_i = 300 \mu\text{m}$ ,  $s = 20 \mu\text{m}$  resulted in close distributions of measured values. Fibers made of soda-lime, borosilicate 3.3 or quartz glass showed significant wider spread of test data.
- The spread of measured values of aluminosilicate fibers was independent from dimension. Fibers of larger dimensions of  $d_o = 400 \mu\text{m}$ ,  $d_i = 300 \mu\text{m}$ ,  $s = 50 \mu\text{m}$  showed the same narrow distribution.
- The increase of the wall thickness at constant inner diameter led to significant higher burst pressure values of the hollow fibers except these made of aluminosilicate glass whereby the dissemination of measured values increased as well.
- Borosilicate fibers in all test series reached the highest single burst pressures; test samples of soda-lime and quartz glass featured comparable high pressure values which always remained slightly below the pressure resistance of borosilicate fibers.

## 6.2 Influence of Aging by Environmental Conditions

Based on the burst pressure of hollow fibers made of different glass materials the influence of glass aging on pressure resistance was investigated. Here two test series for which the hollow fibers were stored at different conditions were carried out. One time the fibers were stored under constant temperature conditions, one time under constant air humidity conditions combined with constant temperature.

The high chemical resistance of glass against a multiple of substances is an outstanding property. But water or even air humidity can lead to chemical attack and corrosion on different glass materials.

### 6.2.1 Aging under Constant Temperature Conditions

Glass fibers with the same inner diameter but different outer diameter were stored under constant temperature conditions of  $T_{\text{storage}} = 35 \text{ }^{\circ}\text{C}$  for one year. The fibers were made of the same four already tested materials. The air humidity in the tempered container was the same as in the laboratory the entire time. The relative atmospheric moisture was monitored daily. The average value of measured air humidity within this year was  $\varphi = 55.0 \%$ . The lowest measured air humidity was  $\varphi = 20.2 \%$  on a dry winter day, the highest air humidity was  $\varphi = 83.2 \%$  on a rainy summer day. The deviation between lowest and highest air humidity amounts to  $\varphi = 63 \%$  of relative air humidity.

After the storage the test samples were prepared according to the procedure explained in chapter 5.2 and the burst pressure of a minimum of 30 samples was determined per series.

Table 16 summarizes the main test parameters of the series which consists of minimum and maximum burst pressure, form-parameter  $b$  and the characteristic pressure  $P$  of Weibull distribution. It can be seen that the fibers with smaller outer diameter performed lower pressure values at the same inner diameter.

Table 16: Minimum and maximum burst pressures with correlating form parameter  $b$  and characteristic pressure  $P$  of tested fibers made of different glasses and dimensions; the hollow fibers were stored for one year under controlled temperature conditions

Glass material	Dimension	Min. burst pressure $p_{\min}$ [MPa]	Max. burst pressure $p_{\max}$ [MPa]	Form parameter $b$	Characteristic pressure $P$ [MPa]
Quartz glass	$d_o = 340 \mu\text{m}$ $d_i = 300 \mu\text{m}$ $s = 20 \mu\text{m}$	17.8	52.1	4.8	42.7
Borosilicate 3.3		21.1	47.5	7.1	36.1
Soda-lime		28.9	48.2	10.4	40.1
Aluminosilicate		25.2	44.4	7.6	35.6
Quartz glass	$d_o = 400 \mu\text{m}$ $d_i = 300 \mu\text{m}$ $s = 50 \mu\text{m}$	57.7	126.3	6.9	106.6
Borosilicate 3.3		50.6	132.4	5.1	89.4
Soda-lime		30.7	122.7	4.0	97.6
Aluminosilicate		32.2	52.9	10.3	42.0

Quartz glass fibers of small dimensions show outstanding pressure resistance in the form of highest maximum burst  $p_{\max}$  and characteristic pressure  $P$  although the form parameter  $b = 4.8$  shows the lowest value in comparison with other test series. Hence, the spread of measured data is wide which is shown by lowest minimum burst pressure.

Borosilicate and aluminosilicate fibers are comparable to each other by exhibiting nearly the same pressure and form-parameter values. Both show similar form parameter of  $b = 7.1$  respectively  $b = 7.6$  but lower characteristic and maximum burst pressure values than quartz glass fibers.

The highest form parameter of  $b = 10.4$  was determined for test samples made of soda-lime. The maximum burst pressure is similar to hollow borosilicate fibers but the minimum burst pressure is significantly higher. This indicates a narrow distribution of measured data.

With regard to the bigger dimensions, it was demonstrated that aluminosilicate fibers show the lowest pressure resistance but also the highest form parameter  $b$ . That behavior is comparable to test series with new samples. Hollow fibers made of the other three glass materials show significantly higher burst pressures those made of aluminosilicate glass. Samples of soda-lime glass exhibit a low value of the form

parameter which indicates a wide distribution with high spread between minimum and maximum burst pressure.

The resultant diagram of failure probability against burst pressure for the smaller dimensions is given in Figure 35. The interpreted distributions seem to be confirmed.

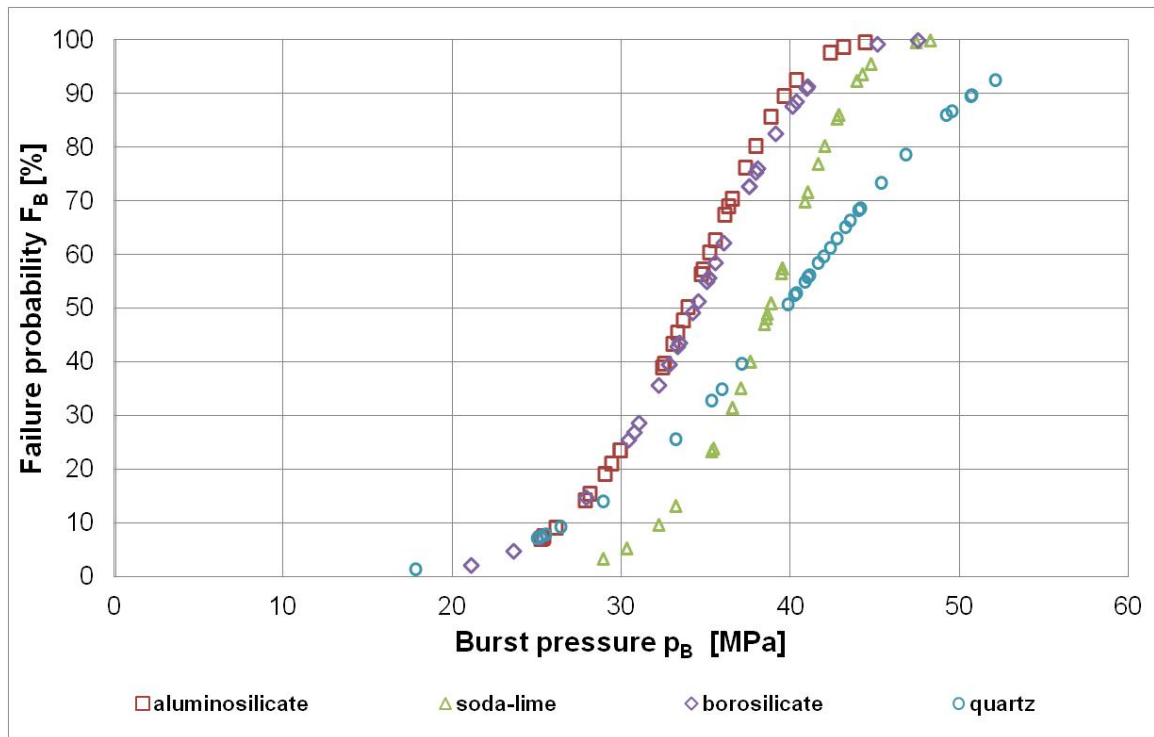


Figure 35: Failure probability curves of fibers made of four different glass types with the dimensions  $d_o = 340 \mu\text{m}$ ,  $d_i = 300 \mu\text{m}$ ,  $s = 20 \mu\text{m}$  aged one year under controlled temperature conditions

The graphs of aluminosilicate and borosilicate test samples show similar development. Also hollow soda-lime fibers curve exhibit almost the same development. But the form parameter  $b$  of soda-lime is higher which results in a slightly steeper gradient. Because the characteristic pressure  $P$  of soda-lime fibers is also higher in comparison to borosilicate 3.3 and aluminosilicate, the graph slid to the right in the diagram. Therefore, not only the distribution of failure probability is narrower but also higher pressures are reachable at same probability of bursting. The distribution of quartz test samples is wider than of the other glass materials. Quartz glass fibers have the lowest minimum burst pressures but the test samples reached also highest maximum burst pressures. Thus, the form parameter  $b$  is lower which causes a significantly lower increase of curve development. In spite of the low  $b$ -value, the high characteristic and maximum burst pressure at failure probabilities above  $F_B = 60 \%$  higher pressure values are appending.

As it can be seen in Table 16, the fibers of larger dimensions exhibit significantly different behavior. In Figure 36 the S-curves of the failure probability is plotted for samples of dimensions  $d_o = 400 \mu\text{m}$ ,  $d_i = 300 \mu\text{m}$ ,  $s = 50 \mu\text{m}$ .

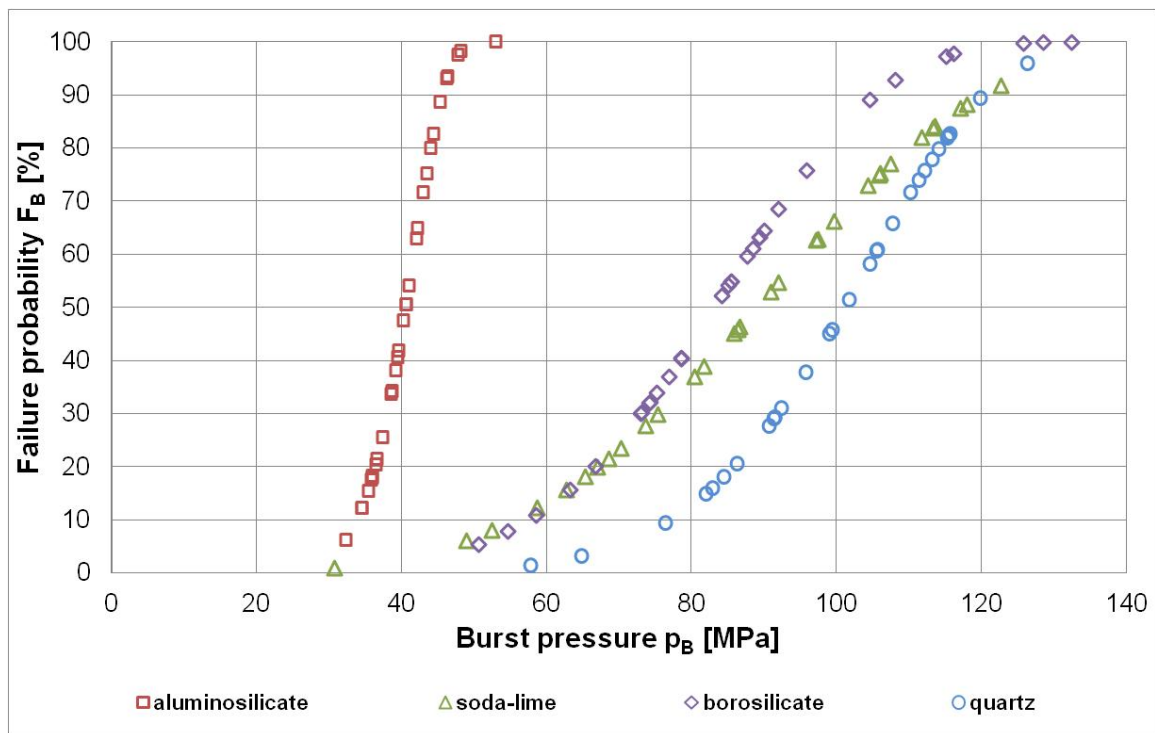


Figure 36: Failure probability curves of hollow fibers made of four different glass types with the dimensions  $d_o = 400 \mu\text{m}$ ,  $d_i = 300 \mu\text{m}$ ,  $s = 50 \mu\text{m}$  aged one year under controlled temperature conditions

Obviously the graphs of quartz, borosilicate 3.3 and soda-lime hollow fibers have higher spread of the measured pressure values compared to the smaller dimensions. Because of the higher reached burst pressures and characteristic pressures  $P$ , the graphs slid to the right. Thus, at a specific failure probability higher corresponding pressure values are reached.

The graph of aluminosilicate glass fibers exhibits a much steeper gradient. The distribution of failure probability  $F_B$  of fibers made of this material with the named dimensions is narrower than these of the other glass materials with the same dimensions but pressure values are much lower. Hence, the approximation to the optimum step function is obvious, though the resistance against inner pressure load of fibers made of aluminosilicate is much smaller than these of quartz, borosilicate 3.3 or soda-lime glass.



A comparison of the current test results of aged fibers (borosilicate 3.3 and aluminosilicate glass) with those of the new hollow glass fibers described in chapter 6.1.2 is listed in Table 17.

Table 17: Characteristic values of hollow borosilicate and aluminosilicate fibers with different dimensions and ages

<b>Glass / Age</b>	<b>Dimension [<math>\mu\text{m}</math>]</b>	<b>Min. burst pressure <math>p_{\text{min}}</math> [MPa]</b>	<b>Max. burst pressure <math>p_{\text{max}}</math> [MPa]</b>	<b>Form parameter b</b>	<b>Characteristic pressure P [MPa]</b>
Borosilicate / new	$d_o = 340$ $d_i = 300$ $s = 20$	21.9	46.3	6.5	36.9
Borosilicate / aged one year		21.1	47.5	7.1	36.1
Aluminosilicate / new		20.7	44.9	7.1	38.0
Aluminosilicate / aged one year		25.2	44.4	7.6	35.6
Borosilicate / new	$d_o = 400$ $d_i = 300$ $s = 50$	61.9	114.2	7.3	89.3
Borosilicate / aged one year		50.6	132.4	5.1	89.4
Aluminosilicate / new		37.5	61.6	7.9	53.5
Aluminosilicate / aged one year		32.2	52.9	10.3	42.0

It can be seen that hollow fibers made of borosilicate 3.3 reached similar burst pressure values. Samples with comparable dimensions exhibit comparable pressure values independent on the age of the fibers. A similar behavior is recognizable for aluminosilicate samples. An influence on the pressure resistance caused by air moisture does not seem to prevail.

Whit regard to quartz fibers it can be seen that the aged hollow fibers reached higher pressure values than the new ones for both dimensions. The characteristic values of test series with new and aged quartz fibers are summarized in Table 18.

Table 18: Characteristic values of hollow quartz fibers with different dimensions and ages

Material / Age	Dimension [ $\mu\text{m}$ ]	Min. burst pressure $p_{\text{min}}$ [MPa]	Max. burst pressure $p_{\text{max}}$ [MPa]	Form parameter b	Characteristic pressure P [MPa]
Quartz / new	$d_o = 340$	11.7	33.8	5.6	28.3
Quartz / aged one year	$d_i = 300$ $s = 20$	17.8	52.1	4.8	42.7
Quartz / new	$d_o = 400$	24.4	94.4	4.2	76.6
Quartz / aged one year	$d_i = 300$ $s = 50$	57.7	126.3	6.9	106.6

Especially for larger dimensions higher pressure ranges for each characteristic pressure value are recognizable as well as a higher form parameter  $b$ . Hollow quartz fibers of smaller dimensions exhibit similar minimum burst pressure independent from the age. But at maximum burst pressure as with characteristic pressure  $P$  an increase by the factor 1.5 is obvious. Thus, the spread of measured values of aged quartz fibers with small dimensions is wider as well as the probability of concurrent failures. Hollow fibers of larger dimensions also exhibit an increase of maximum burst pressure and characteristic pressure  $P$  by the factor 1.5 for aged samples. Additionally, the minimum burst pressure even shows an increase by the factor 2.3. Consequently the spread the resulting failure probability is narrower and a possible collapse is more predictable. Based on the test results a positive influence on the pressure resistance of quartz fibers by aging can be concluded.

Aged hollow fibers made of soda-lime glass with smaller dimensions have a significantly higher form parameter  $b$  due to higher minimum burst pressure but comparable maximum burst pressures between new and aged test samples, as summarized in Table 19.

The result is a narrow distribution of failure probability and an obviously higher characteristic pressure  $P$ . Looking at the larger dimensions, no significant difference by aging is detectable. An increase of the maximum burst pressure  $p_{\text{max}}$  and the characteristic pressure  $P$  by the factor 1.2 is recognizable but the form parameter remains nearly at the same value. Consequently, the results of samples made of soda-lime do not show a clear trend of the influence of aging on the pressure resistance.

Table 19: Characteristic data of soda-lime fibers with different dimensions and age

Material / Age	Dimension [ $\mu\text{m}$ ]	Min. burst pressure $p_{\text{min}}$ [MPa]	Max. burst pressure $p_{\text{max}}$ [MPa]	Form parameter b	Characteristic pressure P [MPa]
Soda-lime / new	$d_o = 340$	14.4	42.8	4.1	33.8
Soda-lime / aged one year	$d_i = 300$ $s = 20$	28.9	48.2	10.4	40.1
Soda-lime / new	$d_o = 400$	31.8	97.8	4.2	82.3
Soda-lime / aged one year	$d_i = 300$ $s = 50$	30.7	122.7	4.0	97.6

Partial significant differences are recognizable in comparisons between new and aged fibers of the same dimension and material. Additionally, the trend of the estimated tensile strength of the different glasses referred to Table 15 is not detectable for aged fibers. As mentioned in chapter 6.1.2 the estimated tensile strength is calculated without consideration of any surface or volume defects.

One reason could be the glass corrosion caused by air moisture which was also investigated by carrying out test series with constant air moisture in chapter 6.2.2. Air moisture could be accumulated on the surface during storage and leads to chemical reactions not only on possible flaws but on the whole surface. The results could be significantly lower mechanical resistance of glass products. In the case of hollow quartz fibers, considerably higher pressure resistance is measured in aged condition independent from dimension. If glass corrosion occurs, the load condition of the sample under consideration is crucial. If stress is acting, stress corrosion is able to occur and leads to fast degradation of mechanical resistance. In the case of tested fibers no load was acting during storage. At appearance of an alkaline reaction under non-load conditions, a defect or crack tip could be rounded and therefore the mechanical sensibility could be decreased [97]. But an alkaline reaction takes place when the water film formed on the glass surface is enriched with alkaline ions as a result of hydrolytic reaction. Indeed, the chemical composition of quartz glass contains other substances in addition to  $\text{SiO}_2$ , but only in traces. Thus, an alkaline reaction caused by dissolved alkaline ions from the glass structure itself is implausible.

Borosilicate 3.3 and aluminosilicate fibers show almost the same results of new and aged hollow fibers. An influence of aging due to air moisture or production parameter is not detectable.

Test samples made of soda glass only show obvious differences by having the small dimensions. Because the chemical composition of that type of glass consists of a high number of alkaline substances, a chemical reaction caused by water is supposable. Rounding of crack tips by this chemical reaction could lead to an increase of pressure resistance, although defects in surface exist.

Another reason for the occurring differences between new and aged fibers might be the fact that the new samples are from a different batch. Care was taken that all test samples within one test series were taken from the same batch. The investigation of influence of aging was done with fibers from another batch.

Glass fibers are produced from glass tubes with a diameter of about  $D_o = 5$  cm. Thereby, the tubes were heated up to a working point with a viscosity of  $\eta = 10^4$  dPa s and afterwards drawn to thin hollow fibers with outer diameters of  $d_o = 100$   $\mu$ m up to  $d_o = 1000$   $\mu$ m and cut into required length. For shipment from manufacturer to test laboratory the fibers were packed in a number of 20 to 50 samples in a plastic bag. Different parameters during production such as drawing temperature and drawing speed or the handling between cutting and packing could be reasons for the partially different test results. The shipment itself also gives possibilities to create new flaws, especially on the surface of the hollow glass fibers. Due to packing not only one but a high number of hollow glass fibers in a small bag contact each other. These results show once again that the pressure resistance is a property not of the glass mixture itself but of the tested product made of the specific glass mixture [5].

Because of the consistently high pressure resistance with comparable failure probability distributions, especially independent on the age, borosilicate 3.3 fibers with the larger dimensions were chosen for further test series.

In addition to borosilicate 3.3, quartz fibers were also chosen. That decision was made due to high pressure resistance in pre-tests and under aged conditions. The determination of pressure resistance and corresponding failure probability of quartz fibers showed high spread of measured pressure values. Nevertheless, high burst pressure values was detected which are indicators for the potential of high mechanical resistance.

Soda-lime and aluminosilicate were excluded from further investigations. Aluminosilicate showed no significant influence of aging on the pressure resistance and resulting failure

probability. But a massive influence on the dimension was detectable, whereby aluminosilicate fibers were the only test samples to show no increase of pressure resistance with larger wall thickness. In contrast to aluminosilicate, soda-lime fibers showed a direct influence on dimension and age. The slight increase of pressure resistance could be affected by glass corrosion caused by air moisture at non-loaded conditions. At loaded conditions, glass corrosions could have the reverse effect.

As result it can be summarized:

- Test series were carried out with four different glass materials and two different dimensions. These fibers were stored at  $T_{\text{storage}} = 35 \text{ }^{\circ}\text{C}$  and relative air humidity of  $\varphi = 55 \%$  for at least one year. The test results were compared with those of new tested fibers. An overview of the development of pressure resistance is given in Table 20.
- Under non loaded storage conditions the effect of aging due to environmental influences was negligible for fibers made of borosilicate.
- The detected deviations were at a scale that these deviations can be attributed to production tolerances. The tested hollow fibers were made of material with the same chemical composition but drawn in different production batches. Changes even in traces may lead to small deviations of test results.

Table 20: Development of burst pressure resistance of glass fibers after aging one year compared new tested fibers by reference to the characteristic pressure P

	<b>Wall thickness s = 20 <math>\mu\text{m}</math></b>	<b>Wall thickness s = 50 <math>\mu\text{m}</math></b>
Borosilicate	Constant	Constant
Aluminosilicate	Decreased	Decreased
Quartz	Increased	Increased
Soda-lime	Increased	Increased

### 6.2.2 Aging under Constant Air Humidity Conditions

Test series with aged hollow fibers made of different glasses showed different effects on pressure resistance and failure probability. Since these results could not be related definitely on either aging by the influence of air moisture or on the history of the hollow glass fibers continuing test series were carried out. Here the source of test samples was

brought into focus. Hollow fibers made of borosilicate 3.3 (DURAN) and quartz glass with dimensions of  $d_o = 400 \mu\text{m}$ ,  $d_i = 300 \mu\text{m}$ ,  $s = 50 \mu\text{m}$  were investigated in test series of new fibers and aged fibers to examine the influence of air moisture. Thereby the tested hollow fibers were taken from the same production batch the test samples of the investigation of different glass types (chapter 6.1.2) were taken from. Hence, any possible influence of different material history was excluded and the results were comparable.

The test samples were glued in stainless steel tubes and stored for 7 weeks in defined air humidity, described in 5.3.2. The test results of borosilicate 3.3 fibers are listed in Table 21. As reference value, the data of new fibers from the same dimensions and batch were used. The new fibers were tested only a few days after delivery.

Table 21: Characteristic test data of borosilicate 3.3 fibers at different air humidity with the dimension  $d_o = 400 \mu\text{m}$ ,  $d_i = 300 \mu\text{m}$ ,  $s = 50 \mu\text{m}$

<b>Air humidity <math>\varphi</math> [%]</b>	<b>Min. burst pressure <math>p_{\min}</math> [MPa]</b>	<b>Max. burst pressure <math>p_{\max}</math> [MPa]</b>	<b>Form parameter <math>b</math></b>	<b>Characteristic pressure <math>P</math> [MPa]</b>
New fiber	61.9	114.2	7.3	89.3
30.9	65.2	138.4	6.8	92.1
75.8	56.0	130.7	6.2	95.2

A consistent behavior of the three test series can be clearly seen. New borosilicate fibers tested at average air moisture of  $\varphi = 55 \%$  exhibit the highest form parameter  $b = 7.3$  but also the lowest characteristic and maximum burst pressure. A slight increase of the minimum burst pressure  $p_{\min}$  and characteristic pressure  $P$  is detectable for hollow fibers stored at  $\varphi = 30.9 \%$  relative air humidity. More obvious is the increase of maximum burst pressure  $p_{\max}$  by the factor 1.2. Through this, the scattering of measured values is wider, which is detectable by a slightly smaller form parameter  $b$ . Also the test results of fibers stored in higher air moisture of  $\varphi = 75.8 \%$  exhibit only small deviations from reference values. However, the highest characteristic pressure  $P$  indicates a narrow distribution of measured burst pressure in high pressure ranges. Generally it can be seen that the test results are similar and comparable. Nevertheless, the higher characteristic pressures  $P$  could be an indication for positive influence of defined air humidity by rounding the edges of defects.

The corresponding distributions of failure probability of the three test series of hollow borosilicate 3.3 fibers are plotted in Figure 37 against the measured burst pressures.

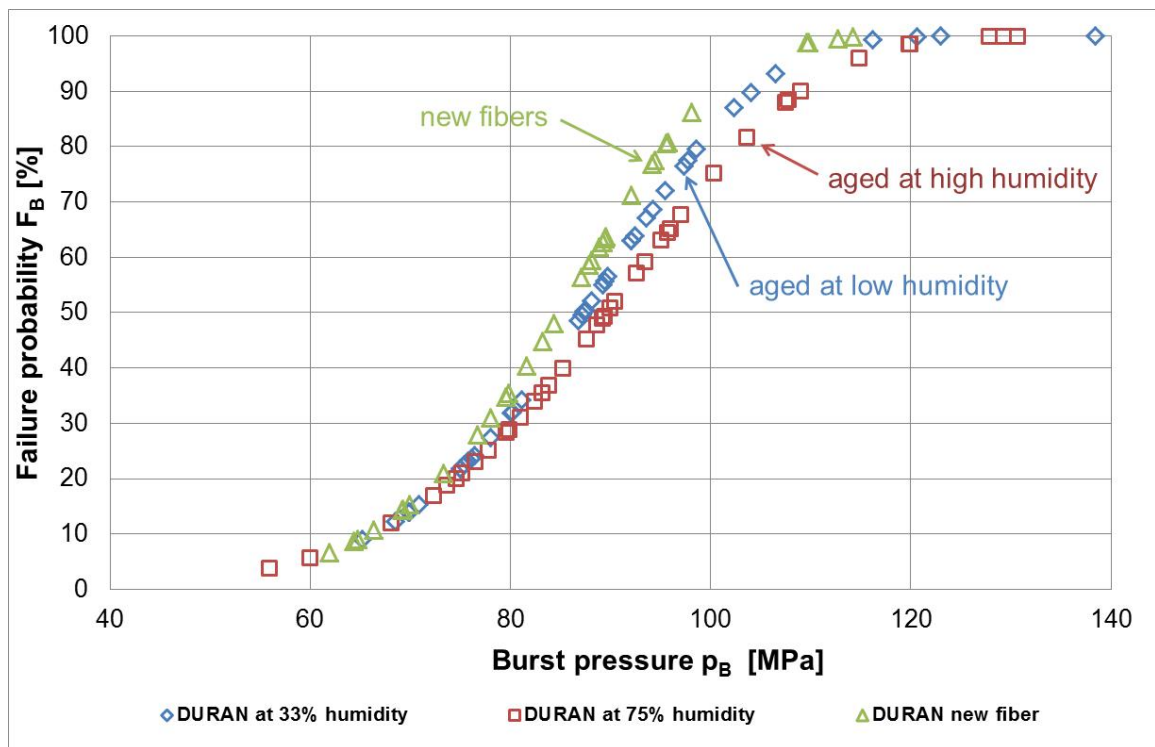


Figure 37: Influence of aging under different humidity on failure probability and pressure resistance of borosilicate 3.3 (DURAN) fibers with the dimensions  $d_o = 400 \mu\text{m}$ ,  $d_i = 300 \mu\text{m}$ ,  $s = 50 \mu\text{m}$

The similar development of all graphs is obvious. Due to similar minimum burst pressure values, the initial points of the graphs are close together. The gentle decrease of form parameter  $b$  with simultaneous slight increase of characteristic pressure  $P$  leads to the displacement of the graphs to the right. However, at pressures above  $p = 80 \text{ MPa}$  a higher pressure resistance of fibers treated with defined constant air humidity is observable. The failure probability  $F_B$  at  $p = 100 \text{ MPa}$  of new fibers is about  $F_B = 90 \%$ . Fibers stored at  $\varphi = 75.8 \%$  air humidity features a failure probability of about  $F_B = 75 \%$  at the same pressure level which is an improvement of about  $20 \%$  in pressure resistance.

In addition to borosilicate 3.3 fibers, test samples made of quartz glass were stored and tested in the same way. The characteristic data of these series are summarized in Table 22. Only small differences between the single test series are detectable. It can be seen

that all characteristic values increase under the influence of defined and constant air humidity.

Table 22: Characteristic test data of hollow quartz fibers stored at different air humidity with the dimensions  $d_o = 400 \mu\text{m}$ ,  $d_i = 300 \mu\text{m}$ ,  $s = 50 \mu\text{m}$

Air humidity $\varphi$ [%]	Min. burst pressure $p_{\min}$ [MPa]	Max. burst pressure $p_{\max}$ [MPa]	Form parameter $b$	Characteristic pressure $P$ [MPa]
New fibers	24.4	94.4	4.2	76.6
30.9	38.4	104.5	5.2	81.1
75.8	39.9	109.0	5.6	82.2

The calculated failure probabilities of quartz samples under the influence of air moisture are shown in Figure 38.

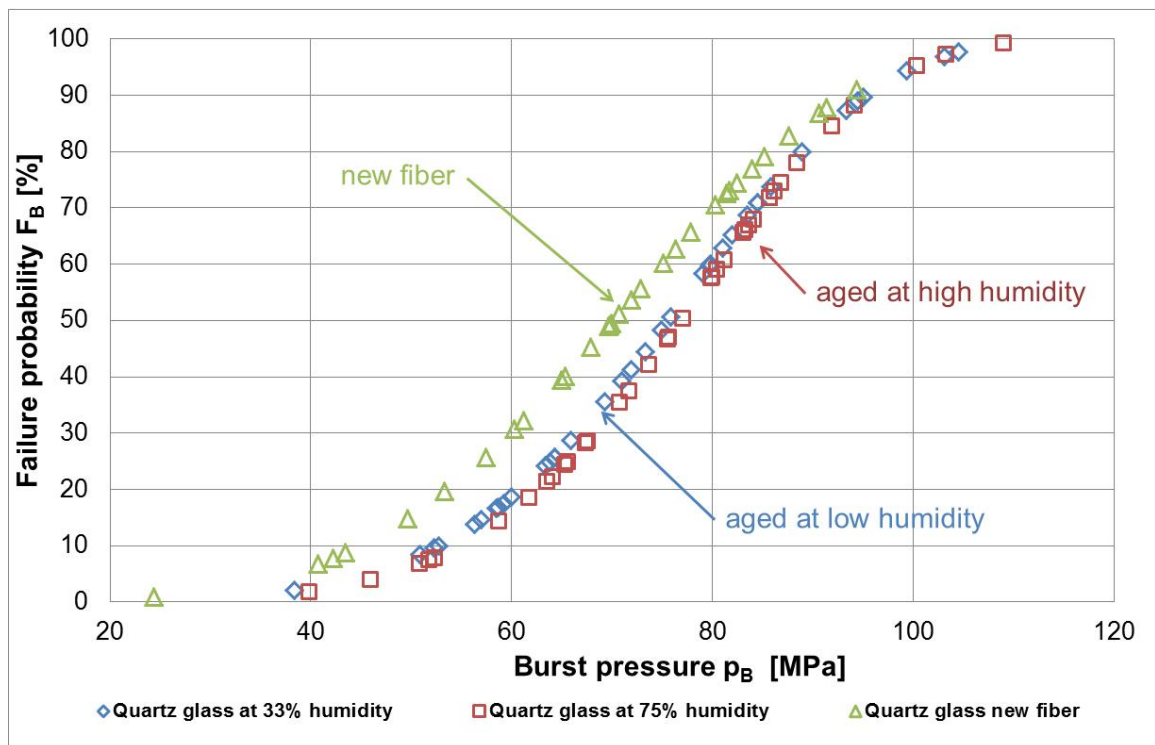


Figure 38: Influence of different humidity on failure probability and pressure resistance of hollow quartz glass fibers with the dimensions  $d_o = 400 \mu\text{m}$ ,  $d_i = 300 \mu\text{m}$ ,  $s = 50 \mu\text{m}$



The three different curves of quartz glass fibers exhibit nearly the same development. Thus, the graph of fibers stored at  $\varphi = 30.9\%$  superimpose this of test samples stored at  $\varphi = 75.8\%$ . At lower pressures, the graph of new hollow fibers deviates from the other two graphs due to the lower minimum burst pressure. At higher pressure values an approximation is observable.

The investigation of the influence of air moisture under non-loaded conditions with defined and constant air moisture and temperature conditions showed no considerable variations with comparable results within the different glass types. Nevertheless, an influence of the different atmosphere on the hollow fibers was observable especially for borosilicate fibers. The presence of air moisture in defined concentrations leads to the increase of the maximum burst pressure and the characteristic pressure  $P$  with simultaneous decrease of form parameter  $b$  and nearly constant minimum burst pressure. Water, even in small concentrations, forms a thin film on the surface of glass and leads to the dissolving of alkaline substances out of the glass network [97]. That chemical reaction can affect particular the surface characteristics in flaws [176].

The distribution of defects in or on the fibers seems to have an important role in that behavior. It can be assumed that the low burst pressures within each test series are caused by test samples with bigger or a high number of defects. Such defects led to stress peaks inside the fiber and caused the breakage. Consequently, test samples with higher burst pressures could exhibit smaller defects or, respectively, a lower number of defects. Hydrolytic reactions on the surface could have influenced the characteristics of the flaws especially of the smaller ones. The edges of defects could be rounded by the hydrolytic reaction on the surface and therefore possible stress peaks under inner pressure could be mitigated or removed [176]. Due to the constant air moisture the hydrolytic reaction featured a higher intensity than in alterable moisture [94]. The decreasing failure probability of samples stored at defined concentration at higher internal pressure in comparison to new fibers could be an indication for this assumption. Therefore borosilicate fibers with small flaws or a low number of defects could withstand higher pressures after being stored in constant air moistures. Bigger flaws were rounded and changed by the chemical reaction as well. Because of the size or the depth a positive influence were not possible.

Also the concentration of the air moisture had a positive influence on the pressure resistance of borosilicate fibers. Test samples stored in a relative air moisture of  $\varphi = 75.8\%$  exhibit lower values of failure probability at higher pressure than those stored at  $\varphi = 30.9\%$ . A higher concentration of water in the atmosphere or often alternating air

moisture benefits the dissolving of alkaline substances out of the network [94]. The edges might be rounded more and therefore the stress distribution at internal pressure is more regular and smoother.

Hydrolytic reaction can take place at all glasses featuring alkaline or earth alkaline substances. Quartz glass is made of pure silica without the addition of any substances. Consequently hydrolytic reaction could not take place on the surface of tested quartz glass fibers. Nevertheless, a comparable trend of increasing pressure resistance was detectable as seen at tests with the borosilicate 3.3 fibers. All characteristic data features higher values when being stored in defined air moisture before testing. Due to impurities in raw material only in traces the presence of water-soluble substances in quartz glass could be possible. In that case hydrolytic reaction might take place on the surface of tested quartz fiber while being stored. Especially in the range between  $p = 40$  MPa and  $p = 80$  MPa a meaningful increase of pressure resistance could be detected in Figure 38. As on the surface of borosilicate fibers a hydrolytic reaction could lead to the rounding of edges of possible flaws. The result can be the reduction of their decreasing influence on the pressure resistance.

Fibers of both materials borosilicate 3.3 and quartz showed a positive effect of air moisture on their pressure resistance under non-loaded conditions where hydrolytic reactions could originate the rounding of edges of surface flaws [176]. Defined and constant air moisture leads to the increase of the resistance against inner pressure. Thereby at higher concentration of air moisture that effect was even higher. Nevertheless, the effect was slightly low. The characteristic values of the test series within one type of glass are still close together. However, the difference of quartz and borosilicate 3.3 fibers was clearly shown. At a defined burst pressure of  $p_B = 80$  MPa fibers made of borosilicate 3.3 exhibit a failure probability of  $F_B = 30$  %. The failure probability of quartz fibers at same burst pressure reached a value of  $F_B = 80$  %. Hence, borosilicate fibers showed a significant higher resistance against inner pressure load in comparison to quartz fibers.

The results of this part of the thesis can be summarized as following:

- Borosilicate and quartz glass fibers with the dimensions  $d_o = 400 \mu\text{m}$ ,  $d_i = 300 \mu\text{m}$ ,  $s = 50 \mu\text{m}$  were tested after storing them for more than 1100 h without inner load in defined air moistures. The test results were compared to measured burst pressures determined with new fibers and are summarized in Table 23.
- Only slight differences under the given circumstances were detected. Hence, the pressure resistance of hollow fibers made of borosilicate or quartz glass was independent on the air moisture under non loaded conditions.
- The high chemical resistance of both glasses excluded possible decreasing effects on the pressure resistance by chemical reactions on the surface. Under non-loaded conditions hydrolytic reactions may even have a positive effect on the resistance against inner pressure by rounding and increasing the radius of surface cracks [94]. Arising stresses inside the material can be distributed more homogeneous and peaks will be reduced.
- Because of the higher burst pressure values independent on air moisture it can be concluded that under given circumstances borosilicate fibers exhibit a higher pressure resistance than those made of quartz.

Table 23: Pressure resistance development of glass fibers aged under the influence of different defined air humidity compared new tested fibers by reference to the characteristic pressure P

	Low air humidity $\varphi = 30.9 \%$	High air humidity $\varphi = 75.8 \%$
Borosilicate	Slightly increased	Slightly increased
Quartz	Increased	Increased

### 6.3 Pressure Resistance at Cyclic and Static Pressure Load

Different literature references give information about the degradation of the tensile strength or eventuation of breakage of containment glass not only by single high stress effects. Dynamic or static pressure load also can lead to reduction of resistance against inner pressure right up to collapse even at pressure load far below the critical stress. This circumstance can be affiliated to material fatigue due to glass corrosion in dilated nanoscale cracks and transformation of mechanical energy to surface energy by forming

new crack surfaces. A possible application of hollow glass fibers as hydrogen storage system deserves the study of the behavior under loaded conditions and possible degradation of pressure resistance due to fatigue.

Indeed, a slight influence of air moisture was shown in prior test series on the pressure resistance of hollow borosilicate or quartz glass fibers. But during the exposure of air moisture, the fibers were not loaded with pressure and hydrolytic reaction could take place especially on the fibers outer surface. Container glass which includes glass tubes and hollow fibers features different thermal and mechanical history of outer and inner surface. The history regarding the effect and reaction with air moisture is different as well. Therefore mostly the outer surface shows hydrolytic reaction further progressed than the inner surface [94]. The effect of hydrolytic reactions on the inner surface thereby is limited by the diffusion of humid air inside the container glass. The most important factor is the open end. In case of tested hollow glass fiber the open end is that small that the diffusion of humid air is degraded by a multitude. Hence, the impact of hydrolytic reactions on the inner surface is negligible in comparison to the effect on the outer surface.

Because of the fact that under loaded conditions stress corrosion could reduce the mechanical resistance of glass many times, the influence of different pressure load conditions were investigated.

### 6.3.1 Cyclic Pressure Load

Hollow fibers made of borosilicate and quartz glass were tested on the influence of air moisture under loaded conditions. Therefore, hollow fibers with the same dimensions as in investigation of air moisture influence ( $d_o = 400 \mu\text{m}$ ,  $d_i = 300 \mu\text{m}$ ,  $s = 50 \mu\text{m}$ ) were pressurized cyclic with gas whereby the number of cycles was defined to  $n_c = (10, 30, 50, 100)$  cycles. Two test gases, nitrogen as well as hydrogen, were used in different test series to compare the results to each other and determine the effect of these two gases on the pressure resistance of hollow glass fibers. After attainment of specific number of cycles the burst pressure of each single fiber was determined. The inner pressure of this investigation was fixed on  $p_{\text{cyclic}} = 50 \text{ MPa}$ . Here the characteristic pressure  $P$  of untreated quartz fibers  $P = 76.6 \text{ MPa}$  was set as reference value for quartz as well as borosilicate samples to ensure the same test conditions and a safety factor of 1.5 was considered.

A summary of distinctive test results of borosilicate fibers loaded with nitrogen is given in Table 24. As reference value the test results of borosilicate fibers were used tested with nitrogen without any cyclic load.

Table 24: Characteristic results of hollow borosilicate fibers ( $d_o = 400 \mu\text{m}$ ,  $d_i = 300 \mu\text{m}$ ,  $s = 50 \mu\text{m}$ ) loaded with nitrogen with different numbers of cycles with  $p_{\text{cyclic}} = 50 \text{ MPa}$

Number of cyclic loads	Min. burst pressure $p_{\text{min}}$ [MPa]	Max. burst pressure $p_{\text{max}}$ [MPa]	Form parameter $b$	Characteristic pressure $P$ [MPa]
0 (reference value)	61.9	114.2	7.3	89.3
10	74.8	145.9	6.8	113.9
30	75.8	122.9	9.9	107.8
50	66.9	146.2	5.6	97.8
100	68.8	140.0	8.1	103.1

The comparison of results of new fibers with those of cyclic loaded fibers points out a clear higher pressure resistance. The treatment of hollow fibers with 10 cycles of  $p_{\text{cyclic}} = 50 \text{ MPa}$  increases the pressure resistance. An enhancement of all pressure values of 25 % eventuates but the form parameter is slightly smaller. That is a result of the higher range between minimum and maximum burst pressure.

The load of 30 cycles with the defined internal pressure leads to comparable high pressure rates like the 10 cycle treatment. Here the maximum reached pressure value shows a small decrease which results in a smaller characteristic pressure  $P$  but a higher form parameter  $b$ . Higher cycle rates of 50 respectively 100 numbers of pressure loads lead to minimum burst pressure values comparable to the untreated fibers. However, the characteristic pressure  $P$  levels at 10 % above the untreated fibers and also the maximum pressures show significantly higher values.

The results of hollow borosilicate fibers tested with  $\text{H}_2$  as test gas as listed in Table 25 show a different behavior than those of fibers tested with  $\text{N}_2$ .

Here the resistance of test samples against inner pressurized hydrogen was determined as reference value and show a broad distribution between minimum and maximum burst pressure. This is confirmed by the low form parameter  $b = 4.8$ . Nevertheless, the high

characteristic pressure of  $P = 104.7$  MPa indicates a high pressure resistance. Test series exposed cyclic pressure loads of hydrogen reach higher minimum burst pressures. Though, the maximum burst pressures of these series lay under the related value of the reference series. Consequently, the measured pressure values follow a closer distribution and the form parameter  $b$  exhibit higher values. Therefore the resulting characteristic pressure  $P$  of cyclic treated test series only gains 90 % of the value of reference series. The comparison to samples tested with nitrogen shows a decreasing influence of cyclic pressure loads with hydrogen.

Table 25: Test results of borosilicate fibers ( $d_o = 400 \mu\text{m}$ ,  $d_i = 300 \mu\text{m}$ ,  $s = 50 \mu\text{m}$ ) loaded with hydrogen with different numbers of cycles with  $p_{\text{cyclic}} = 50$  MPa

Number of cyclic loads	Min. burst pressure $p_{\text{min}}$ [MPa]	Max. burst pressure $p_{\text{max}}$ [MPa]	Form parameter $b$	Characteristic pressure $P$ [MPa]
0 (reference value)	45.8	132.5	4.8	104.7
10	63.5	121.2	9.3	94.2
30	65.0	110.2	9.1	94.6
50	58.1	101.4	8.7	90.1
100	75.1	121.4	9.1	93.0

The same investigation was done with quartz glass fibers whereby similar developments could be detected by testing the fibers with nitrogen as shown in Table 26.

A treatment of 10 cycles with  $p_{\text{cyclic}} = 50$  MPa leads to an increase of characteristic pressure by the factor 1.25 which is a result of the narrower distribution of individual burst pressures and the resulting higher form parameter  $b = 7.2$ . An increase of cycles to 30 respective to 50 entails the same form parameter  $b$  but lower characteristic pressures  $P$ . Hence, the pressure values did not fall below the values of reference series without cyclic treatment. Outstanding is the form parameter  $b = 10.5$  of test series treated with 100 cycles of  $p_{\text{cyclic}} = 50$  MPa before determination of burst pressure. Even though the maximum burst pressure is comparable to test series with 50 cycles the higher minimum burst pressure leads to closer distribution of individual measured pressure values.

Table 26: Significant results of quartz fibers ( $d_o = 400 \mu\text{m}$ ,  $d_i = 300 \mu\text{m}$ ,  $s = 50 \mu\text{m}$ ) tested with nitrogen with different numbers of cyclic pressure load of  $p_{\text{cyclic}} = 50 \text{ MPa}$

Number of cyclic loads $n_c$	Min. burst pressure $p_{\text{min}}$ [MPa]	Max. burst pressure $p_{\text{max}}$ [MPa]	Form parameter $b$	Characteristic pressure $P$ [MPa]
0 (reference value)	24.2	94.4	4.2	76.6
10	60.2	109.9	7.2	95.6
30	53.2	107.7	7.3	84.0
50	58.0	117.9	7.2	85.9
100	67.7	115.2	10.5	89.9

The data of hollow fibers made of quartz glass tested with hydrogen are listed in Table 27. Here comparable characteristic pressure can be seen for all test series. The deviations between the different numbers of cyclic pressure load are only small. That development is valid for all characteristic data listed in this table.

Table 27: Distinct test data of quartz fibers ( $d_o = 400 \mu\text{m}$ ,  $d_i = 300 \mu\text{m}$ ,  $s = 50 \mu\text{m}$ ) tested with hydrogen and different numbers of pressure load cycles

Number of cyclic loads $n_c$	Min. burst pressure $p_{\text{min}}$ [MPa]	Max. burst pressure $p_{\text{max}}$ [MPa]	Form-parameter $b$	Characteristic pressure $P$ [MPa]
0 (reference value)	57.8	108.7	7.7	84.7
10	54.9	117.1	7.3	83.3
30	58.3	102.3	8.9	85.4
50	61.5	100.7	7.2	79.7
100	58.7	97.3	8.3	85.5

A minimum of 30 test samples of each series was tested to generate a convincing Weibull evaluation. Due to the lower pressure resistance of hollow quartz fibers here massive difficulties occur. During the cyclic pressure treatment with nitrogen a multitude of fibers collapsed under the influence of pressure of  $p_{\text{cyclic}} = 50 \text{ MPa}$  or below before

reaching the defined number of pressure cycles. The test series with 50 and 100 cycles were especially involved. Test series with H<sub>2</sub> leads to even more difficulties so the determination of pressure resistance after 100 cycles was aborted after 10 determined burst pressure values.

The development of resistance against inner pressure under the influence of cyclic pressure and different test gases is displayed in Figure 39 whereby the characteristic pressures are plotted as an important parameter of Weibull evaluation of each tested series against the number of pressure cycles.

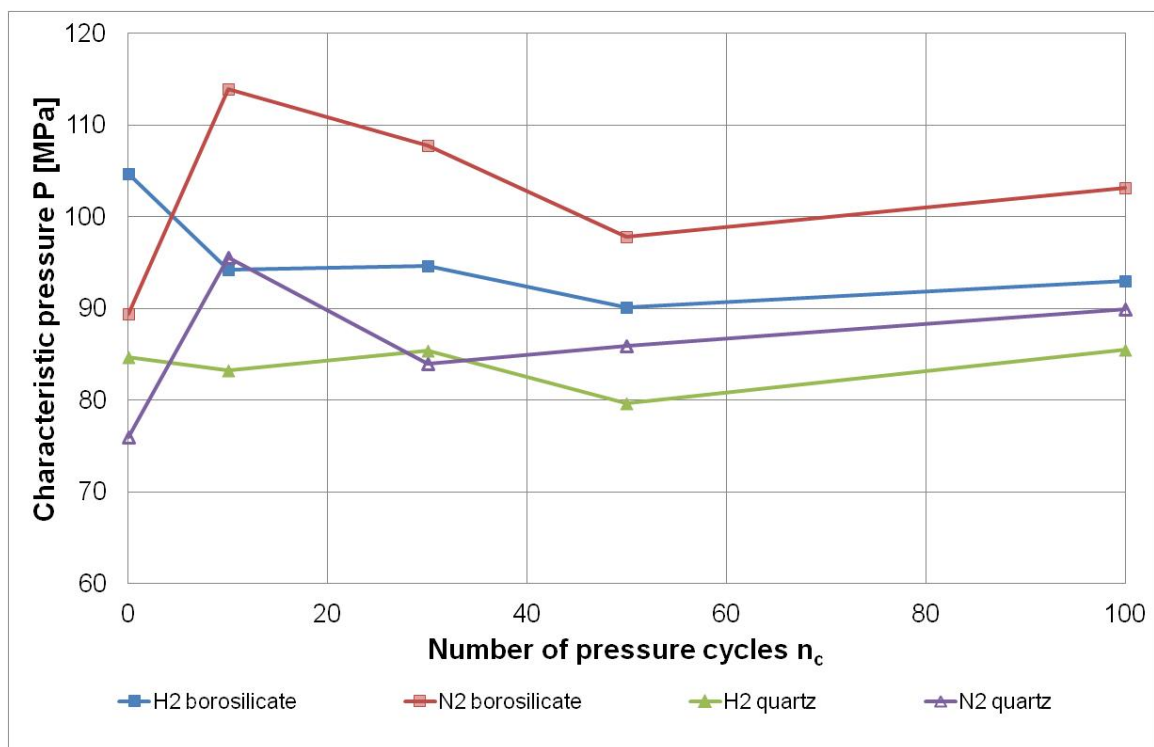


Figure 39: Characteristic pressures of hollow quartz respective borosilicate fibers (both  $d_o = 400 \mu\text{m}$ ,  $d_i = 300 \mu\text{m}$ ,  $s = 50 \mu\text{m}$ ) after cyclic treatment of  $p_{\text{cyclic}} = 50 \text{ MPa}$  with the test gases nitrogen and hydrogen

Plotting the characteristic pressure  $P$  against the number of pressure cycles shows the development of pressure resistance under the influence of N<sub>2</sub> and H<sub>2</sub> at cyclic loads. Borosilicate fibers tested and being loaded 10 times with N<sub>2</sub> show an initial increase of pressure resistance of 30 %. Hereafter, the characteristic pressure decreases steadily. At 50 and 100 cycles the characteristic reaches comparable values with only a small deviation. Nevertheless, all determined characteristic pressures lie above the characteristic pressure of the reference series.



The pressure resistance of borosilicate fibers under the influence of hydrogen is clearly different. Without any cyclic pressure treatment the pressure resistance is higher than those determined with  $N_2$  by the factor 1.2. But with the exposure of 10 times cyclic load the characteristic pressure decreases significantly below the value of hollow borosilicate fibers tested with nitrogen. Furthermore, a similar development like borosilicate tested with nitrogen is detectable. A minimum of characteristic pressure is reached at 50 times of pressure load. The further increase of the number of cycles leads to a slight increase of characteristic pressure but remains under the reference value tested without cyclic load.

Setting focus on hollow quartz fibers charged with nitrogen, the treatment with 10 cycles of  $p_{\text{cyclic}} = 50$  MPa leads to an initial increase of pressure resistance. After that, the resistance decreases again at 30 cycles but does not fall below the value of untreated new hollow fibers. Further increase of numbers of cycles results in slightly increasing pressure resistance.

Like borosilicate tested with hydrogen also quartz fibers charged with hydrogen exhibit a higher characteristic pressure. The exposure of cyclic load here leads only to small deviations of pressure resistance. Therefore, the graph shows a nearly constant level of pressure resistance. Due to the initial increase of quartz fibers tested with nitrogen the characteristic pressures  $P$  of hollow fibers charged with hydrogen exhibit lower resistance against inner pressure load.

The test series with different air moistures under non loaded conditions showed negligible influence of even high air moisture. But studies about the cyclic loading behavior of glass bars showed a heavy impact on their mechanical resistance and loadability. With rising number of cycles, the loadability and resulting tensile strength of test samples decreased significantly [158], whereby the development of the tensile strength plotted against the number of cycles displayed a steady almost linear decrease.

Nevertheless, the results of cyclic load of hollow glass fibers tested with inner pressure show different behavior. The inner load entails the opening of nanoscale flaws on the outer surface of the fiber where air moisture could intrude and leads to stress corrosion cracking by hydrolytic reactions [159], [160] which cause the fatigue of the material. But the results do not show a steady decrease in pressure resistance. Contrary an initial increase of resistance eventuates by the use of nitrogen as test gas. Here a possible resistance-reinforcing effect of nitrogen could be the trigger. The treatment of different steel alloys with nitrogen rich gases under the influence of heat is called nitriding and leads to the hardening of the surface [159], [162], [163]. The effect of surface hardening

by implantation of nitrogen ions was also detectable for different glasses [164]. Comparable effects are recognizable at the exposure of the inner surface to nitrogen. Therefore, it could lead to the initial increase of pressure resistance of borosilicate as well as quartz fibers. Hence, nitrogen can intrude in possible flaws on inner surface and an adsorption of nitrogen could lead to an increase of the pressure resistance. But the following decrease of pressure resistance can be explained by acting fatigue due to hydrolytic reactions in the open flaws. The higher number of inner pressure loads cause an increased number of opening of defects on outer surface where air moisture is able to react with the glass and leads to a degradation of the resistance against inner pressure. The interaction of a reinforcing effect of nitrogen and a decreasing effect of hydrolytic reaction inside of the defects of outer surface results in a nearly constant pressure resistance at 50 and 100 cycles which is above the value of new fibers without cyclic pressure treatment.

The pressure resistance of new fibers independent of the material is higher by using hydrogen. In that only short time of contact between inner surfaces and hydrogen adsorption of hydrogen is able to occur, as in the case of nitrogen. Due to the smaller size of molecular hydrogen, the velocity of that process is much higher. Thus the intrusion of hydrogen in surface flaws leads to a short-time increase of mechanical resistance caused by bracing the chemical structure of glass which only exists in short-range order. Thus, blemishes which even occur in pure quartz glass are stabilized and the resistance against inner pressure thereby is shortly raised. Due to the chemical relatives of hydrogen to water and air moisture, the effects of hydrogen on the mechanical resistance of glass should be the same. Hydrogen is in contact with the inner surface of the fiber so possible hydrolytic reactions could not only act on outer surface defects but also at inner surface defects. However, a significant degradation of pressure resistance is only detectable for borosilicate fibers. Quartz fibers exhibit nearly constant pressure resistance which could be a result of the high chemical resistance of quartz glass.

Additionally, it is clearly recognizable that the development of characteristic pressures of quartz fibers is comparable to the graphs of borosilicate if the same test gas is used during determination of burst pressures. Nonetheless, a serious difference in the pressure level is clearly detectable and point out again the lower pressure resistance of quartz glass fibers in direct comparison to borosilicate 3.3. It is assumed that the lower pressure resistance is influenced not only by the air moisture and its effect under loaded conditions but also by the influence of the used test gas. However, quartz glass shows

significantly lower resistance at inner pressure load, wherefore only borosilicate was chosen as material for the test samples of further test series.

As result of the cyclic pressure study it can be summarized that:

- Dynamic internal pressure load on hollow fibers made of borosilicate and quartz glass with varied numbers of cycles led to remarkable results.
- When nitrogen was used as test gas a significant initial increase of characteristic pressure  $P$  was detected for both borosilicate and quartz glass samples. Afterwards, the pressure resistance decreased again but remained at levels above the resistance against inner pressure of new “unstressed” samples. It can be assumed that higher cycle numbers led to the effect of stress corrosion cracking by hydrolytic reactions on the outer surface of the fibers due to air moisture [159] which resulted in decreasing pressure resistance. The diffusion of nitrogen in the glass material was advanced by increasing number of cycles and counters the decreasing influence of hydrolytic reactions. Equilibrium seemed to be adjusted as nearly constant characteristic pressures  $P$  were determined for each material.
- Hydrogen as test gas effected an initial decrease of pressure resistance of borosilicate fibers but hereafter nearly constant resistance was recognized. Test samples made of quartz glass showed no significant deviations in pressure resistance which indicated negligible effects of hydrogen. Here the theoretical high chemical resistance was relevant. The initial pressure resistance of hollow glass fibers independent on material was higher when tested with hydrogen. The coefficient of diffusion in the material exhibited a distinct higher value wherefore it can be concluded that a stiffening of the network was reached faster compared to the influence of nitrogen.
- Again, a lower pressure resistance of quartz glass fibers than this of borosilicate fibers was detected.

### 6.3.2 Static Pressure Load

Besides the influence of cyclic loads, also the effect of long term static load on the pressure resistance of glass fibers was investigated. Here only test samples made of borosilicate were tested. Series with quartz glass fibers were not carried out due to the results of prior tests. Thus, hollow quartz fibers showed in most cases significant lower resistance against inner pressure load as borosilicate fibers.

The test samples were loaded up with an inner pressure of  $p_{\text{static}} = 50$  MPa. The same inner pressure was set for the investigation of cyclic pressure influence and to ensure comparable results no change of inner pressure was done. The inner pressure was kept constant for different periods of time which are defined to  $t_{\text{static}} = (300; 1800; 3600)$  s. After completion of time period the individual burst pressure was determined.

At first the effect of static pressure was determined by using nitrogen as test gas. The results listed in Table 28 are related to borosilicate fibers tested with different time periods under the influence of nitrogen. Evident is the constant increase of minimum burst pressure with increasing the time period of pressure load.

Table 28: Distinct test results of borosilicate fibers ( $d_o = 400 \mu\text{m}$ ,  $d_i = 300 \mu\text{m}$ ,  $s = 50 \mu\text{m}$ ) loaded with static pressure of  $p_{\text{static}} = 50$  MPa with nitrogen for different time periods before determining the burst pressures

Time period $t_{\text{static}}$ [s]	Min. burst pressure $p_{\text{min}}$ [MPa]	Max. burst pressure $p_{\text{max}}$ [MPa]	Form parameter $b$	Characteristic pressure $P$ [MPa]
0 (reference value)	61.9	114.2	7.2	89.3
300	67.6	137.7	8.0	106.0
1800	73.1	130.0	8.1	105.0
3600	82.8	129.3	9.6	112.0

The following Weibull statistics shows that the form parameter  $b$  exhibits a constant increase by rising duration of static pressure. This is an indicator for closer distributions of burst pressures and is confirmed by the maximum reached burst pressures. Here the development follows after an initial significant increase of around  $\Delta p = 20$  MPa but then a steady decrease. Thus, the spread of measured values decreases. The resulting characteristic pressure as indicator of the resistance against inner pressure increases initially by the factor 1.2 at a treatment of  $t_{\text{static}} = 300$  s with nitrogen. At  $t_{\text{static}} = 1800$  s duration time no change in pressure resistance is detectable though after  $t_{\text{static}} = 3600$  s of load the pressure resistance increases again.

The test series of static load under the influence of hydrogen results in complete different development of distinct values as listed in Table 29.

Table 29: Distinct test results of borosilicate fibers ( $d_o = 400 \mu\text{m}$ ,  $d_i = 300 \mu\text{m}$ ,  $s = 50 \mu\text{m}$ ) loaded with static pressure of  $p_{\text{static}} = 50 \text{ MPa}$  with hydrogen for different time periods before determining the burst pressures

<b>Time period <math>t_{\text{static}}</math> [s]</b>	<b>Min. burst pressure <math>p_{\text{min}}</math> [MPa]</b>	<b>Max. burst pressure <math>p_{\text{max}}</math> [MPa]</b>	<b>Form parameter <math>b</math></b>	<b>Characteristic pressure <math>P</math> [MPa]</b>
0 (reference value)	45.8	132.5	5.3	104.7
300	77.3	128.9	8.1	114.7
1800	80.6	129.2	11.1	108.5
3600	62.5	123.7	8.4	95.5

The reference value already shows a significant high spread between minimum and maximum burst pressure value which is the reason for a low form parameter. Nonetheless, the characteristic pressure  $P$  exhibits a higher value than fibers tested with nitrogen because of the high number of measured pressures in high pressure regions. The effects of  $t_{\text{static}} = 300 \text{ s}$  of inner pressure is an increase of form parameter  $b$  due to significantly higher minimum burst pressures. The closer distribution of measured data leads to an increase of characteristic pressure  $P$  although the maximum burst pressure is smaller than those of the reference test series. Admittedly, the form parameter  $b$  of  $t_{\text{static}} = 1800 \text{ s}$  of static load with hydrogen results in an obviously high value, hence, the measured data are close together. Nonetheless, the decreased characteristic pressure  $P$  shows a displacement of burst pressures to a lower level. The prolongation of duration time to  $t_{\text{static}} = 3600 \text{ s}$  again leads to a decrease of characteristic pressure  $P$ . Here consistently lower pressure indicates a lower pressure resistance of the hollow glass fibers.

Besides the influence nitrogen and hydrogen had on the static fatigue of fibers of borosilicate, the effect of static pressure load with nitrogen and subsequent determination of burst pressure with hydrogen was tested. That test series was carried out on the basis of test results of cyclic pressure treatment which showed a reinforcing impact on the pressure resistance of the fibers.

Table 30: Distinct test results of borosilicate fibers ( $d_o = 400 \mu\text{m}$ ,  $d_i = 300 \mu\text{m}$ ,  $s = 50 \mu\text{m}$ ) loaded up with static pressure of  $p_{\text{static}} = 50 \text{ MPa}$  with nitrogen for different time periods; burst pressures were determined by using hydrogen

<b>Time period <math>t_{\text{static}}</math> [s]</b>	<b>Min. burst pressure <math>p_{\text{min}}</math> [MPa]</b>	<b>Max. burst pressure <math>p_{\text{max}}</math> [MPa]</b>	<b>Form parameter <math>b</math></b>	<b>Characteristic pressure <math>P</math> [MPa]</b>
0 (reference value)	45.8	132.5	5.3	104.7
300	74.9	121.1	10	107.4
1800	65.8	119.2	9.8	102.2
3600	75.8	140.9	9	109.1

The reference value is the burst pressure test series with hydrogen. A treatment with  $p_{\text{static}} = 50 \text{ MPa}$  of nitrogen before determining the burst pressures with hydrogen causes an increase of minimum but a decrease of maximum pressure value. That behavior is comparable to the hollow fibers tested only with hydrogen. The Weibull form parameter rises due to the closer distribution and results in a higher characteristic pressure. Moreover, the prolongation of time period leads to unsteady development of test results. A decrease of pressure resistance is detectable at a time period of 30 minutes nitrogen whereas the exposure of nitrogen over  $t_{\text{static}} = 3600 \text{ s}$  results in an improvement of the measured pressure values.

A comparison and visualization of the development of pressure resistance of borosilicate fibers is displayed in Figure 40. The characteristic pressure  $P$  is plotted against the time period  $t_{\text{static}}$  and illustrates the resistance against inner pressure influenced by the impact of different gasses at static load.

The characteristic pressure represents the pressure with a failure probability  $F_B = 63.2 \%$  and, hence, indicates the inflection point of cumulated failure probability if Weibull distribution is used as an evaluation instrument.

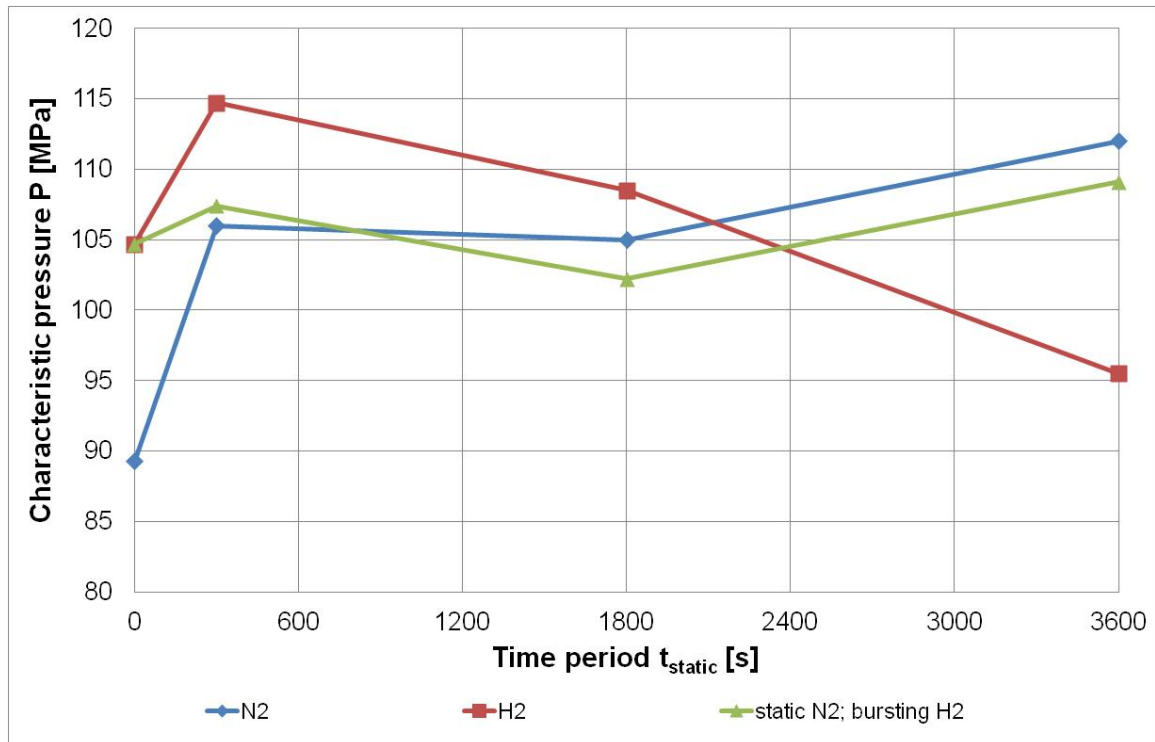


Figure 40: Characteristic pressures  $P$  of fibers made of borosilicate glass ( $d_o = 400 \mu\text{m}$ ,  $d_i = 300 \mu\text{m}$ ,  $s = 50 \mu\text{m}$ ) plotted against time period of static pressure load with  $p_{\text{static}} = 50 \text{ MPa}$  and test gases hydrogen and nitrogen

The higher initial pressure resistance of fibers tested with hydrogen is clearly detectable. As a result of the same reference values as used for the cyclic investigation, the same explanation is valid for that behavior. The adsorption of molecular hydrogen in flaws of inner surface leads to a bracing of chemical structure of glass due to a possible incorporation of molecular hydrogen. The size effect accelerates this process because of the low size of hydrogen molecules. The effect of static treatment of hydrogen over 300 seconds leads to a significant pressure resistance increase. It can be assumed that molecular hydrogen intrudes in defects of inner surface and affects improvement. Hydrogen diffusion into the glass material can be neglected or is not progressed far enough due to the short time period of hydrogen exposure to the glass and the temperature dependency of diffusion coefficient of hydrogen in glass. Nevertheless, the increasing effect on the pressure resistance is not that distinct as the effect of nitrogen. Different investigations on the field of hydrogen diffusion in glass were carried out. Thereby a proportional behavior of temperature and diffusion coefficient could be observed. With increasing temperature the diffusion coefficient increases as well [60] - [62], [165]. For a temperature of  $T = 23 \text{ }^\circ\text{C}$  the diffusion coefficient of hydrogen in glass was determined to  $D = 0.093 \times 10^{-14} \text{ m}^2 \text{ s}^{-1}$  [62] and increases to  $D = 0.44 \times 10^{-14} \text{ m}^2 \text{ s}^{-1}$  at

$T = 50\text{ }^{\circ}\text{C}$  [62]. Also possible hydrolytic reactions which are blamed for the decrease of mechanical resistance at static and cyclic load could not effect high crack propagation in that short time period. Further increase of exposure time to pure hydrogen results in a steady decrease of the pressure resistance. In this case, a diffusion of hydrogen in the glass material cannot be excluded in discussions of influences. Also the influence of fatigue, caused by the ambient conditions on the outer surface, increases noticeable.

The influence of nitrogen causes lower initial resistance against inner pressure load for new fibers but also a massive increase of pressure resistance by increasing the time of exposure. At  $t_{\text{static}} = 300\text{ s}$  of pressure load with  $p_{\text{static}} = 50\text{ MPa}$  of nitrogen the increase of the pressure resistance is more distinct than that of fibers treated with hydrogen for the same time. It can be assumed that flaws enable the intrusion of nitrogen in the structure and imperfections (points of disconnection) in low-range order and could be closed by it. The resistance against the inner pressure is increased by that stiffening of chemical structure. The effect remains the same at prolongation of exposure time but the impact is much smaller which is shown by constant or only slight increase of the pressure resistance by increasing the time period to  $t_{\text{static}} = 1800\text{ s}$  and  $t_{\text{static}} = 3600\text{ s}$  respectively. Here again, an increasing effect on resistance against inner pressure of the fibers is recognizable.

Treating the fibers with nitrogen for a specific time period before load them with hydrogen until the collapse eventuates causes a similar development of the characteristic pressure  $P$  against the time like at treatment only with nitrogen. Indeed the initial point is higher. That is a result of using the same reference series as for fibers treated with hydrogen. The pressure resistance after  $t_{\text{static}} = 300\text{ s}$  of nitrogen treatment and subsequently bursting with hydrogen is comparable to the resistance of fibers treated and burst with nitrogen. The adsorption of nitrogen or even occurring diffusion leads to that similar resistance against inner pressure. Hydrogen leads to higher pressure resistance due to the higher process velocity of accretion. Hereafter the pressure resistance falls below the graph of nitrogen treated fibers at  $t_{\text{static}} = 1800\text{ s}$  of static load. But from there the pressure resistance rises again with same gradient as the graph of nitrogen treated fibers. Summarized the deviations of pressure resistance of hollow borosilicate fibers burst with hydrogen but treated with nitrogen are very small. Hence, it can be assumed that during the treatment with nitrogen over different time periods a layer is formed and slow down the diffusion of hydrogen. That process is comparable to the effects of shielding occurring under the influence of argon on different metal alloys [166]. Consequently, the fibers exhibit the resistance against inner pressure of fibers burst with nitrogen while the determination of burst pressure is carried out with



hydrogen as test gas. The occurring degradation with prolongation of time period of inner pressure load under the influence of pure hydrogen can be avoided.

Against the results published in different references [158], [167] - [171], the influence of cyclic and static pressure load did not lead to a degradation of pressure resistance of tested fibers in general. The influence of inner pressure load effects a modification of mechanical resistance but the used glass material as well as the used test gas causes partly significant differences.

It can be summarized that the determined pressure resistance of quartz glass is smaller than of hollow borosilicate fibers due to the high purity of quartz glass the opposite can be assumed. Nevertheless, the influence of cyclic loaded hydrogen on the pressure resistance of quartz glass fibers is negligible within the measuring inaccuracy.

Hollow fibers made of borosilicate glass exhibit higher pressure resistance but the influence of hydrogen is more distinct. Both static and cyclic pressure loads thus causes decrease of pressure resistance. However, the treatment of fibers with nitrogen is able to avoid the influence of hydrogen on the resistance against inner pressure.

The results of the study of the influence of static load can be summarized as following:

- The pressure resistance of borosilicate fibers was tested with different gases under the influence of static pressure load of different time periods.
- Pure hydrogen led to initial higher pressure resistance followed by an increase of characteristic pressure. Static loads for extended time periods resulted in significant decrease of pressure resistance. Hence, the decreasing effect of hydrogen on the pressure resistance of borosilicate fibers was proven and seemed to be reinforced by glass corrosion caused by open surface flaws and intruding air humidity.
- A permanent load of test samples made of borosilicate glass showed a positive effect of nitrogen on the pressure resistance. Static load of nitrogen led to initial increase of pressure resistance like the cyclic treatment and also to further increase by extending the time durations for inner loads.
- A comparable behavior was observed for hollow fibers which were treated with nitrogen for a specific time period and afterwards loaded up with hydrogen until the collapse eventuated. It can be assumed that diffusion of nitrogen in the material took place during static treatment and the introducing amount of hydrogen during the burst pressure test was reduced massively.

#### 6.4 Impact of Dimension Variations on the Pressure Resistance

The investigation of solid glass fibers and rods by Griffith showed an influence of diameter and age on the tensile strength of test samples [7]. The mechanical resistance of glass fibers of different dimensions and ages were determined in tensile tests and compared to each other. Thereby the decrease of diameter led to an increase of the measured tensile strength which is attributed to a severely reduced probability of defects per defined sample length at decreased sample diameter.

Hence, in theory, the mechanical resistance and loadability of glass fibers normalized on the cross section will increase with decreasing diameter. This assumption is based on the investigation of Griffith [7]. The effect of reduced defect probability should also be verifiable for hollow fibers and should show similar characteristics also at pressure resistance tests.

Therefore different test series were carried out with hollow fibers made of borosilicate glass to investigate the influence of dimensions. Based on the results of test series carried out with fibers made of different glass materials borosilicate glass were chosen as material for further tests.

##### 6.4.1 Fixed Ratio of Outer to Inner Diameter

In a first investigation the influence of wall thickness on resistance against internal pressure test samples with three different ratios of outer diameter to inner diameter ( $d_o / d_i$ ) were tested. The diameter ratios can also be given as free space FS in percent which describe the open area of the cross section of a single fiber in radial direction and is calculable by:

$$FS = \left( \frac{d_i}{d_o} \right)^2 * 100 \quad (6.1).$$

The fixed diameter ratios were specified to

1.  $d_o / d_i = 1.33$  (FS = 56 %);
2.  $d_o / d_i = 1.25$  (FS = 64 %);
3.  $d_o / d_i = 1.15$  (FS = 75 %).

For each of these ratios at least eight different wall thicknesses were tested. The dimensions of all test series are listed in Table 31. It can be seen that a variation of wall thickness led to a variation of outer and as well as of the inner diameter due to the fixed

diameter ratio and free space. Therefore, fibers with highest wall thickness exhibit also the largest outer and inner diameter.

Table 31: Specifications of tested borosilicate hollow fibers with respect to  $d_o / d_i$  ratio, each series has a consecutive number independent on diameter ratio

Serial No.	Diameter Ratio	outer diameter $d_o$ [ $\mu\text{m}$ ]	inner diameter $d_i$ [ $\mu\text{m}$ ]	wall thickness $s$ [ $\mu\text{m}$ ]
1	1.33	300	225	37.5
2		350	263	43.5
3		400	300	50.0
4		450	338	56.0
5		750	563	93.5
6		1,400	1,050	175.0
7		1,650	1,236	207.0
8		2,300	1,725	287.5
9	1.25	150	120	15.0
10		200	160	20.0
11		250	200	25.0
12		300	240	30.0
13		370	296	37.0
14		500	400	50.0
15		750	600	75.0
16		950	760	95.0
17		1,500	1,200	150.0
18	1.15	300	263	18.5
19		350	303	23.5
20		600	520	40.0
21		650	563	43.5
22		860	745	57.5
23		1,000	867	66.5
24		2,000	1,730	135.0
25		3,750	3,250	250.0

A summary of the test results of fibers with fixed diameter ratio of  $d_o / d_i = 1.33$  is listed in Table 32.

Table 32: Distinctive test results of borosilicate fibers with different wall thicknesses and fixed diameter ratio of  $d_o / d_i = 1.33$

Serial No.	Dimensions ( $d_o$ ; $s$ ) [ $\mu\text{m}$ ]	Min. burst pressure $p_{\min}$ [MPa]	Max. burst pressure $p_{\max}$ [MPa]	Form parameter $b$	Characteristic pressure $P$ [MPa]
1	300; 37.5	30.0	107.6	3.1	48.3
2	350; 43.5	53.7	119.6	6.1	103.2
3	400; 50.0	55.1	124.5	6.6	106.8
4	450; 56.0	52.0	132.5	5.3	102.5
5	750; 93.5	37.7	97.7	4.3	69.4
6	1,400; 175.0	33.7	69.6	7.5	53.6
7	1,650; 207.0	26.8	60.1	6.1	47.8
8	2,300; 287.5	19.6	52.9	4.3	42.8

It can be seen that the distinctive pressure values increase at first at increasing the wall thickness from  $s = 37.5 \mu\text{m}$  of serial number 1 to  $s = 50 \mu\text{m}$  of serial number 3 whereby the characteristic pressure  $P$  rises significantly by the factor 2.2. The form parameter  $b$  is doubled as well as at the first two wall thickness and diameter increases but the maximum burst pressure  $p_{\max}$  is only raised by the factor  $d_o / d_i = 1.15$ . That development is a clear indicator for a narrower distribution of burst pressures and therefore failure probability. The further increase of wall thickness accompanied by increase of diameter leads to a recurrence decline of the characteristic pressure  $P$  and the form parameter  $b$ . Also the minimum and maximum burst pressures show consentaneous decreasing values. The only exemption is the maximum burst pressure of serial number 4 which shows an enhancement in comparison to serial number 3.

Table 33 summarizes the test results of minimum burst pressure, maximum burst pressure, form parameter  $b$  and characteristic pressure  $P$  of test series with fixed diameter ratio of  $d_o / d_i = 1.25$ .

Table 33: Distinctive test results of borosilicate fibers with different wall thicknesses and fixed diameter ratio of  $d_o / d_i = 1.25$

Serial No.	Dimensions ( $d_o$ ; $s$ ) [ $\mu\text{m}$ ]	Min. burst pressure $p_{\min}$ [MPa]	Max. burst pressure $p_{\max}$ [MPa]	Form parameter $b$	Characteristic pressure $P$ [MPa]
9	150; 15.0	40.2	91.5	7.2	68.8
10	200; 20.0	47.3	88.3	7.0	70.5
11	250; 25.0	54.2	104.9	7.4	84.1
12	300; 30.0	29.4	112.3	4.3	90.4
13	370; 37.0	51.9	100.4	6.5	82.2
14	500; 50.0	34.5	101.2	4.6	71.9
15	750; 75.0	21.9	64.2	4.4	50.5
16	950; 90.0	27.3	64.3	5.2	49.4
17	1500; 150.0	19.7	52.1	4.7	41.3

Again, a first increase of distinctive pressure values is recognizable at increasing wall thickness. The values of maximum burst pressure and characteristic pressure show a continual rise from serial number 9 to serial number 12. The Weibull form parameters of these test series are similar. An outstanding test series represents serial number 12. Here the characteristic pressure  $P$  as well as the maximum burst pressure reaches their maximum out of all test series with diameter ratio of  $d_o / d_i = 1.25$ . But the minimum burst pressure shows an explicit lower value. Hence, the form parameter is obvious smaller than these of serial number 9 to 11 due to the high spread between minimum and maximum reached burst pressure. Nevertheless, serial number 12 with a wall thickness of  $s = 30 \mu\text{m}$  constitutes an inflection point of the pressure resistance. Thereby, another increase of wall thicknesses leads to the decrease of the distinctive pressure values and indicates a reduction of pressure resistance.

The results of diameter ratio  $d_o / d_i = 1.15$  exhibit a different development of distinctive pressure values, listed in following table.

Table 34: Distinctive test results of borosilicate fibers with different wall thicknesses and fixed diameter ratio of  $d_o / d_i = 1.15$

Serial No.	Dimensions ( $d_o$ ; $s$ ) [ $\mu\text{m}$ ]	Min. burst pressure $p_{\min}$ [MPa]	Max. burst pressure $p_{\max}$ [MPa]	Form-parameter $b$	Characteristic pressure $P$ [MPa]
18	300; 18.5	18.4	71.1	4.1	43.9
19	350; 23.5	17.6	72.5	4.1	62.3
20	600; 40.0	17.6	46.4	5.6	33.7
21	650; 43.5	31.4	111.2	5.0	67.0
22	860; 57.5	16.2	40.7	5.5	32.7
23	1,000; 66.5	12.6	41.4	5.1	30.7
24	2,000; 135.0	9.7	29.5	4.9	21.9
25	3,750; 250.0	10.3	20.8	6.2	16.0

Like the larger diameter ratios a first increase of characteristic pressure  $P$  by the factor of almost 1.5 although the form parameter  $b$  of serial number 18 and 19 as well as their minimum and maximum burst pressure are nearly the same. Therefore, it shows that the majority of measured pressure values of serial number 19 were in a higher pressure range than these of serial number 18. Furthermore, at serial number 20 the characteristic pressure  $P$  decreased whereby the minimum burst pressure is comparable to serial number 18 and 19. Due to the obviously lower maximum burst pressure the resulting pressure resistance of this series is decreased. This progressive decrease of pressure resistance could be verified by further increase of wall thickness up to the largest diameter. Thus, the decrease of pressure resistance is not only indicated by the decrease of the characteristic pressure  $P$  but also by the reduction of minimum and maximum burst pressure values. The form parameters of all test series are similar and exhibit only small deviations. However, the development is interrupted by serial number 21 with a wall thickness of  $s = 43.5 \mu\text{m}$  whereby an increase of all pressure values indicates an improvement of resistance against internal pressure at this wall thickness. Nevertheless, it remains at this single outlier.

A plot of the characteristic pressure against the wall thickness given in Figure 41 elucidates the development of the resistance against internal pressure while increase of wall thickness.

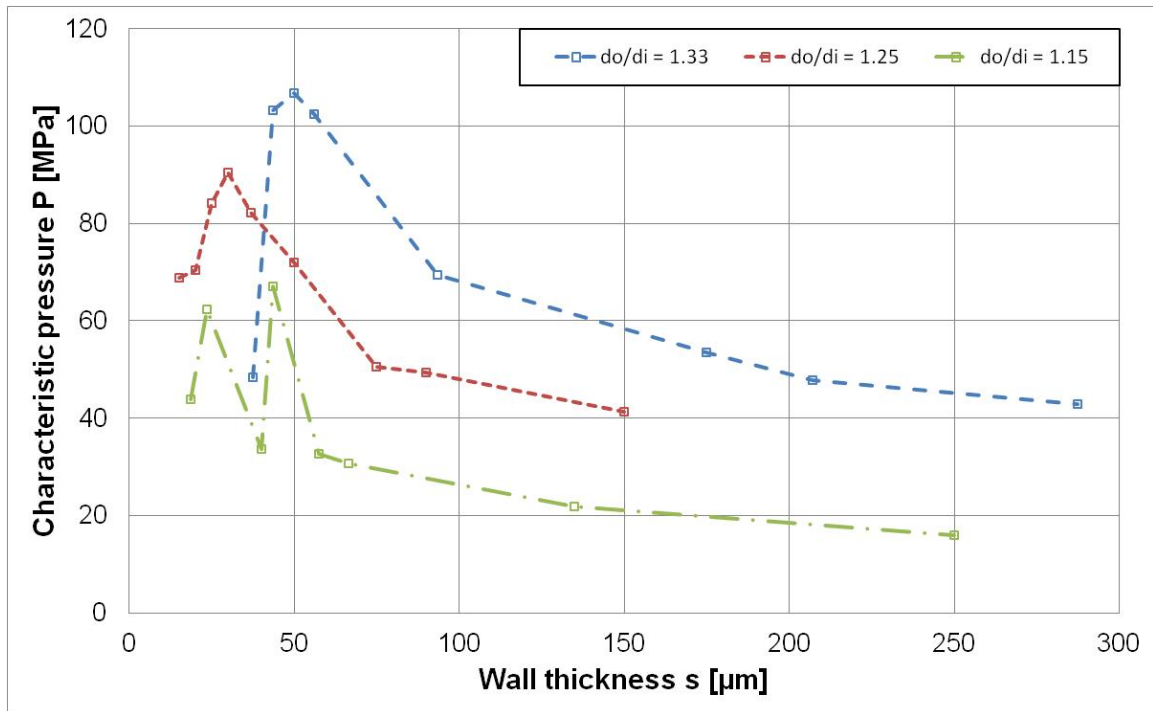


Figure 41: Characteristic pressure  $P$  for hollow borosilicate fibers with different fixed diameter ratios plotted against the corresponding wall thickness  $s$

Thereby the characteristic pressure  $P$  is an important Weibull parameter and gives crucial information about the inflection point of failure probability distribution. Here the failure probability reaches a value of  $F_B = 63.2\%$  and exhibits the step of the optimal function. Additionally, information about the position of the graph in the failure probability diagram can be identified from the characteristic pressure.

What is clear to see is the initial increase of characteristic pressure  $P$  at wall thickness decrease for all three diameter ratios. The highest characteristic pressures were reached at wall thicknesses between  $s = 30\ \mu\text{m}$  and  $s = 50\ \mu\text{m}$ . Moreover, further enhancement of wall thickness leads to reduced resistance against internal pressure. Important to know is the development of diameter ratio  $d_o / d_i = 1.15$  between  $s = 23.5\ \mu\text{m}$  and  $s = 43.5\ \mu\text{m}$  wall thickness. Here, after the initial increase of characteristic pressure a reduction and new increase of pressure resistance is detectable insofar as the graph exhibits two inflection points. The reason of that unsteady trend could not be detected.

Decreasing characteristic pressures indicate higher failure probabilities at a specific internal pressure due to the displacement of S-curves to lower pressure values. The failure probability of hollow glass fibers with diameter ratio of  $d_o / d_i = 1.25$  and selected wall thicknesses is displayed in the example in Figure 42.

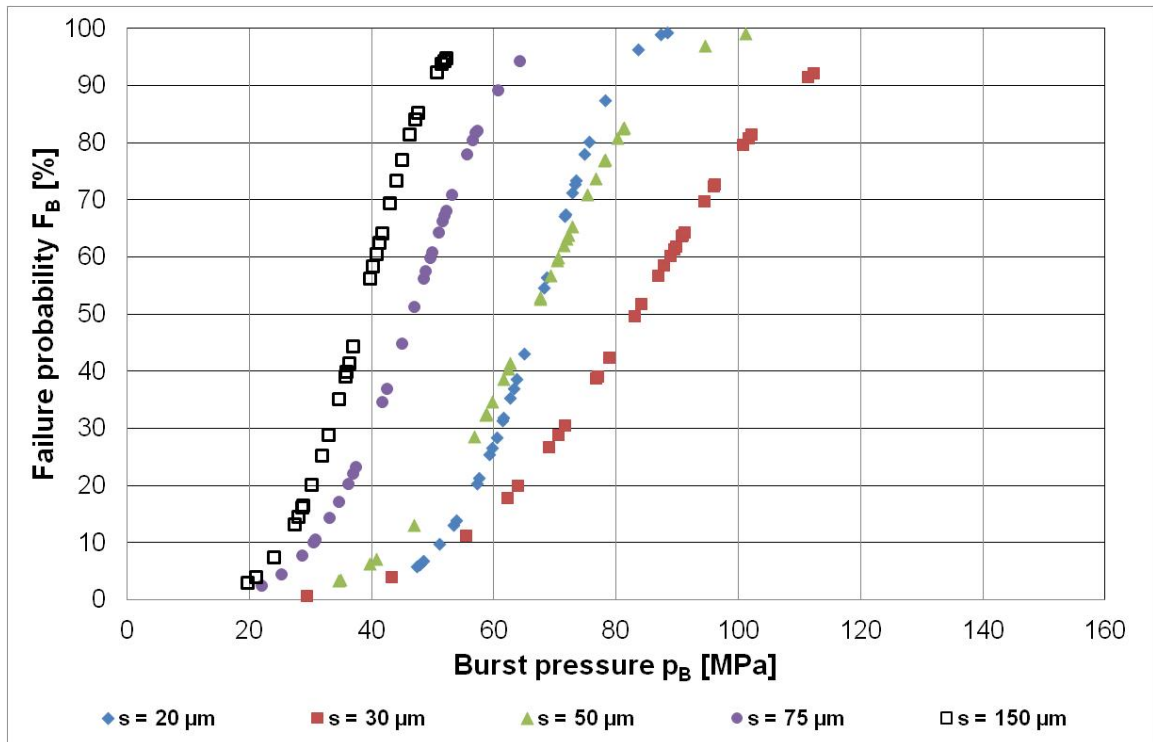


Figure 42: Failure curves against burst pressure of fibers with selected wall thicknesses and a fixed diameter ratio of  $d_o / d_i = 1.25$

Due to the initial increase of characteristic pressure  $P$  at the increase of wall thickness from  $s = 20 \mu\text{m}$  to  $s = 30 \mu\text{m}$  the failure curve slid to the right. As a consequence, the failure probability at a specific pressure value increases significantly. Due to decreasing characteristic pressure at wall thicknesses above  $s = 30 \mu\text{m}$ , the related graphs slide to the left to lower pressure values. As a result, the failure probabilities increase at a specific pressure.

The behaviors of distinctive test results show the same development for all three fixed diameter ratios. The increase of wall thickness initially accompanies with an increase of pressure resistance indicated by the characteristic pressure  $P$  of each test series. However, further increase of wall thickness leads to a maximum characteristic pressure  $P$  which is exhibited as an inflection point. Moreover, every increase of wall thickness leads to a reduction of pressure resistance. A uniform wall thickness as inflection point cannot be detected. The decreased pressure resistance of hollow fibers with wall thicknesses between  $s = 30 \mu\text{m}$  to  $s = 50 \mu\text{m}$  seems to correlate with foreign influences. During transportation and preparation of test samples every contact to the glass surface could lead to defects. Apparently, the thin wall thickness is more susceptible against such defects. This view is encouraged by the results of serial number 1. The test series of fibers with smallest wall thickness within the diameter ratio  $d_o / d_i = 1.33$  shows a



significant lower value of characteristic pressure. Therefore, series with wall thickness below a value of  $s = 40 \mu\text{m}$  are less meaningful in relation to the influence of wall thickness on pressure resistance.

Related to the main trend the highest pressure levels have been detected for hollow fibers with a diameter ratio of  $d_o / d_i = 1.33$  which is an effect of the inner volume of the hollow fibers. It can be approximately explained with the calculation formula for cylindrical, thin-walled vessels made of steel [172]:

$$\sigma_t = \frac{p d_o}{2 s} \quad (6.2)$$

where  $\sigma_t$  is the tangential stress in the wall,  $p$  the internal pressure,  $d_o$  the outer diameter and  $s$  the wall thickness.

With decreasing diameter ratio, the ratio between outer diameter and wall thickness increases. If the internal pressure  $p$  and the wall thickness  $s$  are fixed, the outer diameter  $d_o$  will increase by decreasing the diameter ratio. The resulting tangential stress inside the wall is much higher for hollow fibers with lower diameter ratio.

Nevertheless, a decrease of the wall thickness leads to an increase of pressure resistance indicated by the increase of the characteristic pressure within each diameter ratio. At wall thicknesses between  $s = 30 \mu\text{m}$  to  $s = 50 \mu\text{m}$  an inflection point occurs and the pressure resistance decreases again which can be an effect of possible defects of the outer fiber surface. The transfer of Griffith's theory from solid fibers to hollow fibers seems to be feasible.

As result of the study of hollow borosilicate glass fibers with different dimensions but fixed ratio of outer to inner diameter it can be summarized that:

- The influence of the wall thickness on the pressure resistance of hollow glass fibers was observed in test series with different glass material and dimensions. The decrease of wall thickness was associated with an increasing pressure resistance.
- Due to fixed ratio of outer to inner diameter a decrease of wall thickness accompanied with a decrease of dimensions.
- At a specific wall thickness a maximum burst pressure was reached for each diameter ratio. A further reduction of the wall thickness led to decrease of pressure resistance. It can be assumed, that defects due to handling and transport affect the surface of the fibers. Defects could be caused and therefore affected the pressure resistance in a negative way. That critical wall thickness was not determined, because it was different for each test series.

#### 6.4.2 Different Wall Thicknesses at Fixed Inner Diameter

The test series with fixed diameter ratios showed the trend of increasing pressure resistance at decreasing wall thickness. Thus, not only the wall thickness was varied but also the inner and outer diameter.

Hence, an investigation of hollow fibers with different fixed inner diameter and varying wall thickness should exclude the influence of varying inner diameter. The results of fixed diameter ratios lead to the assumption that the inner diameter and resulting inner volume and surface have a large influence on the pressure resistance of hollow glass fibers. Samples of five different inner diameters were tested whereby at each inner diameter also five different wall thicknesses were available. Due to the change of supplier the used fibers were made of another borosilicate glass whose chemical composition is slightly different to the previous tested borosilicate 3.3.

The preparation of test samples includes the investigation under the microscope. The surface was checked for visible defects and the diameter of tested fibers was reviewed. Partly distinct deviations between desired and actual value of inner diameter and wall thickness were detected. For the evaluation of burst pressure test results the average diameter and wall thickness value of five hollow fibers were determined. The resulting average actual diameters and wall thicknesses together with the desired values are listed in Table 35. Outstanding were the results of the test series with the smallest inner diameter (serial number 1 to 5). Hollow glass fibers of serial number one to three with small wall thicknesses and high free space ratio especially exhibited massive deviations not only from desired inner diameter but also from the desired wall thickness. The hollow fibers from serial number four and five with high wall thicknesses nearly showed the desired dimensions. Here comparability was not given without restrictions. The other test series with higher inner diameter showed similar behaviors but the deviations between desired and actual values was not that large so the test results should be meaningful and comparable to each other.

Table 35: Specifications (real and desired) for hollow borosilicate fibers with fixed inner diameter  $d_i$ , but different wall thicknesses  $s$  (desired values given in brackets)

Serial No.	outer diameter $d_o$ [ $\mu\text{m}$ ]	inner diameter $d_i$ [ $\mu\text{m}$ ]	wall thickness $s$ [ $\mu\text{m}$ ]	Free space FS [%]
1	181.2 (139.8)	159.4 (127)	10.9 (6.4)	77.5 (83)
2	200.2 (147.4)	163.0 (127)	18.6 (10.2)	66.3 (73)
3	189.8 (160.0)	151.0 (127)	19.4 (16.5)	63.4 (64)
4	200.2 (195.6)	123.8 (127)	38.2 (34.3)	38.2 (43)
5	275.2 (259.8)	124.8 (127)	75.2 (66.4)	20.6 (24)
6	208.3 (195.6)	183.5 (178)	12.4 (8.8)	77.7 (83)
7	230.2 (208.4)	189.2 (178)	20.5 (15.2)	67.6 (73)
8	235.2 (223.6)	186.6 (178)	24.3 (22.8)	62.3 (64)
9	275.5 (272.0)	173.7 (178)	50.9 (47.0)	39.8 (43)
10	371.0 (363.4)	175.2 (178)	97.9 (92.7)	22.3 (24)
11	292.1 (292.2)	257.3 (266)	17.4 (13.1)	77.6 (83)
12	321.7 (309.8)	265.5 (266)	28.1 (21.9)	68.2 (73)
13	342.6 (332.8)	273.2 (266)	34.7 (33.4)	63.7 (64)
14	418.6 (409.0)	265.8 (266)	76.4 (71.5)	40.3 (43)
15	546.9 (546.0)	258.9 (266)	144.0 (140.0)	22.4 (24)
16	402.8 (388.6)	365.0 (356)	18.9 (16.3)	82.1 (83)
17	419.2 (414.0)	345.0 (356)	37.1 (29.0)	67.8 (73)
18	453.0 (444.6)	361.6 (356)	45.7 (44.3)	63.7 (64)
19	558.2 (543.6)	352.0 (356)	103.1 (93.8)	39.8 (43)
20	735.0 (727.4)	352.4 (356)	191.3 (185.7)	23.0 (24)
21	508.8 (500.4)	464.4 (457)	22.2 (21.7)	83.3 (83)
22	548.6 (533.4)	455.4 (457)	46.6 (38.2)	68.9 (73)
23	583.4 (571.6)	465.8 (457)	58.8 (57.3)	63.8 (64)
24	726.8 (698.6)	457.6 (457)	134.6 (120.8)	39.7 (43)
25	935.6 (934.)	458.6 (457)	238.5 (238.9)	24.0 (24)

The distinctive test results of all test series are summarized in Table 36 together with actual inner diameter, wall thickness and resulting free space. Comparing the measured pressure values within the test series of similar inner diameters it is conspicuous that with decreasing wall thickness and consequently increasing free space a decreasing pressure resistance is detectable.

Outstanding are the test series with free spaces of FS = 20 % to FS = 24 % (serial no. 5, 10, 15, 20 and 25) which exhibit the highest wall thickness for respective inner diameter. A complete test series was possible only with fibers of an inner diameter of about  $d_i = 460 \mu\text{m}$ . Decreasing diameter on same free space leads to pressure resistances which exceeded the pressure limit of the experimental setup of  $p_{\text{system}} = 150 \text{ MPa}$ . If pressure values are listed in the table up to maximum five burst pressures could be determined for the respective series.

An analysis of distinctive test results shows a clear connectedness between wall thickness and characteristic pressure  $P$ . A constant linear behavior is not detectable but it can be recognized proportionality between these values. A roughly estimated ratio between characteristic pressure  $P$  and wall thickness  $s$  can be determined whereby a reduction of wall thickness by the factor 2 leads to a decrease of pressure resistance indicated by characteristic pressure by nearly the same factor.

Admittedly, an estimated ratio between pressure resistance and wall thickness at similar inner diameter can be seen but this is not applicable in general to each step of wall thickness decrease. The determined burst pressure values show no consistent distribution. Therefore, the minimum burst pressures of series two and three are comparable to each other which can be explained by only small differences in wall thickness. A comparison of maximum burst pressures shows a significant higher pressure value for serial number three with only slightly higher wall thickness. Due to that higher spread a lower form parameter results for serial number three. Analogous behaviors of pressure values and form-parameters are detectable also for series with higher inner diameter but similar free space of about FS = 65 %.

Table 36: Test results of hollow borosilicate fibers with similar inner diameter but varied wall thicknesses

Serial No.	Dimensions (d <sub>i</sub> ; s) [μm]	Free space FS [%]	p <sub>min</sub> [MPa]	p <sub>max</sub> [MPa]	Form parameter b	P [MPa]
1	159.4; 10.9	77.5	25.6	54.6	8.8	41.7
2	163.0; 18.6	66.3	41.9	75.5	8.7	54.8
3	151.0; 19.4	63.4	43.1	97.9	5.6	80.7
4	123.8; 38.2	38.2	101.3	>150	10.3	140.8
5	124.8; 66.4	20.6	>150	Not determinable (*)		
6	183.5; 12.4	77.7	17.2	57.8	4.8	44.3
7	189.2; 20.5	67.6	36.8	60.5	9.0	52.2
8	186.6; 24.3	62.3	48.7	99.8	7.4	72.7
9	173.7; 50.9	39.8	86.9	150.0	9.1	118.3
10	175.2; 97.9	22.3	56.8	>150	Not determinable (*)	
11	257.3; 17.4	77.6	12.2	46.6	4.5	36.4
12	265.5; 28.1	68.2	41.2	78.3	8.5	55.2
13	273.2; 34.7	63.7	22.4	71.6	4.8	58.1
14	265.8; 76.4	40.3	49.4	131.2	5.1	96.9
15	258.9; 144.0	22.4	128.5	>150	Not determinable (*)	
16	365.0; 18.9	82.1	10.8	30.0	5.3	24.2
17	345.0; 37.1	67.8	30.2	57.3	8.8	45.9
18	361.6; 45.7	63.7	31.2	68.9	6.9	52.9
19	352.0; 103.1	39.8	42.9	130.8	5.1	110.2
20	352.4; 191.3	23.0	Not determinable (*)			
21	464.4; 22.2	83.3	12.1	28.3	6.3	21.7
22	455.4; 46.6	68.9	26.0	47.0	9.3	39.8
23	465.8; 58.8	63.8	26.8	53.4	6.6	43.7
24	457.6; 134.6	39.7	32.9	110.7	4.1	80.5
25	458.6; 238.5	24.0	85.9	>150	10.5	119.7

\* Burst pressure >150 MPa = maximum operating pressure of the experimental setup

The decrease of wall thickness not only leads to the decrease of pressure resistance but also to an increase of failure probabilities at inner pressure load. The Weibull diagram for hollow fibers of serial number one to four with smallest inner diameter is displayed in Figure 43.

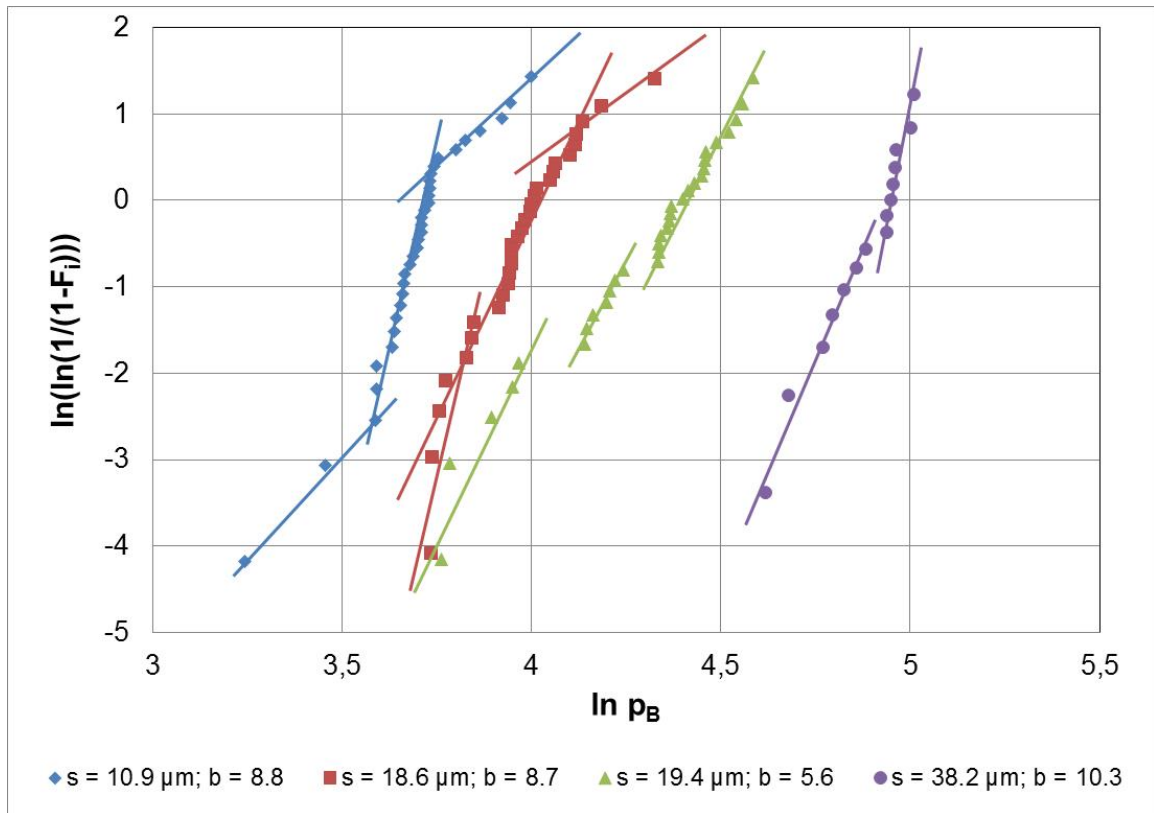


Figure 43: Weibull diagram of hollow borosilicate fibers with inner diameter of about  $d_i = 150 \mu\text{m}$  and different wall thicknesses, double logarithmic function of estimated failure probability  $F_i$  plotted against logarithmic burst pressure  $p_B$

Clearly recognizable is the displacement of graphs to the left with a decrease of related wall thickness. A similar development and displacement can be observed for fibers with higher inner diameters and decreasing wall thicknesses. Obvious, the different slopes on the graph are more related to a wall thickness of  $s = 10.9 \mu\text{m}$ . Fibers with a higher wall thicknesses feature different slopes as well. But these are not that significantly proceeded. The distinctions between the varying slopes could be explained by different failure reasons which lead to the collapse. Nevertheless, a good accordance to a linear slope is given for all graphs. The corresponding form parameters  $b$  are given in diagram for each test series. Single defect populations each with specific failure behavior might

be the reason for the observable behavior as shown in Figure 44. Hence, e.g. surface flaws can lead to complete different collapse behavior than volume defects.

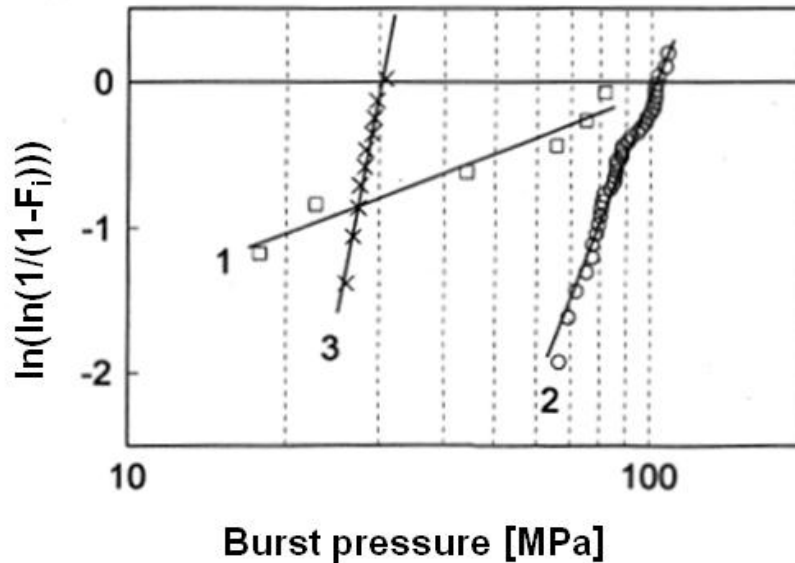


Figure 44: Defined defects of different populations on beverage bottle surface caused distinctions in burst pressures, according graphs in Weibull diagram exhibited different slopes and distributions [97]

The shown diagram is the result of burst pressure tests of glass beverage bottle according to DIN EN ISO 7458 with defined defects in test samples. According to the defects the Weibull distributions were calculated and plotted in one diagram. It can be seen that the different types of defects caused different behaviors in failure. Bubbles (graph no. 1) induced a wide spread of data by showing low failure stress. Bottles with solid enclosures and inhomogeneities in the glass exhibited a consistent and straight development with a high slope (graph no. 2). Additionally the test samples with solid enclosures featuring higher failure stresses than test samples with bubbles as defect. Test samples with defined procured defects by grit blasting showed a straight distribution with a high slope as well (graph no. 3). The curve is comparable to these of solid enclosures. However, the failure stresses exhibited lower values.

A differentiation of types of defects before testing the fibers was not possible. The investigation under the microscope did not show any visible flaws on the surface or inside the wall of the hollow fibers. Comparing it to the graphs in Figure 44 inhomogeneities or enclosures can be assumed as failure reason due to the comparable high slope.

The resulting failure probability curves, associated with Figure 43, plotted against the burst pressures are given in Figure 45 are calculated with linear slope designated for each curve.

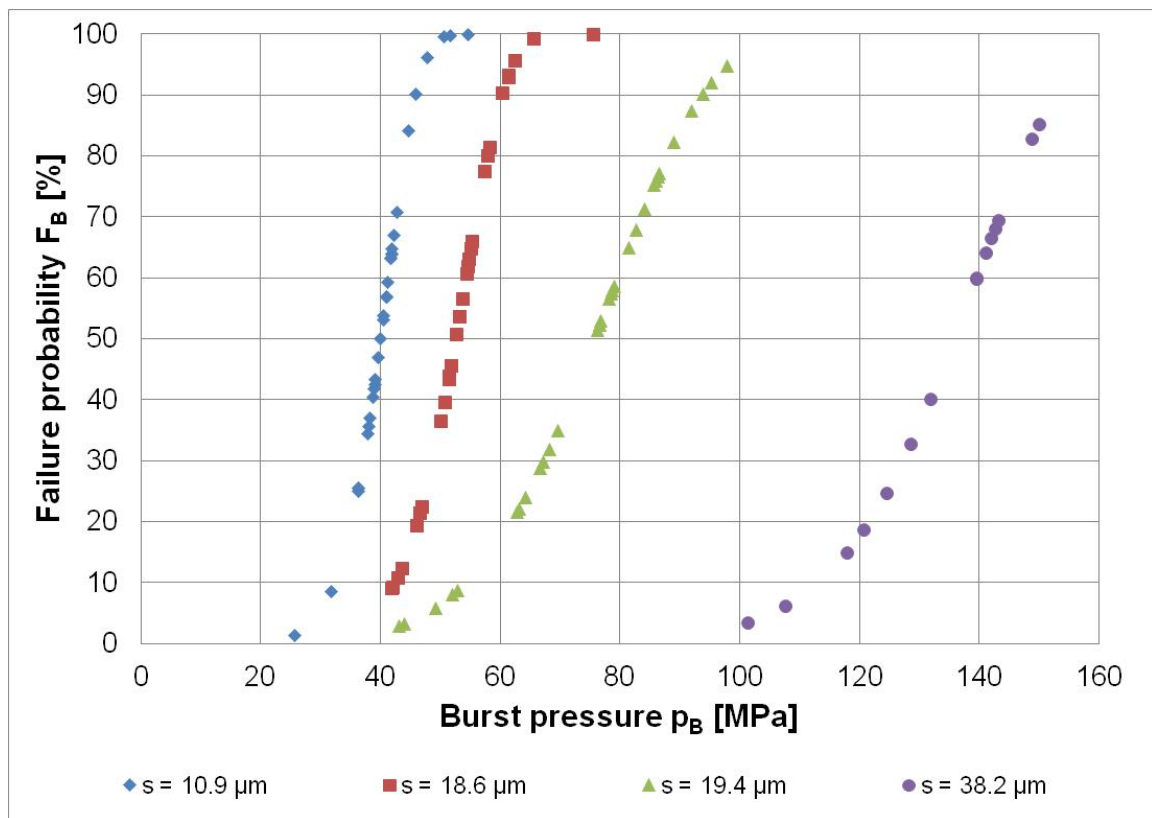


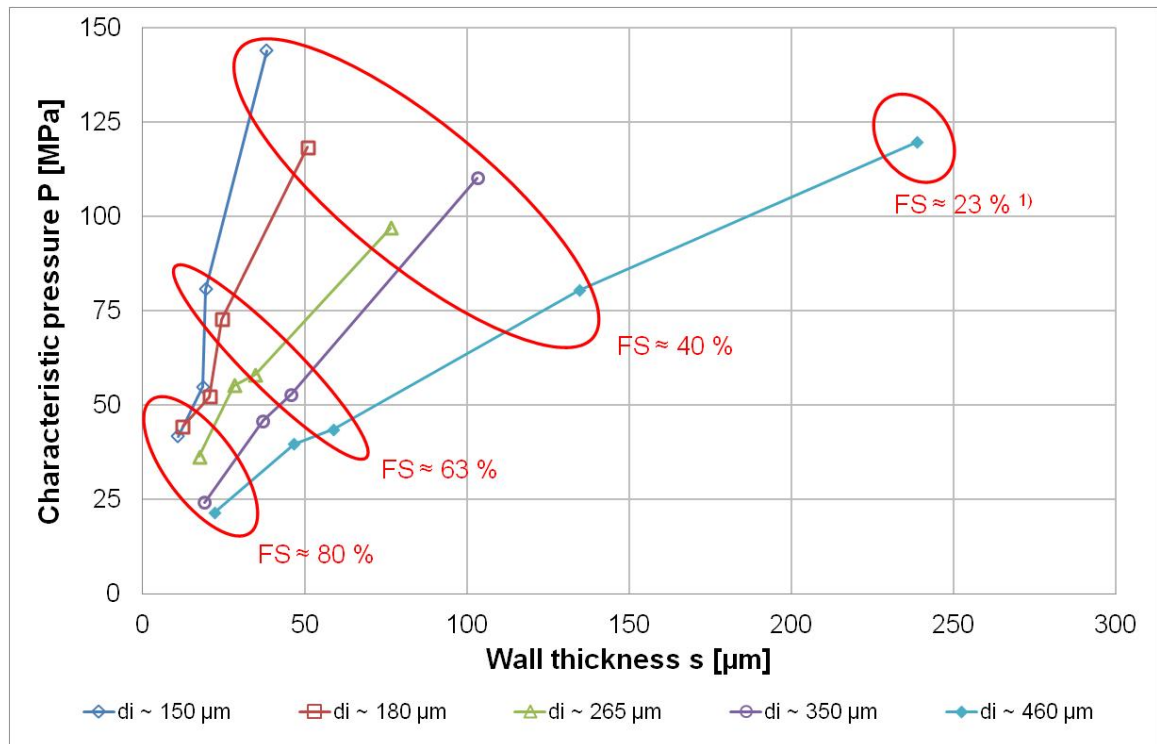
Figure 45: Failure probability  $F_B$  plotted against burst pressure  $p_B$  for hollow borosilicate fibers of inner diameter of about  $d_i = 150 \mu\text{m}$

The diagram points out distinct differences of pressure resistance and failure probabilities of hollow fibers with different wall thicknesses but similar inner diameters. It can be seen that test samples of highest wall thickness of  $s = 38.2 \mu\text{m}$  exhibit failure probabilities in the range of  $F_B = 5 \%$  at burst pressures of around  $p_B = 100 \text{ MPa}$ . Hollow fibers with halved wall thicknesses show the same inner pressure load failure probabilities of about  $F_B = 95 \%$ . Therefore, a collapse at these pressure values is almost predictable. Furthermore, wall thickness reductions lead to failure probabilities of  $F_B = 100 \%$ . Weibull diagrams and failure curve diagrams of fibers with larger diameters show similar developments at decreasing wall thicknesses but almost smaller pressure values.

For clarification of linear connectedness of pressure resistance and wall thickness in Figure 46 the relationship of both parameters is shown. Therefore, the characteristic



pressure of fibers with similar inner diameter is plotted against the related wall thicknesses.



1) Only series with  $d_i = 460 \mu\text{m}$  could be tested since other series with  $\text{FS} = 23\%$  features  $p_B \geq 150 \text{MPa}$  which is the maximum operating pressure of test setup

Figure 46: Characteristic pressure of hollow fibers with different fixed inner diameter plotted against wall thickness, the encircled values are valid for hollow glass fibers with similar free spaces but different inner diameter

Regarding the different inner diameter again, the nearly linear development of the curves is recognizable. A decrease of wall thickness by the factor two leads nearly to a linear decrease of characteristic pressure by the same factor. The slope of the graphs increases by decreasing inner diameter but the relation keeps the same.

Setting focus on samples of different inner diameter but similar free space another fact can be seen in Figure 46. Here the decrease of wall thickness leads to a decrease of the inner diameter as well. In the diagram selected free spaces of different inner diameters are encircled whereby the increase of characteristic pressure is detectable at decreasing wall thickness. That behavior is comparable to the test results presented chapter 6.4.1. As an example the failure probability of fibers with similar free space of about  $\text{FS} \approx 63\%$  but decreasing wall thickness and diameter is plotted in Figure 47.

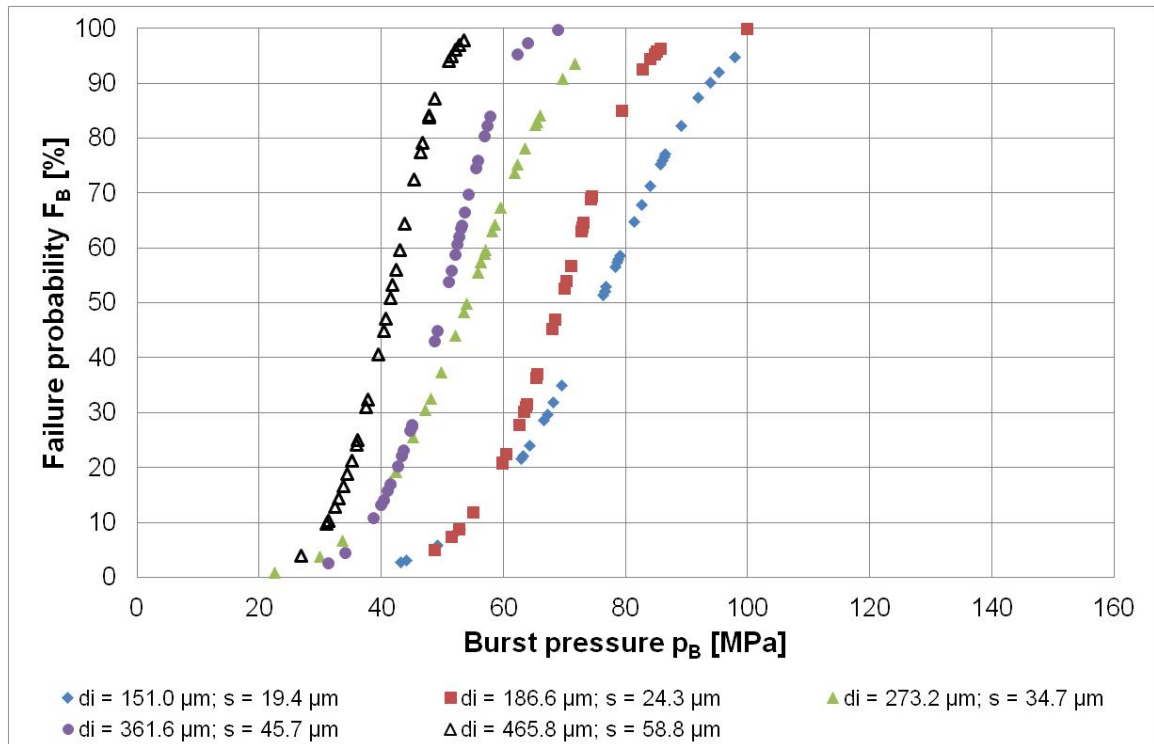


Figure 47: Failure probability of hollow fibers with comparable free space of about  $FS = 63\%$  but decreasing wall thickness and inner diameter plotted against related burst pressure values

Here the displacement of failure S-curves to the right can be detected by decreasing wall thickness and diameter. Clear to see is the achievement of significantly higher burst pressures at same failure probability with smaller dimensions. Additionally, it can be seen that the slope of S-curves is decreasing at smaller diameter and wall thicknesses. The sensitivity of hollow fibers made of the same glass material against surface damages caused by foreign contact is the same. But the decreasing slope of S-curves at decreasing dimensions indicates that the influence of such defects is much higher at smaller wall thicknesses. Therefore, the minimum burst pressures plotted in Figure 47 are closer together than the maximum burst pressure values.

A clear connection between wall thickness and inner diameter is detectable. Although, a variation of two dimension parameters occurred the constant inner diameter at different wall thicknesses led to similar inner volumes and surfaces. That behavior can be explained with formula 6.2 [172]:

$$\sigma_t = \frac{p d_o}{2 s} \quad (6.2).$$

Thus the outer diameter  $d_o$  can be substituted by:

$$d_o = d_i + 2s \quad (6.3).$$

The resulting formula (6.4) shows clearly the connection of reachable tangential stress and wall thickness at constant inner diameter:

$$\sigma_t = \frac{p}{2} \frac{(d_i + 2s)}{s} \quad (6.4).$$

Constant inner diameter  $d_i$  and increasing wall thickness  $t$  lead to a decrease of second fraction of formula (6.4). Therefore, at a constant inner pressure the tangential stress in the wall of a fiber will decrease and less load acts on the material. Consequently, at constant tangential stress the increase of wall thickness leads to increasing pressures that the hollow fiber is able to withstand.

A decrease of wall thickness at constant inner diameter implicates a decreasing pressure resistance of hollow glass fibers. The single burst pressure values as well as the failure probability distribution of single test series of similar test samples exhibit that trend. Griffith's theory of increasing tensile strength at decreasing dimension is not transferable directly to hollow glass fibers with constant inner diameter but varied wall thicknesses. The reduction of wall thickness leads to a decrease of glass volume per defined length but at inner pressure and similar inner diameter the surface on which the pressure load is able to act remains nearly the same.

However, the test results show an increase of burst pressure resistance and a displacement of failure probabilities to higher pressure levels with a decrease of wall thickness which accompanies with a decrease of diameter as plotted in Figure 46 and Figure 47. In that case the theory of Griffith is also applicable on hollow glass fibers. Due to reduction of inner diameter the volume and inner surface decreases as well. Compared to the results of different diameter ratios in chapter 6.4.1, a clear difference is detectable. With a reduction of wall thickness and diameter the pressure resistance against inner load increases up to an inflection point. From that point further decrease of dimension leads to decreasing pressure resistance. The reason for that behavior may be assumed in defects caused by handling. The actual results do not exhibit such a clear inflection point at evaluation of pressure resistance at fixed free spaces. The related results of one defined free space ratio do not describe a steady behavior rather an inflection point in a defined range of wall thickness does not exist.

It can be summarized that:

- Decreasing wall thickness at constant inner diameter accompanied with decreasing resistance against inner pressure. In that case Griffith theory is not valid on hollow fibers and the pressure resistance follows the Barlow's formula. Decreasing wall thicknesses led to decreasing pressure resistances.
- Keeping the free space constant Griffith's theory was valid also for hollow glass fibers. The reduction of wall thickness accompanied with a reduction of the outer and inner diameter and resulted in higher pressure values. Under these circumstances small and thin walled hollow glass fibers showed an increased pressure resistance with smaller wall thicknesses.
- Consequently, the reduction of the wall thickness led to an increased pressure resistance but a simultaneous decrease in size had to be proceeded as well.

### 6.5 Comparison of different Borosilicate Glasses

The investigations regarding the effect of different dimensions on the pressure resistance were conducted with hollow glass fibers comprised of different types of borosilicate glass due to a change in supplier.

The fibers with fixed ratio of outer diameter to inner diameter (chapter 6.4.1) were made of borosilicate 3.3 (DURAN). The fibers with fixed inner diameter but varying wall thickness (chapter 6.4.2) were made of borosilicate C5. Both glasses are classified in the group of borosilicate glasses but differ from each other in chemical composition. To investigate the effect of the different types of glasses from the same family on the pressure resistance of hollow glass fibers test samples had to be made by the same manufacturer. Therefore influences of production could be excluded. The used borosilicate glasses and their chemical main components are listed in Table 37. Mainly changes can be observed in the percentages of  $\text{SiO}_2$ ,  $\text{Al}_2\text{O}_3$  and  $\text{B}_2\text{O}_3$ . All substances are network former [3] whereby  $\text{Al}_2\text{O}_3$  and  $\text{B}_2\text{O}_3$  can act as a stabilizer as well [3], [78].

Table 37: Chemical main components of tested borosilicate glass fibers, as determined in chemical analysis

<b>Components [ma-%]</b>	<b>Borosilicate 3.3 (DURAN) [148], [154]</b>	<b>Borosilicate C5 [151]</b>	<b>Borosilicate C1S [177]</b>
SiO <sub>2</sub>	80.5	72.0	65.0
Na <sub>2</sub> O	3.5	6.7	2.5
Al <sub>2</sub> O <sub>3</sub>	2.4	6.8	7.3
K <sub>2</sub> O	0.5	2.4	3.0
B <sub>2</sub> O <sub>3</sub>	12.8	11.4	18.0
BaO			2.6

The changes of chemical composition entail variations in physical properties which are given in Table 38. The characteristic temperatures like annealing, softening and working point are different for each type. Consequently the thermal history after drawing the thin hollow fibers out of the glass tube differs for each type. Also the mechanical properties changed with varying the chemical composition, as can be seen in the different Young's modulus of borosilicate 3.3 and C5.

The investigation of the effect of the different borosilicate glasses on the pressure resistance contained four test series with a minimum sample size of 30 samples per series. A direct comparison of all three glasses to each other was not possible due to the non-existence of suitable raw-tubes. During the drawing process the dimension is reduced many times. The open area and the ratio of diameter to wall-thickness were not substantially changed. Consequently borosilicate C5 was taken as a reference value and compared once to borosilicate C1S and twice to DURAN.

Table 38: Physical properties of tested borosilicate glasses

Physical property	Borosilicate 3.3 (DURAN) [148], [154]	Borosilicate C5 [151]	Borosilicate C1S [177]
Density [ $\text{g cm}^{-3}$ ]	2.23	2.33	2.27
Transformation temperature $T_g$ [ $^{\circ}\text{C}$ ]	525		465
Annealing point [ $^{\circ}\text{C}$ at $10^{13}$ dPa s]	560	570	480
Softening point [ $^{\circ}\text{C}$ at $10^{7.6}$ dPa s]	825	785	715
Working point [ $^{\circ}\text{C}$ at $10^4$ dPa s]	1260	1140	1130
Young's modulus E [( $\text{kN mm}^{-2}$ )]	63	102	
CTE $\alpha_{25-300^{\circ}\text{C}}$ [( $1 \text{ K}^{-1}$ ) $10^{-6}$ ]	3.3	5.5	4.7

Hollow fibers made of borosilicate C5 and C1S featured dimensions of  $d_o = 488 \mu\text{m}$ ,  $d_i = 441 \mu\text{m}$  and a wall thickness of  $s = 23 \mu\text{m}$ . The characteristic test results are given in Table 39. It is predictable that the results are quite similar. The characteristic pressures  $P$  and the maximum burst pressures of both test series are close together. The lower form parameter of borosilicate C1S can be explained by the lower minimum burst pressure which created a wider spread of the measured data.

Fibers made of DURAN as well as the corresponding borosilicate C5 fibers had the dimensions of  $d_o = 478 \mu\text{m}$ ,  $d_i = 400 \mu\text{m}$  and  $s = 39 \mu\text{m}$ . The outer diameter is nearly the same of C1S fibers but the wall thickness is almost doubled. Therefore higher burst pressure was expected which can be seen by comparison of both C5 test series. The doubling of wall thickness at the same outer diameter led to a doubling of minimum and maximum burst pressure as well as characteristic pressure value. A comparison of borosilicate C5 to DURAN fibers shows a significant difference. All pressure values of DURAN fibers are 30% lower than those of borosilicate C5. The form parameter exhibits

a higher value of  $b = 10.6$  which can be attributed to the lower range between minimum and maximum burst pressure.

Table 39: Characteristic test results of hollow glass fibers made of three different borosilicate glasses and different dimensions

Material	Dimension [ $\mu\text{m}$ ]	Min. burst pressure $p_{\text{min}}$ [MPa]	Max. burst pressure $p_{\text{max}}$ [MPa]	Form parameter $b$	Characteristic pressure $P$ [MPa]
C5	$d_o = 488$	13.0	26.9	7.1	22.5
C1S	$d_i = 441$ $s = 23$	10.4	26.5	5.6	21.8
C5	$d_o = 478$	29.0	50.2	8.5	43.1
DURAN	$d_i = 400$ $s = 39$	21.6	36.8	10.6	31.4

A visualization of calculated failure probabilities plotted against the burst pressure is given in Figure 48. Thereby the distinctions between the different borosilicate glasses can be seen.

Comparing the S-curves of borosilicate C5 and borosilicate C1S with a wall thickness of  $s = 23 \mu\text{m}$  a likewise development of both graphs is observable. The similar test results of minimum and maximum burst pressure, as well as characteristic pressure and form factor, which are illustrated in Table 39, lead to comparable progression and slope of both curves; especially, in the upper range both curves overlay each other.

What is clear to see is the difference of the S-curve of borosilicate C5 glass with higher wall thickness to the curve of borosilicate 3.3. Comparing both graphs of borosilicate C5 to each other, the doubling of pressure resistance by doubling the wall thickness is detectable. The curve of borosilicate C5 with higher wall thickness slid to the right of the diagram significantly. Borosilicate 3.3 shows a complete different behavior. The corresponding graph slid only slightly to the right due to the higher wall thickness. A sharper increase of the curve can be recognized because of the smaller range between the minimum and the maximum value of burst pressures. Nevertheless, the pressure resistance of borosilicate 3.3 is much smaller than of borosilicate C5.

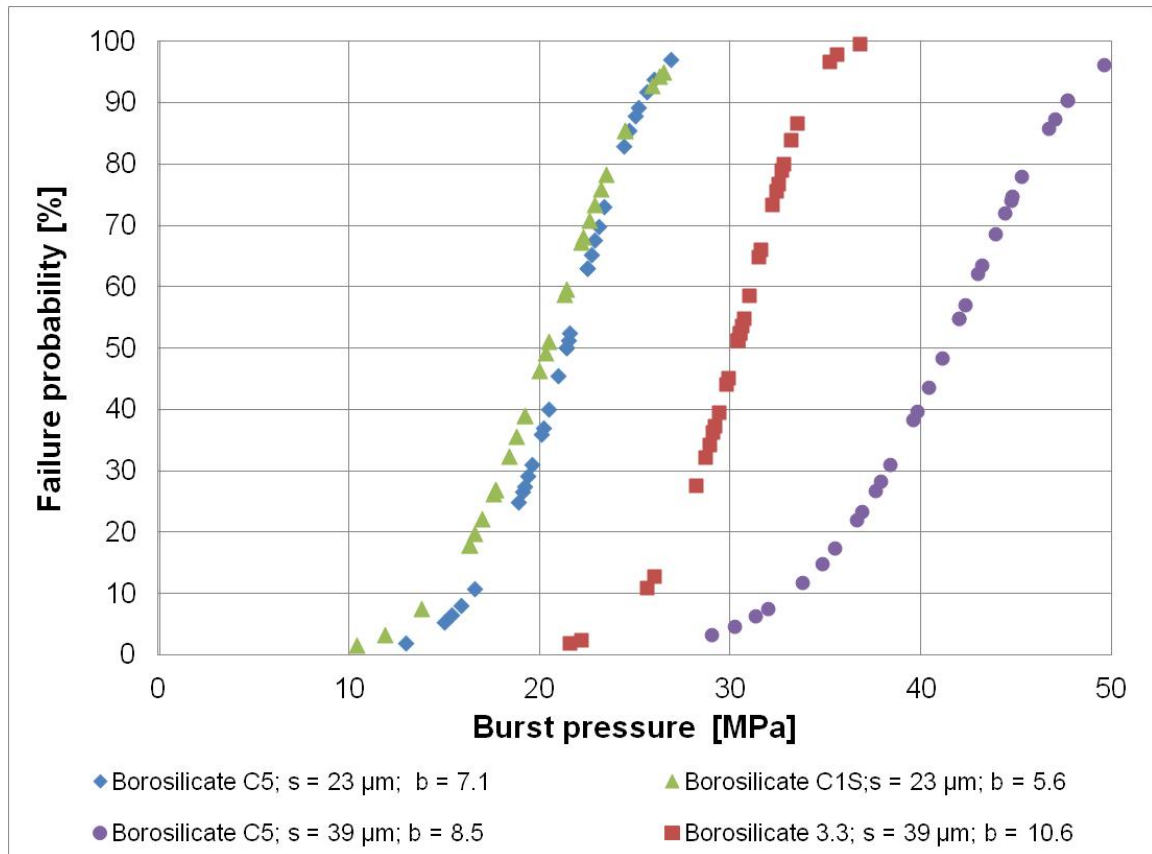


Figure 48: Failure probability of hollow fibers made of different types of borosilicate glass with similar outer diameter but different wall thickness ( $d_o = 488 \mu\text{m}$ ,  $d_i = 441 \mu\text{m}$ ,  $s = 23 \mu\text{m}$  respectively  $d_o = 478 \mu\text{m}$ ,  $d_i = 400 \mu\text{m}$ ,  $s = 39 \mu\text{m}$ )

A conclusion of the varying pressure resistance of the different borosilicate glasses could be given by the differences in chemical composition. The addition of substances to the glass mixture leads to changes in a multitude of chemical as well as mechanical properties of the glass itself. Alkaline and earth alkaline components cause a decrease of melting and working temperature in comparison to pure quartz glass [3], [4]. Simultaneously the network structure of the glass is weakened due to the formation of disconnecting points by breaking the bridge structure oxygen [3]. The addition of  $\text{Al}_2\text{O}_3$  and  $\text{B}_2\text{O}_3$  leads to the reduction of disconnecting points and a stabilization of the network. The stabilizing effect depends on the concentration in the chemical mixture and the percentage of alkaline and earth alkaline components [3], [4]. Attention should be paid especially to the concentration of  $\text{B}_2\text{O}_3$ . Due to its open structure, high concentrations lead to the destabilization of the network structure which appears, for example, in the decrease of the Young's modulus [3].

A comparison of the chemical compositions given in Table 37 reveals main distinctions in the percentage of  $\text{SiO}_2$ ,  $\text{Al}_2\text{O}_3$  and  $\text{B}_2\text{O}_3$ . Borosilicate C5 and C1S reached nearly the



same test results with fibers of similar dimensions. Thereby C5 glass features a significantly higher percentage of  $\text{SiO}_2$  than C1S glass. Nevertheless, the burst pressures and both failure probability curves showed similar developments. Alkaline like  $\text{Na}_2\text{O}$  and  $\text{K}_2\text{O}$  lead to the degradation of solidity of the network structure of glass. Borosilicate C5 contains about 10% of these two alkaline substances. However, the addition of 6.8% of  $\text{Al}_2\text{O}_3$  and 11.4 % of  $\text{B}_2\text{O}_3$  acts against that effect and stabilizes the glass structure.

Borosilicate C1S contains less  $\text{SiO}_2$  as the main network builder. The concentration of  $\text{Al}_2\text{O}_3$  increases slightly from 6.8% to 7.3%. But the  $\text{B}_2\text{O}_3$  concentration in comparison to borosilicate C5 significantly increases from 11.4% to 18.0%. Due to that high percentage  $\text{B}_2\text{O}_3$  loses the stabilizing effect and the resulting network exhibits a wide and open structure. In that case, however, the addition of alkaline substances reinforces the open network of boron and leads to a stiffening. Therefore the slight increase of  $\text{Al}_2\text{O}_3$  and the presence of alkaline substances act on the network-weakening effect of boron and stabilize the glass network and thus a similar pressure resistance can be achieved.

The comparison of borosilicate C5 and C1S to borosilicate 3.3 shows an obvious higher percentage of  $\text{SiO}_2$  but lower amounts of alkaline substances. However, borosilicate 3.3 exhibits the lowest amount of alumina oxide of the three tested glasses. At the same time, the concentration of boron oxide is slightly higher than borosilicate C5. It can be assumed that the existing concentration of boron oxide leads to a strength-decreasing influence by opening the network [3]. The missing stabilizing effect of  $\text{Al}_2\text{O}_3$  and the small amounts of potassium and sodium oxide cannot act against that influence. Therefore the structure of the network is weaker than the other borosilicate glasses and in the comparison of Young's modulus of borosilicate C5 and 3.3. The higher Young's modulus of a material the higher is the stiffness of its structure. The elastic modulus of borosilicate C5 is almost doubled in comparison to borosilicate 3.3. A value of elastic modulus of borosilicate C1S was not available in the literature. Hence, it can be assumed that the amount of alumina oxide and boron oxide influence the mechanical resistance of the glass and both interact. Consequently a weakening effect of boron oxide on the solidity of the network can be countered by the addition of alumina oxide.

The chemical resistance of glass can be influenced massively by the addition of  $\text{B}_2\text{O}_3$  [4]. Its positive effect on the firmness of the network seems to be mainly linked to the concentration and the presence of  $\text{Al}_2\text{O}_3$ . Similar concentrations of  $\text{B}_2\text{O}_3$  but obvious distinctions in the amount of  $\text{Al}_2\text{O}_3$  of borosilicate 3.3 in comparison to C5 lead to significant decreases of pressure resistance. Borosilicate C5 and C1S exhibit comparable or even higher percentages of  $\text{B}_2\text{O}_3$  than borosilicate 3.3. The increase of

alumina and alkaline oxides in the mixture of the glass acts against the negative effect of boron and lead to higher resistance against inner pressure load.

All samples were investigated under the light microscope before preparing and testing. No relevant or meaningful defects on the surface or in the volume could be detected. Therefore the different behaviors can be attributed to the effect of chemical composition in all probability.

In following the test results of glass fibers made of different borosilicate glasses can be summarized as:

- In comparison to borosilicate C5 fibers made of borosilicate 3.3 and borosilicate C1S were produced and tested. Differences of their chemical composition led to deviations of physical properties of the borosilicate glasses. Both types borosilicate C5 and C1S exhibited a lower amount of silica as main component.
- The amount of  $Al_2O_3$  was increased which acts as network stabilizer. The effect on the glass structure thereby depends on the concentration. The percentage of boron oxide, as well classified as stabilizer, was decreased for borosilicate C5 and increased for borosilicate C1S.
- Borosilicate C5 reached significant higher pressure resistances as borosilicate 3.3. The slightly higher amount of boron oxide of borosilicate C5 with concurrent increase of aluminum oxide led to a stiffening of the network.
- The effect of the even higher percentage of  $Al_2O_3$  in borosilicate C1S was equalized by the high amount of  $B_2O_3$ . Nevertheless, C1S featured similar results of pressure resistance as borosilicate C5. Consequently increasing the amount of  $Al_2O_3$  in borosilicate glasses leads to increased pressure resistance.

Table 40: Development of pressure resistance of different borosilicate fibers compared to a borosilicate C5 fiber

	<b>C1S</b>	<b>DURAN</b>
Pressure resistance	Slightly decreased	Decreased

## 6.6 Pre-stressed Glass Fibers

The mechanical resistance and loadability of glass is dependent on the surface quality and the thermal history of the sample [94]. Stress, formed in the material during cooling, can weaken the structure due to inhomogeneous distribution. Different processes like annealing can be applied to reduce or eliminate such negative acting stress distributions. The application of tempering glass not only eliminates inhomogeneous thermal stress peaks but also forms a specific desired distribution of stress inside the glass. Therefore the glass is prestressed by compressive stress in the outer layer and tensile stress in the inner layer [6], [95] as described in chapter 4.4.1.

However, the method of tempering glasses is not applicable at wall thicknesses below 3 mm [6]. Therefore the preload of hollow glass fibers by using a combination of different glass materials was investigated. Due to the different coefficients of thermal expansion (CTE), the glass materials exhibit different behaviors during heating and cooling process. Non-uniform expansion and shrinkage of different glasses will lead to a specific stress distribution in the wall of the fiber. Before drawing the thin hollow fibers two glass tubes with appropriate dimensions were stuck into each other. During the drawing process the acting heat fused the glass materials and a uniform fiber made of two raw glass tubes was generated.

The results from the comparison of different borosilicate glasses showed the influence of chemical composition on the pressure resistance of the test samples. Due to the high and comparable resistance against inner pressure of borosilicate C5 and C1S (see chapter 6.5) these two materials were chosen for the production of pre-stressed test samples. The physical properties of borosilicate C5 and C1S are listed in Table 41. The deviations of characteristic thermal points were a big challenge during drawing. The working points of both glasses are quite similar but the softening point exhibits a difference of 70 K. Hence, deformations or flow of C1S could happen much earlier than with borosilicate C5.

Table 41: Thermal properties of tested borosilicate glasses C5 and C1S

<b>Physical property</b>	<b>Borosilicate C5 [151]</b>	<b>Borosilicate C1S [177]</b>
Annealing point [°C at 10 <sup>13</sup> dPa s]	570	480
Softening point [°C at 10 <sup>7.6</sup> dPa s]	785	715
Working point [°C at 10 <sup>4</sup> dPa s]	1140	1130
CTE $\alpha_{25-300^{\circ}\text{C}}$ [(1 K <sup>-1</sup> ) 10 <sup>-6</sup> ]	5.5	4.7

Nonetheless hollow fibers in three different dimensions were produced. While the dimensions were not exactly the same they exhibited a good comparability. In theory, the inner fiber layer would be under compression stress and the outer layer under tensile stress if the glass tube with the lower CTE is placed as inner tube. Due to the lower CTE the shrinking of inner layer during cooling is less than the outer layer. Therefore further shrinking of the outer layer will occur when the shrinking of the inner layer is finished. The outer layer will remain under tensile stress and compresses the inner layer. If the assembly of the materials is done in the opposite manner i.e., the glass with lower CTE is placed as the outer tube as opposed to after cooling, the inner layer will remain under tensile stress and the outer layer under compressive stress.

The characteristic test results of combined fibers as well as those of the reference are listed in Table 42. As reference value, the test results of fibers made of only one tube of C5 but similar dimensions were used. Comparing the test data of test samples with similar dimensions a pattern is observed. Comparing the combined fibers to the reference series made of borosilicate C5, it can be seen that the combination of two tubes comprised of C5 leads to a decrease of pressure resistance. The characteristic pressures  $P$  of all tested dimensions of C5-C5-combination exhibit a decrease of 10% for the smallest dimensions and up to 25% lower value for the largest fibers. The minimum and maximum burst pressures show lower values as well. Outstanding is the test series of C5-C5 with intermediate dimensions. Here a significant small minimum burst pressure of  $p_{\min} = 10.2$  MPa is recognizable. The maximum burst pressure is like

the characteristic pressure 20% below the according values of the reference series. As a consequence the form parameter of that series is distinctively smaller due to the higher spread between minimum and maximum value.

Test series C5-C1S-combination, where the first termed glass is the outer layer, shows lower pressure resistance. Here only fibers of the smallest and largest dimensions were available. However, both series are quite similar. A comparison to the reference series shows values of the characteristic pressure 5% below the corresponding data of the reference. In contrast the form parameters of C5-C1S fibers exhibit higher values than the references. Indeed, the range between minimum and maximum burst pressure value is smaller in comparison to C5 fibers. Nevertheless, both values are smaller than these of the reference.

Borosilicate C1S assembled as outer layer and borosilicate C5 as inner layer leads to an increase of characteristic pressure  $P$  of about 30% for intermediate and largest dimensions and even 40% for fibers with smallest dimensions. The maximum burst pressure of all three tested series with above-mentioned combination increased as well in comparison to the reference. Thereby the range of increase varies with dimensions. The fibers with the smallest dimensions show an improvement of 30% of maximum value. The intermediate fibers exhibit only 10% improvement whereby the largest fibers have an increase of maximum reached burst pressure of about 50% in comparison to C5 fibers of similar dimension. However, the form parameters of tested series of C1S-C5 fibers feature lower data due to wider distribution of measured pressure data between minimum and maximum value. What is remarkable is the fact that the minimum burst pressures of the combined C1S-C5 fibers of the smallest and largest dimensions are comparable to the C5-C5 combination which showed the lowest pressure resistance in the comparison. The test series of C1S-C5 fibers with intermediate dimensions features a minimum burst pressure comparable to the corresponding reference series.

Table 42: Characteristic test results of pre-stressed hollow glass fibers with different dimensions, whereby the fibers were combined from two borosilicate tubes with different coefficient of thermal expansion (CTE)

Material combination (outside - inside)	Dimension [ $\mu\text{m}$ ]	Min. burst pressure $p_{\text{min}}$ [MPa]	Max. burst pressure $p_{\text{max}}$ [MPa]	Form parameter b	Characteristic pressure P [MPa]
C5 (reference)	$d_o \approx 210$ $d_i \approx 170$ $s \approx 20$	41.9	75.5	8.7	55.0
C5 - C5		35.1	62.6	8.2	50.3
C5 - C1S		35.9	62.0	9.3	52.7
C1S - C5		36.1	96.2	5.9	77.4
C5 (reference)	$d_o \approx 320$ $d_i \approx 250$ $s \approx 35$	41.2	78.2	8.5	55.1
C5 - C5		10.5	62.6	2.9	44.6
C5 - C1S		No convenient raw material available			
C1S - C5		40.9	87.4	6.8	71.3
C5 (reference)	$d_o \approx 400$ $d_i \approx 320$ $s \approx 40$	30.2	57.3	8.8	45.9
C5 - C5		22.0	45.9	7.9	34.5
C5 - C1S		29.5	50.5	9.4	44.5
C1S - C5		22.3	84.8	4.5	61.0

The calculated failure probabilities of fibers having small dimensions plotted against the corresponding burst pressure are shown in Figure 49 to visualize the results.

It can be seen that the curve of the reference C5 fibers is quite similar in development to the curves of C5-C5 and C5-C1S combinations due to the comparable form parameters. Both graphs of C5-C5 and C5-C1S combination slid to the left which indicates the lower pressure resistance whereby the degradation is in the range of 5% for C5-C1S and 10% for C5-C5, respectively. The curve of C1S-C5 combined fibers slid to the right which indicates an improved pressure resistance. A failure probability of  $F = 30\%$  appears at pressure of  $p = 65$  MPa whereas all other test series features the same failure probability at pressures of about  $p \approx 45$  MPa.

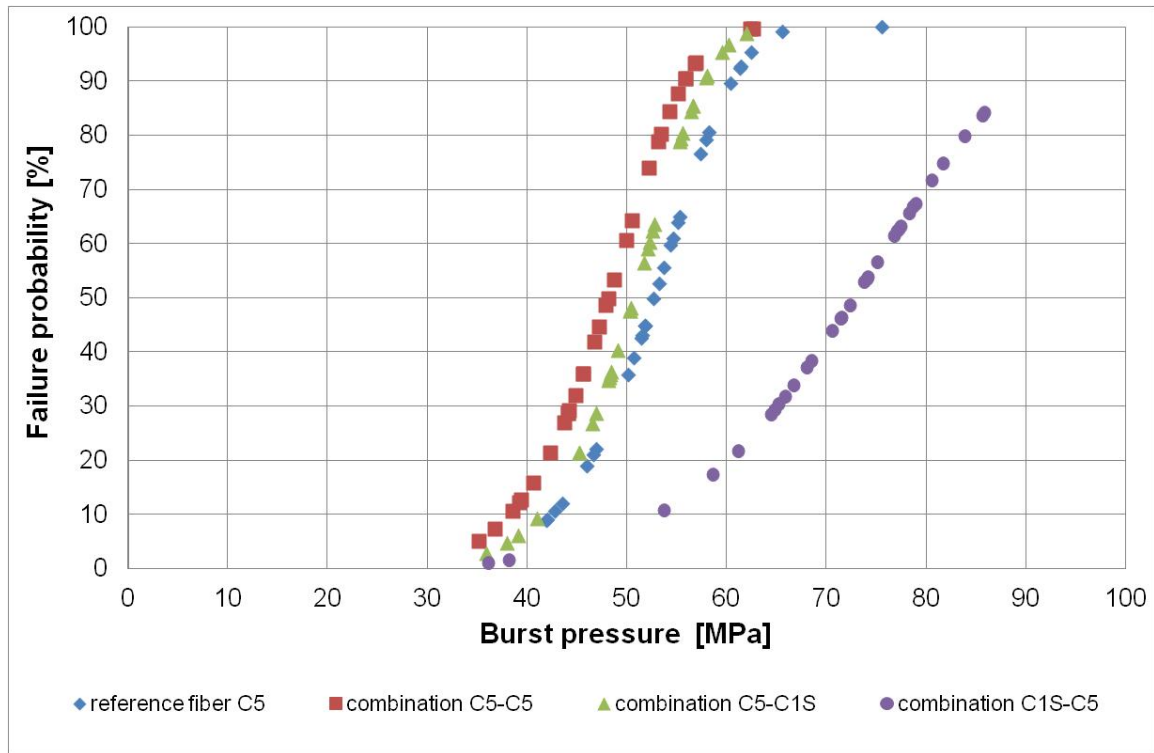


Figure 49: Failure probability of pre-stressed hollow fibers with comparable dimensions ( $d_o \approx 210 \mu\text{m}$ ,  $d_i \approx 170 \mu\text{m}$ ,  $s \approx 20 \mu\text{m}$ ), pre-stressed condition reached by combination of glasses with different CTE

However, the minimum burst pressure of C1S-C5 combination is comparable to these of C5-C5 and C5-C1S combination. Here two outliers were measured and can be detected in the diagram. If outliers were measured these data can be neglected in the analysis [138] when a clear deviation to the rest of the test results is recognizable. Due to the good interpolation of both outliers they were considered in the Weibull analysis. Therefore the initial point of the graph is in the same range of the other graphs. The rest of the measured burst pressure values of C1S-C5 combination with small dimensions are located in a significantly higher pressure region. The graph slides to the left but also features a lower slope because of wider distribution of measurement data.

Figure 50 displays the Weibull S-curves of tested fibers with intermediate dimensions of  $d_o \approx 320 \mu\text{m}$ ,  $d_i \approx 250 \mu\text{m}$  and  $s \approx 35 \mu\text{m}$ . A comparable behavior to the smaller fibers can be detected.

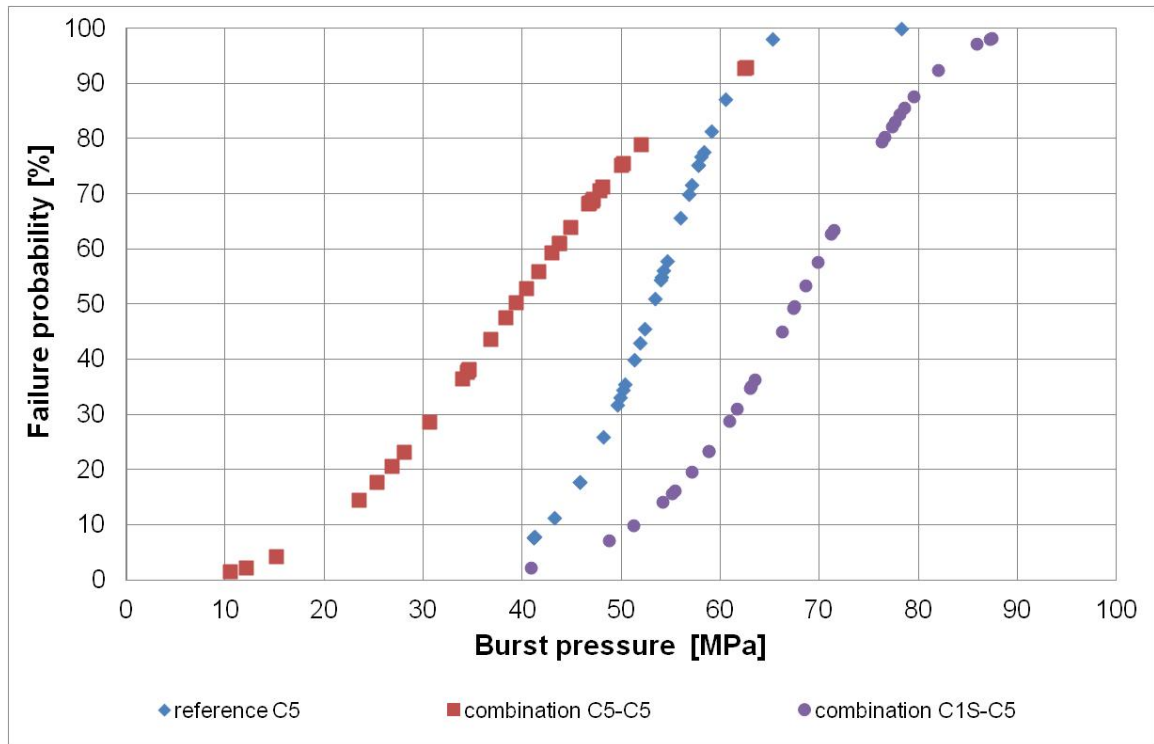


Figure 50: Failure probability of pre-stressed hollow fibers with comparable dimensions ( $d_o \approx 320 \mu\text{m}$ ,  $d_i \approx 250 \mu\text{m}$ ,  $s \approx 35 \mu\text{m}$ ), pre-stressed condition reached by combination of glasses with different CTE

A test series of C5 fibers was taken as a reference. Attention should be paid to the similar pressure resistance in comparison to the reference fibers with smaller dimensions. In addition to the pressure range, the development of the graph is comparable as well.

The graph of fibers combined from two C5 tubes shows lower resistance against inner pressure load. Once again the curve slides to the right, however, the slope and development of the curve is not similar to the reference series, as seen in Figure 49 which charts fibers having small dimensions. The spread of measured burst pressure values is considerably wider and is reflected in the lower slope of the S-curve. However, in the upper pressure region a convergence to the reference can be detected. Nevertheless, the pressure resistance is obviously lower.

Fibers combined from C1S as outer layer and C5 as inner layer show comparable development in failure probability with both fibers with smaller dimensions and the reference series. Here, too, the initial point of the graph is in the same range than the references series due to similar minimum burst pressures. The development is



consistent but features a lower slope because of the lower form parameter and wider spread of measured pressure values.

A combination of C5 as outer tube and C1S as inner tube was not available in the desired dimensions and is therefore missing in the diagram.

For the largest dimensions the failure probabilities for tested series were calculated as well. The originated diagram is given in Figure 51.

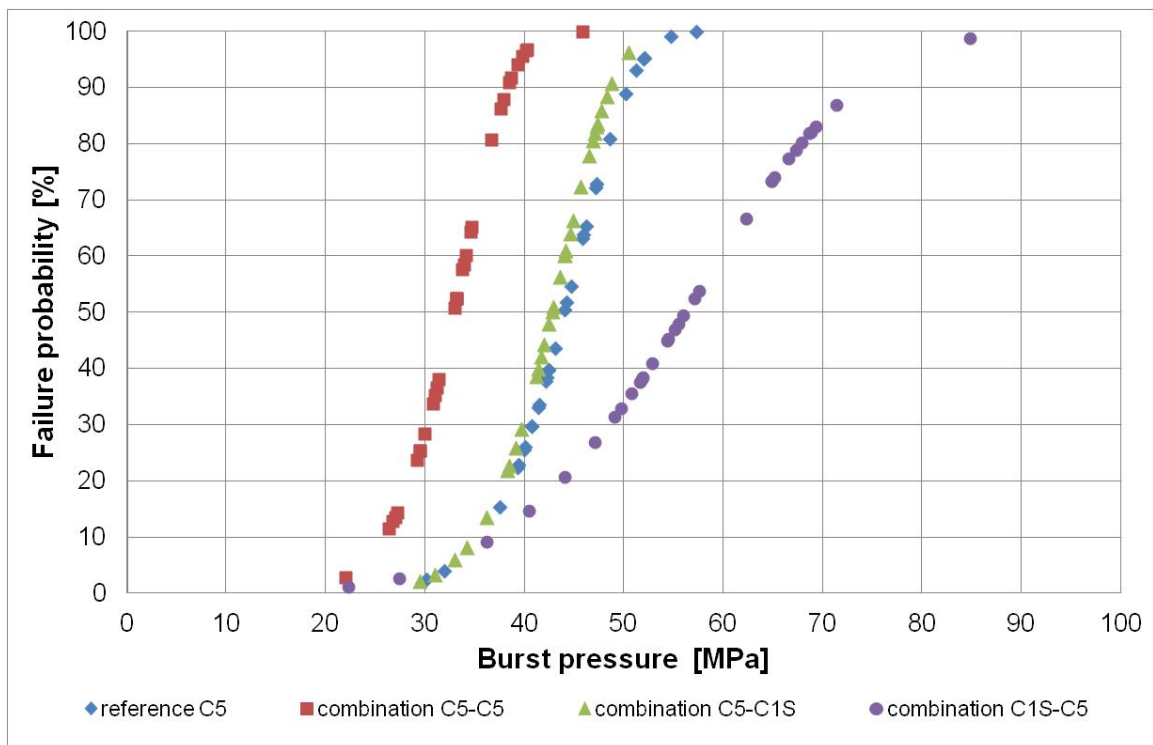


Figure 51: Failure probability of pre-stressed hollow fibers with comparable dimensions ( $d_o \approx 400 \mu\text{m}$ ,  $d_i \approx 320 \mu\text{m}$ ,  $s \approx 40 \mu\text{m}$ ), pre-stressed condition reached by combination of glasses with different CTE

The reference series characterize a clear S-form with high slope. The pressure resistance in the current dimension is lower than the smaller dimension due to the effect of size (chapter 6.4). A comparison of pure C5 fibers and the combination C5-C5, which are made of two C5 tubes, shows similar slope and development of both graphs. Again, the curve of C5-C5 combination slides to the left and indicates a lower pressure resistance. It seems that the decrease of pressure resistance of C5-C5 combination increases with increasing diameter.

Fibers combined from C5 as outer layer and C1S as inner layer exhibit nearly the same resistance against inner pressure than pure C5 fibers. The graphs of both test series

nearly overlay each other especially in lower pressure range. In upper devolution the curve of C5-C1S combined fibers features a slightly higher slope, which is a consequence of the lower maximum burst pressure. Nevertheless, the characteristic pressure of both curves is comparable and this represents the inflection point.

The graph of the combination C1S-C5 shows a significantly lower slope as in the other diagrams. A wide spread between minimum and maximum burst pressure leads to the plotted distribution of failure probabilities. The initial point of the graph is comparable to C5-C5 combination. Nevertheless, the majority of samples of C1S-C5 fibers burst at higher pressures than the other series. Therefore, the graph slides to the right and indicates an improvement of pressure resistance.

Comparing the listed test results and the plotted diagrams it is detectable that the combination of borosilicate C1S as outer layer and borosilicate C5 as inner layer entailed an improvement of resistance against inner pressure. Three different dimensions led to similar developments of the plotted graphs. It should be noted that the minimum burst pressures of the C1S-C5 combined fibers, independent on the dimension, showed lower values than the reference series. However, the majority of tested samples exhibited burst pressures higher than those of the other combinations. It was the only combination of different tubes that were drawn to hollow fibers which featured an increase of pressure resistance.

In theory the combination of two glasses with different CTE have a pre-stressing effect on the hollow glass fiber like the process of tempering because of the different shrinking during cooling. Due to the small wall thickness in the range between  $s = 20 \mu\text{m}$  and  $s = 40 \mu\text{m}$  that treatment is not suitable for the glass fibers. The combination of two tubes of borosilicate should have no effect on the performance at inner pressure load. Due to same material all physical parameters are similar and no pre-stressing effects would occur. During drawing of the fibers both tubes were fused. Investigations of cross sections of C5-C5 combined fibers under the light microscope showed a unique wall without any signs of detachment of both layers. Before the drawing process both tubes were stuck into each other. Thereby some place between the outer surface of inner tube and the inner surface of outer tube was necessary to ensure the combination without any slip agents, as these could remain and prevent the fusion of the tubes. Nevertheless, while the tubes were stuck together foreign particles could be inserted in the gap and caused some surface defects at the interface of outer and inner layer. The formation of hollows between the tubes is possible as well. Those could be caused either by foreign particles or an incomplete fusion of both tubes.

An incomplete fusion of the tubes could be affected by the gap. Both tubes had to be heated to the temperature necessary for drawing. The heat impact is from outside so the outer tube was heated completely before the inner tube. Therefore there was an opportunity for the drawing process to have begun too early. Furthermore, the gap had to be compensated by the flow of the material. The drawing speed of one tube had to be faster than the other. Due to the higher temperature of the outer layer the outer tube could be forced to bulging by applying on the inner tube. That change of form and free space, together with different temperatures of inner tube and outer tube, could cause the incomplete fusion of the tubes and therefore cause the lower pressure resistance.

Combined fibers of C5-C1S borosilicate had pressure resistance comparable to pure borosilicate C5. The graphs showed similar developments and slopes. But degradation in pressure resistance of about 5% could be detected. The investigation under the light microscope showed a clear boundary between the inner and the outer layer, which is displayed in Figure 52.

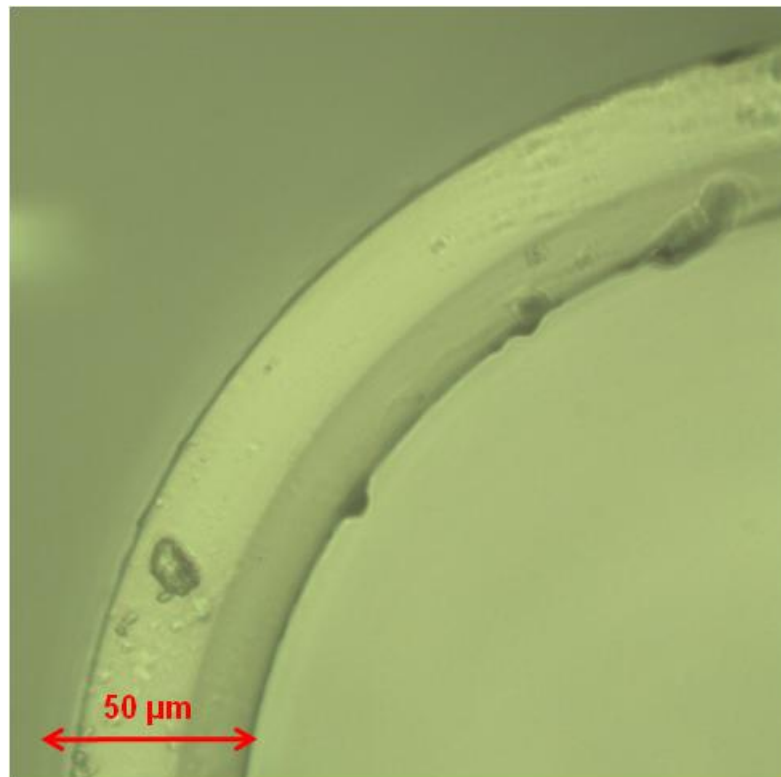


Figure 52: Microscopic view of C5-C1S combined fiber ( $d_o \approx 400 \mu\text{m}$ ,  $d_i \approx 320 \mu\text{m}$ ,  $s \approx 40 \mu\text{m}$ ) with clear boundary of inner and outer layer, magnified 400 times

The usage of borosilicate C5 as outer layer with higher CTE leads to a pre-stressing effect. The inner layer should be under compression stress after cooling and the outer

layer should exhibit tensile stress, while the compression of the inner layer should operate against a load appeared by inner pressure. Borosilicate C5 features a higher temperature level at the characteristic points, which could have a positive influence on the drawing process. If the outer layer is heated completely the inner layer could be heated completely as well due to the lower working point. At the boundary (seen in Figure 52), foreign material can cause the formation of surface defects in surface of fusion. In addition to defects, the formation of hollows is possible as well.

In addition to the boundary line, the thicknesses of the inner and outer layer are also detectable. An uneven distribution between outer and inner layer can be seen. The inner layer, pre-stressed with compression, represents only 40% of total wall thickness. The compression acts against the inner pressure load which has a homogeneous load distribution over the complete inner diameter. Because of the small layer thickness the effect of compression stress is limited and an increase of resistance against inner pressure does not eventuate. The outer layer is pre-stressed with tensile stress which can affect the pressure resistance of the hollow fiber in a negative way. The loadability of glass depends on the surface quality, the quantity and the size of surface flaws [94]. If inner pressure acts on a not prestressed hollow fiber tensile load on the outer surface will occur and might present defects which support the crack propagation until an eventual collapse. In the case of pre-stressed fibers with tensile stress in the outer layer any surface defect on the outer surface can decrease the pressure resistance of a single fiber by a multitude. Due to the present tensile stress a specific load acts on flaws and may lead to the propagation of defects without pressure load. Stress corrosion, caused by air humidity, may also occur on the flaws and accelerate crack propagation. Under the influence of inner pressure the tensile stress at outer surface continues to increase and accelerates the crack propagation once again. Therefore it can be assumed that the increasing effect of the compressed inner layer on the pressure resistance is reversed by the tensile stressed outer layer.

Fibers combined of borosilicate C1S as outer layer and borosilicate C5 as inner layer exhibited highest pressure resistance. The examination under the microscope showed a clear boundary line between the different glasses, as in the case of reversed glass material assembly. A view of a cross section of a combined C1S-C5 fiber with dimensions  $d_o \approx 400 \mu\text{m}$ ,  $d_i \approx 320 \mu\text{m}$  and  $s \approx 40 \mu\text{m}$  is displayed in Figure 53.

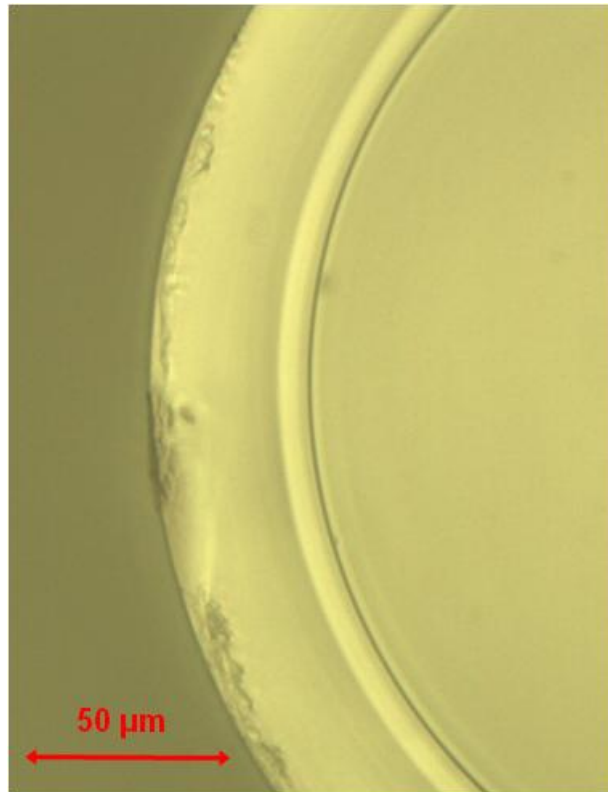


Figure 53: Microscopic picture of C1S-C5 fiber ( $d_o \approx 400 \mu\text{m}$ ,  $d_i \approx 320 \mu\text{m}$ ,  $s \approx 40 \mu\text{m}$ ) with clear borderline between inner C5 layer and outer C1S layer

Again a boundary of both layers is detectable. Due to the present stresses the refraction index is changed and the materials appear in different brightness. The inner layer consisting of borosilicate C5 is stressed with tensile stress because of its higher CTE and therefore possesses a higher shrinking rate during cooling. What is striking is the different thickness of the layers. The outer layer consisting of C1S borosilicate glass contains of about 80% of the total wall thickness. Since the compressed layer is located on the outside of the fiber the influence of defects of the outer surface on the pressure resistance of the material is low. The compression stress acts against the opening of the flaws so that no stress corrosion can occur. Under the influence of inner pressure load the compressed outer layer will act against the opening and increase of defects as well. Due to the high layer thickness in relation to total wall thickness the described effect is amplified and may lead to the improvement in pressure resistance. Nevertheless, the measured minimum burst pressure of C1S-C5 combined fibers exhibited low values comparable to C5-C5 combined fibers with lowest resistance against inner pressure. Here again the contamination of boundary line with foreign particles, like, dust can lead to the formation of hollow or defects which decrease the pressure resistance of the single test samples.

In spite of the investigation, what was demonstrated was the potential of pressure resistance improvement of hollow glass fibers by pre-stressing them. Thereby it has to be considered to ensure the present of compression stress in the outer layer of combined fibers. Compression stress inside the inner layer did not lead to any improvement of the resistance against inner pressure.

An opportunity for further increase of pressure resistance of combined hollow glass fibers could be the production from three tubes. Thus, the outer and the inner layer should be under compression stress and the intermediate layer should be under tensile stress. Hence, the same stress distribution like in tempered flat glass would be present and not only the outer surface but also the inner surface would be pre-stressed with compression. The probability of stress corrosion on the inner surface of thin hollow glass fibers is very low but, nevertheless, it could happen. If the inner surface is compressed to any surface flaw it cannot be opened nor can it decrease the pressure resistance of the fiber. Additionally, the compression acts against the elastic expansion, which is caused by inner pressure load. In case of three layers, two pre-stressed by compression, the increasing effect on the maximum stress could be increased significantly.

The test results can be summarized as following:

- A combination of glasses with different coefficients of thermal expansion (CTE) may pre-stress the fibers during cooling process by different rate of shrinking.
- Borosilicate C5 exhibited a CTE by the factor 1.2 higher than C1S wherefore the shrinking rate will be increased compared to C1S. Indeed, a combination of C1S as outer and C5 as inner glass layer led to an improvement in the range between 30% and 40%, respectively, referred to the characteristic pressure of the test series.
- The combination of glass with low CTE outside and higher CTE inside led to compressive stress at the outer surface and tensile stress at the inner one. Consequently, small Griffith flaws, not visible by investigation with light microscope, were closed or even exhibited decreased size at pressure load.
- Other combinations of C5-C5 and C5-C1S featured decreased pressure resistance.

Table 43: Development of pressure resistance of combined fibers compared to a borosilicate C5 fiber (uncombined)

	<b>C5-C5</b>	<b>C5-C1S</b>	<b>C1S-C5</b>
Pressure resistance	Decreased	Decreased	Increased

## 6.7 Aluminosilicate Glasses

The investigation of glass fibers made of different borosilicate glasses showed the positive influence of alumina oxide with regard to pressure resistance. An increase of the  $\text{Al}_2\text{O}_3$  concentration led to an improvement of resistance against inner pressure. Thus, the percentage of boron oxide had to be constant. A simultaneous increase of  $\text{Al}_2\text{O}_3$  and  $\text{B}_2\text{O}_3$  entailed an almost constant pressure resistance.

Tests with aluminosilicate fibers as described in chapter 6.1 showed inconsistent results. Fibers with two different dimensions made of four diverse glass types were tested for pressure resistance. Fibers with small dimensions showed high pressure resistance comparable to borosilicate fibers. However, fibers with large dimensions exhibited the lowest resistance against inner pressure. Therefore aluminosilicate was not considered for further test series. Contrary to the test results of large fibers, pressure resistance data for solid aluminosilicate fibers with diameters in the range of  $d = 10 \mu\text{m}$  given in literature are in the range of  $\sigma \approx 5500 \text{ MPa}$  [103] at ambient conditions. At cryogenic temperature the tensile strength of such fibers is about  $\sigma \approx 8500 \text{ MPa}$  [103] and, hence, converges to the theoretical strength of glass.

For a comprehensive investigation of the influence of  $\text{Al}_2\text{O}_3$  on the resistance against inner pressure of hollow glass fibers test series with fibers made of different types of aluminosilicate were carried out. The main components of the chemical composition of the used glasses are listed in Table 44. Aluminosilicate 0812 was previously used in the investigation of pressure resistance of different glasses, as described in chapter 6.1. Aluminosilicate 0813 was chosen because of its higher percentage of  $\text{Al}_2\text{O}_3$  and significantly lower concentration of  $\text{B}_2\text{O}_3$ , which can be seen in Table 44 below. The lower concentration of boron oxide was balanced by higher concentration of  $\text{CaO}$ . Other components and their concentrations were comparable to aluminosilicate 0812. The results of both aluminosilicate glasses were compared to results of borosilicate C5 fibers, determined as borosilicate glass fibers with the highest pressure resistance.

Due to the unavailability of aluminosilicate glass tubes of both types with same free space the compared fibers did not have the exact same dimensions, there were slight differences. As conducted in previous investigations, two different dimensions were tested to examine not only the impact of the material, but the size effect as well. The test results of both aluminosilicate glasses are listed in Table 45.

Table 44: Chemical main components of tested aluminosilicate glass fibers given in technical data sheets of the manufacturer

Components [ma-%]	Aluminosilicate 0812 (Schott 8252) [150], [177]	Aluminosilicate 0813 (Schott 8253) [178]	Borosilicate C5 [151]
SiO <sub>2</sub>	60.0	61.0	72.0
Na <sub>2</sub> O	0.02	0.02	6.7
Al <sub>2</sub> O <sub>3</sub>	14.0	16.5	6.8
B <sub>2</sub> O <sub>3</sub>	4.5	0.5	11.4
BaO	9.0	8.0	
CaO	10.0	13.0	
MgO	2.5		
K <sub>2</sub> O			2.4

Table 45: Characteristic test results of hollow aluminosilicate fibers with different dimensions, the fibers were made of two types of aluminosilicate glass with different composition, borosilicate C5 fibers conduce as reference

Material	Dimension (d <sub>o</sub> ; d <sub>i</sub> ; s) [μm]	Min. burst pressure p <sub>min</sub> [MPa]	Max. burst pressure p <sub>max</sub> [MPa]	Form parameter b	Characteristic pressure P [MPa]
Alumino 0812	340; 300; 20	20.7	44.9	7.1	38.0
Alumino 0813	300; 240; 30	31.2	101.1	5.8	64.4
Boro C5	320; 260; 30	41.2	78.3	8.5	55.1
Alumino 0812	400; 300; 50	37.5	61.6	7.9	53.5
Alumino 0813	400; 320; 40	50.7	102.3	7.1	79.5
Boro C5	420; 340; 40	30.2	57.3	8.8	45.9



Test results with hollow fibers made of aluminosilicate 0812 glass with dimensions of  $d_o = 340 \mu\text{m}$ ,  $d_i = 300 \mu\text{m}$  and  $s = 20 \mu\text{m}$  showed high resistance against inner pressure in comparison to hollow fibers made of other glasses like borosilicate 3.3 or quartz glass (chapter 6.1). Comparing these results to measured data of fibers from aluminosilicate 0813 and borosilicate C5, the lowest pressure resistance is detectable for hollow fibers made of aluminosilicate 0812. Samples from aluminosilicate 0813 with  $d_o = 300 \mu\text{m}$ ,  $d_i = 240 \mu\text{m}$  and  $s = 30 \mu\text{m}$  exhibit 55% improvement in minimum burst pressure. The maximum burst pressure is more than double compared to the other aluminosilicate and the characteristic pressure is nearly double as well. The form parameter  $b$  is smaller than the value of aluminosilicate 0812 due to the higher spread as well as the increase of improvement, which is nearly 55% at minimum and about 120% at maximum burst pressure value.

Also the data of borosilicate C5 features higher value than aluminosilicate 0812. The minimum burst pressure is twice as high as the according value of aluminosilicate 0812 and even 10 MPa higher than the value of 0813. Nevertheless, the characteristic pressure and the maximum burst pressure of borosilicate C5 are higher than those of aluminosilicate 0812, but remain below the values of according data of samples from aluminosilicate 0813.

With regard to the larger dimensions a similar behavior can be detected. Again test samples made of aluminosilicate 0813 exhibit the highest measured values of minimum and maximum burst pressure. An improvement of 35% at minimum and 40% at maximum burst pressure compared to aluminosilicate 0812 is discernible. The characteristic pressure  $P$  actually increased by the factor 1.5.

Nevertheless, aluminosilicate 0812 fibers with large dimensions of  $d_o = 400 \mu\text{m}$ ,  $d_i = 300 \mu\text{m}$  and  $s = 50 \mu\text{m}$  features higher pressure resistance than borosilicate C5 which is indicated by higher reached pressure values. The maximum burst pressure reaches a comparable range but still remains below the value of aluminosilicate 0812. Indeed, the form parameter  $b$  is the highest in comparison which stands for a narrow distribution of measured values. However, the minimum burst pressure as well as the characteristic pressure of borosilicate C5 have smaller values than those of aluminosilicate 0812 and therefore indicate a lower resistance against inner pressure load.

The calculated failure probabilities of the three tested glasses with small dimensions are plotted against the single burst pressure values and shown in Figure 54. Again, the

visualization gives a proper way of comparison of the different behaviors and pressure resistances of the test series.

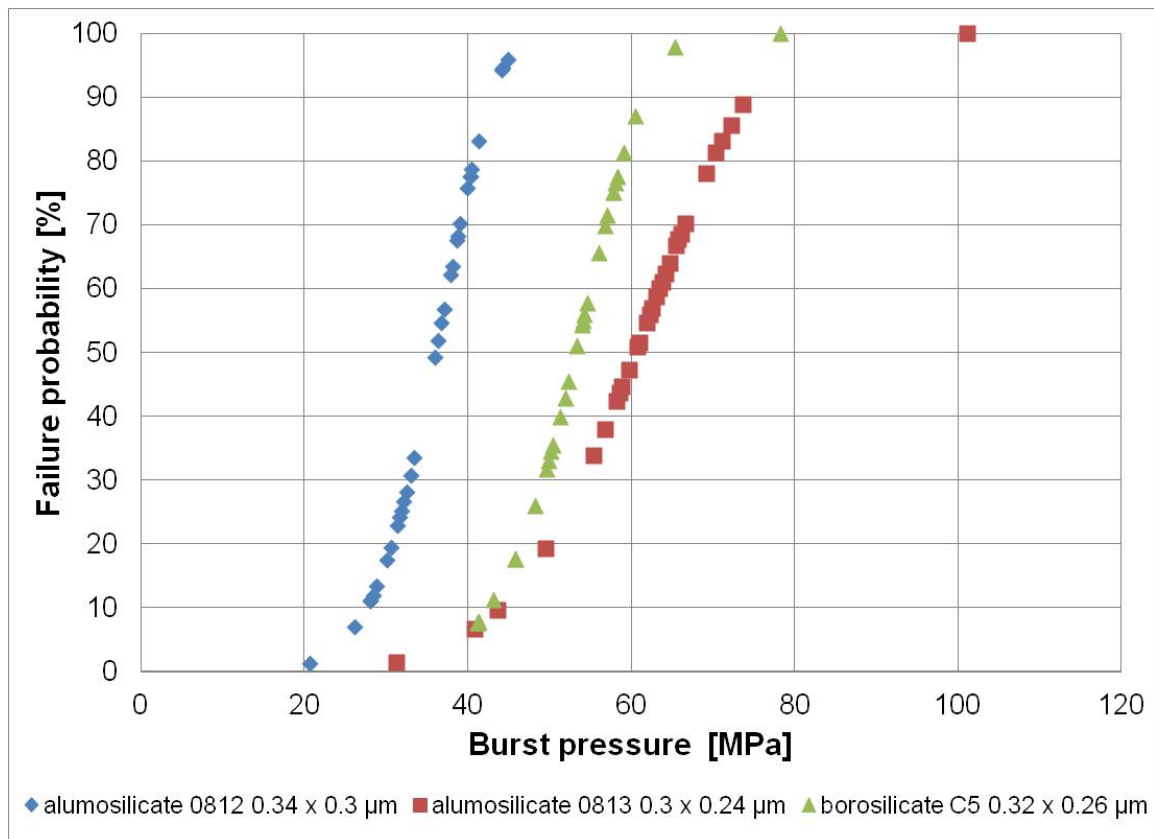


Figure 54: Comparison of the failure probability of hollow aluminosilicate glass fibers with similar dimensions in the range of  $d_o \approx 320 \mu\text{m}$ ,  $d_i \approx 250 \mu\text{m}$  and  $s \approx 30 \mu\text{m}$  but different glass mixture, as comparison value the test results of borosilicate C5 fibers were plotted

The graph of aluminosilicate 0812 test samples represents an S-curve with clear and sharp development. Due to the high slope a convergence to an ideal step function is detectable. The graph of aluminosilicate 0813 does not exhibit such a high slope but slides to the right significantly, as illustrated in the diagram. This is a distinct indicator for higher pressure resistance due to higher burst pressure reached by the test samples. Indeed, the minimum burst pressures as initial points of the curves are close together. Nevertheless, an improvement of almost 50% is detectable at the initial point. The maximum values of both series feature a significant distinction which leads to the lower slope of aluminosilicate 0813 but also leads to an improvement of 120% in maximum.

The form and development of the graph of borosilicate C5 are comparable to aluminosilicate 0812. Similar to aluminosilicate 0813, the graph slides to the right and indicates a higher pressure resistance.

Calculations of failure probabilities of test series with larger dimensions were done and visualized as well. The diagram is given in Figure 55 whereby again the failure probability is plotted against the burst pressure of single test samples.

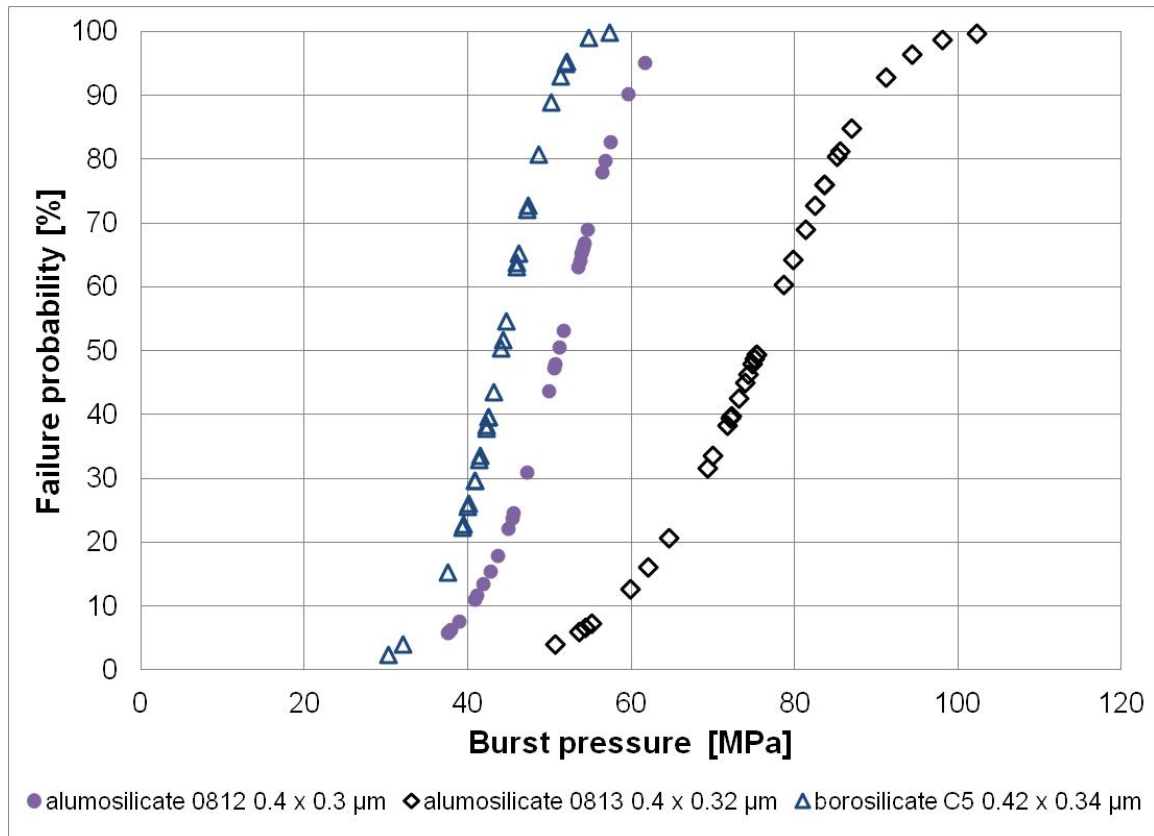


Figure 55: Comparison of the failure probability of hollow aluminosilicate glass fibers with similar dimensions in the range of  $d_o \approx 400 \mu\text{m}$ ,  $d_i \approx 300 \mu\text{m}$  and  $s \approx 50 \mu\text{m}$  but different glass mixture, as reference value the results of borosilicate C5 fibers was taken

In comparison to the test samples with smaller dimensions, the graph of aluminosilicate 0812 represents a clear and sharp S-curve with high slope. Again the curve of aluminosilicate 0813 shows a lower slope which indicates a wider spread of measured pressure values. However, the graph slides to the right. As a result, the pressure resistance of aluminosilicate 0813 is higher than aluminosilicate 0812 of similar dimensions.

The graph of borosilicate C5 again shows similar development and form than the graph of aluminosilicate 0812. But the graph of C5 slides to the left compared to 0812. Therefore the resistance against inner pressure of borosilicate glass in tested dimensions is lower than aluminosilicate glass independent of composition.

The comparison between the two different aluminosilicate glasses repeatedly demonstrated the influence of chemical composition on the mechanical properties. During previous investigations of borosilicate glass fibers the impact of boron and alumina oxide on the pressure resistance was examined (chapter 6.5). An increase of alumina oxide at the same time as a decrease of the percentage of boron oxide leads to an improvement of pressure resistance. The addition of alkaline and alkaline earth oxides in general leads a weakening of the silica network due to the breaking of bridge oxygen [3]. The formation of disconnecting points leads to decreasing temperatures which are important in the manufacturing and processing of glass [3], [4].  $\text{Al}_2\text{O}_3$  and  $\text{B}_2\text{O}_3$  are classified as stabilizers and can effectuate a reduction of disconnecting points dependent on their concentration. The physical properties of glass thereby are dependent, most notably on the percentage of boron oxide, which has an open structure. In high concentrations boron oxide has a destabilizing effect [4], [2] whereby the limiting concentration depends on the types of additives and their percentage.

The two examined glass types from the aluminosilicate group exhibited different chemical compositions. Independent of the dimensions, fibers made of aluminosilicate 0813 featured the highest resistance against inner pressure load. The measured burst pressures and the resulting characteristic pressures of fibers of small, as well as of large dimensions, reached values that are nearly twice as much as in the comparison with aluminosilicate 0812.

The chemical composition of the two glass types might be the reason for that behavior. The percentage of silica as the main component and network former in both glasses exhibited nearly the same value. Nevertheless, aluminosilicate 0812 had 14.0% of alumina oxide and 4.5% of boron oxide. In contrast, aluminosilicate 0813 featured a percentage of  $\text{Al}_2\text{O}_3$  of 16.5% and an almost negligible amount of 0.5% boron oxide.

Compared to the reference glass borosilicate C5 the amount of  $\text{B}_2\text{O}_3$  is low. However, attention has to be paid to the amount of silica which is significantly higher for borosilicate. Therefore it can be assumed that the effect of boron and alumina oxide in the composition of borosilicate is different to the effect in aluminosilicate. The concentration of 4.5% of  $\text{B}_2\text{O}_3$  in 0812 can lead to a decrease of resistance due to the small percentage of 60% silica. Therefore it can be assumed that the concentration of

4.5%  $B_2O_3$  exceeded the limiting concentration of stabilizing effect and boron oxide became a network modifier. An exact value of the limiting concentration of  $B_2O_3$  is not given in the literature due to its dependency on the percentage of silica and any other component [3], [4]. Therefore for each chemical composition it is varying.

Aluminosilicate 0813 featured only 0.5% of boron oxide but a simultaneously higher percentage of alumina oxide.  $Al_2O_3$  led to a stiffening of the network structure due to the effect of a network builder. The very low percentage of 0.5%  $B_2O_3$  led to an increasing impact on the mechanical resistance as well. In that low concentration boron oxides acts as a network builder and a reduction of disconnecting points is effectuated by  $Al_2O_3$  and  $B_2O_3$ .

The used reference material borosilicate C5 had a significantly higher percentage of 72% of  $SiO_2$  wherefore a higher amount of network builder is available. The limiting concentrations of  $Al_2O_3$  and  $B_2O_3$  changed in comparison to aluminosilicate.  $Al_2O_3$  did not have to act as a network builder in that dimension as in the aluminosilicate glasses with only 60% of silica. Nevertheless, fibers of C5 showed contrasting results in pressure resistance. Samples of small dimensions reached burst pressures between both aluminosilicate glasses, while fibers of large dimensions reached the smallest pressure resistance compared to aluminosilicate glasses.

At this juncture the deviation in dimensions had to be considered. Focusing on the small dimensions fibers made of aluminosilicate 0812 exhibited the smallest wall thickness which could be an advantage. However, the test samples had the largest diameter as well. Hence, the tested samples exhibited different inner surfaces and volumes which acted on those surfaces. Smaller wall thickness led to higher pressure resistances in earlier investigations only in union with smaller dimensions.

The comparison of test samples of large dimensions led, however, to a completely opposite result. In comparison with borosilicate C5 and aluminosilicate 0813, fibers made of aluminosilicate 0812 had the highest wall thicknesses. In addition, samples of 0813 and C5 exhibited higher inner diameters. Nevertheless, aluminosilicate 0813 showed the highest resistance against inner pressure load independent of dimension.

The investigation of hollow glass fibers made of different aluminosilicate glasses showed the positive effect of high percentages of  $Al_2O_3$  on the pressure resistance. Indeed, the deviations in dimensions had to be considered. However, the higher percentage of alumina oxide led to higher reached burst pressures by having both smaller and larger wall thicknesses. Therefore the effect of dimensions could be exceeded. In comparison

to borosilicate fibers with similar dimensions higher pressure resistance can be reached as well.

As result of this investigation it can be summarized that:

- Fibers of two different aluminosilicate glasses in two different dimensions were investigated. Aluminosilicate 0813 featured higher percentage of  $\text{Al}_2\text{O}_3$  and significant lower amount of boron oxide compared to aluminosilicate 0812.
- Aluminosilicate 0813 showed an improvement in pressure resistance by pressurized fibers. Based on the characteristic pressure of test series the increased aluminum oxide amount led to an improvement between 50% and 70% compared to aluminosilicate 0812 with lower  $\text{Al}_2\text{O}_3$  amount.
- Compared to borosilicate C5 glass as well an improvement was detected of 15% and 70%, respectively. Consequently, the increase of  $\text{Al}_2\text{O}_3$  with simultaneous decrease of  $\text{B}_2\text{O}_3$  led to improved pressure resistance as seen for borosilicate glass as well.
- Aluminosilicate 0813 exhibited constantly the highest burst pressure resistance in this study.

Table 46: Development of pressure resistance of aluminosilicate fibers compared to a borosilicate C5 fiber

	<b>Aluminosilicate 0812</b>	<b>Aluminosilicate 0813</b>
Small dimension	Decreased	Increased
Large dimension	Increased	Increased

### 6.8 Influence of Variation of Production Parameter on the Pressure Resistance

The pressure resistance of hollow glass fibers can be affected by the chemical composition of the used, as shown in chapter 6.5 and 6.7. Thus, the concentration of  $\text{Al}_2\text{O}_3$  and  $\text{B}_2\text{O}_3$  affected the pressure resistance of tested hollow glass fibers.

The condition of the glass surface is an important factor which influences the global strength of the material [94], [95] and, finally, the maximum stress inside a component. The property of the surface can be changed by different environmental factors, as outlined in chapter 6.2 and 6.3. Furthermore, the mechanical resistance and the condition of the surface can be affected by different production parameters due to the impact of the thermal and mechanical history of the material [3], [94], [97]. In addition to

the working temperature, the cooling rate also influences possible stresses inside the glass and thus the loadability. Different processes, such as annealing, can be used to relax the material and increase the mechanical resistance [3].

The drawing process of hollow glass fibers depends on different production parameters. Glass tubes with diameters of about  $D_0 = 50$  mm were heated up in a furnace and drawn to small hollow fibers. The most important process parameters are:

- The input of glass into the furnace, defined as down speed  $S_{dn}$ ,
- The output of glass out of the furnace, defined as drawing speed  $S_{dr}$ ,
- The drawing temperature inside the furnace  $T_d$ .

Changes of these parameters results in differences of following drawing properties:

- Residence time of glass inside the furnace  $t_R$ ,
- Drawing stress which acts on the material  $\sigma_D$ ,
- Drawing viscosity  $\eta_D$ .

Each change of any parameter leads to different mechanical as well as thermal history of the material and might influence the pressure resistance of the produced hollow glass fibers.

Therefore an investigation of the effect of production parameters was carried out with five different test series. Single process parameters were changed and compared to a reference series. The tested samples were hollow fibers made of borosilicate 3.3 (DURAN) glass tubes of the same batch. Reference series hollow glass fibers were produced at defined process parameters. In order to examine each influence different parameters were changed which resulted in different drawing properties.

### 6.8.1 Increase of Residence Time

The residence time of glass inside the furnace during the drawing process depends on both the down speed and the drawing speed. An increase of residence time requires the decrease of the process velocity, which results in slower input as well as output of glass, and consequently in longer heating time. At higher process velocity the glass will not reach the predefined working temperature and the material flow will be decelerated because of a high viscosity. A slower drawing process supports the flow of the material which is necessary at the drawing process to reach the deformation of the glass tube to the smaller size.

Two process parameters were changed during the drawing of fibers with increased residence time. The down speed as well as the drawing speed was decreased whereby

it had to be considered that the ratio of both parameters remain almost the same. The ratio between drawing speed and down speed was defined as drawing ratio DR:

$$DR = \frac{S_{dr}}{S_{dn}} \quad (5.5).$$

The process parameters of the reference series A and series B with increased residence time are listed in Table 47. It can be seen that the draw ratios of the tested series are similar. The differences of both ratios are demonstrated by small deviations in changes of down and drawing speed. Thereby the down speed of series B is decreased by the factor 1.4 compared to series A, whereas the drawing speed is decreased by the factor 1.5. Nevertheless, the comparable draw ratios result in similar dimensions. The drawing temperature of tested fibers remains the same to exclude an influence of temperature on the viscosity.

The increased residence time should result in homogeneous heating of the glass tube. Due to the longer duration inside the furnace the material had more time to reach the defined drawing temperature and viscosity. Therefore the flow behavior of the glass is supported and the acting drawing stress is decreased during drawing process. The processing of glass is not fixed at a specific temperature value. Rather, it is spread by a temperature region which is different for each glass type. The viscosity of glass should be in a range between  $\eta = 10^{12}$  dPa s and  $\eta = 10^{3.5}$  dPa s [2]. In that region the temperature is above the transformation temperature  $T_g$  but below the melting temperature  $T_m$ . The longer the residence time the lower the drawing stress on the material and the stress inside the material after cooling should be reduced.

The characteristic test results of series A and B are listed in Table 48. Series B with increased residence time exhibits considerable lower values not only for the minimum burst pressure but also for maximum and characteristic pressure. The minimum burst pressure decreased about 75%. For the maximum burst pressure a degradation of 30% can be detected as well as for the characteristic pressure P. Due to the wide spread between minimum and maximum burst pressure the form parameter b of series B exhibits a lower value than the according parameter of series A.



Table 47: Process parameters of hollow DURAN glass fibers with different residence time but similar dimensions of  $d_o \approx 490 \mu\text{m}$ ,  $d_i \approx 420 \mu\text{m}$  and  $s \approx 35 \mu\text{m}$ , whereby series A represents the reference series

Test series	$S_{dn}$ [cm h <sup>-1</sup> ]	$S_{dr}$ [m s <sup>-1</sup> ]	DR	$T_d$ [°C]
Series A (reference)	2.54	1.47	206,692	910
Series B (increased residence time)	1.78	0.96	192,612	910

Table 48: Distinct test results of borosilicate DURAN glass fibers with comparable dimensions, series B produced with increased residence time but same drawing temperature

Test series	Dimension ( $d_o$ ; $d_i$ ; $s$ ) [ $\mu\text{m}$ ]	Min. burst pressure $p_{min}$ [MPa]	Max. burst pressure $p_{max}$ [MPa]	Form parameter $b$	Characteristic pressure $P$ [MPa]
Series A (reference)	492.0; 421.8; 35.1	15.3	38.8	5.2	28.6
Series B	487.8; 415.0; 36.4	4.1	26.0	3.2	20.4

A visualization of the resulting failure probabilities against the measured burst pressure of each single fiber of both series is given in Figure 56.

The diagram provides a good opportunity to compare the two graphs. The distinct difference of both series is detectable. The graph of series B slides significantly to the left and an S-shape of the curve is observable only slightly. This behavior is attributed to the small form parameter  $b$  of series B. Both aforementioned characteristics indicate a lower pressure resistance of tested samples of series B compared to the reference series A, whose graph illustrates a clear detectable S-shape and significantly higher burst pressures. Furthermore, the failure probability exhibits a considerable lower value. At an inner pressure of  $p = 20 \text{ MPa}$  series A achieves a failure probability of  $F_B = 15\%$ , while series B at same inner pressure exhibits a distinctly higher value of  $F_B = 60\%$ .

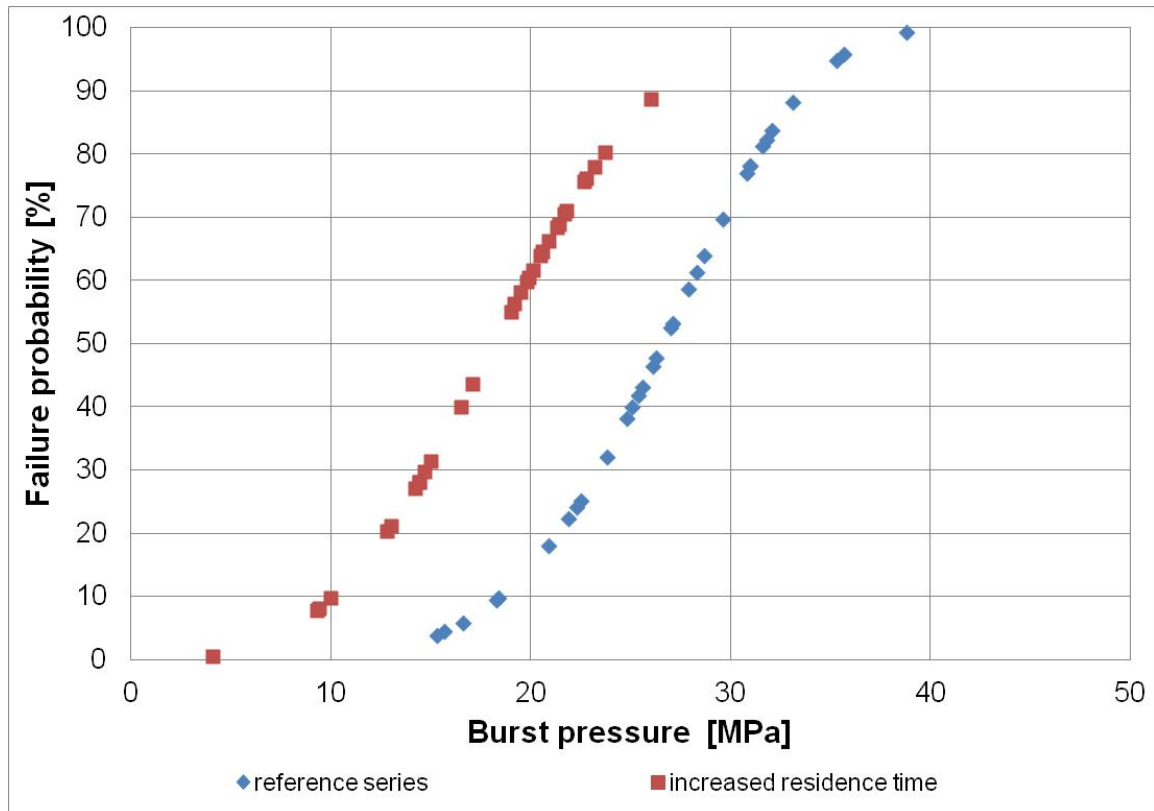


Figure 56: Influence of increased residence time during drawing process on failure probability of hollow DURAN fibers with  $d_o \approx 490 \mu\text{m}$ ,  $d_i \approx 420 \mu\text{m}$  and  $s \approx 35 \mu\text{m}$

The increase of the residence time of DURAN fibers leads to a significant decrease of the resistance of the glass fibers against inner pressure load. The higher residence time should lead to a homogeneous heating of the complete wall thickness of the glass tube before drawing. The viscosity and the drawing stress inside the material during drawing process should be decreased simultaneously. However, the test results showed that the assumed behavior did occur.

The investigation of the fibers under the light microscope showed defects on the surface of the reference series A as well as on the surface of samples of series B. Figure 57 shows the surface of a test sample of series A.

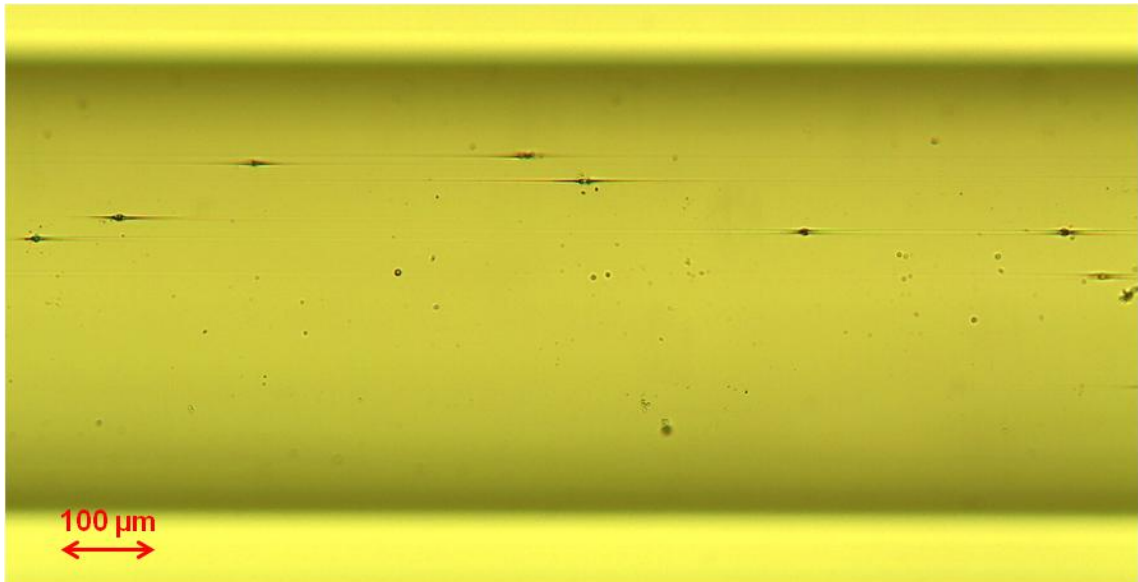


Figure 57: Surface defects of hollow DURAN fiber of series A with  $d_o \approx 490 \mu\text{m}$ ,  $d_i \approx 420 \mu\text{m}$  and  $s \approx 35 \mu\text{m}$  (magnified 100 times), test samples act as reference in investigation of the effect of product parameter on pressure resistance

The surface exhibits different small defects which are surrounded by short stripes in drawing direction. It can be assumed that those defects were originated by enclosures inside the glass tube before the drawing process. Such enclosures can be composed of refractory material of the melting pot during the production of the glass tubes, which are used for drawing the tested fibers. Raw material which did not melt completely and remained in an original state in the molten mass, due to insufficient homogenization, can form such enclosures as well. Additionally, impurities like dust or particles of the refractory material of the furnace could be deposited during drawing process on the soft surface of the heated glass.

Independent from the original similar surface, defects could be detected on the surface of series B which can be seen in Figure 58.

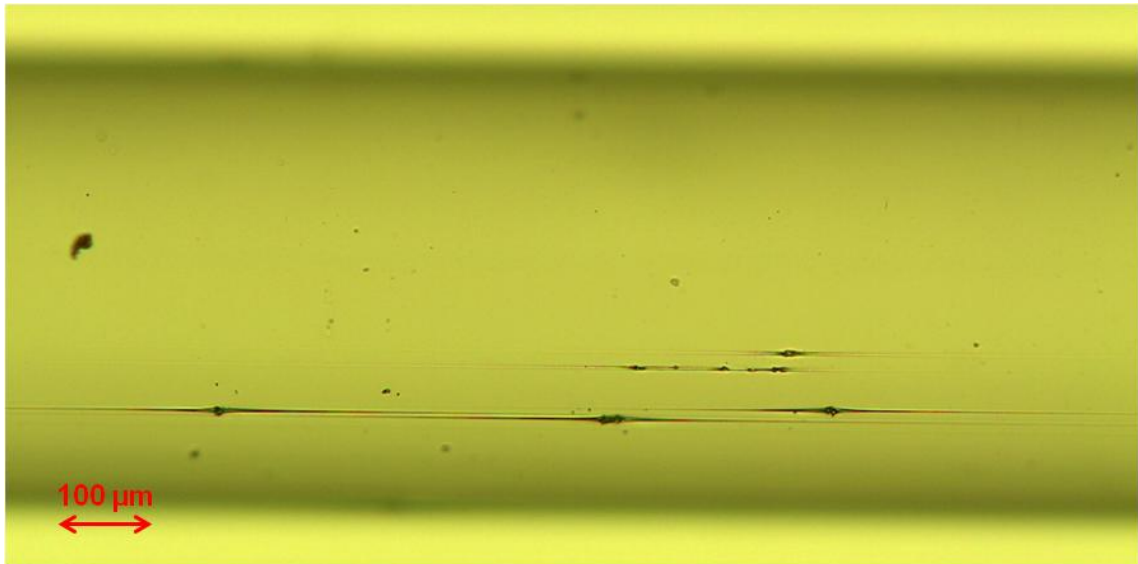


Figure 58: Surface defects of Duran fiber of series B with  $d_o \approx 490 \mu\text{m}$ ,  $d_i \approx 420 \mu\text{m}$  and  $s \approx 35 \mu\text{m}$  (magnified 100 times) produced at increased residence time

The defects show the same shape and comparable size to the defects on fiber surface of series A in Figure 57. A difference can be seen in the length of the stripes surrounding the defects in drawing direction. The stripes on series A surface had a length of about  $l = 100 \mu\text{m}$ , while the stripes in Figure 58 on the surface of series B fibers exhibited a length of about  $l = 400 \mu\text{m}$  up to  $l = 500 \mu\text{m}$ .

The increased residence time led to a homogeneous heating as well to lower viscosity of the processed glass. Due to the longer duration inside the furnace and the homogeneous heating the temperature at the diminution of the glass during drawing process reached higher values and as a result, the viscosity was lower. Consequently the flow characteristics of the glass were different and much lower drawing stress was necessary for producing the small hollow fibers from the glass tube. The lower viscosity and accordingly higher temperature in drawing region led to a slower cooling of the drawn fibers wherefore the formation of the stripes surrounding the surface defects were forwarded.

The stripes represented a kind of indentation or crack in direction of highest stress. At an acting inner pressure load the highest stress acts in tangential direction [172] which can be calculated by formula 5.2. Therefore the stripes forwarded the bursting of the hollow fibers whereby the length seemed to influence the pressure resistance in a negative way. The longer the detectable stripes the lower the measured burst pressure.

### 6.8.2 Increase of Drawing Stress

The stress which acts on the glass during the drawing process can influence the pressure resistance, thus high drawing stress could be frozen in a glass structure and produce a prestressed fiber during the cooling process. The cooling process happens very quickly after leaving the furnace because of the small size of the fiber.

Increasing the drawing stress can be realized by lower drawing temperature but keeping the drawing speed constant, or by higher drawing speed but similar drawing temperature. The process parameters of tested hollow fibers are listed in Table 49. What is clear to see is the increase of drawing speed by the factor 3 whereby the down speed is slightly decreased. The process temperature is elevated to ensure the drawability otherwise the material would rip during drawing or the free space (the open area of the hollow fiber) would be changed. Increasing the drawing speed but holding the down speed on a similar level led to a massive increased drawing ratio DR by the factor 4, which is associated with decreasing dimensions of produced fibers.

Table 49: Process parameters of hollow DURAN glass fibers with increased drawing stress and dimensions of  $d_o \approx 490 \mu\text{m}$ ,  $d_i \approx 420 \mu\text{m}$  and  $s \approx 35 \mu\text{m}$  (series A) and  $d_o \approx 270 \mu\text{m}$ ,  $d_i \approx 240 \mu\text{m}$  and  $s \approx 15 \mu\text{m}$  (series C)

Test series	$S_{dn}$ [cm h <sup>-1</sup> ]	$S_{dr}$ [m s <sup>-1</sup> ]	DR	$T_d$ [°C]
Series A (reference)	2.54	1.47	206,692	910
Series C (increased drawing stress)	1.78	4.21	844,703	965

The resulting smaller dimensions of fibers of series C compared to test samples of test series A are summarized together with the characteristic test results in Table 50. It is observable that increasing the draw ratio DR by the factor 4 leads to decreased dimensions by the factor 2. Consequently, the diameters and the wall thickness of series C fibers are only half as big as the reference series. With regard to the pressure values concerning both series it is rather strange that series C with smaller dimensions exhibits lower pressure values than the reference series. The minimum burst pressure is decreased by the factor 1.2 which could be affiliated to an outlier in test series. But the characteristic and the maximum burst pressure exhibit debased values as well. Thereby the factor of degradation is about 2. However, the spread between minimum and

maximum burst pressure is minimized wherefore the form parameter  $b$  is higher than the according parameter of the reference series.

Table 50: Characteristic test results of DURAN glass fibers at inner pressure load, the fibers were produced at different drawing speed and stress

Test series	Dimension ( $d_o$ ; $d_i$ ; $s$ ) [ $\mu\text{m}$ ]	Min. burst pressure $p_{\min}$ [MPa]	Max. burst pressure $p_{\max}$ [MPa]	Form parameter $b$	Characteristic pressure $P$ [MPa]
Series A (reference)	492.0; 421.8; 35.1	15.3	38.8	5.2	28.6
Series C	266.8; 238.0; 14.4	12.9	18.9	11.7	16.3

The significant difference between reference series A and test series C produced with increased drawing stress becomes more clearly in Figure 59. The calculated failure probabilities are plotted against the single burst pressures in a diagram in typical S-curves resulting from Weibull distribution.

The diagram points out significant deviation between reference series A and test series C. Clear to see is the wider spread of the reference series and consequently a lower value of the form factor of  $b = 5.2$ . Therefore the slope of the graph is lower but the development of the graph exhibits a consequent progression. The initial points of both graphs represent the minimum burst pressures of both series and lay roughly in the same pressure range. However, the test samples of the reference series reach higher burst pressures without showing any outliers.

In stark contrast to above results, the graph test series C features a high slope which approaches to the ideal step function very well because of the high form factor of  $b = 11.7$ , resulting from the narrow distribution of measured pressure results between minimum and maximum burst pressure. A straight progression is observable without any detectable outliers, as well as the graph slides to the left in comparison to the location of curve of the reference series. Therefore a degradation of pressure resistance of hollow fibers produced with higher drawing stress can be determined.

A higher drawing speed but nearly the same down speed led to much smaller hollow fibers. The enhancement of drawing speed by the factor 4 led to a bisection of dimensions, but unchanged free space of produced fibers. Test results of former investigations with fibers of similar free space showed increasing pressure resistance

with decreasing dimensions, as described in chapter 6.4. Fibers with same free spaces were produced from the same glass tube independent on the size. The differences of dimensions were made by changes of the drawing speed whereby higher drawing speed caused smaller hollow fibers.

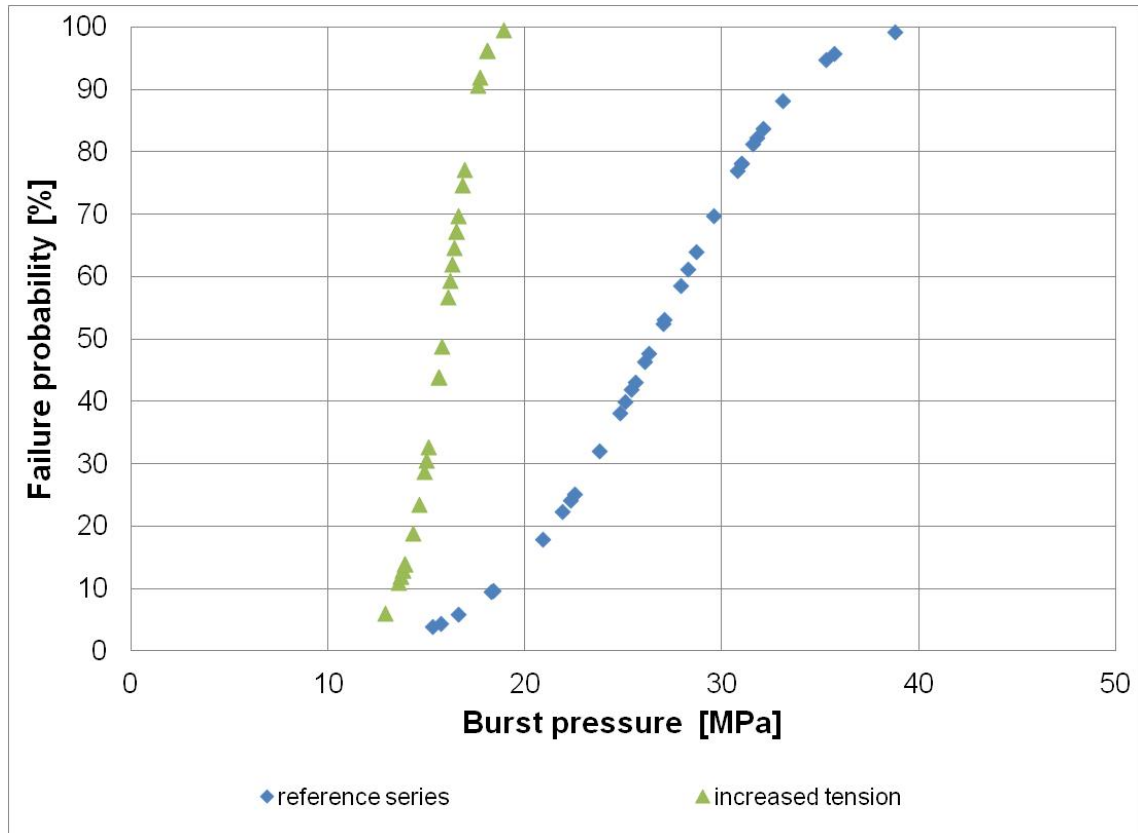


Figure 59: Influence of increased drawing stress on the failure probability of DURAN fibers, increasing the drawing speed led to increased drawing stress

Hence, tested fibers of series C should have showed similar behavior with an improvement of measured burst pressures. Not only the size effect but also the increased stress during drawing process should have led to an improvement of pressure resistance. During cooling the stress should have been frozen in the fibers. It was assumed that the fibers would be prestressed and therefore the pressure resistance could be increased. However, the opposite occurred and smaller fibers showed a degradation of pressure resistance of about 50%. The increased drawing stress on the glass was acting mainly in axial direction. At internal pressure load the highest stress acted in tangential direction. The axial stress at similar loaded conditions had only half the size of the tangential stress [172], and was not responsible for the bursting of test samples.

The investigation of test samples of series A under the light microscope showed surface defects in detectable sizes. Due to using glass tubes from the same batch to draw the fibers of both, series A as well as series C, the surface of fibers of series C exhibited also detectable surface defects as shown in Figure 60.

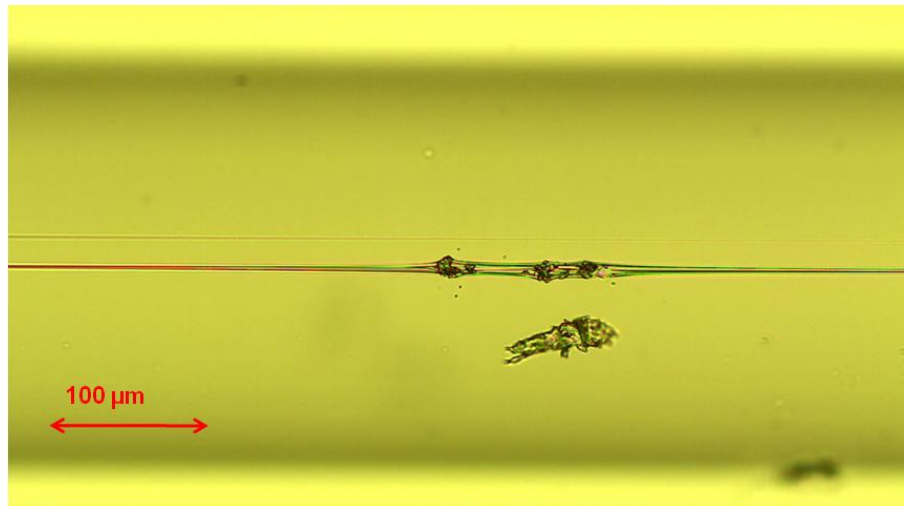


Figure 60: Surface defects of Duran fiber of series C with  $d_o \approx 270 \mu\text{m}$ ,  $d_i \approx 240 \mu\text{m}$  and  $s \approx 15 \mu\text{m}$  produced at increased drawing stress (magnified 100 times)

The detected defects had the same shape as seen on series A and B. Comparing Figure 60 to the picture of series A in Figure 57 it can be seen that the defects had the same size of about  $30 \mu\text{m}$ . With regard to the reduced fiber size they are much bigger. The effect on the pressure resistance of the tested fibers was considerable stronger. The increased drawing speed also led to much longer stripes surrounding the defects in the drawing direction, which again reduced the pressure resistance by acting as a groove in the surface. At acting inner pressure the tangential stress led to bursting of the test sample by forming a stress peak.

It can be assumed that the detected defects decreased the pressure resistance and therefore the improving effect of decreasing size was lost.

### 6.8.3 Increase of Drawing Temperature

The temperature at which glass is manufactured affects the viscosity of the material. The higher the temperature during production process the lower is the viscosity of the material [2] [3]. The increase of the drawing temperature should support the flow of the material as supposed for increased residence time. Thereby the down and drawing speed remain unchanged.



A test series with DURAN fibers produced at an elevated temperature level was carried out and compared to the reference series. An additional series was produced at increased drawing temperature and residence time in order to decrease the viscosity and ensure a homogeneous temperature distribution.

The production parameters of tested series are summarized in Table 51. All listed series exhibits similar draw ratios wherefore the fibers of the three series have similar dimensions with only small deviations. The drawing temperature of series D was elevated about  $\Delta T = 70$  K. Down and drawing speed are similar to the data of the reference series. The fibers of series E were drawn the same increased temperature as series D. Furthermore, the residence time was increased as was a decrease of down and drawing speed.

Table 51: Process parameters of hollow DURAN glass fibers with different drawing temperature and residence time and similar dimensions of  $d_o \approx 490 \mu\text{m}$ ,  $d_i \approx 420 \mu\text{m}$  and  $s \approx 35 \mu\text{m}$

Test series	Down speed $S_{dn}$ [cm h <sup>-1</sup> ]	Drawing speed $S_{dr}$ [m s <sup>-1</sup> ]	Draw ratio DR	Drawing temperature $T_d$ [°C]
Series A (reference)	2.54	1.47	206,692	910
Series D (increased $T_d$ )	2.54	1.34	188,413	982
Series E (increased $T_d$ and $t_R$ )	1.65	0.83	180,949	982

Decreasing the viscosity by increasing the drawing temperature supports the flow of the material. The stress, which acts on the material during drawing process at unchanged drawing speed, is decreased so that the produced fibers should exhibit a more relaxed stress distribution. An additional increase of residence time can lead to further decrease of drawing stress.

The characteristic test results of fibers of series D and E are listed in Table 52 and compared to the reference series. The comparison of pressure data of series D and series A shows an almost constant displacement of series D to lower values. The minimum and the maximum burst pressure as well as the characteristic pressure decrease by the factor 1.4 to 1.6. The form parameter  $b$  changes slightly because of the

lower range between minimum and maximum burst pressure and therefore lower spread of measured data.

A similar behavior can be observed for test results of series E but the additional increase of the residence time leads to a further decrease of pressure data. Compared to series A the results of series E are consistently decreased by the factor 2. Again the form parameter  $b$  rises due to the lower spread between minimum and maximum pressure value.

Table 52: Distinct test results of DURAN fibers of similar dimensions with different drawing temperatures and residence times

Test series	Dimension ( $d_o$ ; $d_i$ ; $s$ ) [ $\mu\text{m}$ ]	Min. burst pressure $p_{\min}$ [MPa]	Max. burst pressure $p_{\max}$ [MPa]	Form parameter $b$	Characteristic pressure $P$ [MPa]
Series A (reference)	492.0; 421.8; 35.1	15.3	38.8	5.2	28.6
Series D (increased $T_d$ )	492.3; 422.8; 34.7	9.3	24.2	5.6	20.3
Series E (increased $T_d$ and $t_R$ )	491.5; 417.5; 37	7.6	19.4	5.9	14.3

Plotting the calculated failure probabilities of the three series listed in Table 52 against the single measured pressure data means that the effect of the changed drawing temperature and residence time becomes clearer. The resulting diagram is given in Figure 61. It should be noted that series D was produced with an increased drawing temperature but similar down and drawing speed. Series E was produced at a similar increased temperature, however, down and drawing speed were decreased in order to increase the residence time. The drawing ratios and the dimensions of the three tested series were similar.

All graphs describe a consistent distributions and a clear detectable S-curve without any outliers. The shift of the graphs of series D in relation to series A is detectable and indicates a degradation of pressure resistance of test samples, which were produced at a higher drawing temperature. As a result of an increase of the residence time of the material inside the furnace during drawing process, a decrease of resistance against inner pressure load is observed by the graph of series E which slides to the left. The increase of the form parameter  $b$  of series D and E is identifiable by a higher slope of the according curves. Therefore the graphs exhibits a better convergence to the ideal saltus function by having a lower pressure resistance.

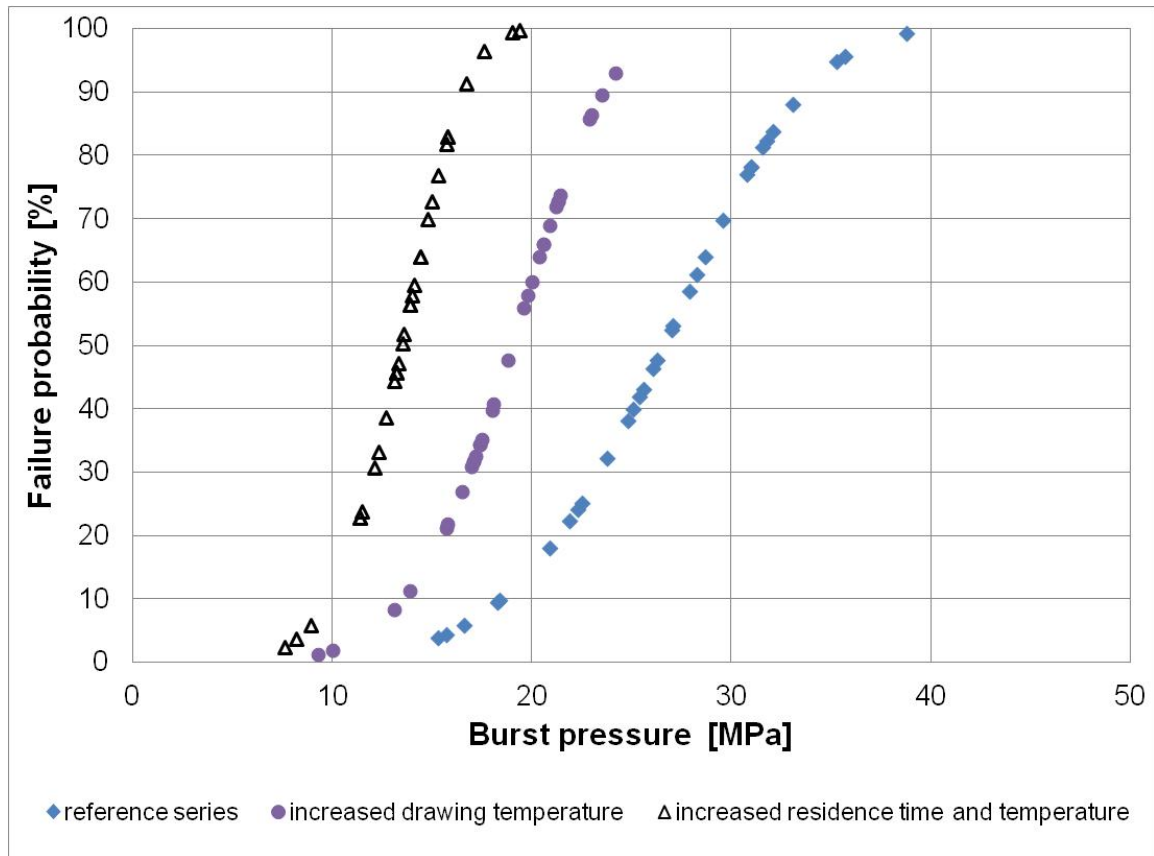


Figure 61: Effect of increased drawing temperature and residence time on failure probability of DURAN fibers with dimensions of  $d_o \approx 490 \mu\text{m}$ ,  $d_i \approx 420 \mu\text{m}$  and  $s \approx 35 \mu\text{m}$  compared to reference series A

Again the change of production parameter which influences directly the viscosity leads to a degradation of the pressure resistance of the tested hollow fibers. In theory, the increased temperature and residence time leads to decreased viscosity wherefore the production and formation process in the glass industry is supported and the viscosity range during processing is between  $\eta = 10^{12} \text{ dPa s}$  and  $\eta = 10^{3.5} \text{ dPa s}$  [2]. The softening point of the used borosilicate DURAN glass is given with  $T = 825 \text{ }^\circ\text{C}$  at  $\eta = 10^{7.6} \text{ dPa s}$  and the working point with  $T = 1260 \text{ }^\circ\text{C}$  at  $\eta = 10^4 \text{ dPa s}$  [148]. Hence, the tested hollow fibers were drawn in given process range but distinct below given working point. Lower viscosity at higher drawing temperature should support the flow behavior of the glass material wherefore the fibers should feature a more relaxed glass structure. Consequently an increase of the resistance against inner pressure should be the following result.

However, the tested fibers provided results that were contrasting in nature vis-à-vis when elevating the process temperature. The light microscopic investigation showed

similar surface defects as detected on the reference series fibers. A microscopic picture is given in Figure 62.

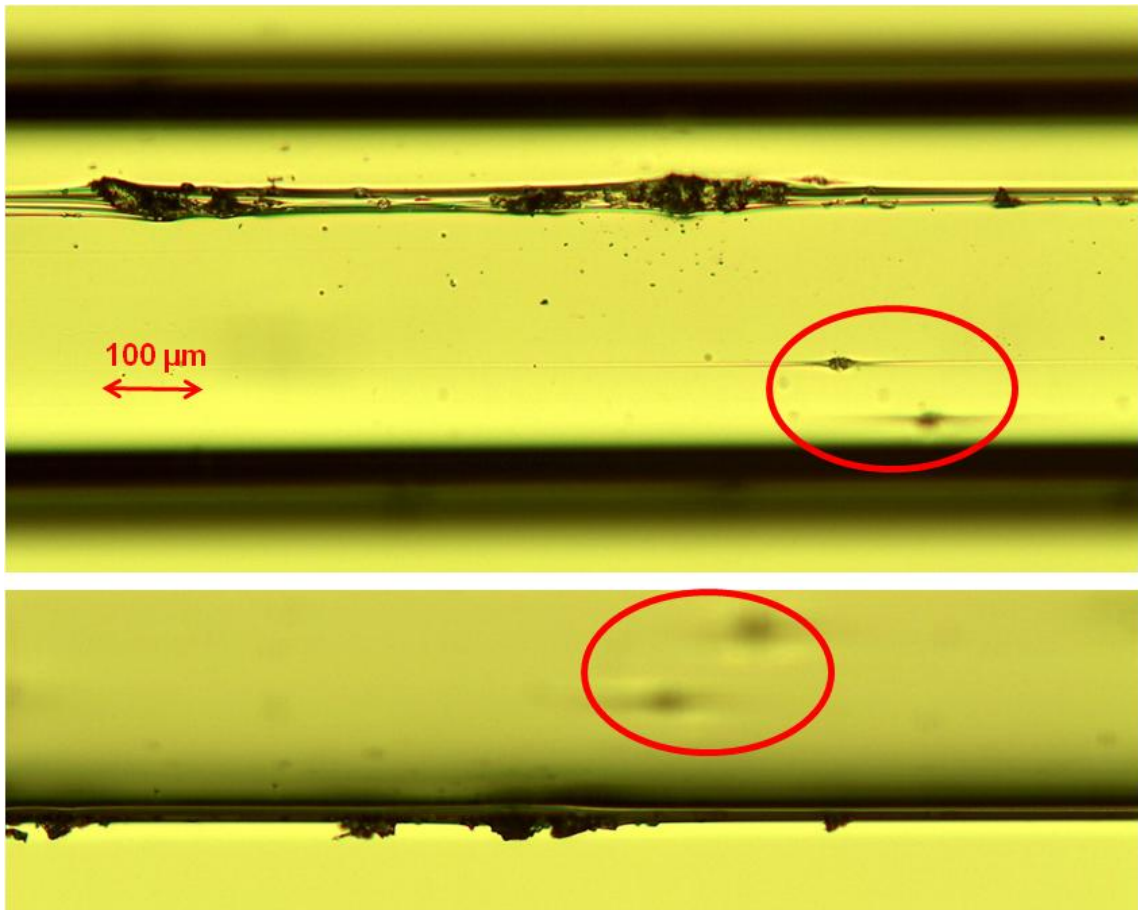


Figure 62: Surface defects on hollow DURAN fiber of series D with dimensions of  $d_o \approx 490 \mu\text{m}$ ,  $d_i \approx 420 \mu\text{m}$  and  $s \approx 35 \mu\text{m}$  (magnified 100 times), fibers were produced at increased drawing temperature compared to reference, both pictures show same fiber but rotated by  $90^\circ$  on lower picture

The surface of fibers of series D exhibited the same defects as on reference series surface with a size of  $30 \mu\text{m}$ . Such defects are surrounded in red in the picture above whereby both pictures show the same defects. In addition to these defects, distinct larger flaws could be detected on single test samples which are shown in Figure 62. In Figure 69, the investigated fiber is rotated by  $90^\circ$  wherefore the elevated structure of the defects becomes clear. Such flaws were an exception rather than the rule and all one has to do is weaken the tested fibers by a multitude and the lower burst pressures can be explained. Not only was the surface of the glass, but also the volume was influenced by such large defects and a characteristic stress peak originated at that location during

inner pressure load. The lower viscosity due to higher drawing temperature supported the formation of the lines and furrows, which surrounded the defects in drawing direction. Consequently the length of the lines was increased due to slower cooling of the fibers. Furthermore, the size of the defects had an effect on the length as well as on the width of the lines. As demonstrated in the pictures above, the large defects originated an indentation of several hundreds of  $\mu\text{m}$  in length and about  $40\ \mu\text{m}$  in width.

Fibers of series E as well featured known surface defects surrounded by lines and stripes in drawing direction shown in Figure 63.

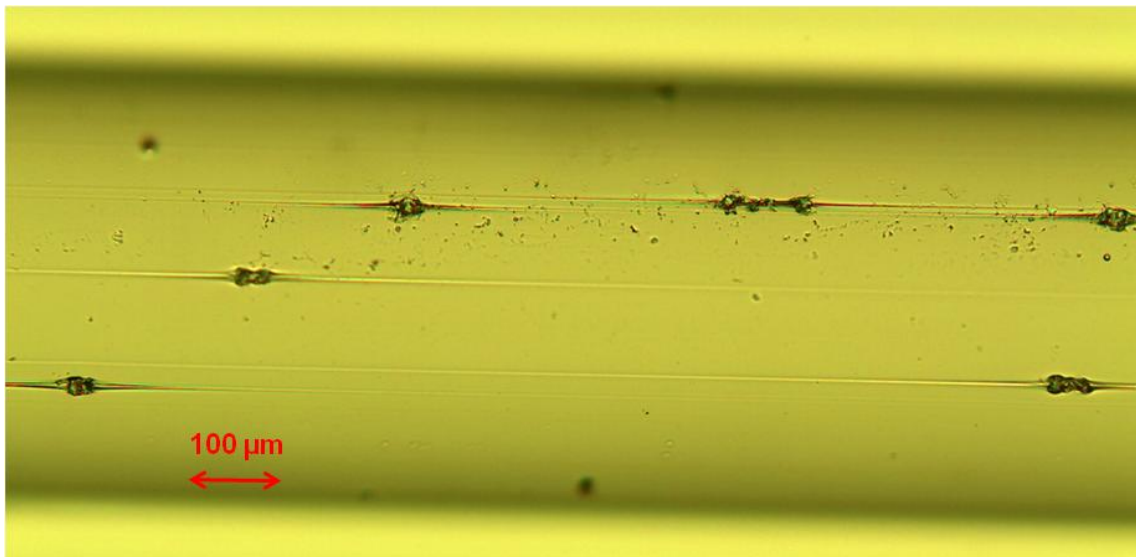


Figure 63: Surface of DURAN fiber of series E with dimensions of  $d_o \approx 490\ \mu\text{m}$ ,  $d_i \approx 420\ \mu\text{m}$  and  $s \approx 35\ \mu\text{m}$  (magnified 100 times)

Again similar flaws are observable on the surface of tested fibers. The size is comparable to these of series A but the higher process temperature and residence time inside the furnace led to longer stripes in drawing directions. The weakening effect due to indentation on the pressure resistance is forced by the increased length of such stripes wherefore a further decrease of pressure resistance can be detected compared to series D.

With regard to all of the results pertaining to the investigated changes of production parameters no improvement could be detected. The assumption of higher pressure resistance by lower drawing stress could not be proven. A lower drawing stress originated by increased residence time, increased drawing temperature or a combination of both and resulting lower local stresses inside the fibers walls did not lead to higher pressure resistance of the tested fibers. Rather, it led to a degradation of it. However,

the determined degradation of the pressure resistance can be ascribed on the influence of surface defects which are detectable on fibers of each tested series even at reference series. The increase of residence time, drawing temperature or both led to a support of the formation of shown stripes and lines in drawing direction. The stripes emanated from the defects wherefore it was not possible to determine the origin of the particles. On the one hand, enclosures inside the glass could be raised to the surface due to the reduction of size during drawing. In addition to the diameters, the wall thickness was also reduced. However, the actual temperature was not high enough to fuse the enclosures and homogenize the glass material which resulted in the enclosures remaining in their size and not rising to the surface. The location of first surface contact was the initial point of the detected lines in drawing direction. On the other hand, particles of the refractory material could be deposited on the hot surface during drawing process and originated some dents as the initial point of the stripes.

The increase of the drawing stress by increased drawing speed to prestressing the fibers was also unsuccessful. The dimensions of test samples were reduced to half of the same free space FS and as a result, the pressure resistance should have been increased and this in direct relation to the results of the experiments concerning size effect, as described in chapter 6.4. However, comparable flaws with the same size as the reference series could be observed and determined on the surface of the small fibers. Due to the smaller dimensions of the fibers, as a result of higher drawing speed, the defects were larger in relation to the fiber diameter. Therefore, the reducing effect on the pressure resistance was higher and a degradation compared to the reference series resulted. Furthermore, the increased drawing speed supported the length of the stripes in drawing direction. Those indentations decreased the pressure resistance due to their axial orientation. During inner pressure load the tangential stress is the highest stress acting on the hollow fiber. The indentations supported the formation of stress peaks due to changing the stress distribution.

The presence of defects of the same size and shape in five different series arose from the use of glass tubes of the same batch for the production of the fibers. Deviations of production parameters could lead to the improvement of the pressure resistance which could not be proven in the tests that were carried out. Therefore it has to be ensured that defect free glass is used in the production process.

An investigation of the raw material showed no enclosures or impurities inside the glass which could be raised to the surface during the drawing process. Therefore test samples of series A to E were investigated by using the energy dispersive X-ray spectroscopy (EDX). The results are summarized in chapter 6.10.3.

As result of the investigation of the influence of varying production parameter it can be summarized that:

- The tensile strength of glass is mainly influenced by the surface property [94], [95]. The effect of different production parameter on the viscosity of borosilicate DURAN glass fibers and their surface was investigated. The residence time, drawing speed and drawing temperature were increased to a reference series wherefore the viscosity and the flow behavior of the glass during drawing process were modified.
- The test results featured a degradation of the pressure resistance by each changed process parameter compared to the reference series.
- An examination of fibers under the microscope showed significant defects even on reference series. All series were produced from glass tubes of the same batch. Therefore the origins of the defects were assumed as enclosures from melting process. The change of production parameters changed the flow characteristics of the glass and supported the formation of stripes and lines in drawing direction beginning at the defects.
- The lower the viscosity by increased temperature, the longer the detectable length of the lines. Due to the effect of the lines in drawing direction the pressure resistance of the tested fibers was decreased significantly.
- In fact, the change of production fibers influences the surface property of glass fibers. A direct coherence could not be determined due to the effect of production parameters on the defect size. The behavior of defect free material could be completely different.

### **6.9 Investigation of the Effect of Surface Coating on Hollow Glass Fibers**

The pressure resistance of hollow glass fibers depends on different parameters such as the characteristics of the type of glass used for the production, the size of the fiber, as well as the presence of defects.

Surface defects heavily influence the mechanical resistance of glass [94]. The origin can be different as shown in previous investigations. Possible impurities of the glass before final formation process as well as dust or hard particles can create surface defects. Another source of surface flaws is the handling during production and packing. The application of a surface coating can prevent surface defects caused by handling.

The application of surface coatings can be done by the using the atomic layer deposition process (ALD). During different steps at elevated temperature a surface coating is generated by a chemical reaction. These processes afford the opportunity of healing existing surface defects by rounding the crack radius or even filling it completely depending on their defect size [136], [137]. Test with glass plates showed an improvement in loadability up to 89% [137].

A further possibility of applying a coating can be realized directly after drawing in the production process. Therefore a polymer like polyacrylate or polyimide is sprayed on the glass fiber and forms a continuous protection shell on the surface against mechanical as well as chemical impacts.

### 6.9.1 ALD-Coated Hollow Borosilicate Glass Fibers

The influence of ALD-coating on the resistance during internal pressure of thin hollow glass fibers were tested with an aluminum oxide coating of four different coating thicknesses of  $s_c = (50, 100, 200, 500)$  nm on the surface of hollow borosilicate C5 fibers. In previous tests, borosilicate glass proved to have the highest resistance when loaded with internal pressure.

The fibers were packed after being produced in special transportation brackets made of stainless steel and transported in a stainless steel box, as shown in Figure 64. The brackets were secured against shifting by screws.



Figure 64: Transport system for coated single fibers consists of stainless steel box (left picture) and the stainless steel brackets (right picture)



The production of the transportation system from stainless steel was necessary because of its inert behavior during the ALD-process. The different coloration of brackets in Figure 64 was related to the different coating thicknesses.

The brackets prevented any contact between the single fibers. The fibers did not have to be removed from the bracket for coating process but the bracket with the located fibers was put in the ALD-chamber and coated as well. The contact surface was kept as small as possible to ensure a homogeneous and large-area application of the coating. Additional possible injuries caused by the steel bracket itself should be hindered.

The ALD-procedure processes stepwise and at each step a thin layer of  $s_c = 0.1$  nm is applied on the surface [137]. The number of steps is repeated until the desired thickness is reached. Consequently thicker coatings require longer process duration. The necessity of heat during ALD-process brought along an influence of temperature wherefore the different coating thicknesses were applied not only at  $T = 300$  °C but also at  $T = 500$  °C. The chosen temperatures are the most used values when ALD coating is applied on glass surface by the enforcing company [136], [137]. The handling and gluing together into the stainless steel pipes was not changed to the untreated single fibers.

In Table 53 the characteristic results of fibers coated at  $T = 300$  °C are listed. As reference value a series of uncoated fibers was tested and listed whereby all fibers were produced from glass tube taken from the same batch. Hence, differences due to deviations in chemical composition can be excluded.

Table 53: Characteristic test results of fibers covered with different coating thickness at a temperature of  $T = 300$  °C, all fibers exhibit dimensions of  $d_o \approx 500$   $\mu\text{m}$ ,  $d_i \approx 465$   $\mu\text{m}$  and  $s \approx 17.5$   $\mu\text{m}$

Serial number	Coating thickness $s_c$ [nm]	Min. burst pressure $p_{\min}$ [MPa]	Max. burst pressure $p_{\max}$ [MPa]	Form parameter $b$	Characteristic pressure $P$ [MPa]
ALD 0 (reference)	uncoated	9.8	19.1	9.3	16.1
ALD 1	50.0	10.7	23.5	6.2	17.9
ALD 2	100.0	11.1	19.0	8.1	15.3
ALD 3	200.0	7.1	21.6	5.6	17.5
ALD 4	500.0	3.9	19.2	2.6	14.2

Comparing the reference series to series ALD 1 a slight increase of all pressure values is noticeable. The minimum burst pressure and the characteristic pressure features an improvement of about 10% with 50 nm coating thickness. However, the form parameter decreases due to a wider spread which is caused by an improvement of about 20% for the maximum reached burst pressure.

The minimum pressure value of series ALD 2 increases again slightly but pressure remains characteristically below the according values of the reference series. The maximum burst pressures of both series are comparable. Indeed, the pressure range between minimum and maximum reached burst pressure is smaller than of the reference series. The accumulation of measured pressure values of ALD 2 leads to a lower form parameter than ALD 0.

Series ALD 3 exhibits a minimum burst pressure by the factor 1.4, which is lower than the reference series. However, the maximum burst pressure and as well the characteristic pressure feature higher values and an improvement of 10%. Therefore an outlier can lead to the lower minimum burst pressure. The resulting wider spread of measured test pressures consequently leads to a decrease of the form parameter  $b$ .

The series ALD 4 with a coating thickness of  $s_c = 500$  nm features a maximum burst pressure comparable to the reference series but the minimum burst pressure remains distinctively below the according value of the reference by having only 40% of the reference. A significantly lower form parameter points out not only a wide spread but together with the decreased characteristic pressure, it indicates a distinct degradation of the pressure resistance.

Theoretically and bottom-up on the literature reference the resistance against inner pressure of the fibers should be increased by filling up small flaws and increasing the radius of larger cracks. The unsteady behavior of test results can be shown more clearly in Figure 65 by plotting the failure probabilities against the burst pressure.

The diagram shows a narrow development of the graphs of the tested series. Series ALD 0 to ALD 2 proceed similar in lower pressure region and the initial points of these curves are close together. The slight improvement of the minimum burst pressures of ALD 1 and ALD 2 constitute that close physical proximity. The graph of ALD 1 then proceeds with a lower slope than the reference series graph but at higher pressure level. The similarity of test results of reference series and series ALD 2 is shown by comparable developments.

The S-curve of ALD 3 with  $s_c = 200$  nm exhibits a comparable development to reference series in the low pressure range whereby the initial point slides to the left. In further development the graph converges to the S-curve of series ALD 1 with  $s_c = 50$  nm. That behavior can be explained by the similar form parameter and characteristic pressure.

A considerable different development shows the S-curve of series ALD 4 with a coating thickness of  $s_c = 500$  nm. The significantly lower minimum burst pressure and the form parameter create the low slope of the graph. Therefore the calculated failure probabilities are much higher for series ALD 4 than for the other series in comparison vis-a-vis up to pressures of  $p = 15$  MPa. It can be seen that no outlier leads to the described development of the graph but a straight and consistent distribution is noticeable.

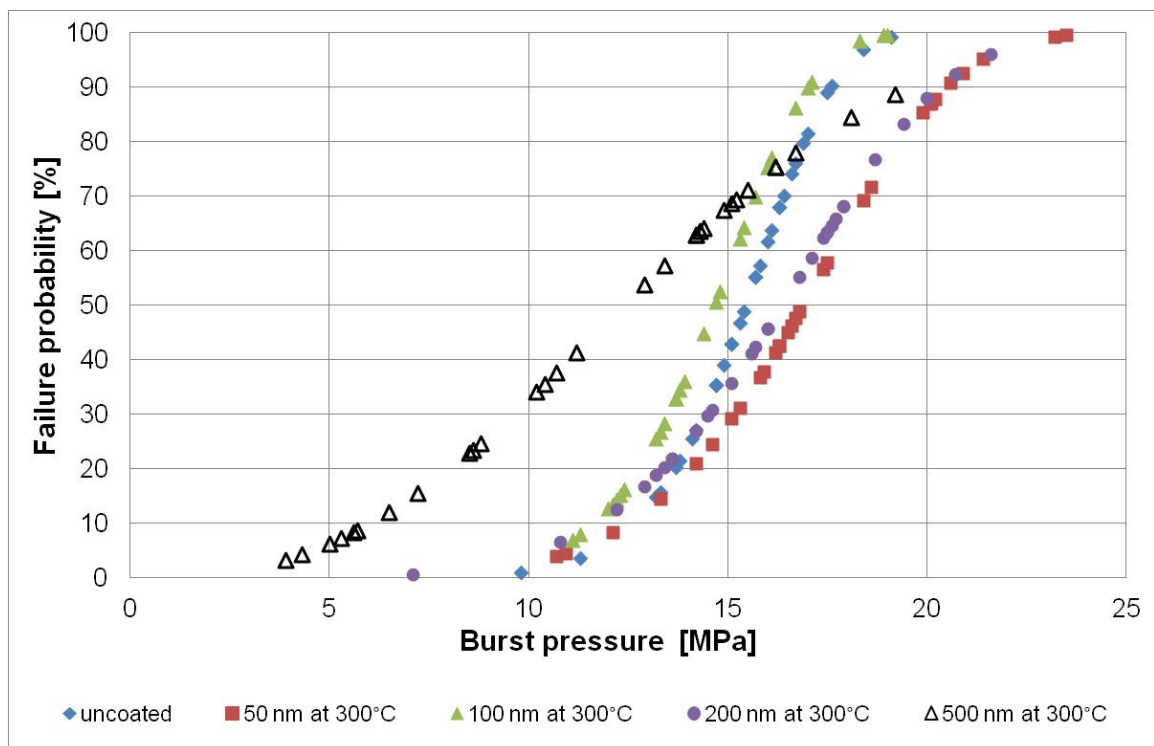


Figure 65: Failure probability of hollow borosilicate C5 fibers covered with ALD-coating of different thicknesses at  $T = 300$  °C, the reference series was carried out without coating and temperature treatment

Furthermore, single hollow borosilicate fibers were coated with the same four thicknesses at a process temperature of  $T = 500$  °C. An elevated process temperature is necessary to deliver the essential energy for the chemical reaction. The increased temperature should accelerate the reaction again and support the formation of the coating layer.

The characteristic results of test series with fibers coated at increased process temperature is listed in Table 54.

Table 54: Characteristic test results of fibers covered with different coating thickness at a temperature of  $T = 500\text{ }^{\circ}\text{C}$ , all fibers exhibit dimensions of  $d_o \approx 500\text{ }\mu\text{m}$ ,  $d_i \approx 465\text{ }\mu\text{m}$  and  $s \approx 17.5\text{ }\mu\text{m}$

Serial number	Coating thickness $s_c$ [nm]	Min. burst pressure $p_{\min}$ [MPa]	Max. burst pressure $p_{\max}$ [MPa]	Form parameter $b$	Characteristic pressure $P$ [MPa]
ALD 0 (reference)	uncoated	9.8	19.1	9.3	16.1
ALD 5	50.0	12.1	20.0	9.8	17.2
ALD 6	100.0	2.3	16.1	2.1	13.1
ALD 7	200.0	8.6	14.3	10.3	11.9
ALD 8	500.0	2.0	21.6	2.6	16.9

The comparison of the reference and series ALD 5 with  $s_c = 50\text{ nm}$  shows a slight improvement of pressure data in the range of 20% at minimum and about 5% at characteristic as well as at maximum pressure. The slight increase of all pressure values leads to comparable form parameters of both series.

Series ALD 6 features a characteristic test result which remains below the data of the reference series. Series ALD 6 has a minimum burst pressure that is decreased by the factor 5 in comparison to the reference series. The maximum and the characteristic pressure values remain at 80% of the according reference value. Due to the large deviation at minimum burst pressure and the approach at maximum burst pressure the spread of the measured values is significantly wider. Consequently series ALD 6 has a small form parameter.

Fibers coated with  $s_c = 200\text{ nm}$  of ALD 7 have pressure values below the reference series. The minimum burst pressure is similar to the value of the reference series by having about 90% of reference value. The deviation gets higher by approaching the maximum burst pressure. Therefore, the characteristic and the maximum burst pressure exhibit only 75% of series ALD 0 values and decreased by the factor 1.3 to 1.4. The

narrow values of minimum and maximum burst pressure are indicative of a consistent distribution, which is shown by the high form parameter of  $b = 10.3$ .

Series ALD 8 with  $s_c = 500$  nm of coating thickness shows a similar behavior to ALD 6. The minimum pressure remains at only 20% of the reference but the maximum burst pressure shows an improvement of about 15%. The characteristic pressure of series ALD 8 also has a higher value compared to ALD 0 and increases about 5%, which indicates a small number of outliers at minimum burst pressure. Nevertheless, the wide spread between minimum and maximum burst pressure originates the small form factor of  $b = 2.6$  which is similar to that of series ALD 6.

Calculating the failure probabilities and plotting it in a diagram against the single burst pressure gives the opportunity to compare the series not only by the characteristic results but on their developments and distributions as well. The diagram is given in Figure 66.

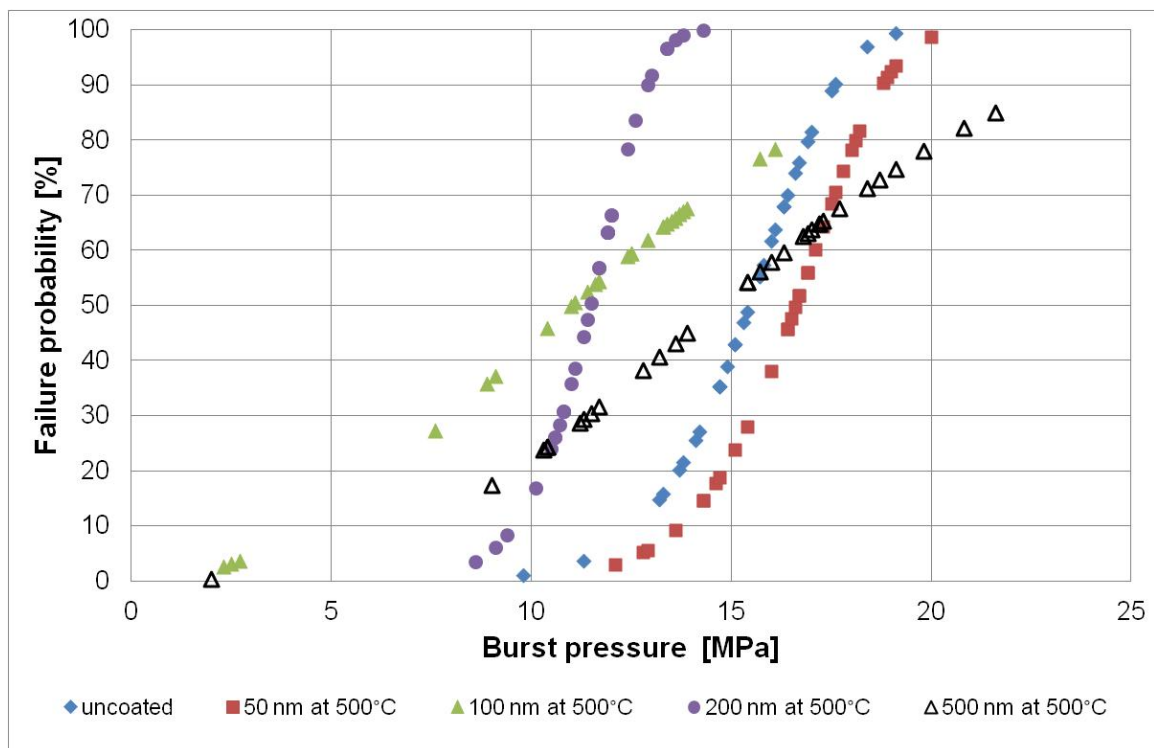


Figure 66: Failure probability of hollow borosilicate C5 fibers with the dimensions of  $d_o \approx 500 \mu\text{m}$ ,  $d_i \approx 465 \mu\text{m}$  and  $s \approx 17.5 \mu\text{m}$  covered with an aluminum ALD-coating of different thicknesses at  $T = 500 \text{ }^\circ\text{C}$ , the reference series was carried out with samples without coating and temperature treatment

The diagram clearly shows the differences between the single tested series. While series ALD 5 and ALD 7 show a comparable development to the reference series ALD 0, they show different locations. The graph of ALD 5 slides to the right which is indicated by the higher pressure values, as seen in Table 54 and, therefore, exhibits an improved pressure resistance. The S-curve of ALD 7 slides to the left wherefore a decreased pressure resistance is shown. Nevertheless, it shows the same narrow and consistent distribution than the reference and ALD 5.

A completely different development regarding the graphs of ALD 6 and ALD 8 can be observed. The graph conforms more of a straight line than an S-curve, resulting from Weibull distribution. It can be seen that the initial points are in the range of  $p = 2$  MPa. However, both graphs exhibit only one and three points, respectfully in that range of initial points wherefore the assumption of outliers is confirmed. Those outliers lead to the small form parameter of both series which is responsible for the low slope and development of the graphs. Nevertheless, the multitude of measured pressure values is below those of the reference series and consequently no improvement can be observed.

The temperature treatments during ALD coating process average a duration of four hours wherefore an annealing effect could be ensued. The used process temperatures of  $T = 300$  °C and  $T = 500$  °C remain distinctively below the annealing point, which is at a temperature of  $T = 570$  °C [151]. However, an annealing effect can be reached at a lower temperature, at strain point of  $T = 530$  °C, which is still above the process temperatures. An investigation of a possible annealing effect of uncoated hollow fibers was carried out. Test samples were temperature treated for four hours at given process temperatures of  $T = 300$  °C and  $T = 500$  °C before being prepared and tested. Again the test series consist of a minimum of 30 samples.

The test results are summarized and listed in Table 55. The comparison of the pressure values of the three series shows only slight deviations. Series ALD 9 treated with  $T = 300$  °C exhibits a slight decreased pressure resistance of the test samples. All pressure results are below the reference values whereby the degradation of pressure resistance is only in the range of 5% to 10%.

ALD 10 treated with  $T = 500$  °C exhibits a degradation of about 5% at minimum burst pressure. However, at maximum burst pressure an improvement of about 15% can be detected. The characteristic pressure of reference series and ALD 10 feature similar values. The wider spread due to decreased minimum but increased maximum burst pressure leads to a smaller form parameter of ALD 10.

Table 55: Characteristic test results of uncoated fibers with dimensions  $d_o \approx 500 \mu\text{m}$ ,  $d_i \approx 465 \mu\text{m}$  and  $s \approx 17.5 \mu\text{m}$  annealed at different temperatures

Serial number	Annealing temperature $T_A$ [°C]	Min. burst pressure $p_{\min}$ [MPa]	Max. burst pressure $p_{\max}$ [MPa]	Form parameter $b$	Characteristic pressure $P$ [MPa]
ALD 0 (reference)	untreated	9.8	19.1	9.3	16.1
ALD 9	300	8.6	18.6	7.1	15.1
ALD 10	500	9.3	21.7	6.5	16.5

Again the failure probabilities were calculated and for better visualization plotted in a diagram against the burst pressure values, which is given in Figure 67.

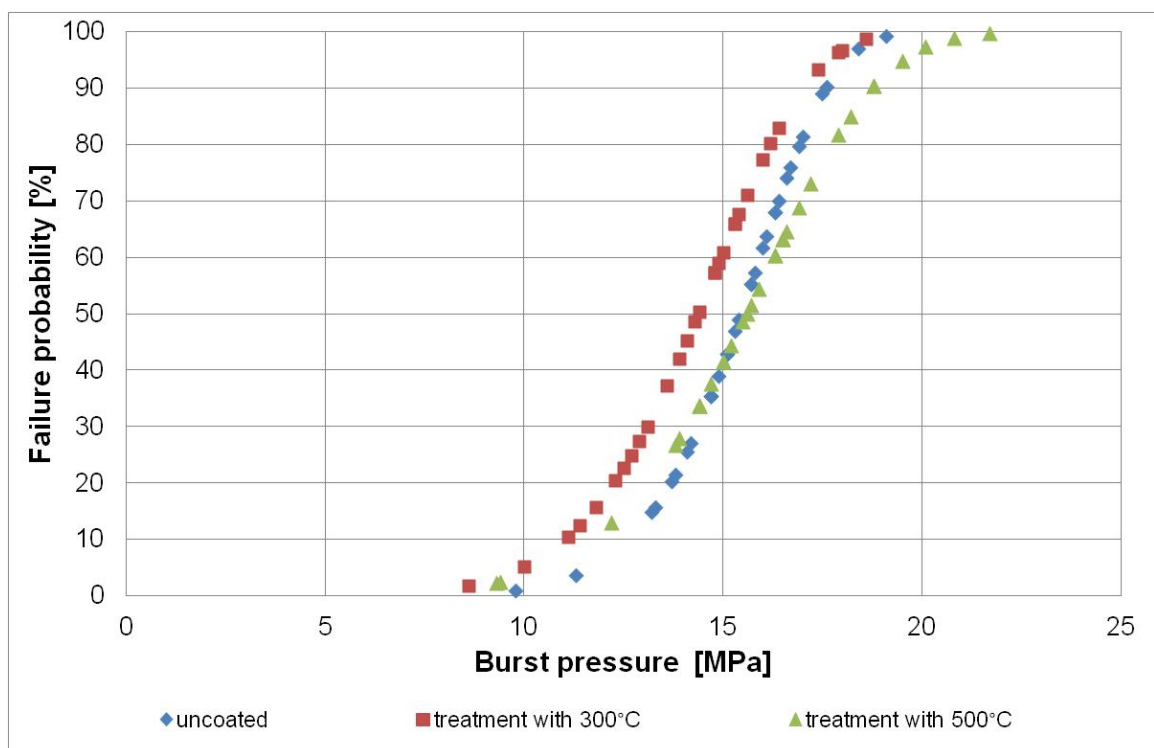


Figure 67: Comparison failure probability of uncoated hollow fibers but different thermal history

In the diagram only slight differences between the single test series can be seen. Nevertheless, it is detectable that both temperature treated series feature initial points

with pressure values below that of the reference series. ALD 9 series approximates in upper pressure region to the graph of the reference series. It shows a consistent development without any outliers but a slightly lower slope compared to ALD 0 graphs due to the lower form factor  $b$ .

The graph of test series treated with  $T = 500\text{ °C}$  subtend the curve of the reference series at a pressure value of  $p = 15\text{ MPa}$ . Below that value the temperature treated series features higher failure probabilities. Above the point of intersection the failure probabilities remains below the value of the reference series at same pressure loads.

The test results of ALD-coated hollow glass fibers did not show a consistent and clear influence of the coating on the pressure resistance of the fibers. The application of aluminum coating at a process temperature of  $T = 300\text{ °C}$  had a positive influence at a coating thickness of  $s_c = 50\text{ nm}$  and  $s_c = 200\text{ nm}$ . Thereby the characteristic burst pressures of the test series were compared to the values of the reference series and they reached pressure values which increased when compared to the uncoated and untreated test samples. The test series with a coating thickness of  $s_c = 100\text{ nm}$  and  $s_c = 500\text{ nm}$  showed a decreased pressure resistance over the complete range.

Test samples coated at  $T = 500\text{ °C}$  as well showed a more distinct result. An improvement of the pressure resistance was detectable only for test samples with a coating thickness of  $s_c = 50\text{ nm}$ . Increasing coating thicknesses was associated with a decrease of the pressure resistance of samples.

It was assumed that the inconsistent results were affected by the influence of temperature during the coating process. An investigation of uncoated fibers using the same production batch showed no crucial impact of pressure resistance. A temperature treatment at  $T = 300\text{ °C}$  led to decreased pressure resistance whereby the treatment at  $T = 500\text{ °C}$  led to increased resistance but only at higher pressure range. In lower pressure range the resistance decreased as well.

The annealing of glass can affect its mechanical resistance by relaxing possible stresses inside the glass. Stress peaks therefore can be reduced or prevented when a load is acting on the annealed material and the distribution inside the glass would be more uniform. However, the annealing of glass takes place in a temperature region between strain and annealing point. Therefore the temperature has to be between  $T = 530\text{ °C}$  (strain point) and  $T = 570\text{ °C}$  (annealing point) [151]. Due to lower temperature in the coating process an annealing of the fibers did not take place which could be confirmed by the treatment and following testing of uncoated single fibers at process temperature and residence time.



Investigating uncoated and coated fibers under the microscope showed different flaws and damages on the surface. The origin and the shape of the defects were different. Surface defects surrounded by straight lines in drawing direction could be observed as well as scratches. Figure 68 shows two pictures of uncoated fibers with a high concentration of defects close together.

The flaws in the left picture can be originated by handling during production and packing. To ensure a fat free surface the fibers have to be handled only with gloves. The particles and elevated structures point out that the possible origin is handling without gloves and the remained fat and humidity formed the detected flaws. The local high concentration of humidity and maybe alkaline pH on the surface led to a degradation of structural resistance by hydrolytic or even alkaline reaction. Therefore the formation of stress peaks during internal pressure load can take place and lead to lower pressure resistances.

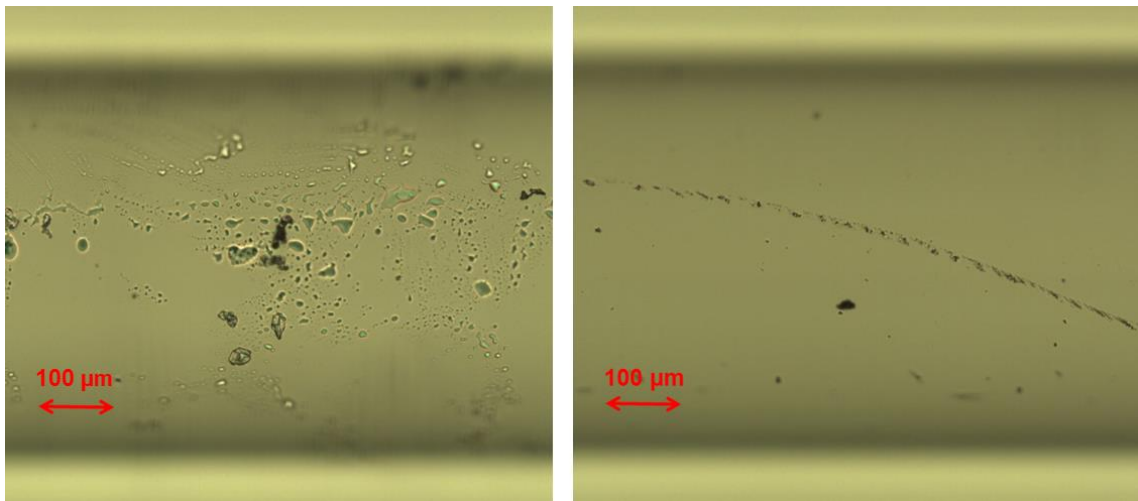


Figure 68: Surface defects of uncoated borosilicate C5 fibers with dimensions of  $d_o \approx 500 \mu\text{m}$ ,  $d_i \approx 465 \mu\text{m}$  and  $s \approx 17.5 \mu\text{m}$

In the left picture of Figure 68 distinct scratches can be detected. Such scratches can be originated by the transportation bracket made of stainless steel. The fibers were transported in a safe manner; neither contact between each other nor impacts from the environment was made. However, during transport the fibers were able to slide inside the bracket. Due to the small contact area between fiber and bracket the shown defects can be created by the movement of the fibers. In addition to the observable flaws possible enclosure was detected. The shape and size was comparable to defects detected on fiber surface in chapter 6.8 and might have been created from enclosures

inside the glass tube. During drawing process the particles keep their size and due to shrinking wall thickness they are transported to the surface and support the formation of straight lines in drawing direction.

Coating the small fibers in a thin layer of ALD-coating can lead to the improvement of pressure resistance by closing present flaws on the surface. Nevertheless, different types of defects were observed during investigation of the coated fibers. Beside scratches and solid particles with straight lines damages in the coatings can also be observed. Figure 69 displays irregularities of the coating. The coating thickness rises from the upper left to the lower right picture from  $s_c = 50$  nm to  $s_c = 500$  nm. Independent from the thickness and the resulting residence time the formation of a consistent layer of coating was disturbed or inhibited by possible impurities on the surface. The dark deposits might be residues of an undesirable decomposition reaction which is not restricted on a small area.

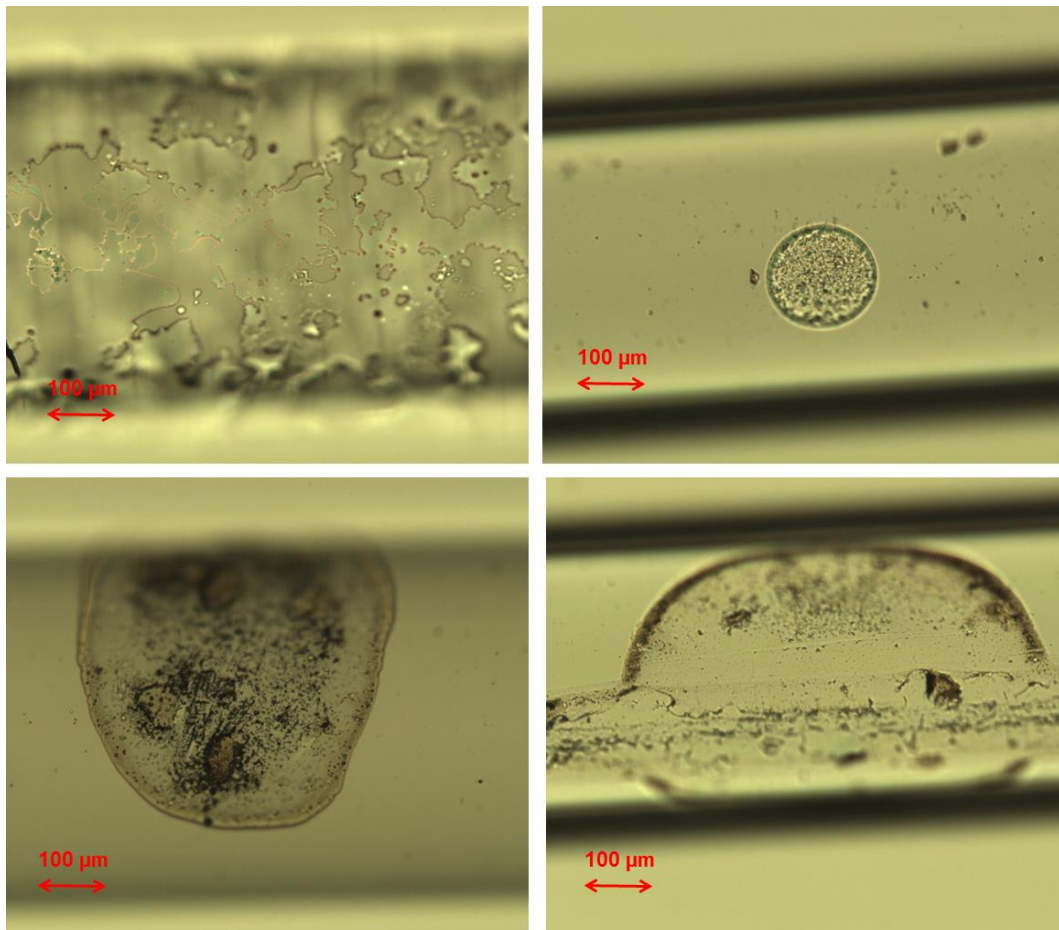


Figure 69: Damages of ALD-coating of different thicknesses applied at  $T = 300$  °C on borosilicate C5 fibers, the layer thickness increases from upper left to bottom right ( $s_c = (50, 100, 200, 500)$  nm)

The deposits of the decomposition reaction can influence the structure by forcing a chemical reaction on the surface of the glass and support the destabilization of the glass structure as alkaline reactions which attack the bonding of silica in the network. Such reactions during ALD-process can occur from impurities on the surface due to handling or non-clean conditions.

Samples coated at  $T = 500\text{ }^{\circ}\text{C}$  were investigated under the microscope. On their surface defects were again noticeable, as seen on the reference series. Also different damages in coating layer could be found, as seen on the surface of fibers coated at  $T = 300\text{ }^{\circ}\text{C}$ . Figure 70 shows different damages on fibers with different layer thickness.

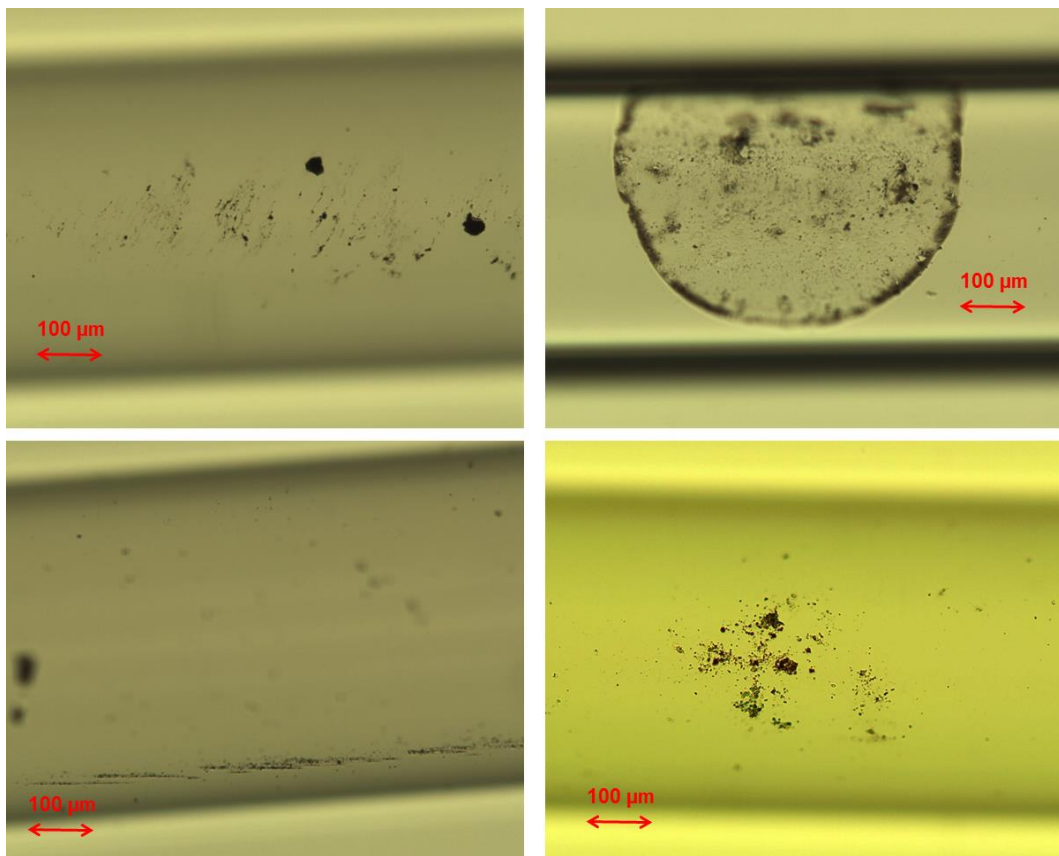


Figure 70: Imperfections of ALD-coating of different thicknesses applied at  $T = 500\text{ }^{\circ}\text{C}$  on borosilicate C5 fibers, layer thickness increases from upper left to bottom right ( $s_c = (50, 100, 200, 500)\text{ nm}$ )

Remains and deposits of possible decomposition reactions were detected on the surface of the fibers. The area was not restricted to a small size, as it could occupy larger sizes and different shapes. Again such deposits can affect a consecutive reaction whereby the

glass network is weakened. In addition to the concentration of scratches, point defects were also noticeable.

Particles, straight lines and stripes act as an indentation of the material and origin of stress peaks which can lead to the exceedance of the critical local stress and therefore the collapse of the fiber. The high number of such flaws detected on the surface led to the low resistance against inner pressure of the fibers. The coating applied on the surface was not able to act against the weakening effect of the defects.

Nevertheless, a completely different behavior of fibers coated at different process temperatures was observable and were influenced by different chemical reactions during ALD-process. The coating with aluminum requires the use of trimethylaluminum (TMA) and water. Above temperatures of  $T = 350\text{ }^{\circ}\text{C}$  TMA becomes unstable and a decomposition reaction begins [179]. The decomposition product can influence the surface of the glass and attack it by chemical reaction. A lower pressure resistance of fibers coated with high layer thickness at  $T = 500\text{ }^{\circ}\text{C}$  can be explained by the aforementioned processes. Furthermore, the decomposition of TMA at the high process temperature can influence the formation of the aluminum oxide layer on the surface of the fibers. If the TMA was decomposed before water steam as second reagent was led into the reaction chamber no coating would form on the fibers. Consequently the present defects cannot be filled or their radius increased by the coating. The coating itself was not identifiable under the microscope although damages and/or side reactions were observable.

An important impact on the pressure resistance in regard to the treatment of the fibers occurs between their production and their testing. The fibers were packed and transported in stainless steel brackets. The contact area was as small as possible. Nevertheless, the fibers were able to slide inside the brackets before being coated. New surface defects were created and could be detected on the surface in shape of sharp scratches. During the coating process the fibers were not removed from the brackets but the brackets were coated as well. Consequently a large area of the surface was coated but the contact area was not coated. After application of the coating the brackets were packed again in a stainless steel box and transported to the testing facility. Again sliding around in the brackets was possible and may support the formation of further defects. The defects caused by possible enclosures in raw tube before drawing and damages of the surface caused by transport in the steel bracket had a stronger impact on the pressure resistance of the borosilicate fibers than the coating with a thin layer of aluminum by using ALD-coating process.

The impact of ALD-Coating on the pressure resistance can be summarized as following:

- In theory small flaws on the surface shell filled up and the radius of larger defects shall be increased [136], [137]. As a result the stress distribution during internal pressure load may have a more homogeneous development.
- Borosilicate C5 fibers were coated by thin alumina layers of four different sizes at varying process temperatures.
- A coating layer of  $s_c = 50$  nm thickness led to a slight improvement of the pressure resistance independent on ALD-process temperature.
- Higher layer thicknesses led to both slight improvement as well as degradation of pressure resistance. A consistent and explainable behavior was not observed.
- The pressure resistance of the tested fibers was influenced more significantly by flaws and defects. Deposits, enclosures and surface scars were determined during microscopic investigation.
- A possible origin of such defects was during both the production process as well as the transportation. The fibers were packed in stainless steel brackets for shipment from the manufacturer to the coater and afterwards to the test facility. The contact surface was already reduced to a minimum. Nevertheless, defects by sliding in the stainless steel brackets were formed and detected.
- Additionally, deposits of decomposition reactions were found on the fiber surface. Debris from handling, cutting and from the environment led to irregular formation of the coating layer.
- Finally, no convincing effect of ALD-coating on the pressure resistance was determinable.

### 6.9.2 Hollow Quartz Glass Fibers with different Coatings

Applying a coating directly during drawing process might have a bigger effect on the resistance against inner pressure of single hollow glass fibers than a coating applied afterwards. In this case glass fibers are protected against mechanical impacts during transport and handling. Coating directly after the drawing process, the fibers are still hot and air moisture is not able to condense on their surface. Coatings, applied by spraying or continuous immersion bath, isolate the glass surface from the environmental conditions and therefore a chemical reaction even by the air moisture is not possible.

Hollow glass fibers made of fused silica glass and coated with soft or hard coating are commercially available in different dimensions. Because of the use of silica glass the

tested fibers are not directly comparable to the investigations done with borosilicate glass fibers. However, the investigations of such fibers can show the potential of coating applied on the fibers surface directly after being drawn. Therefore the sample size was limited to ten samples per series. Table 56 summarizes the properties of tested fibers. Two different outer diameters are given in table whereby  $d_{o\ all}$  stands for the outer diameter of the coated fiber and  $d_{o\ glass}$  for the outer diameter of the hollow fiber without regard of the coating. The fiber dimensions were chosen to compare the samples of different manufacturers. Comparable dimensions to the already tested borosilicate fibers were not available. Most producers use a hard coating made of polyimide whereby the fiber is drawn through a continuous immersion bath. A cover of acrylate is sprayed and remains soft.

Table 56: Properties of different coated hollow silica fibers

Manufacturer	Short term	Coating material	$d_{o\ all}$ [ $\mu\text{m}$ ]	$d_{o\ glass}$ [ $\mu\text{m}$ ]	$d_i$ [ $\mu\text{m}$ ]	$s_c$ [ $\mu\text{m}$ ]	$FS_{glass}$ [%]
NKT	HC-1550	acrylate	250	122	72	128	34.8
Postnova	PN 280/360	polyimide	380	332	278	48	70.4
	PN 250/350		363	320	254	43	62.8
	PN 180/260		267	243	189	24	60.5
	PN 100/160		169	142	104	27	53.6
Polymicro	PM 530/660	polyimide	661	615	540	46	77.0
	PM 250/350		359	319	247	40	59.9
	PM 100/170		169	147	102	22	48.3
CeramOptec	CO 250/350	polyimide	345	312	247	33	62.5
University of Florida	UF 360/480	acrylate	483	432	362	51	70.3

Due to the limitation of the sample size a complete Weibull evaluation was not done to coated silica fibers. Nevertheless, the characteristic test results summarized in Table 57 give an overview about the measured pressure values. In addition to the minimum and maximum burst pressure the average value is also given. The average burst reveals the trend of the distribution of measured data.

The comparison of the test results reveals that the maximum burst pressure of seven test series is not determinable. The pressure limit of the test setup of  $p_{\max} = 150$  MPa is too low for the exact determination wherefore it is not possible to determine the exact pressure resistance of the according series, even series with high diameters exhibit burst pressure values above  $p = 100$  MPa.

Series HC-1550 exhibits a minimum burst pressure of  $p_{\min} = 53.0$  MPa. The maximum value is not determinable and has to be defined as  $p_{\max} \geq 150$  MPa. The average pressure value of  $p_{\text{average}} = 114.5$  MPa reveals a distribution of measured values in high pressure range.

Fibers of PN-series feature increasing pressure resistance with decreasing dimensions. The minimum as well as the average burst pressure value increases with smaller diameters. Outer diameters of the fiber below  $d_o = 250$   $\mu\text{m}$  lead to maximum pressure resistance above setup limit. The rather low minimum burst pressure of series PN 100/160 of  $p_{\min} = 48.8$  MPa indicates a decreasing pressure resistance compared to series with larger dimensions. The high average burst pressure value of  $p_{\text{average}} = 138.3$  MPa identify the minimum value as an outlier and points out the high resistance against inner pressure load of the series.

The PM-series exhibit a similar behavior and significantly high pressure values. Even fibers of the series PM 530/660 with the largest diameter in comparison exhibit a maximum burst pressure of  $p_{\max} = 104.2$  MPa and indicate a high pressure resistance. With decreasing dimensions again the measured pressure value increase and the maximum values are above setup limit. Series PM 100/170 features a significantly low minimum burst pressure. Again the average burst pressure of  $p_{\text{average}} = 135.7$  MPa indicates that measured data as an outlier.

The comparison of test series with different dimensions and free space ratios reveals the necessity of a standardized parameter of the maximum stress inside the glass fiber wall. Therefore, the tangential stress at measured burst pressure was calculated by using Barlow's formula [172] :

$$\sigma_t = \frac{p d_o}{2 s} \quad (6.2).$$

The resulting normalized stress of the tested fibers was calculated for the measured maximum burst pressure and is given in Table 57. Outstanding results are noticeable for the series PM 530/660 and UF 360/480 by having  $\sigma_{t \max} = 854.4$  MPa and  $\sigma_{t \max} \geq 925.7$  MPa.

Table 57: Characteristic test results of coated silica fibers with different dimensions

Fiber	$d_o$ glass [ $\mu\text{m}$ ]	$d_i$ [ $\mu\text{m}$ ]	$p_{\min}$ [MPa]	$p_{\max}$ [MPa]	$p_{\text{average}}$ [MPa]	$\sigma_{t \max}$ [MPa]
HC-1550	122	72	53.0	>150.0 <sup>1)</sup>	114.9	>366.0
PN 280/360	332	278	16.3	35.0	25.4	215.2
PN 250/350	320	254	20.6	63.8	36.0	309.3
PN 180/260	243	189	78.7	>150.0 <sup>1)</sup>	130.7	>675.0
PN 100/160	142	104	48.8	>150.0 <sup>1)</sup>	138.3	>560.5
PM 530/660	615	540	12.0	104.2	72.5	854.4
PM 250/350	319	247	79.5	>150.0 <sup>1)</sup>	133.6	>664.6
PM 100/170	147	102	9.0	>150.0 <sup>1)</sup>	135.7	>490.0
CO 250/350	312	247	13.6	>150.0 <sup>1)</sup>	75.3	>720.0
UF 360/480	432	362	13.6	>150.0 <sup>1)</sup>	93.8	>925.7

1) Burst pressure above test setup limit

The carried out test series reveals the high pressure resistance of hollow glass fibers even those with large dimensions. In Table 58 the maximum burst pressure of all series with  $p_{\max} \geq 150$  MPa are calculated by formula (6.2). Thereby the maximum reached tangential stress of PM 530/60 of  $\sigma_{t \max} = 854.4$  MPa was taken. Outstanding are the results of series PN 100/160 and PM 100/170 by having a calculated maximum burst pressure of  $p_{\max} \geq 200$  MPa even at free space ratios of about 50%. The calculated maximum burst pressure of series UF 360/480 is below the determined  $p_{\max} \geq 150$  MPa which indicates an even higher reachable pressure resistance for coated silica fibers.



Table 58: Calculated maximum burst pressures  $p_{max}$  of coated silica fibers,  $p_{max}$  was not determinable up to the limit of experimental limit, as  $\sigma_{t\ max}$  the value of PM 530/660 was taken

Fiber	$d_o$ glass [ $\mu\text{m}$ ]	$d_i$ [ $\mu\text{m}$ ]	FS <sub>glass</sub> [%]	Calculated $p_{max}$ [MPa]
HC-1550	122	72	34.8	350.2
PN 180/260	243	189	60.5	189.9
PN 100/160	142	104	53.6	228.6
PM 250/350	319	247	59.9	192.8
PM 100/170	147	102	48.3	261.6
CO 250/350	312	247	62.5	178.0
UF 360/480	432	362	70.3	138.4

The investigation of coated silica fibers of different manufactures showed the potential of coatings applied directly after drawing as part of the production process. Compared to silica fibers investigated in chapter 6.1 the maximum burst pressures were doubled. Uncoated silica fibers with dimensions of  $d_o = 400\ \mu\text{m}$ ,  $d_i = 300\ \mu\text{m}$  and  $FS = 56\%$  reached maximum burst pressures of  $p_{max} = 94.4\ \text{MPa}$ . Coated fibers with comparable FS ratio of series PM 250/350 exhibited burst pressures above setup limit and were calculated to  $p_{max} = 192.8\ \text{MPa}$ .

The calculation of tangential stress of the coated fibers gives the possibility to compare fibers of different dimensions by a normalized value. Therefore fibers of different material as well as dimensions can be contrasted. That perception is used especially in chapter 6.11. In addition, the uncoated borosilicate fibers are comparable to the coated silica fibers. The highest reached tangential stress of borosilicate C5 fiber was  $\sigma_{t\ max} = 479.9\ \text{MPa}$  at a burst pressure of  $p_B = 97.9\ \text{MPa}$  calculated for single fibers of dimensions  $d_o = 190\ \mu\text{m}$ ,  $d_i = 151\ \mu\text{m}$  and  $FS = 63\%$ . Consequently the pressure resistance is only 50% of the according value of coated silica fibers.

The high pressure resistance determined during the investigation of coated single silica fibers of different dimensions can be led back to the effect of coating. The mechanical impact on the fibers surface was reduced to a minimum by outer influences and also possible attack by air moisture was prevented. Nevertheless, the comparison between coated silica and uncoated borosilicate fibers showed a significant deviation in pressure resistance. That improvement can be attributed by the coating. However, the fact of different glass types used for the production of tested hollow glass fibers influences the pressure resistance as well. In fact, the tensile strength of the glass is a surface property [94]. But the change and weakening of the network structure of borosilicate glass by chemical components of alkaline group makes the glass more resistant against further flaws. Quartz glass like fused silica is much more susceptible against surface defects [115]. Consequently the determined improvement of pressure resistance by application of a coating on the surface of silica fibers cannot be associated on the protective effect of the coating itself. The usage of different material had an influence as well. Nevertheless, the increase of the resistance against inner pressure load by applying a coating on the surface of borosilicate fibers directly in production process can be reached and has to be investigated.

As results of the investigation of coated silica fibers it can be outlined that:

- Pure silica fibers covered by a coating directly during drawing process commercially available with hard or soft coating were tested.
- The pressure resistance of several test series exceeded the limit of test setup by having a maximum burst pressure of  $p_{\max} \geq 150$  MPa.
- The calculated tangential stress of  $\sigma_t = 854.4$  MPa of test series with largest dimension in test exceeded the highest according value of uncoated borosilicate fiber by the factor of almost 2. Based on that the theoretical maximum burst pressure of fiber with smaller dimensions featured value of up to above  $p = 200$  MPa.
- The high potential of an applied coating layer on the surface of glass fibers directly during the drawing process was shown. A coherence of high pressure resistance with the effect of the coating or the used silica glass was not determined. Therefore the effect on borosilicate fibers have to be proven as well.
- A coating being applied after the drawing process does not improve the pressure resistance. To ensure an effective protection against surface defects and environmental conditions the coating has to be applied during drawing process.

## 6.10 Investigation on Defects

Evaluations of different test series showed partly significant deviations between comparable types of hollow fibers. Thus, with similar glass materials and dimensions different pressure resistances are detectable. Especially on hollow fibers with similar free space or diameter ratios but varying wall thicknesses, higher spread of measured values are recognizable on thinner wall thicknesses. It is assumed that defects caused by different effects have stronger influence on the failure behavior by decreasing the wall thickness. Therefore, the fibers were investigated under the microscope on defects which are able to degrade the mechanical resistance by a multitude. Under acting load, crack tips generate stress peaks inside the material whereby the related stress value exceeds the resistance of the material significantly. The following investigation should summarize possible defects on the surface or inside the material which are considered as reasons for deviations of the pressure resistance of hollow glass fibers.

### 6.10.1 Volume Defects

Performed investigations of hollow glass fibers with the assistance of the SEM showed the opportunity to detect flaws like bubbles or stones as volume defects as displayed in Figure 71. The investigation of volume defects by using SEM requires the preparation of cross sections of single fibers. These were fixed in epoxy and afterwards a cross section was carved out by grinding. This method of mechanical treatment causes the straight lines detectable on the SEM pictures.

The cross section of a single hollow quartz fiber shows the existence of small volume flaws in even small dimensions of  $s = 50 \mu\text{m}$ . The material of the wall of the hollow fiber part of the wall was partially abraded during preparation. The detected flaws exhibit a size of only  $2 \mu\text{m}$  to  $3 \mu\text{m}$  in width. The complete flaw row has a length of about  $85 \mu\text{m}$  and could be defined as a row of enclosure bubbles as a result of the production process. During melting gas bubbles are formed in the molten mass and different materials are added to the mixture to clad out the gas bubbles by the formation of even more bubbles. The higher number of gas bubbles leads to agglomeration of smaller bubble to bigger ones. Therefore, the upswing increases and the cladding out is accelerated. However, the sharp lines and edges partly recognizable inside of the defect indicates another possibility of formation of these defects. The different refraction indexes substantiate the suspicion of unmixed areas caused by non-molten material which could be abraded by grinding. The exact reason of the present flaws could not be detected.

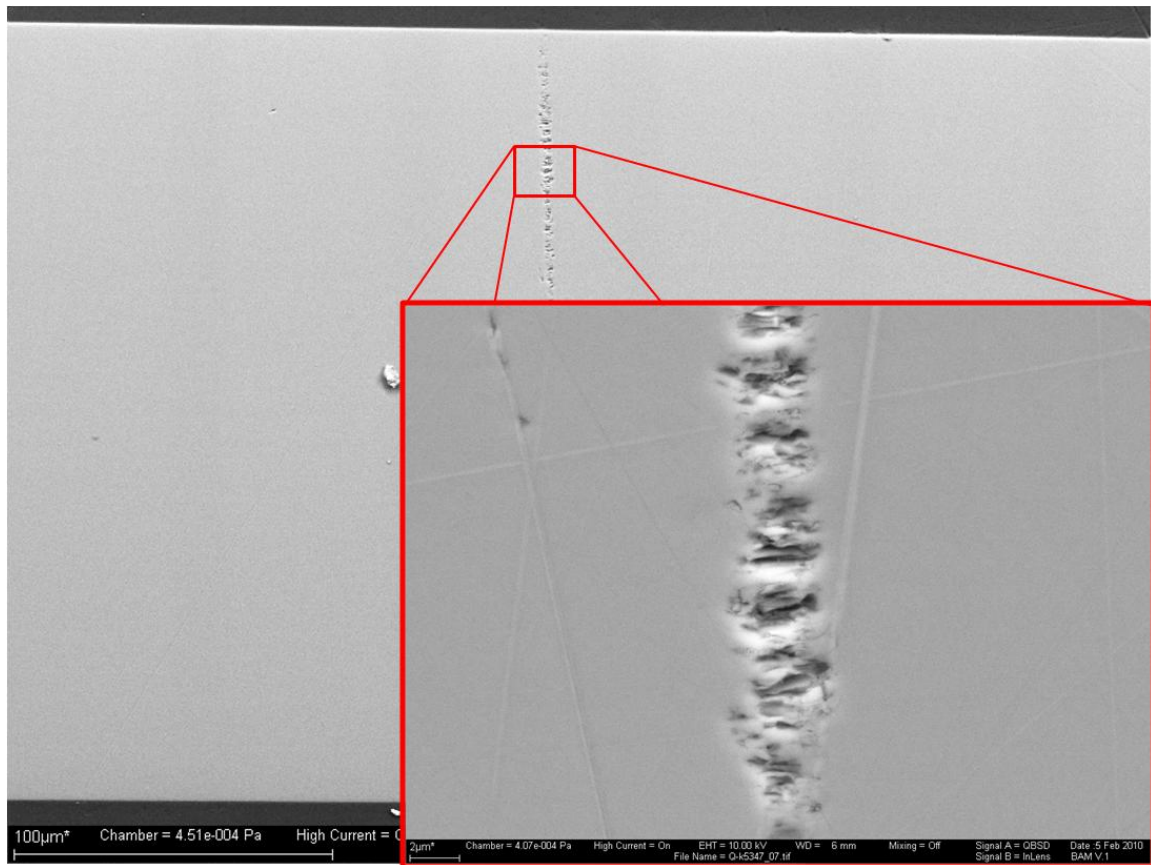


Figure 71: Volume defects inside the wall of single quartz fiber with the dimensions  $d_o = 400 \mu\text{m}$ ,  $d_i = 300 \mu\text{m}$ ,  $s = 50 \mu\text{m}$

Not only quartz fibers were investigated with SEM but also hollow fibers made of other glass materials. Furthermore, in these fibers volume defects could be detected as shown in Figure 72.

The bright region displayed in the figure represents the wall of a hollow borosilicate fiber with a wall thickness of  $s = 50 \mu\text{m}$  whereby the darker regions represents the epoxy which was necessary to fix the samples for grinding. Again, enclosures are detectable which could be identified in that case clearly as gas bubbles. The size of detected flaws is again about  $3 \mu\text{m}$  as detected in the quartz glass fiber. Remarkable is the significant lower number of defects caused by gas enclosures. The visible spalling at the rough inner surface can be affiliated to the sample preparation by grinding and represent no defects. Because of the small sample size the epoxy was not able to fulfill the complete inner volume of the hollow fibers and wherefore this surface was not completely stabilized. Compared to other materials the size of the detected enclosures is small. In relation to the small wall thickness of only  $s = 50 \mu\text{m}$  a defect size of about  $2 \mu\text{m}$  to  $5 \mu\text{m}$

is quite big. The resulting stress peaks will lead to the exceeding of the maximum local stress and, consequently, to the collapse of the loaded fiber.

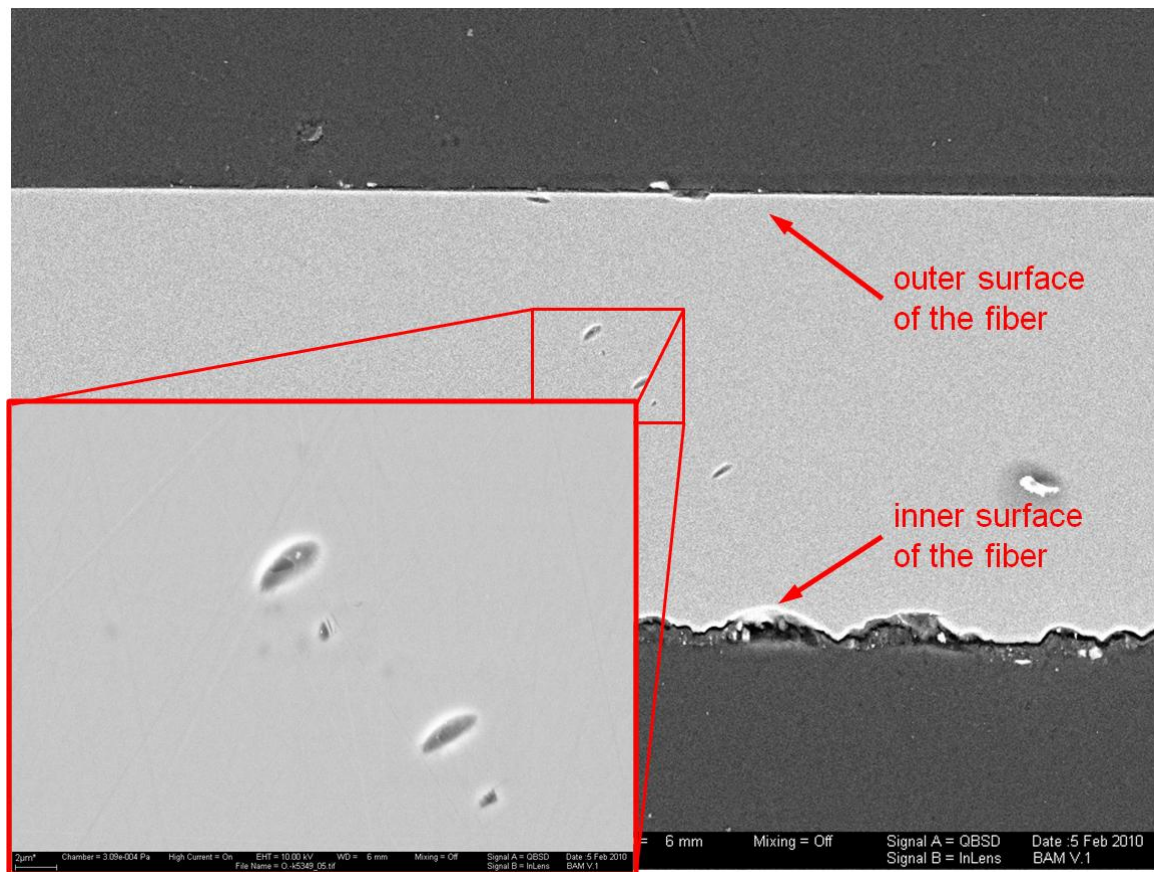


Figure 72: Cross section of borosilicate fiber with the dimensions  $d_o = 400 \mu\text{m}$ ,  $d_i = 300 \mu\text{m}$ ,  $s = 50 \mu\text{m}$ , the enclosures of gas bubbles are detectable, rough inner surface caused by grinding during the preparation

The detected defects could create a different stress distribution under loaded conditions. Stress peaks and structural collapse can be the consequence in surrounding glass. The investigation of volume defects by SEM entails the destruction of the investigated sample. Nondestructive test methods like AFM or light microscope are not applicable for the detection of volume flaws, described in chapter 4.3.2.

The expertise of single hollow fibers under the light microscope leads to the detection of other types of defects which could occur in the bulk of the material. Here the molten end is the region where these flaws were detectable. The gas tightness of the fibers is reached by sealing one end of the hollow fiber by melting whereas the other end is untreated to ensure the introduction of test gases. The end is exposed to a flame and the glass heated up above the transformation temperature  $T_g$ . Due to softening of the

glass and the aspiring of the smallest surface tension the end of the fiber collapsed and formed a glass pellet. That procedure is done completely manually without any automation. Hence, deviations in heat exposure time can result in different rates of heat conduction and melting process. Therefore, every molten end exhibits a different form and appearance and the formation of defects is forced. As possible flaws, a wire is formed passing at the former interface of the inner surface and passes through the pellet, as visible exemplarily in Figure 73.

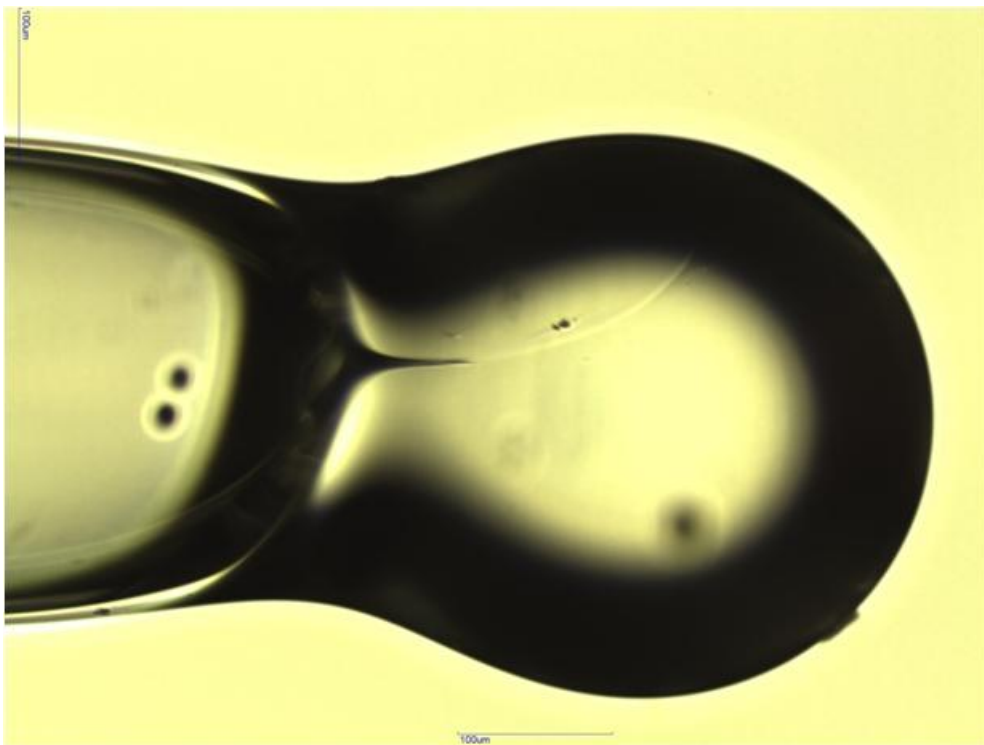


Figure 73: Sealed end of a single borosilicate fiber with dimensions  $d_o = 310 \mu\text{m}$ ,  $d_i = 270 \mu\text{m}$ ,  $s = 20 \mu\text{m}$ , magnified 200 times, wire visible passing through the glass pellet, generation of a sharp peak at bottom

It can be seen that the inner surface shows a round crossover from the wall to the bottom but in the center of the hollow fiber a sharp peak formed as a sinkhole was generated which ends a fine line running through the pellet. The peak does not allow a smooth distribution of stress inside the fiber end but rather generates stress peaks and a higher probability of failure.

That behavior can be determined on hollow fibers of different outer diameters and wall thicknesses. Due to the manual process and different contact time of the glass to the flame the form and depth of possible formed defects in the end pellet can vary.



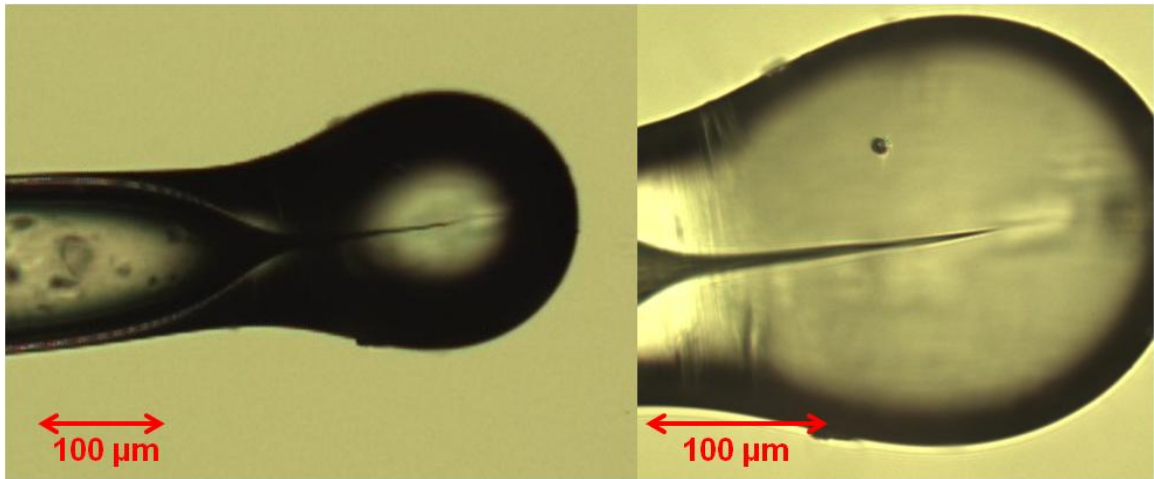


Figure 74: Sealed end of a single borosilicate fiber with dimensions  $d_o = 150 \mu\text{m}$ ,  $d_i = 100 \mu\text{m}$ ,  $s = 15 \mu\text{m}$ , magnified 100 times (left) and 400 times (right), detection of sharp peak

Figure 74 shows a very thin single hollow fiber and point out the difficulties of the manual process of sealing. Indeed, the molten pellet exhibits a ball shape which indicates the formation of smallest surface. Again, a sharp peak at the bottom is recognizable which looks like more than a tapering. Here under loaded conditions gas can intrude and a massive stress peak is formed by acting pressure.

With increasing diameter and wall thickness the time of heating up the material should increase as well. If the time is too short the area of temperatures in the material above is then too small and the end is not closed gas tight as visualized in Figure 75.

The hollow fiber shown exhibits a small channel at the end. During testing such defects leads to leakage and exhaustion of gas at pressurization. Therefore, no collapse of the fiber eventuates. Fibers with such defects were not considered during the analysis. Nevertheless, uncomplete closed fibers cannot be used in a possible application wherefore displaying such defects is important as well.

Different forms and appearance of the molten end were detected not only for borosilicate fibers as shown in the figures but also for test samples made of the other investigated glass materials. Pictures look the same whereby different temperatures have to be applied due to different transformation temperature  $T_g$ .

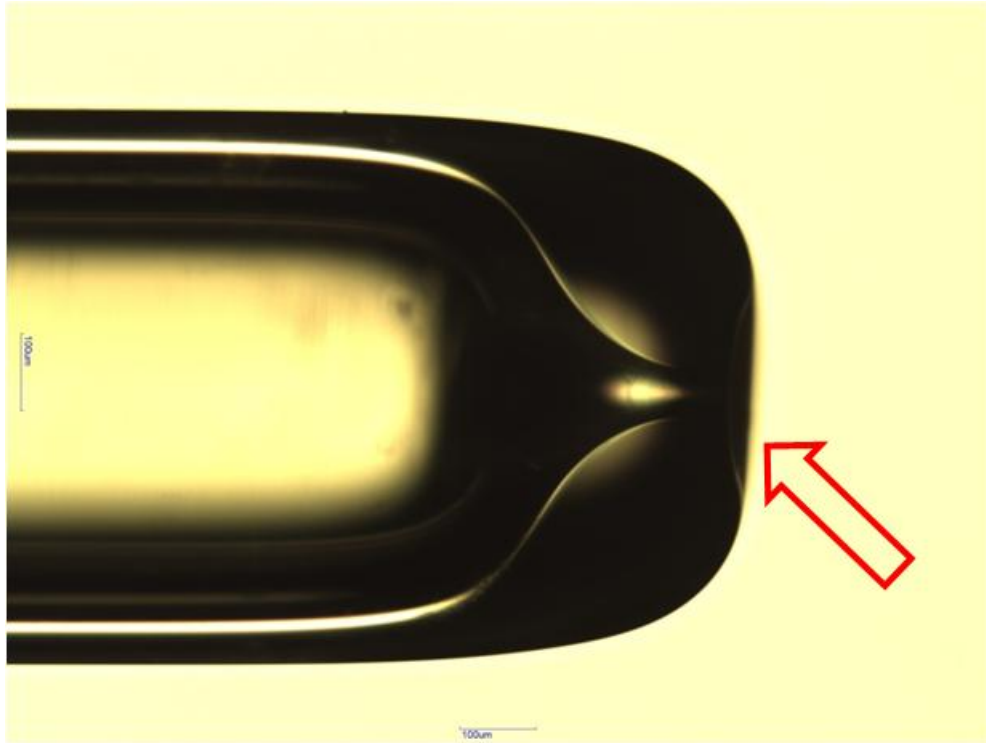


Figure 75: Uncomplete sealed end of single borosilicate fiber with  $d_o = 700 \mu\text{m}$ ,  $d_i = 460 \mu\text{m}$ ,  $s = 120 \mu\text{m}$ , magnified 100 times, open channel visible at the end resulting in gas leakage

The investigation of volume defects can be outlined as following:

- The detection of volume defects partly was not possible without destruction of the test sample, because of the small size of fibers existing enclosures was very small.
- Investigations of cross section in axial direction of single fibers pointed out the enclosures of gas bubbles which was able to create stress peaks under loaded conditions. Here the size of the enclosed bubble was in the range of  $2 \mu\text{m}$  to  $3 \mu\text{m}$  and represented, in relation to the wall thickness of the hollow glass fiber, large defects. Nevertheless, such defects could not be detected under the light microscope.
- Another volume defect was the formed pellet at the molten end. Here one end of the single hollow fiber was sealed by melting. At the connection of the former inner surface a small inhomogeneity was clearly detected. The sealing was done manual for every hollow fiber wherefore every molten end looked individual.
- Also the changeover from fiber wall to molten bottom exhibited differences in appearance and development. The formation of a sharp peak was detected.
- Volume defects caused stress peaks when load was acting inside the material and could be the location of initial break.



### 6.10.2 Surface Defects

The investigation of the hollow fibers surface under the microscope was carried out to detect significant flaws which could cause stress peaks under the influence of inner pressure. Here the examination of the surface leads to different visualization of surface defects. The detected defects could not be directly identified as reason for a failure under load conditions. If a smooth and defect free surface was observed, the opportunity of existing Griffith flaws is still given. The sizes of such cracks increase and might become visible when pressure is applied inside of the fibers. In that state fibers are not examinable because of hazard of bursting.

The detected flaws varied significantly in form and size. The examination of single hollow fibers made of different glass materials under light microscope showed a smooth surface nearly without defects. Nevertheless, defects could be detected on test samples independent of the material. Reasons could be found in the production process as well in transportation conditions. With the following pictures flaws should be characterized, potential causer should be identified and the effects on pressure resistance should be discussed.

The hollow fiber in Figure 76 exhibits a smooth surface. However, clusters of small defects which could be characterized as localized spalling are detectable. Enclosed gas bubble in low distance to surface could be opened during drawing process due to reheating the material to temperatures above transformation temperature  $T_g$ . The gas trapped in the hollows has a different expansion behavior under the influence of heat and the pressure inside the bubble will increase by heating. The glass material loses stability with increasing temperature. If the pressure inside the bubble and the therefore acting stress on the glass material exceed the critical stress which is decreased by heat treatment, the bubbles will be opened and the characteristic defects will be formed. The existence of such bubbles was shown and confirmed by investigation of potential volume defects.

During the production process a glass tube is heated up and drawn to thin hollow glass fibers. In the heated area of the glass tube an area of tapering is formed. There a size reduction takes place caused by the force applied by the drawing facility. The small size of hollow glass fibers after leaving the tapering area indicates a rapid cooling rate due to small volume. In Figure 77 straight lines are observable on the top.

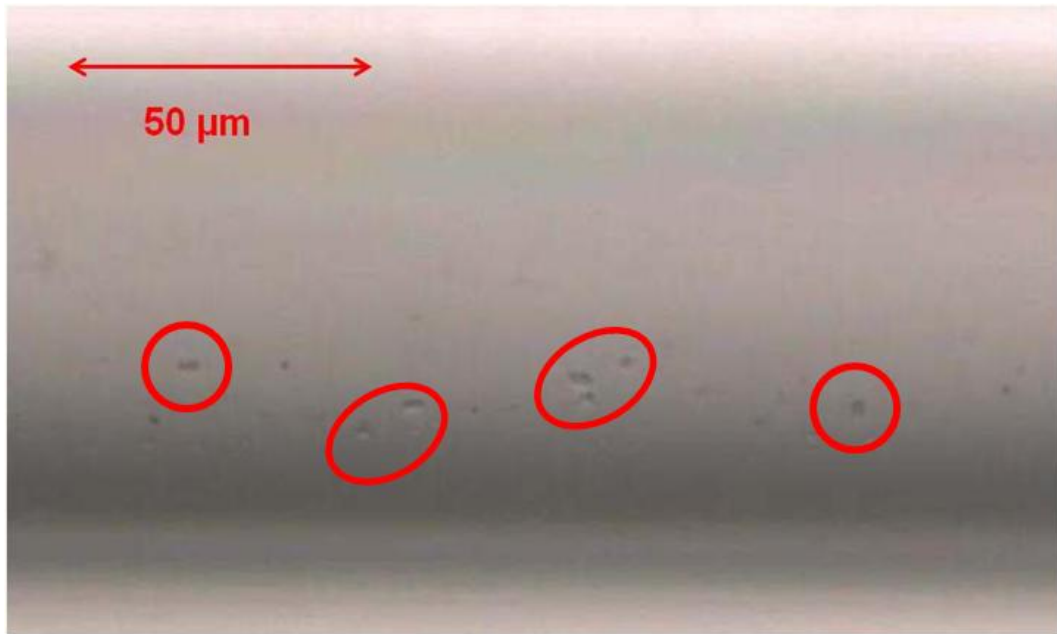


Figure 76: Surface of a hollow aluminosilicate fiber, detection of flatting or spalling on the surface was done under light microscope

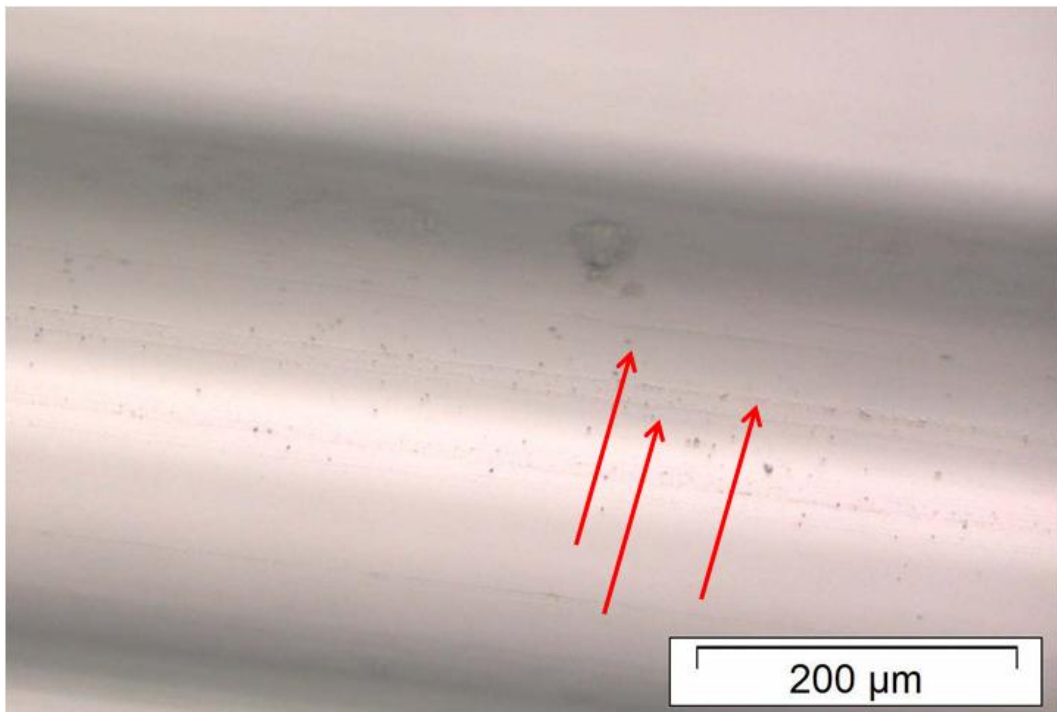


Figure 77: Quartz fiber surface under the microscope, straight lines detectable which could be caused during drawing process

Due to the consistency of the lines and the steady development parallel to the long axis the supposition can be made that these lines are formed by a drawing tool. Here wheels with rubber surface, respectively, rubber bands are in direct contact to the glass surface to apply the traction wherefore specific contact pressure is necessary. Although the temperature must have decreased to protect the rubber against decomposition the glass still exhibits increased temperature which could lead to decreased viscosity and formation of imprints.

The shipment from manufacturer provides opportunities for the formation of flaws as well. The hollow fibers were packed not separately but in amounts of around 50 pieces in small plastic bags. Due to the direct contact between the single fibers and the possibility of individual movement, potential of defect formation was given. Figure 78 displays such type of defects.

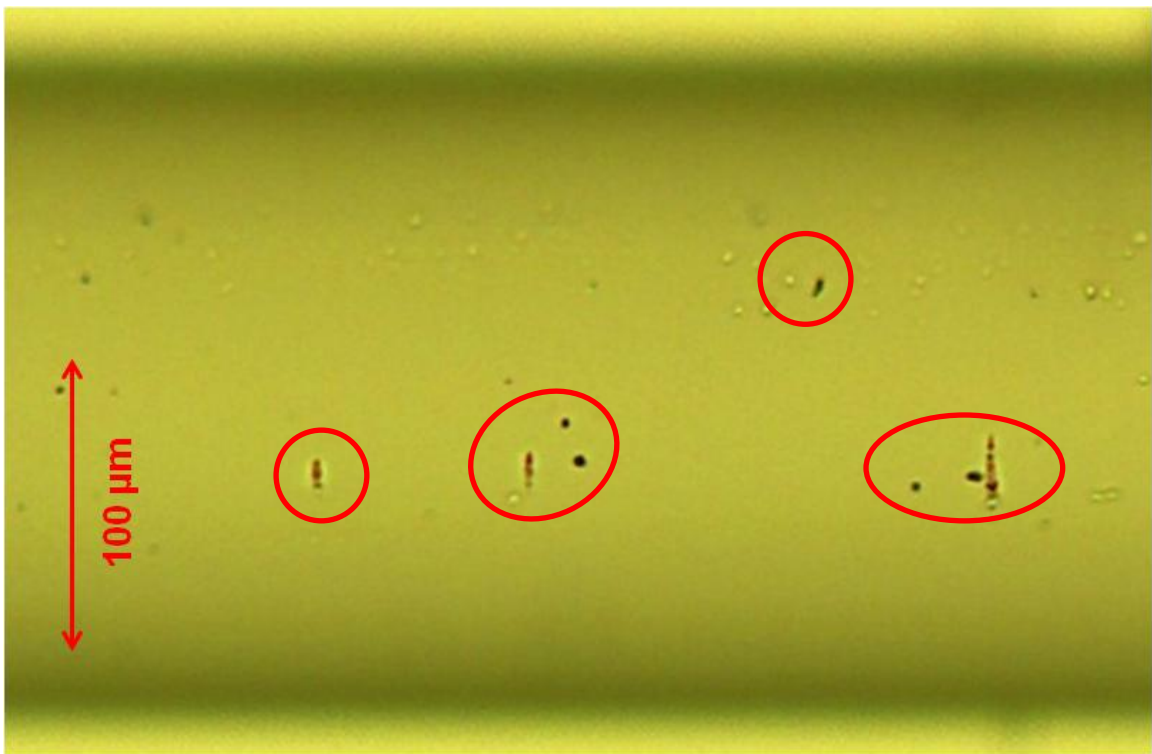


Figure 78: Hollow fiber surface with scratches, potential results transportation damages

The visible scratches on the surface orthogonal to the long axis of the hollow fiber with different sizes of 15 μm to 30 μm encourage the assumption that such defects are the result of abrasion between single fibers during transportation. Such defects could also be formed during drawing caused by contact with parts of the production plant

responsible for the guidance. Like the contact to traction device, such contacts at even higher temperatures also could affect flaws.

Obviously surface defects which could be detected on the outer surface of single hollow glass fibers are displayed in the following figure.

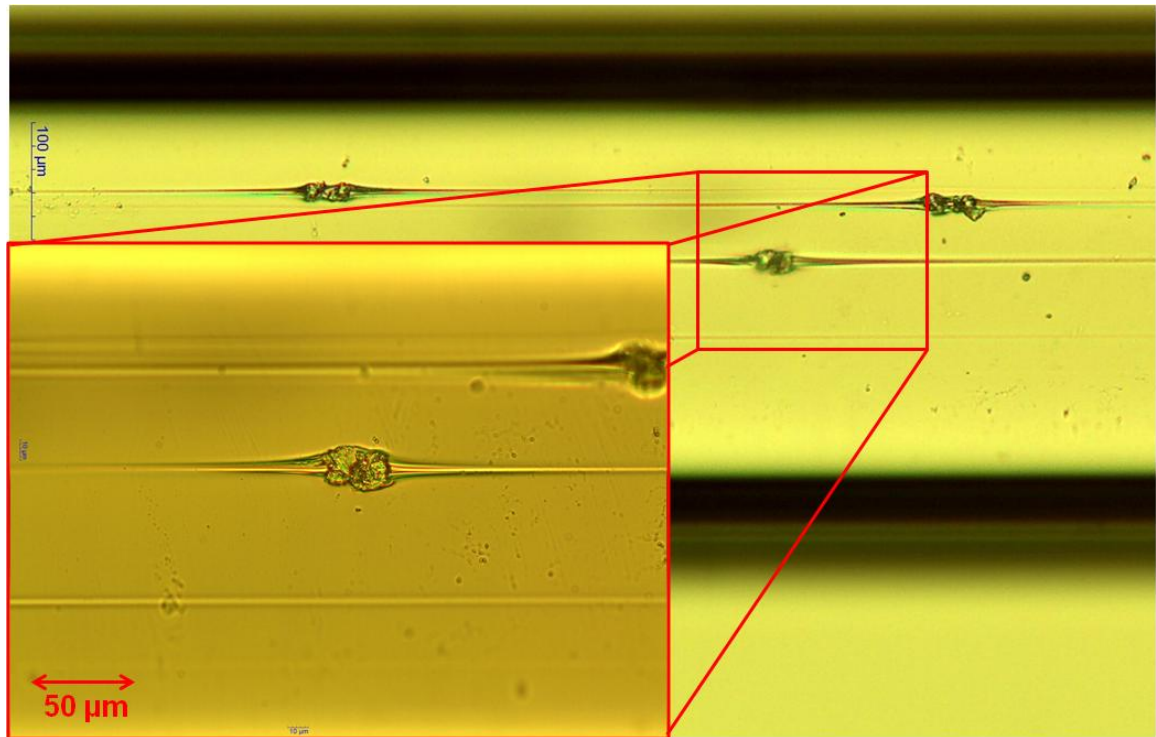


Figure 79: Borosilicate fiber with enclosures which are located at the surface

The displayed type of defect was detectable on different single hollow fibers in different quantities. Remarkable is the size of the defect of about 50 μm and the straight lines moving away from the center. Thus, the lines are parallel to the draw direction which indicates the formation during the drawing. The glassy look of the center points out that the defect could be defined as a knot. These can be characterized as glassy foreign objects in the glass material with high viscosity which inhibits a deformation during production or formation process. The lines, following the draw direction, are surrounding material with lower viscosity comparable to those of the borosilicate glass. The viscosity of that material is decreased by heating during formation process and admits a deformation. The size of the knot itself is not changed by formation process because the prevalent temperature is not high enough to melt the knot. Deviations in draw temperature also could lead to such defects. Thereby small particles of the furnace can be removed from the refractory material by the influence of higher temperatures and due to convection attached to the hot and weak surface of the glass. These particles are not

meltable and remain on the surface during drawing. The impact position is deformed and leads to straight lines while tapering and drawing. However, the investigation of a part of a raw tube before drawing process shows no enclosures or knots in the material wherefore the assumption of refractory particles seems to be right. Hollow fibers exhibiting such defects on the surface reached significantly lower burst pressures, so the pressure resistance is decreased many times. A chemical analysis of the defect center could give some indications of the origin and was done by using EDX. It is given in chapter 6.10.3 and discussed in detail.

The cutting of single fibers to length is a manual process where defect formation can take place. The hollow fibers were scratched with a glass cutter, a diamond added plate, and afterwards broken at the scratches by bending force. Here different breakage properties could be detected or the open end gives some indicates of it.

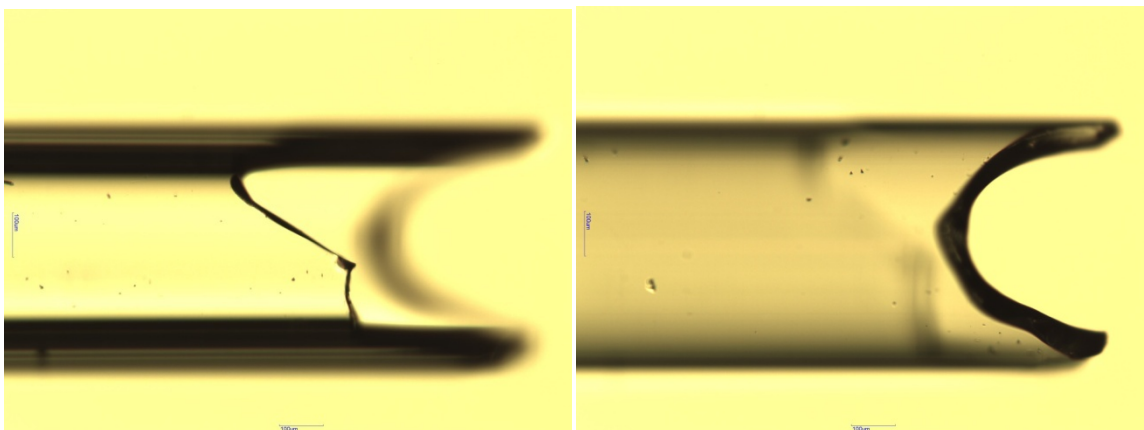


Figure 80: Open end of a borosilicate glass fiber with  $d_o = 570\mu\text{m}$ ,  $d_i = 460\mu\text{m}$ ,  $s = 50\mu\text{m}$ , magnified 100 times, taped in different levels

Caused by round shape of the hollow fibers the scratches are located only in one small region and will lead to the initial breakage when bending force is applied. The resulting rough fractured surface of a fiber with wall thickness of about  $s = 50\mu\text{m}$  is clearly noticeable in Figure 80 but further possible small cracks are not detectable. Fibers with even smaller diameters and wall thickness show the same fractured surface at the open end (Figure 81).

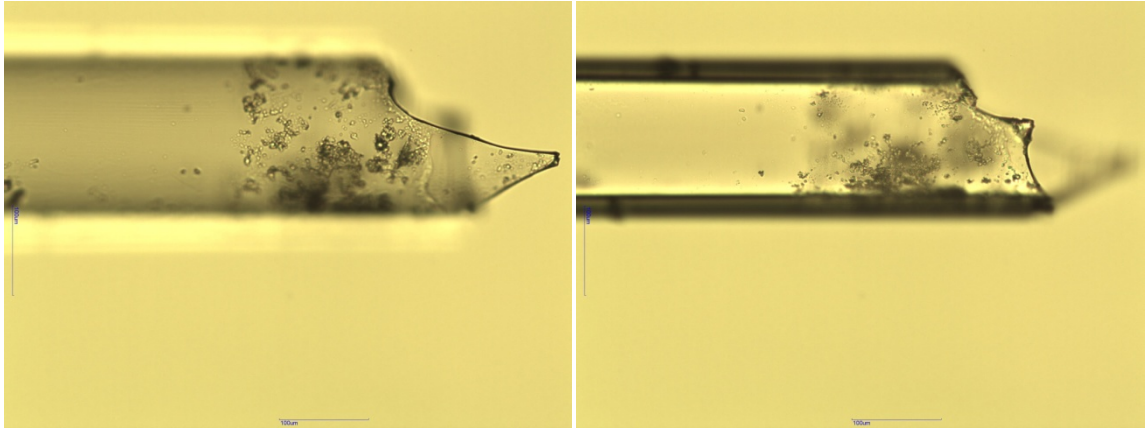


Figure 81: Open end of a borosilicate glass fiber with  $d_o = 180 \mu\text{m}$ ,  $d_i = 160 \mu\text{m}$ ,  $s = 10 \mu\text{m}$ , magnified 200 times, taped in different levels

At these levels visible precipitates can be defined as dust and glass powder remains after breaking at the inner surface of the hollow fiber. Again the sharp edges on breaking line are detectable but no further crack which indicates a damage of the structure or a massive influence on the pressure resistance. Nevertheless, at thicker wall thicknesses and diameter the breakage behavior is completely different. The scratches are produced in the same way but breakages exhibit a nearly straight break at the marked position, shown in Figure 82.

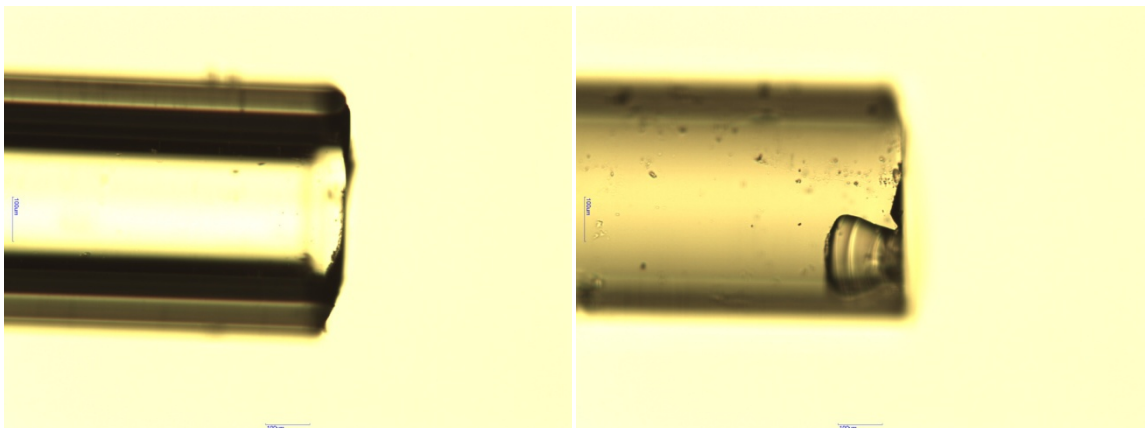


Figure 82: Open end of two different borosilicate fibers with  $d_o = 540 \mu\text{m}$ ,  $d_i = 360 \mu\text{m}$ ,  $s = 50 \mu\text{m}$ , magnified 100 times

Clearly identifiable is the straight edge of breakage at both open ends. Here the material thickness leads to a minor impact and influence on the material. During the scratching the fibers with the glass cutter at specific force acts on the fibers surface and dependent on that force, size and depth varies. If it is assumed that the force is the same for every



type of fiber, larger hollow fibers with higher wall thickness will be marked only at surface whereby at thinner fibers the wall could be penetrated partially. That damage in surface and structure leads to different breakage behavior.

The developments in quality management result in prevention of most types of volume defects, so the mechanical loadability of glasses is rather a surface property [97]. However, the investigation showed the existence of volume defects by enclosed gas bubbles or knots.

The investigation of hollow fibers surface showed the importance of the surface quality. Different flaws were detected. The origin of these defects could not be clearly identified. Additionally, the existence of surface flaws did not lead to decreased loadability implicitly. It was not possible to associate possible surface defects with the initial break of a fiber. The velocity of crack propagation increases by increasing inner pressure.

The distribution of stress in peaks at the tip of existing cracks not only effects crack propagation but also the opening of defects which enable faster degradation by environmental influences. Thus, the existence of Griffith flaws could not be proved because of the nanometer or micrometer size. Even with SEM such flaws could not be detected. The limitation of pressure resistance by surface defects could be countered by the application of a surface coating. Defects due to the handling and transport could be prevented.

As result of the investigation of hollow glass fibers on surface defects it can be summarized that:

- Different surface defects were detectable by investigating the hollow fibers under a light microscope. The assessment of exact reasons of such flaws was not able in each instance. In most cases the origin can be ascribed to transport and handling.
- Different defects surrounded by lines in drawing directions can be ascribed to enclosures in the raw material. During drawing process those were not molten and remain in the glass material. Due to reduction of size the surface was pierced through.
- A connection between detected surface flaws and the point of initial break was not successful by using a high-speed camera because of the high velocity of crack propagation under loaded conditions.

### 6.10.3 Investigation of Glass Fiber Surface by SEM and EDS

Detecting the surface of hollow glass fibers by using the scanning electron microscope (SEM) allows for a much higher resolution. Additionally, the investigation of the origins of defects can be done by energy dispersive X-ray spectroscopy (EDS). The excitation of the surface by consistent energy leads to the emission of x-rays by the material. Thereby each element exhibits a characteristic X-ray emission and can be identified.

Single fibers made of borosilicate DURAN glass exhibited a significant defect rate by showing different types of flaws on the surface which are surrounded by stripes in drawing direction. That typical defect is shown in Figure 83.

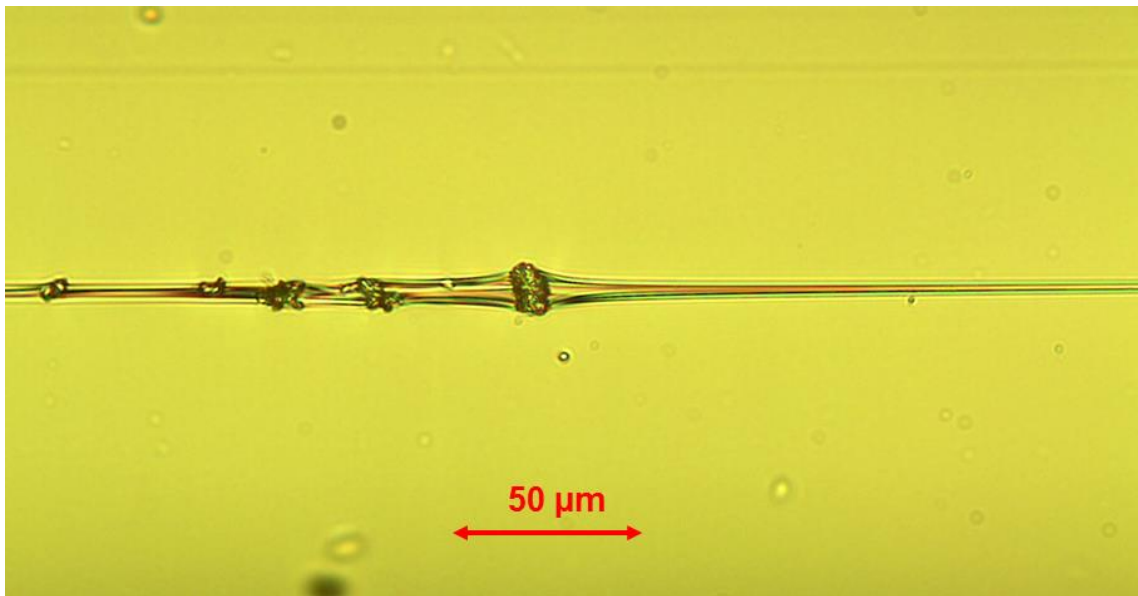


Figure 83: Typical surface defect on borosilicate glass fibers with dimensions of  $d_o \approx 490 \mu\text{m}$ ,  $d_i \approx 420 \mu\text{m}$  and  $s \approx 35 \mu\text{m}$ , magnified 400 times

The defects and the stripes in drawing direction can be detected. The usual size was in the range of  $20 \mu\text{m}$  up to  $35 \mu\text{m}$ , but larger particles were observed as well.

Using the light microscope the existence of flaws can be determined. The origin of the defects was not investigable. Such particles on the surface, as demonstrated in picture above, can create deposits of refractory material of the furnace inner surface. Another possible source is in enclosures inside the glass material which are originated in the melt during glass production and classified as stones. Impurities of raw materials with higher melting temperatures form such enclosures remain inside the material. Inhomogeneous temperature distribution can create stones as well. In this case even pure raw material may remain unmelted and form enclosures like stones.



The origins of such flaws were investigated under the SEM by the application of EDS. In addition to the above described defects, deposits on the surface in different shapes were observable. Figure 84 displays a concentration of different defects. Each of them was investigated and the chemical components were determined. Therefore four different marks on the surface are noticeable.

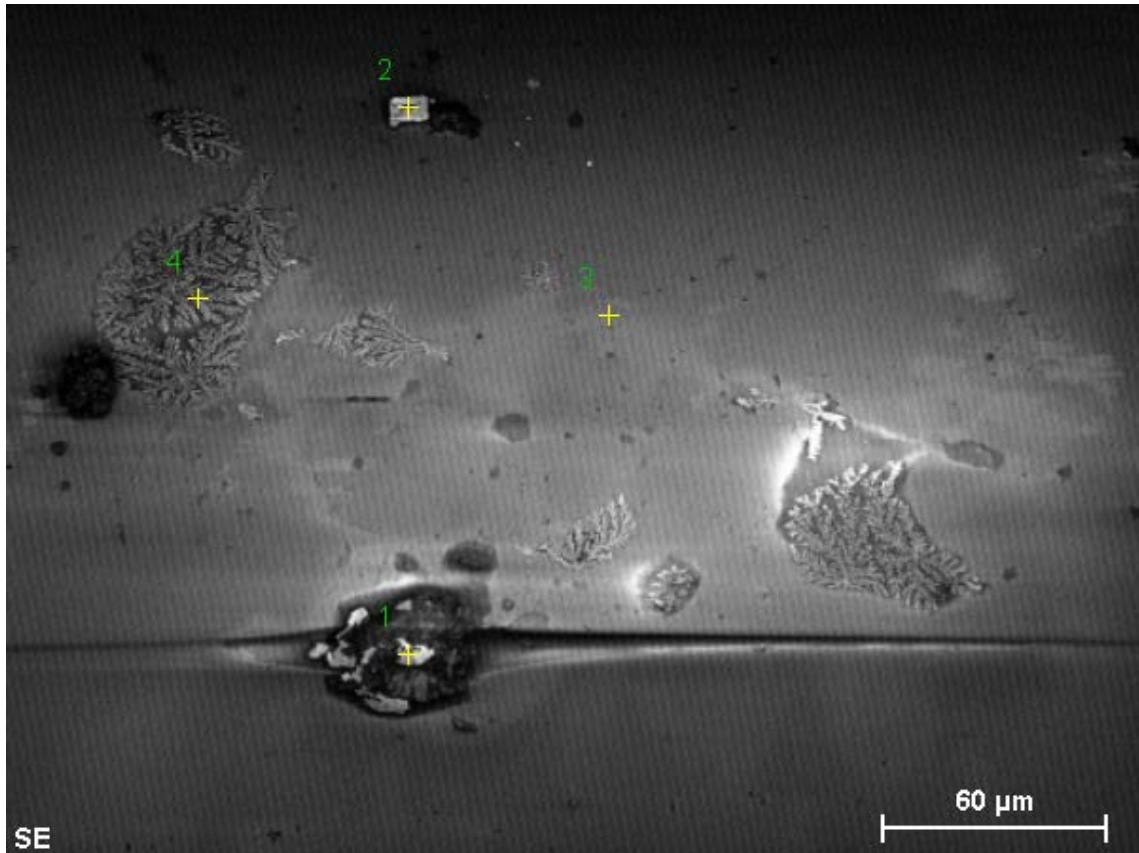


Figure 84: Surface defects on borosilicate DURAN fibers with dimensions of  $d_o \approx 490 \mu\text{m}$ ,  $d_i \approx 420 \mu\text{m}$  and  $s \approx 35 \mu\text{m}$ , four different measuring points are marked and the chemical elements were investigated

The picture presents different types of defects each with a unique shape. In the lower part of the picture is a particle surrounded by stripes in drawing direction which is marked as measuring point no. 1. The indentation of the glass material by the stripes is noticeable as the elevated structure of the particle. The second measuring point is a cuboid structure at the upper margin marked by no. 2. The cubic shape leads to the assumption that the detected particle could be a salt crystal. Furthermore, crystal structures with slightly elevated structure are observable in different regions of the picture. Measuring point no. 4 was set directly on a crystal structure to investigate its chemical composition. A defect-free region of the surface was examined by setting

measuring point no. 3. Therefore, the results of measuring points no. 1, no. 2 and no. 4 should be validated and confirmed.

In the following picture the measured spectrum of measuring point no. 1 is plotted. The large defect with a size of about 25  $\mu\text{m}$  is expected to be refractory material or even an enclosure remained in glass from the production process.

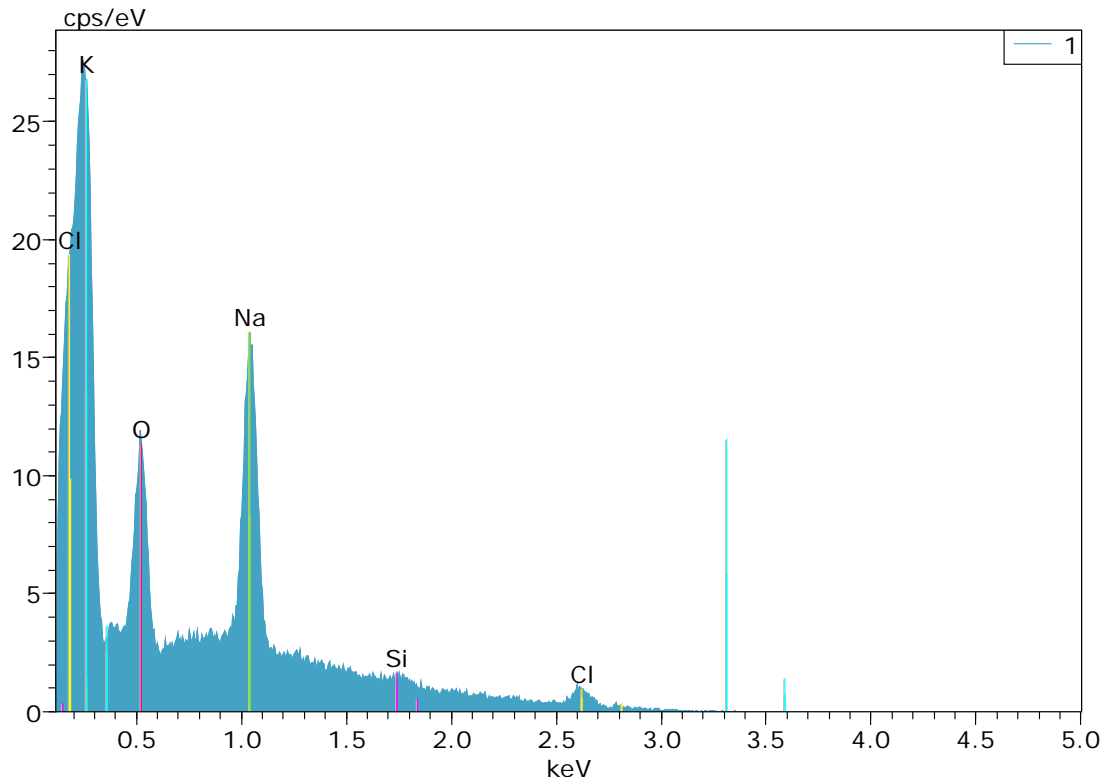


Figure 85: EDS-spectrum of measuring point no. 1 defined in Figure 84, significant peaks for the elements Na, K, and Cl are detectable

The diagram shows clearly significant peaks for the elements potassium (K), sodium (Na), oxygen (O) and chlorine (Cl). The origin of such particles from refractory material from the inner furnace surface can be excluded. Most refractory materials consist of a high percentage of  $\text{Al}_2\text{O}_3$  and a peak of Al has to be detected. The addition of  $\text{Na}_2\text{O}$  and  $\text{K}_2\text{O}$  in the chemical composition of DURAN glass leads to the reduction of the melting point. Nevertheless, the main component is still silica with a percentage of 80.5% [3], [148]. Due to the negligible peak of silica the examined particle can be identified as an enclosure created during melting process of the glass. During the production of the glass tubes and subsequently the hollow glass fibers, the temperatures were not high enough to melt the remaining solid particle. The drawing to fibers and the simultaneous

reduction of size and wall thickness led to the shift of the enclosure from the volume to the surface of the material.

The cubic shape of the particle defined as measuring point no. 2 led to the assumption that it is a salt crystal. The according spectrum is given in Figure 86.

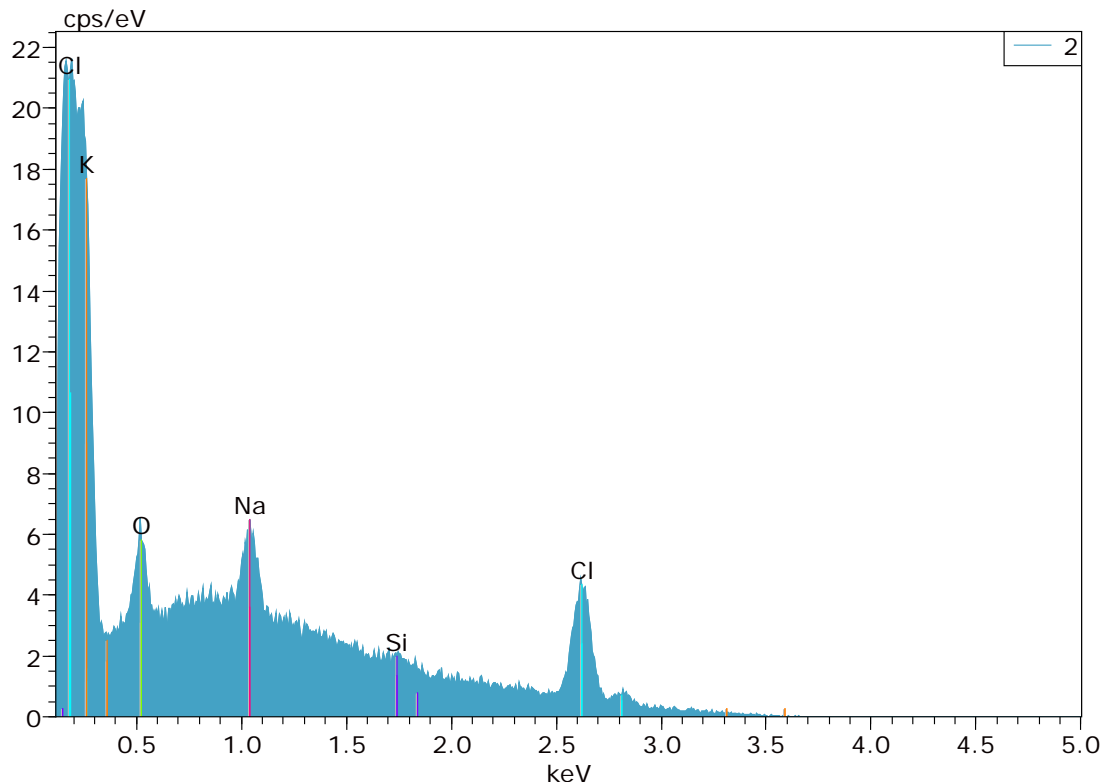


Figure 86: EDS-spectrum of cubic shaped particle on DURAN fiber surface

Measuring point no. 2 features significant peaks for the elements K, Na and Cl. The cubic shape and the distinct peaks for Na and Cl indicate the presence of a sodium chloride crystal on the surface of the examined fiber. The drawing temperature of the DURAN fiber was given as  $T = 910\text{ }^{\circ}\text{C}$  [148] which is above the melting temperature of NaCl of  $T = 810\text{ }^{\circ}\text{C}$  [15]. However, during drawing process the salt crystal might be molten but remained in glass material. A shift from the volume to the surface might take place and after leaving the furnace and cooling down the cubic shape were formed again. Afterwards the crystal remained on the surface. The origin can be found in impurities of raw material. NaCl is available as mineral in natural appearance. The contamination of raw materials of glass production even in traces can lead to the enclosure of the crystals in the material.

A comparable result was observable for the elevated crystal structure at measuring point no. 4 as can be seen in Figure 87.

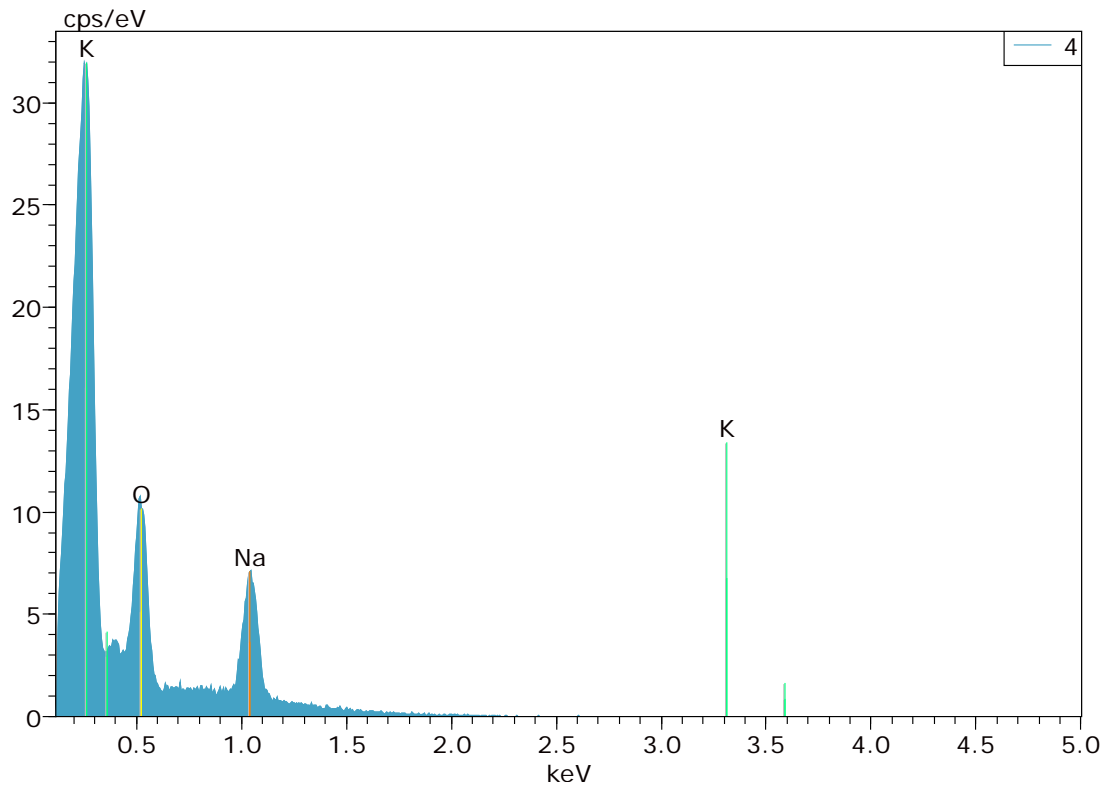


Figure 87: EDS spectrum of measuring point no. 4 with elevated crystal structures on fibers' surface

The sharp peak for K is observable in the spectrum distinctly. Additionally a clear peak of Na and O is detectable. The crystal structure therefore can be identified as  $K_2O$  and  $Na_2O$  which is crystallized out at the surface of the hollow fiber. The behavior can be explained by inhomogeneous parts of the melt and local high concentration of the components. During tube and fiber production the material shifted to the surface and a crystallization process takes place. However, the presence of  $Na_2O$  and  $K_2O$  on the surface leads to a possible chemical reaction which can modify the structure of the glass network. Both compounds are hygroscopic and form in compound with water or even air moisture hydroxides. These products may lead to an alkaline reaction on the glass surface. In addition to alkaline compounds being dissolved from the structure, the silica network is attacked by such reactions. The mechanical resistance can be decreased by a multitude in that region and a possible initial point of breakage is formed.

In addition to the examination of the irregularities, a defects free area was defined as measuring point no. 3, and it was investigated as well. The results are given in typical EDS spectrum in Figure 88.

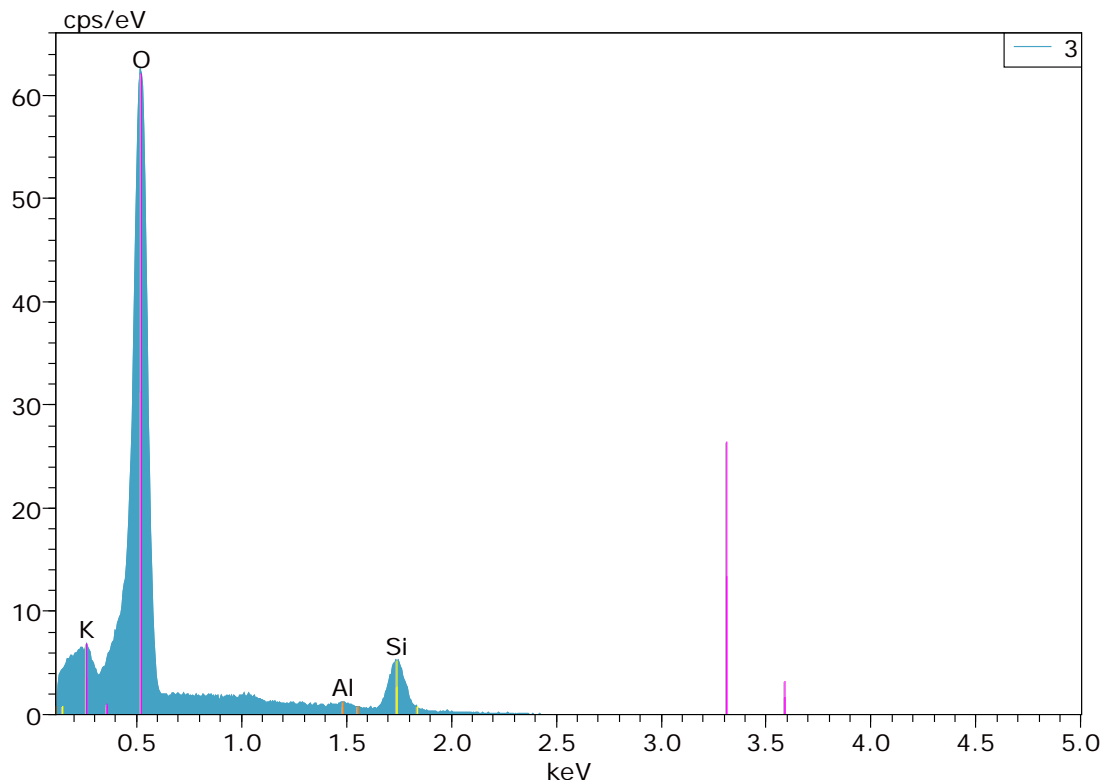


Figure 88: EDS spectrum of measuring point no. 3 of a defect free area of the DURAN fiber surface

A distinct sharp peak of oxygen and silica is noticeable beside low peaks of K and Al. Silica is determined as the main component beside  $K_2O$  and  $Al_2O_3$ . The absence of a peak for  $B_2O_3$  as component can be explained with the inactivity of the element boron in EDS procedure.

Investigating the origin of defects under the SEM by using EDS procured good results. The chemical composition of a small region is determinable and therefore the origin of defects can be declared as enclosures from production process. The high resolution of the SEM allows the visualization of the surface in detail and even small defects were found like the crystal structure of measuring point no. 4.

Nevertheless, the investigation of hollow glass fibers under the light microscope is a fast and economic way of quality control. In many cases no defects were detectable on the surface by using the light microscope. The large scale defects found on the surface of

the DURAN fibers showed the benefit of the light microscope as well as of the SEM. A combination of both methods will be the best way for quality control of further test series.

Present flaws created by impurities or inhomogeneous regions in production process restricted on only a small number of test series. A direct coherence between defects and low pressure resistance could not be observed or declared. However, flaws on the surface can act as indentation where the material is weakened by having lower wall thickness and stress peaks arise under acting load. Deposits of chemical compound like detected NaCl or Na<sub>2</sub>O may lead to local restricted chemical reactions on the surface. Due to their hygroscopic property water from air moisture is ligated and hydrolytic or even alkaline reactions can take place which weaken the structure.

The investigation of surface defects by SEM and EDS can be outlined as following:

- Using the SEM and EDS the chemical composition of defined regions can be examined and therefore possible origins were found.
- Surface defects surrounded by lines in drawing direction as shown in previous subchapter was proven as enclosures of Na<sub>2</sub>O, K<sub>2</sub>O and NaCl. The formation of such flaws in melting process may have no influence on the mechanical resistance of large-scale and thick-walled glass products and components. Because of keeping their size during drawing of thin hollow fibers a significant effect on the pressure resistance of those fibers occurred.
- Consequently a combination in usage of light microscope and SEM/EDS will be an efficient way in detection of defects and determining their origins.

### 6.11 Calculation of Defect Sizes

The investigation of hollow glass fibers revealed different defects existing in the glass material on the surface. However, most fibers exhibited a smooth and defect free surface which presents no reason for failure under non-loaded conditions.

In 1921 the study of Griffith led to the development of a formula to calculate the size of defects which causes the failure. Here at crack tip equilibrium of energy  $U$  was assumed between mechanical energy  $U_M$  and surface energy  $U_S$ . Thus, the mechanical energy  $U_M$  is composed of the elastic energy of the material  $U_E$  and the potential energy  $U_A$

$$U = U_M + U_S = U_E + U_A + U_S \quad (6.5).$$

If the acting load is strong enough to propagate the crack the mechanical energy will decrease due to the loss of elasticity in the crack region ( $U_E$ ) and potential energy ( $U_A$ )

caused by changing position. The equilibrium is obtained by formation of new surfaces and consequently new surface energy.

The mechanical energy is a function of the acting load  $\sigma_F$ , the radius of the critical defect  $c$  and the Young's modulus  $E$  of the material:

$$U_M = - \frac{\pi c^2 \sigma_F^2}{E} \quad (6.6).$$

The surface energy is described as a function of the normalized fracture surface energy  $\gamma$  and the radius of defect again in formula (6.7):

$$U_S = 4 c \gamma \quad (6.7).$$

Combine formula (6.6) and (6.7) and assumed equilibrium of energy:

$$\frac{dU}{dc} = 0 \quad (6.8)$$

yield to Griffith criteria:

$$\sigma_F = \sqrt{\frac{2 E \gamma}{\pi c}} \quad (3.5).$$

Hence, the critical defect size is calculable with the knowledge of the acting load  $\sigma_F$ .

A multitude of single fibers were tested and leads to various burst pressure results. The application of Barlow's formula:

$$\sigma_t = \frac{p d_o}{2 s} \quad (5.2)$$

initializes the opportunity of calculation of the tangential stress in the material occurring at burst pressure. Thus, a normalized stress  $\sigma_t$  of hollow fibers is given which causes the individual failure at a specific crack and is definable as critical stress of the related fiber. The calculated stress is directly proportional to the burst pressure and dependent on both the outer diameter and the wall thickness as well. It can be seen that with constant free space the resulting stress at a specific pressure should be the same theoretically. Thus, the free space is synonymous to the ratio of the outer diameter to the wall thickness. Test series in chapter 6.4 showed that hollow glass fibers exhibit a different behavior. Decreasing wall thicknesses and constant free space ratios lead to increasing pressures. Consequently, the tangential stress inside of the fiber wall increase as well. Figure 89 shows exemplary the behavior of hollow borosilicate C5 glass fibers with a free space of  $FS = 63\%$ .

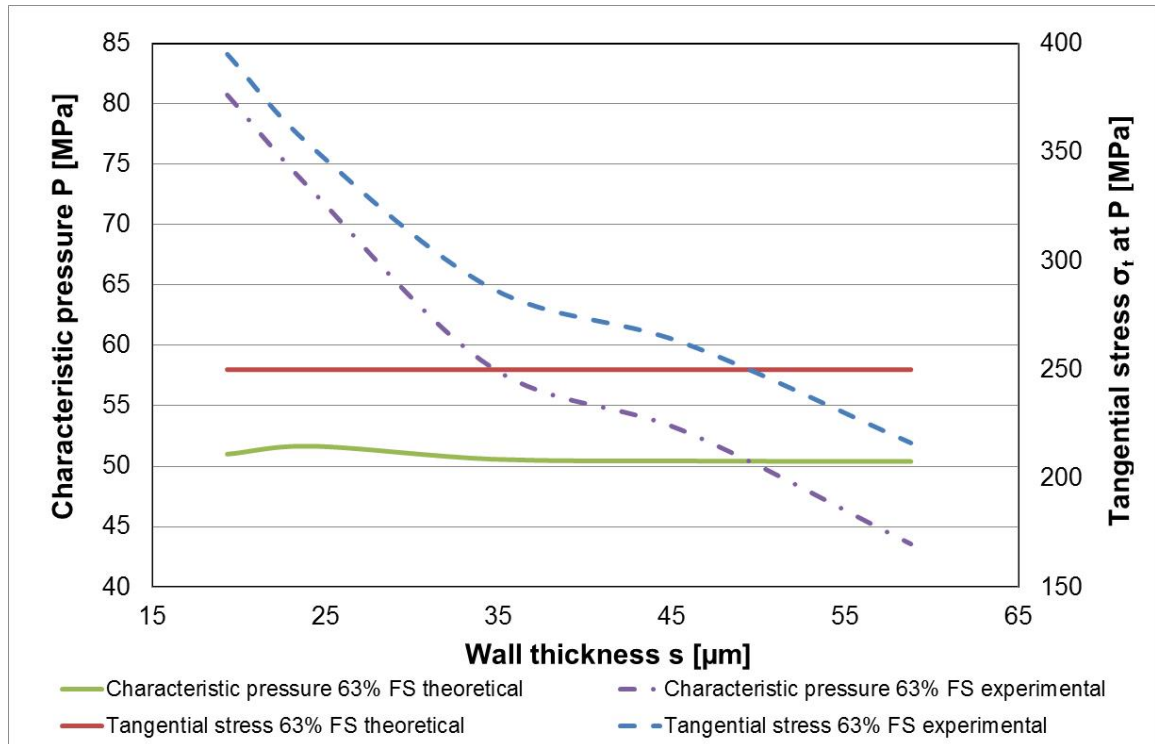


Figure 89: Characteristic pressure of hollow borosilicate fibers against wall thickness, theoretical calculation in comparison to experimental results

The development of theoretical values compared to the experimental measured results is completely different. The theoretical pressure development nearly describes a straight line at constant pressure value caused by uniform ratio of outer diameter and wall thickness. Variations in dimensions and resulting differences in free space of about 0.5 % result in the slight deviations of ideal behavior. As calculation basis, a tangential stress of  $\sigma_t = 250$  MPa was adopted which is also plotted in the diagram. The development of experimental results points out precisely the increase of pressure resistance as well as tangential stress by decreasing wall thickness. Due to the constant diameter to wall thickness ratio, the diameters decrease as well. The characteristic pressure  $P$  exhibit a steady increasing development like the tangential stress  $\sigma_t$ .

The calculation of the tangential stress  $\sigma_t$  can be done for every single measured burst pressure value. Because of the assumption that tangential stress  $\sigma_t$  at individual burst pressure  $p_B$  can be equated with the acting load  $\sigma_F$  at the critical flaw radius of individual hollow fiber the equation:

$$\sigma_F = \sigma_t \quad (6.9)$$

leads to formula (6.10):



$$\sqrt{\frac{2 E \gamma}{\pi c_0}} = \frac{p d_o}{2 s} \quad (6.10).$$

Solving that formula to the critical crack radius results in formula (6.11):

$$c_0 = \frac{8 E \gamma}{\pi} \left( \frac{s}{d_o p} \right)^2 \quad (6.11).$$

With this formula the opportunity is given to calculate the radius of the crack  $c_0$  at which the acting load initiates the initial break. The total size of the crack thereby can be calculated by formula (6.12):

$$C = 2 c_0 \quad (6.12).$$

Exemplary characteristic values of tested hollow glass fibers with a free space of  $FS \approx 80 \%$ ,  $FS \approx 63 \%$  and  $FS \approx 40 \%$  together with calculated critical crack size  $C$  at characteristic pressure  $P$  of the related test series with same parameters are listed in Table 59. Moreover, some of the listed parameters are required for the calculation. Young's modulus and normalized fracture surface energy were given in literature [3], [148], [151], [173]. The listed values are exemplary for the dominant development of defect size dependent on hollow fibers wall thickness and measured burst pressures. Therefore, the calculation is valid for every single fiber and individual measured pressure.

Again, it can be seen that significant variations in dimensions exist. Consequently, the free spaces vary as well. Nevertheless, a clear trend is detectable by comparison of data. Decreasing wall thickness at similar free space is associated with increasing characteristic pressure. The direct proportionality of tangential stress  $\sigma_t$  to pressure values during decreasing the wall thickness leads to increasing tangential stress values as well.

The critical crack size exhibit a complete deviance due to the squared reciprocal function of the tangential stress in formula (6.11) where the size of the critical flaw decreases with decreasing wall thickness. That behavior comes along with the theory of Griffith that also the probability of critical flaws per volume element decreases with decreasing wall thickness. It should be noted that calculated defects here only exhibit magnitudes in very low micrometer scale. Hence, a detection of defects beforehand of the burst pressure tests is not possible. However, a critical defect size can be calculated which has to be excluded to reach a predefined performance range.

Table 59: Characteristic data and calculated critical crack size of hollow borosilicate fibers with similar free spaces

Inner diameter $d_i$ [ $\mu\text{m}$ ]	Wall thickness $s$ [ $\mu\text{m}$ ]	Free space FS [%]	Characteristic pressure $P$ [MPa]	Tangential stress $\sigma_t$ [MPa]	Critical crack size $C$ [ $\mu\text{m}$ ]
159.4	10.9	77.5	41.7	348.0	0.22
183.5	12.4	77.7	44.3	373.4	0.19
257.3	17.4	77.6	36.4	305.5	0.28
365.0	18.9	82.1	24.2	257.9	0.40
464.4	22.2	83.3	21.7	249.2	0.42
151.0	19.4	63.4	80.7	395.0	0.17
186.6	24.3	62.9	72.7	351.8	0.22
273.2	34.7	63.6	58.1	314.4	0.32
361.6	45.7	63.7	52.9	262.2	0.38
465.8	58.8	63.8	43.6	216.3	0.56
123.8	38.2	38.2	143.9	368.9	0.19
173.7	50.9	39.8	118.3	320.4	0.26
265.8	76.4	40.3	96.9	287.2	0.37
352.0	103.1	39.8	110.2	298.3	0.30
457.6	134.6	39.7	80.5	217.4	0.56

A clear visualization of the ratio of tangential stress to size of defects, which lead to the failure of tested samples, is plotted in Figure 90.

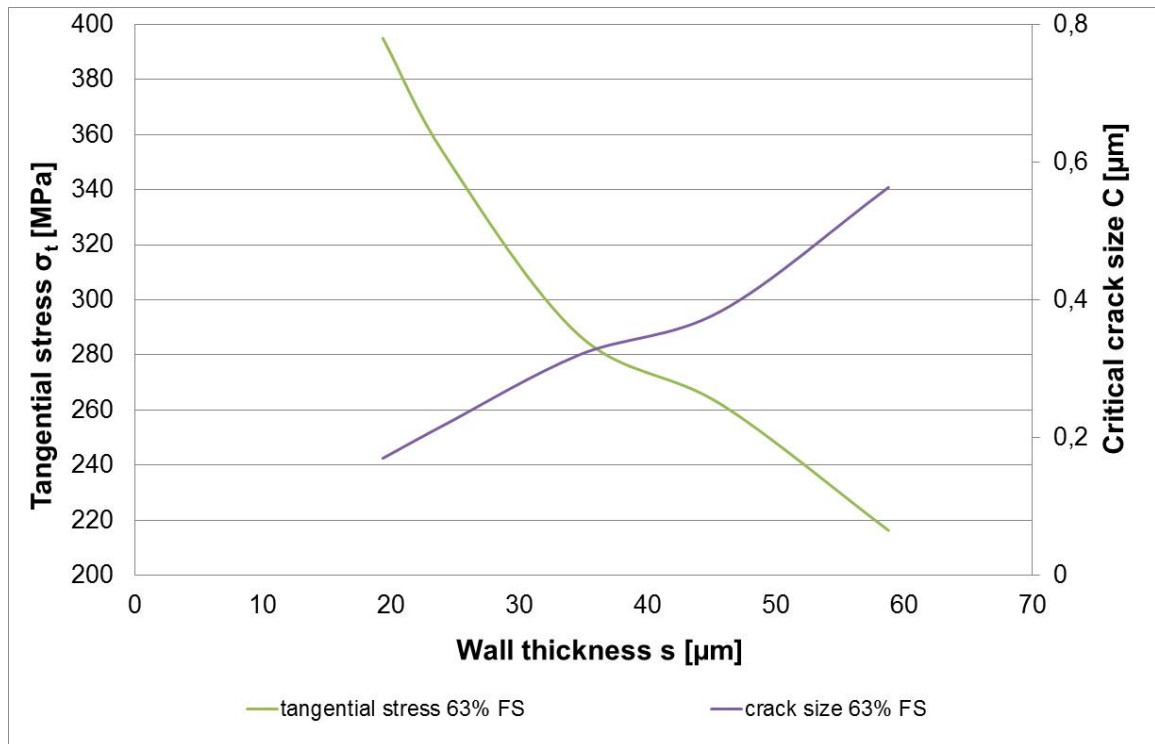


Figure 90: Tangential stress plotted against wall thickness for borosilicate fibers with free space of FS = 63%; development of related critical crack size C in micrometer is given as well

The diagram points out the increasing values of tangential stress of characteristic pressure with decreasing wall thicknesses but nearly constant free space. Besides the higher reachable stress also smaller critical defect sizes are calculable. Hence, higher pressure resistance of hollow fibers is associated with smaller defects.

An appropriate method to compare test results of hollow glass fibers with different dimensions to each other and demonstrate improvements or degradations of performance of single test series is the calculation of occurring tangential stress at specific burst pressures. The calculated stress value is normalized and directly proportional to the burst pressure.

It can be summarized that:

- The calculation of tangential stress inside the fibers' wall from burst pressure values by Barlow's formula showed direct proportional.
- Equating the tangential stress with the acting load of the Griffith criteria, the calculation of critical crack size of every single hollow fiber was possible. An inversely proportional behavior occurred so with increasing pressure resistance the calculation led to decreasing results of the critical defect size.
- The critical crack sizes  $C$  which led to failure in carried out test series of this thesis under the assumption of Barlow's formula and Griffith criteria were in the range of  $C = 0.1 \mu\text{m}$  to  $C = 1.0 \mu\text{m}$ .
- By using that method a critical defect size can be calculated which has to be excluded for reaching a predefined performance level at defined fiber size.

## 6.12 Influence of Defects on Pressure Resistance of Hollow Glass Fibers

Thin hollow glass fibers feature an outstanding mechanical resistance by being loaded up with internal pressure. The theoretical tensile strength of glass can be calculated as  $\sigma_{\text{th}} \approx 12,900 \text{ MPa}$  [3] and  $\sigma_{\text{th}} \approx 7,000 \text{ MPa}$  [5], respectively. The practical tensile strength of the material glass is decreased many times by the presence of different defects which can be classified as material-dependent defects or production-dependent defects. Such defects can originate different local stresses in the considered component wherefore the stability, calculable from the theoretical tensile strength, will not be reached. The following subchapters point out the characteristics and origins of defect types by reference to the carried out test series and examinations.

### 6.12.1 Material-dependent Defects

Glass features an irregular and random network structure of silica tetrahedrons in contrast to the regular and ordered crystalline lattice structure of e.g. quartz crystals. The main component  $\text{SiO}_2$  forms the amorphous structure without showing any long-range order.

The addition of alkaline oxides leads to modification of the network due to splitting bridge ring oxygen structures by alkaline oxide ions [3], [4]. The formed disconnecting points in structure engender different changes of physical as well as chemical glass properties. The generated points of imperfections are material-dependent defects influenced by the chemical composition of the glass. The appearance in the amorphous structure is

irregular as well. The formation of points of disconnection in glass structure varies the mechanical properties of glass by reducing the stiffness of the network. Therefore such material-dependent defects lead to lower pressure resistance. With the addition of network stabilizer e.g.  $\text{Al}_2\text{O}_3$  and  $\text{B}_2\text{O}_3$  the reducing effect of network modifier on network stability can be antagonized as investigated in chapter 6.5 and 6.7. Here the concentration of stabilizer has to be considered. The exceeding of a limiting concentration results in the change of effect of the stabilizer on the network. Below the limiting concentration stabilizer acts as a network builder, above that concentration the effect will be comparable to that of a modifier. Moreover, the limiting concentration depends on the chemical composition and the amount of silica.

Chemical properties of glass are modified as well by the addition of different substances. The addition of alkaline oxides entails the reduction of chemical resistance compared to quartz glass which is only attackable by alkaline reactions and two acids (fluoric acid and aqua regia) [3], [94], [95]. Modified glasses are attackable additionally by acid and hydrolytic reaction on the surface. Alkaline reactions reduce the loadability of glass components by destroying the silica network. However, acid and hydrolytic reactions dissolve alkaline ions from the network wherefore modified glasses are susceptible against such reactions. The enrichment of alkaline in water or acid may lead to the change of the reaction into a more corrosive acting alkaline reaction.

Consequently, material-dependent defects are directly dependent on the chemical composition of the used glass material, and influence the physical and chemical properties of the glass in a similar manner. However, the prior impact on the pressure resistance of hollow glass fibers results from production-dependent defects.

### **6.12.2 Production-dependent Defects**

Production-dependent defects can occur in all steps of the production of glass. The focus of this subchapter is set on the production of hollow glass fibers from glass melt to the final fiber.

The melting process exhibits the first opportunity for the formation of defects in glass material. Thereby enclosures are formed and may remain in the glass until the final product. Possible origins can be impurities of the raw material, particles of refractory material of the melting pot or inhomogeneous temperature and material distribution. The formation of stones or knots is the result of described origins. Due to the high melting temperature of such particles they remain in solid state in molten glass mass. During further temperature treatments of formation processes the temperatures remain certainly

below the required melting temperature of the particles. Consequently, solid enclosures can be present from the melting process until the final product. Such defects could be determined in hollow glass fibers, as examined in chapters 6.8 and 6.10.3.

The homogenization of molten glass mass is done by gas bubbles [114] introduced via cones in a melting pot wall. Another method of homogenization is the addition of gas forming chemical compounds to the glass melts which do not modify the network structure but decompose it by high temperatures to gases. If the upswing of bubbles is too small they can remain in the material and form defects as well. The size of remaining bubbles in material could be different and small bubbles were determinable as volume defects in the wall of hollow glass fibers (chapter 6.10.1).

After the glass melting process tubes with different diameters were formed from molten mass. The origin of production-dependent defects is restricted to solid particles from ambient air and the refractory material of formation tools. The deposition of such particles can effect indentations, crater-shaped pits and lines in drawing directions. Such defects in most cases are detected by quality assurance but cannot be excluded completely. Scars and scratches formed by tools can be healed by further drawing process of thin hollow glass fibers.

The drawing of fibers from glass tubes as a final formation and production step involves also the possibility of defect formation. Enclosures formed during melting process may be transported to the surface. The size of the glass tube is reduced by a multitude whereby the enclosure size remains unchanged. At the initial point of surface contact indentations will be formed in drawing direction due to the flow of the glass (chapters 6.8 and 6.9.1). The material is weakened due to lower wall thickness and new stress peaks arises at the indentation during inner pressure load. Furthermore, scars and scratches formed by the tractor are possible defects during drawing process.

The cutting, transportation and general handling may cause the formation of new flaws. Cracks and outbursts at the cutting edge shown in chapter 6.10.2 as well as scratches on the surface can be reduced or completely excluded by the application of a coating directly during drawing process. The positive effect on the pressure resistance of hollow glass fibers were investigated and determined in chapter 6.9.2.

Described defects were detectable as surface or volume flaws on fibers investigated as part of this work. The presence of defects could not be attributed to low pressure resistance. However, it can be assumed that defects led to local stress peaks which exceeded the maximum loadability of the material and causing a bursting of the fiber.

As result of the study of influences of defects on the pressure resistance of hollow glass fibers can be outlined that:

- Occurring defects in glass are classifiable in two different types: the material-dependent and the production-dependent defects.
- Material-dependent defects are attributed to the irregular network structure of glass and the formation of points of disconnection dependent on the chemical composition. Their influence on the pressure resistance is negligible compared to the effect of production-dependent flaws.
- Production-dependent flaws can be originated from the first melting process to the final formation process. Enclosures of solid particles or bubbles in molten mass are typical melting flaws and were determined in hollow glass fibers in chapters 6.8 and 6.9.1. Such imperfections remained in the glass and led to more defects in further production steps when being transported to the surface.
- Scars and scratches are healed in each further production step with applied heat but may remain from last hot production step.
- The effect of environmental conditions like air moisture after the final production step has to be counted as production-dependent defect as well. The covering of the juvenile surface by a coating during production step can exclude or reduce that effect wherefore the pressure resistance is increased (chapter 6.9.2).

## 7 Conclusions and Perspectives

### 7.1 Conclusions

The main objective of this thesis was to investigate and determine the influences on the resistance of hollow glass fibers against internal pressure load. Thereby the determined burst pressures were taken for the evaluation as the most important and meaningful property of the hollow glass fibers regarding the main objective. From the results the following conclusions can be drawn:

- The theoretical tensile strength of glass can be estimated as a tenth of the Young's modulus [5]. The practical tensile strength is decreased by a multitude by different influences but should follow the theoretical trend. Tests with hollow glass fibers made of four different glasses with varying mechanical properties showed complete different results. Finally, hollow borosilicate glass fibers exhibited the highest resistance against inner pressure while having the lowest Young's modulus. Therefore, no coherence of theoretical trend and practical pressure resistance was identifiable.
- Aging under non-loaded conditions led to different changes of the pressure resistance of hollow glass fibers. The investigation of four different glass materials aged under defined temperature conditions but varying air humidity led to slight deviations of pressure resistance of aged hollow fibers compared to new fibers. Hollow fibers made of borosilicate or aluminosilicate glass showed slight decrease in pressure resistance. On the contrary quartz and soda-lime glass fibers exhibited an increase in pressure resistance when being aged. Summarizing borosilicate fibers showed the smallest change of pressure resistance. It can be concluded that under non-loaded conditions no significant effect of aging by altering air moisture is influencing the pressure resistance of hollow glass fibers. Furthermore, it can be concluded that under given condition borosilicate showed the lowest effect on pressure resistance of all tested glasses.
- The exposure of borosilicate and quartz hollow glass fibers to defined air humidity and temperature conditions caused slight increase in the pressure resistance. Because of the higher measured burst pressure values it can be concluded that under given circumstances borosilicate glass fibers exhibit a higher pressure resistance than those made of quartz.



- The exposure of nitrogen on the glass can lead to an increase of the pressure resistance of hollow glass fibers. Cyclic and static load with nitrogen led to an increase of resistance against inner pressure compared to the initial pressure resistance of new hollow glass fibers. It can be concluded that nitrogen diffused in the material and led to increasing pressure resistance by filling imperfections in the glass structure. New glass fibers made of borosilicate or quartz glass featured higher initial burst pressure when being tested with hydrogen compared to those being tested with nitrogen. The exposure of hydrogen on the glass in cyclic or static loads led to the decrease of pressure resistance. In conclusion from the results of fibers tested with hydrogen it can be assumed that a decrease of pressure resistance eventuated due to the missing filling of imperfections. The size of hydrogen molecules is much smaller than this is nitrogen. The diffusion of the molecules in the glass material is much faster. The higher initial burst pressure as well as the initial increase of pressure resistance can be assumed as reason for that behavior. Due to the small size, the molecules will not remain in the glass network and permeates through the glass material, wherefore the increasing effect is reversed at further load. However, it is possible to encounter the decreasing effect of hydrogen on the pressure resistance by static load with nitrogen before being loaded with hydrogen.
- The pressure resistance of hollow glass fibers can be influenced by the dimension. Following the theoretical considerations the tensile strength of glass should be a constant value. Practical investigations with solid fibers showed a contrary behavior and an increasing tensile strength with decreasing diameter [7]. However, the decrease of wall thickness at constant inner diameter followed the theory of Barlow's formula [172] and led to decreased pressure resistance. Nevertheless, the tangential stress calculated with the formula showed increasing values. The simultaneous decrease of wall thickness and outer diameter at constant ratio of outer to inner diameter led to increased pressure resistance of hollow glass fibers. It can be concluded that the pressure resistance is heavily dependent on the dimension of the fiber. Furthermore, it can be concluded that Griffith's theory of increasing loadability with decreasing material thickness is also valid for hollow glass fibers. At fixed inner diameter the tangential stress increases with decreasing wall thickness although the pressure resistance is decreased.

- Test series with different borosilicate glass fibers of different chemical compositions showed a positive effect of high percentages of aluminum oxide. The pressure resistance was decreased by increasing slightly the amount of boron oxide and obvious reduction of aluminum oxide. A simultaneous increase of aluminum oxide and boron oxide led also to a decrease in pressure resistance. Aluminosilicate fibers from two different compositions were tested as well. The increase of aluminum oxide with coincident reduction of the amount of boron oxide led to the increase of pressure resistance. Compared to the test results of borosilicate fibers with highest pressure resistance even higher resistance against inner pressure load was detectable. It can be concluded that a high amount of aluminum oxide lead to higher pressure resistance of borosilicate as well as of aluminosilicate glass fibers when it is combined with a low amount of boron oxide.
- The effect of the combination of two glasses with different coefficient of thermal expansion (CTE) on the pressure resistance of hollow glass fibers is dependent on the compilation. An increase of pressure resistance can be reached when the glass with the low CTE is on the outside and the glass with the high CTE is on the inside. The opposite combination resulted in decreased burst pressures. In conclusion, the glass with the high CTE as inner layer of the combined fiber led to the pre-stressing of the outer surface of hollow glass fibers. The resulting compression stress counteracted the tensile stress acting at inner pressure load. Consequently, an increase of pressure resistance can be reached.
- An increasing effect on the pressure resistance can be reached by an effective surface coating. Coated hollow fibers made of quartz glass exhibited a constant high resistance against inner pressure load, wherefore a higher pressure resistance can be concluded as result of fewer defects on the fiber surface. The coating has to be applied on the hollow glass fiber directly after being drawn as part of the production process. A subsequent application by using the ALD-method did not lead to higher pressure resistance due to already existing surface defects. Concluding, an adequate healing or filling of such damages was not possible.
- Defects of different species and sizes were detectable not only under the light microscope but as well by using the SEM. The origin of single surface defects was defined by using EDS. Furthermore, the number of defects on single test samples varied significantly. Due to the big differences in size, origin and number

of defects a wide spread of burst pressures in the single test series occurred. It can be concluded that as adequate statistical method for the evaluation of the single test series and the comparison of them to each other the Weibull distribution was the suitable instrument.

- Material-dependent defects are caused by the irregular network of the material glass. Their appearance can be affected by the chemical composition and the amount of additives. Their influence on the pressure resistance is marginal compared to production-dependent defects.
- Production-dependent defects are most influencing parameters on the pressure resistance. Such defects can occur both as volume defects and as surface defects. Especially defects on the surface generate significant stress peaks under acting load. The avoidance of such flaws has to be first priority and can be reached by applied surface coatings.

The intention for this detailed study on the pressure resistance of hollow glass fibers at internal pressure load was to determine the general applicability of hollow glass fibers as gas storage system. According to the above mentioned examinations, it can be stated that the build-up of a storage system consisting of hollow glass fibers is possible in principle. However, critical remains the fact that any existent defect leads to decreasing pressure resistance regardless of whether being material-dependent or production-dependent.

The impact of defects on the pressure resistance can cause problems for continuous production of gas storage systems with consistent quality. An intended storage pressure of a high pressure gas storage system of  $p_{\text{storage}} = 70 \text{ MPa}$  and a not-standardized safety factor of 2 require a minimum burst pressure of  $p_{\text{min}} = 150 \text{ MPa}$  which are achievable only with well optimized production methods, quality checks and surface/system coatings. The avoidance of production-dependent defects of any origin thereby is important.

Furthermore, the gravimetric storage capacity of the hollow fibers has to be considered. Materials with gravimetric storage capacities of about  $\text{gsc} \approx 8 \text{ wt } \%$  already exist [33], [34]. A competitive value of  $\text{gsc} = 10 \text{ wt. } \%$  at intended storage pressure and safety factor requires a minimum free space of  $\text{FS} = 90\%$ . On the one hand, the production of single hollow fibers with 90% free space lead automatically to very thin fiber walls. The tests showed that an increase of pressure resistance can only be reached by the decrease of wall thickness and diameter. Fibers with such a big free space ratio have to be very thin

in diameter to withstand inner pressure. Furthermore, the following handling is therefore critical and further defects can be added easily. On the other hand, tested fibers with a free space ratio of even  $FS = 83\%$  (chapter 6.4.2) were actually not able to withstand inner pressures of  $p = 150 \text{ MPa}$  maybe due to above mentioned handling problems. Finally, single hollow fibers are not feasible for storing sufficient amounts of gas due to their small free volume. To be competitive to other gas storage systems thousands of hollow fibers needs to be bundled to realize gas storage in kg- or  $\text{m}^3$ -scale. The results of this thesis can be used for numerical simulations of the pressure resistance not only of single but also for bundled hollow fibers. The stress distribution inside the material and the bundle can be calculated and may lead to improvements of the pressure resistance especially of bundled structures.

Consequently, a competitive high pressure storage system for gas made of single hollow glass fibers is possible but feasibility has to be checked for each case individually. The safety of a storage system with pressure of  $p = 70 \text{ MPa}$  cannot be ensured due to the decreasing effect of any defect in the material on the pressure resistance. The avoidance of defects regardless of their origin thereby has to be ensured. Nevertheless, the systems can offer some unique advantages. Especially the bundling of thousands of hollow fibers can be realized such that the gas storage systems are free in shape and volume. Furthermore, the gas storage systems made of glass are not that susceptible like other systems with respect to hydrogen losses by permeation, degradation of materials by hydrogen corrosion or thermal resistance in refilling processes.

## 7.2 Perspectives

The conducted test series showed the potential of hollow glass fibers to withstand high internal pressures and therefore the possibility for an application as storage material for high pressure gas storage systems. Glass structures as storage material could be used in a wide field of applications. Therefore, further parameter and their influence on the pressure resistance should be considered and investigated in future.

Reaching competitive amounts of stored gas brings along the necessity of bundling a multitude of single hollow fibers to complex structures. However, the investigated influences on pressure resistance and corresponding results are valid for single hollow glass fibers. The effect of bundling thousands of them to complex structures may lead to different impacts on the behavior. The mechanical interaction is not regarded in carried out test series. Glass as amorphous material features elastic deformation under the influence of acting loads until the critical stress is reached. If the single fibers are

charged by inner pressure, expansion will occur until the collapse eventuates. Because of the fact, that single hollow fibers do not interact with any other objects, no outer action of force influences the expansion. In a bundle or structure of a multitude of fibers the individual hollow fibers will expand as well and influence each other.

The investigated effects of environmental influences especially the air humidity showed no significant impact under non-loaded conditions. Under loaded conditions another behavior could occur and influence the pressure resistance in different ways. Tests with single test samples made of quartz glass and being coated directly after drawing showed a massive improvement of pressure resistance. This exceeded the limit of used test apparatus which is actually at  $p_{\text{system}} = 150 \text{ MPa}$ . The influence on the pressure resistance of borosilicate fibers applied with a coating should be investigated as well as the effect of aging under loaded conditions.

The pre-treatment of hollow glass fibers with nitrogen showed a significant increasing impact on the pressure resistance. That effect is maybe to amplify by prolongation of time duration of pre-treatment. In that case, nitrogen can diffuse much deeper inside the glass material and the stiffening of chemical structures, especially in points of disconnection, can lead to even higher mechanical loadability. In this context the long-time effect of the pre-treatment should be investigated as well. Storing hydrogen for a longer time period in glass fibers or structures, reinforced by nitrogen pre-treatment, can lead to the diffusion of hydrogen inside of the glass as well. Due to the significant smaller size of hydrogen molecules, hydrogen can diffuse even deeper in the material as nitrogen or accumulate in defects of the chemical structures which are too small for the nitrogen molecules. Hence, the increasing effect of nitrogen can be reversed by the influence of hydrogen. With respect of the intension of the future use of hollow glass fibers in gas storage systems the effect of nitrogen should be investigated in detail. Different test series in prior project state showed a similar effect of argon [12]. Due to the larger size of the molecules, more precisely the atoms, argon is able to occupy large flaws in the chemical structures. Therefore, the increasing effect on the maximum stress is possibly amplified by using argon instead of nitrogen. Furthermore, the long-term stability during dynamic and static inner pressure load has to be investigated more extensive by increase the number of cycles and the extension of time duration.

The application of hollow glass fibers structures as high pressure storage system could be realized not only for hydrogen but also for other gases. Therefore, the permeability of glass against the different gases has to be investigated. The permeation of glass against hydrogen and helium was already investigated and published in different papers. The permeation of hydrogen and helium through glass is strongly dependent on the

---

temperature [60]. However, at room temperature and increased pressures of  $p = 10$  MPa no permeability of hydrogen but significant permeability against helium was detectable [61]. Summarized, the permeability against helium is much higher as these against hydrogen. The prospective examination should not only be in respect to the glass. Regarding the buildup of complex storage systems all used components have to feature a similar low permeability against gas and as well as a comparable long term durability.

## 8 List of references

- [1] J.-D. Wörner, J. Schneider, A. Fink: **Glasbau - Grundlagen, Berechnung, Konstruktion**, Springer Verlag, Berlin Heidelberg, (2001)
- [2] H. Müller-Simon: **Überblick über die praxisrelevanten Größen**, in *HVG - Fortbildungskurs 2009 - Physikalische und chemische Eigenschaften von Gläsern und Glasschmelzen - Werkstoffdaten für die Praxis*, Verlag der Deutschen Glastechnischen Gesellschaft, Offenbach/Main (2009), pp. 1-12,
- [3] H. Scholze: **Glass. Nature, Structure and Properties**, Springer Verlag, Berlin Heidelberg, (1994)
- [4] A. K. Varshneya: **Fundamentals of Inorganic Glasses**, 2<sup>nd</sup> Edition, Society of Glass Technology, (2006)
- [5] J. R. Varner: **Festigkeit und Bruchmechanik von Glas**, in *HVG-Fortbildungskurs 2001 - Festigkeit von Glas*; Verlag der Deutschen Glastechnischen Gesellschaft, 2. Auflage, Offenbach/Main (2003), pp. 25-38
- [6] E. Wagner: **Glasschäden - Oberflächenbeschädigungen Glasbrüche in Theorie und Praxis**, Hofmann Verlag, Fraunhofer IRB Verlag, 3. Überarbeitete Auflage, (2008)
- [7] A.A. Griffith: **The Phenomena of Rupture and Flow in Solids**, *Philosophical Transactions of the Royal Society of London, Series A, Containing Papers of a Mathematical or Physical Character* 221 (1921), pp. 163-198
- [8] M. Rexer: **Festigkeit gespannter Glasstäbe**, *Zeitung für Technische Physik* 20 (1939), pp. 4-13
- [9] K. Holtappels, M. Beckmann-Kluge, et al: **Hydrogen storage in glass capillary arrays for portable and mobile systems**, in *Proceedings of the 3rd International Conference on Hydrogen Safety (ICHS)*, Ajaccio, France, (2009), paper 242
- [10] M. Gebauer: **Untersuchung der Druckfestigkeit von Kapillaren verschiedener Materialien**, Technische Fachhochschule Berlin, (2009)

- 
- [11] D. Eliezer, K. Holtappels, M. Beckmann-Kluge: **An Innovative Technology for Hydrogen Storage in Portable and Mobile Systems**; in *Proceedings of the World Hydrogen Energy Conference 2010 (WHEC)*, Essen; Germany, (2010), pp. 33-36
- [12] C. Gröschl: **Steigerung der Druckfestigkeit von Glasstrukturen**, Master Thesis; Free University Berlin; 2010
- [13] L. Schlapbach, A. Züttel: **Hydrogen-storage materials for mobile applications**, *Nature* 414 (2001), pp. 353-358, DOI: 10.1038/35104634
- [14] R. Lide: **CRC Handbook of Chemistry and Physics**, CRC Press, 90<sup>th</sup> Edition, (2010)
- [15] Paetec, Gesellschaft für Bildung und Technik mbH: **Formeln und Tabellen für die Sekundarstufen I und II**, 6th revised edition, Paetec, Ges. für Bildung und Technik; Berlin, (1996)
- [16] M. Müller: **Die Entwicklung von Energieversorgungssystemen mit PEM-Brennstoffzellen**, *gwf Gas Erdgas* 144 (2003), pp. 411-415
- [17] G. W. Mair: **Prüfung/wiederkehrende Prüfung von Composite Druckgefäßen**, in: **6. Fachgespräch Druckgefäße**, Berlin, (2010)
- [18] C. Red: **The outlook for composite pressure vessels**, *Composites technologies* 15 (2009), pp. 32-36
- [19] Metal Mate Corp.: **High Pressure Composite Cylinder**, *Technical Datasheet and Product Portfolio*, Metal Mate Company Limited, (2008)
- [20] J. Garcke, P. Treffinger, L. Jörissen: **Wasserstoffspeicherung und Verkehr**, in *ForschungsVerbund Sonnenenergie - Themen 2001 - Integration Erneuerbarer Energien in Versorgungsstrukturen* (2001), pp. 100-113
- [21] D. O. Berstad, J.H. Stang, et al: **Comparison criteria for large-scale hydrogen liquefaction processes**, *International Journal of Hydrogen Energy* 34 (2009), pp. 1560-1568, DOI: 10.1016/j.ijhydene.2008.11.058
- [22] P. Di Profio, S. Arca: **Comparison of hydrogen hydrates with existing hydrogen storage technologies: Energetic and economic evaluations**, *International Journal of Hydrogen Energy* 34 (2009), pp. 9173-9180, DOI: 10.1016/j.ijhydene.2009.09.056



- [23] D. K. Ross: **Hydrogen storage: The major technological barrier to the development of hydrogen fuel cell cars**, *Vacuum - Surface Engineering, Surface Instrumentation & Vacuum Technology* 80 (2006), pp. 1084-1089, DOI: 10.1016/j.vacuum.2006.03.030
- [24] J. Wolf, Linde Gas AG: **Liquid Hydrogen Tank & Filling Systems for Vehicles**; in **ForschungsVerbund Sonnenenergie - Workshop Wasserstoffspeicherung**, Günzburg, (2001), pp. 6-9
- [25] U.S. Department of Energy: **Technical Assessment: Cryo-Compressed Hydrogen Storage for Vehicle Applications**, U.S. Department of Energy Hydrogen Program, revised edition (2008)
- [26] M. Kampitsch, BMW Group: **BMW – Cryocompressed Hydrogen Refueling**, in: **WHEC World Hydrogen and Energy Conference 2012**, Toronto, Canada, (2012)
- [27] R.K. Ahluwalia, T.Q. Hua, J.K. Peng, R. Kumar: **System Level Analysis of Hydrogen Storage Options**, in: **2010 DOE Hydrogen Program Review**, Washington, DC, (2010)
- [28] I.P. Jain, L. Chhagan, A. Jain: **Hydrogen storage in Mg: A most promising material**, *International Journal of Hydrogen Energy* 35 (2010), pp. 5133-5144, DOI: 10.1016/j.ijhydene.2009.08.088
- [29] A. Otto: **Wasserstoffspeicherung in Niedertemperatur-Metallhydriden**, in: **ForschungsVerbund Sonnenenergie - Workshop Wasserstoffspeicherung**, Günzburg (2001), pp. 20-26
- [30] V. Güther, A. Otto: **Recent developments in hydrogen storage applications based on metal hydrides**, *Journal of Alloys and Compounds* 293-295 (1999), pp. 889-892, DOI: 10.1016/S0925-8388(99)00385-0
- [31] B. Sakintuna, R. Lamari-Darrim, M. Hirscher: **Metal hydride materials for solid hydrogen storage: A review**, *International Journal of Hydrogen Energy* 32 (2007), pp. 1121-1140, DOI: 10.1016/j.ijhydene.2006.11.022
- [32] O. Friedrichs, T. Klassen, J.C. Sanchez-Lopez, R. Bormann, A. Fernandez: **Hydrogen sorption improvement of nanocrystalline  $MgH_2$  by  $Nb_2O_5$  nanoparticles**, *Scripta Materialia* 54 (2006), pp. 1293-1297, DOI: 10.1016/j.scriptamat.2005.12.011

- [33] T. Klassen, W. Oelerich, R. Bormann: **Nanocrystalline Mg-based Hydrides: Hydrogen Storage for the Zero-Emission Vehicle**, *Materials Science Forum* 360-362 (2001), pp. 603-608
- [34] P.-A. Huhn, M. Dornheim, T. Klassen, R. Bormann: **Thermal stability of nanocrystalline magnesium for hydrogen storage**, *Journal of Alloys and Compounds* 404-406 (2005), pp. 499-502, DOI: 10.1016/j.jallcom.2004.10.087
- [35] G. Barkhordarian, T. Klassen, R. Bormann: **Fast hydrogen sorption kinetics of nanocrystalline Mg using Nb<sub>2</sub>O<sub>5</sub> as catalyst**, *Scripta Materialia* 49 (2003), pp. 213-217, DOI: 10.1016/S1359-6462(03)00259-8
- [36] R. H. Crabtree: **Hydrogen storage in liquid organic heterocycles**, *Energy and Environmental Science* 1 (2008), pp. 134-138, DOI: 10.1039/B805644G
- [37] C. Morris: **Brennstoffzelle ist nicht gleich Brennstoffzelle**, *Telepolis*, online magazine (2004), <http://www.heise.de/tp/artikel/18/18767/1.html>
- [38] M. Meister, Siemens AG: **Security for use in power generation plant, has hydrogen-absorbing substance provided in container that is permanently connected to component, where permanent connection is made by absorbing and storing hydrogen in material**, German Patent DE102012220106 A1, (2014)
- [39] J.L.C. Rowsell, O.M. Yaghi: **Metal-organic frameworks: a new class of porous materials**, *Microporous and Mesoporous Materials* 73 (2004), pp. 3-14, DOI: 10.1016/j.micromeso.2004.03.034
- [40] M.P. Suh, et al: **Hydrogen Storage in Metal-Organic Frameworks**, *Chemical Reviews* 112 (2011), pp. 782-835
- [41] L.J. Murray, M. Dinca, J.R. Long: **Hydrogen storage in metal-organic frameworks**, *Chemical Society Reviews* 38 (2009), pp. 1294-1314, DOI: 10.1039/B802256A
- [42] Y. Yan, et al: **Exceptionally high H<sub>2</sub> storage by a metal-organic polyhedral framework**, *Chemical Communications* 9 (2009), pp. 1025-1027, DOI: 10.1039/B900013E
- [43] J.L.C. Rowsell, O.M. Yaghi: **Strategien für die Wasserstoffspeicherung in metall-organischen Kompositgerüsten**, *Angewandte Chemie* 117 (2005), pp. 4748-4758, DOI: 10.1002/ange.200462786

- [44] N.L. Rosi, J. Eckert, M. Eddaoudi, D.T. Vodak, J. Kim, M. O'Keeffe, O.M. Yaghi: **Hydrogen Storage in Microporous Metal-Organic Frameworks**, *Science* 300 (2003), pp. 1127-1129, DOI: 10.1126/science.1083440
- [45] M.U. Niemann, et al: **Nanomaterials for Hydrogen Storage Applications: A Review**, *Journal of Nanomaterials* 2008 (2008), pp. 1-9, DOI: 10.1155/2008/950967
- [46] A.C. Dillon, M.J. Heben: **Hydrogen storage using carbon adsorbents: past, present and future**, *Applied Physics A - Materials Science and Processing* 72 (2001), pp. 133-142, DOI: 10.1007/s003390100788
- [47] L. Zhou, Y. Zhou, Y. Sun: **A comparative study of hydrogen adsorption on superactivated carbon versus carbon nanotubes**, *International Journal of Hydrogen Energy* 29 (2004), pp. 475-479, DOI: 10.1016/S0360-3199(03)00092-2
- [48] S.J. Gregg, K.S.W. Sing: **Adsorption, Surface Area and Porosity**, 2<sup>nd</sup> Edition, Academic Press, London, (1982)
- [49] A. Anson, M.A. Callejas, A.M. Benito, W.K. Maser, M.T. Izquierdo, B. Rubio, J. Jagiello, M. Thommes, J.B. Parra, M.T. Martinez: **Hydrogen adsorption studies on single wall carbon nanotubes**, *Carbon* 42 (2004), pp. 1243-1248, DOI: 10.1016/j.carbon.2004.01.038
- [50] C. Liu, Y.Y. Fan, M. Liu, H.T. Cong, H.M. Cheng, M.S. Dresselhaus: **Hydrogen storage in single-walled carbon nanotubes at room temperature**, *Science* 286 (1999), pp. 1127-1129, DOI: 10.1126/science.286.5442.1127
- [51] M. Herr, J. A. Lercher: **Hydrogen Storage in Microspheres - Final Report**, ET Energie Technologie GmbH: ESA Contract No. 16292/02/NL/PA, (2003)
- [52] J.E. Shelby, M. Hall: **A Radically New Method for Hydrogen Storage in Hollow Glass Microspheres**, in *DOE U.S. Department of Energy Hydrogen Program*, Progress Report, (2004)
- [53] G.G. Wicks, L.K. Heung, R.F. Schumacher: **Microspheres and Microworlds**, *American Ceramic Society Bulletin* 87, (2008), pp. 23-28
- [54] R.J. Teitel: **Microcavity Hydrogen Storage - Final Progress Report**, Brookhaven National Laboratory, Upton, New York, (1981)

- [55] D.K. Kohli, R.K. Kahrdekr, R. Singh, P.K. Gupta: **Glass micro-container based hydrogen storage scheme**, *International Journal of Hydrogen Energy* 33 (2008), pp. 417-422, DOI: 10.1016/j.ijhydene.2007.07.044
- [56] G.D. Rambach: **Hydrogen Transport and Storage in engineered Glass Microspheres**, Sandia National Laboratory, Livermore, (1994)
- [57] J.E. Shelby: **Glass Microspheres for Hydrogen Storage**, in **DOE U.S. Department of Energy Hydrogen Program, 2008 Annual Progress Report**, DOE US Department of Energy, (2008)
- [58] V.V. Budov: **Physicochemical processes in producing hollow glass microspheres**, *Glass and Ceramics* 47 (1990), pp. 9-10, DOI: 10.1007/BF01196172
- [59] M.L. Schmitt, J.E. Shelby, M.M. Hall: **Preparation of hollow glass microspheres from sol-gel derived glass for application in hydrogen gas storage**, *Journal of Non-Crystalline Solids* 352 (2006), pp. 626-631, DOI: 10.1016/j.jnoncrysol.2005.11.057
- [60] G.A. Williams, J.B. Ferguson: **The Diffusion of Hydrogen and Helium through Silica Glass and other Glasses**, *Journal of the American Ceramic Society* 44 (1922), pp. 2160-2167, DOI: 10.1021/ja01431a010
- [61] H.M. Elsey: **The Diffusion of Helium and Hydrogen through Quartz Glass at Room Temperature**, *Journal of the American Ceramic Society* 48 (1926), pp. 1600-1601, DOI: 10.1021/ja01417a501
- [62] L. Shang, I. Ming Chou, W. Lu, R.C. Burruss, Y. Zhang: **Determination of diffusion coefficients of hydrogen in fused silica between 296 and 523 K by Raman spectroscopy and application of fused silica capillaries in studying redox reactions**, *Geochimica et Cosmochimica Acta* 73 (2009), pp. 5435-5443, DOI: 10.1016/j.gca.2009.06.001
- [63] N. Kurita, N. Fukatsu, H. Otsuka, T. Ohashi: **Measurements of hydrogen permeation through fused silica and borosilicate glass by electrochemical pumping using oxide protonic conductor**, *Solid State Ionics* 146 (2002), pp. 101-111, DOI: 10.1016/S0167-2738(01)00989-4
- [64] J.E. Shelby: **Handbook of Gas Diffusion in Solids and Melts**, ASM International, 1996

- [65] J.L. Barton, M. Morain: **Hydrogen Diffusion in Silicate Glass**, *Journal of Non-Crystalline Solids* 3 (1970), pp. 115-126
- [66] S. Shetty, M. Hall: **Facile production of optically active hollow glass microspheres for photo-induced outgassing of stored hydrogen**, *International Journal of Hydrogen Energy* 36 (2011), pp. 9694-9701, DOI: 10.1016/j.ijhydene.2011.04.195
- [67] D.B. Rapp, J. E. Shelby: **Photo-induced hydrogen outgassing of glass**, *Journal of Non-Crystalline Solids* 349 (2004), pp. 254-259, DOI: 10.1016/j.jnoncrysol.2004.08.151
- [68] R.T. Tsugawa, I. Moen, P.E. Roberts, P.C. Souers: **Permeation of helium and hydrogen from glass-microsphere laser targets**, *Journal of Applied Physics* 47 (1976), pp. 1987-1993, DOI: 10.1063/1.322924
- [69] N.K. Zhevago, V.I. Glebov: **Hydrogen storage in capillary arrays**, *Energy Conversion and Management* 48 (2007), pp. 1554-1559, DOI: 10.1016/j.enconman.2006.11.017
- [70] N.K. Zhevago, E.I. Denisov, V.I. Glebov: **Experimental investigation of hydrogen storage in capillary arrays**, *International Journal of Hydrogen Energy* 35 (2010), pp. 169-175, DOI: 10.1016/j.ijhydene.2009.10.011
- [71] K. Holtappels, M. Beckmann-Kluge, M. Gebauer, D. Eliezer: **Pressure Resistance of Glass Capillaries for Hydrogen Storage**, *Materials Testing* 53 (2011), pp. 14-18, DOI: 10.3139/120.110195
- [72] C. Gröschl, R. Meyer, K. Holtappels, M. Beckmann-Kluge, D. Eliezer: **A New Technology for Hydrogen Safety: Glass Structures as a Storage System**, in *H2Expo*, Hamburg, Germany, (2011)
- [73] R. Meyer: **A New Technology for Hydrogen Safety: Glass Structures as a Storage System**, in *Proceedings of the 4th International Conference on Hydrogen Safety (ICHS)*; San Francisco, CA, USA, (2011)
- [74] N.K. Zhevago, A.F. Chabak, E.I. Denisov, V.I. Glebov, S.V. Korobtsev: **Storage of cryo-compressed hydrogen in flexible glass capillaries**; *International Journal of Hydrogen* 38 (2013), pp. 6694-6703, DOI: 10.1016/j.ijhydene.2013.03.107

- 
- [75] DIN Deutsches Institut für Normung e.V.: **DIN 1259 - 1: Glas - Teil 1: Begriffe für Glasarten und Glasgruppen**, Beuth Verlag GmbH, Berlin, (2001)
- [76] W.H. Zachariasen: The atomic arrangement in glass, *Journal of the American Chemical Society* 54 (1932), pp. 3841-3851, DOI: 10.1021/ja01349a006
- [77] [www.benbest.com/cryonics/lessons.html](http://www.benbest.com/cryonics/lessons.html); January 2013
- [78] K.-Ch. Thienel: **Werkstoffe des Bauwesens - Glas**, Universität der Bundeswehr München, (2008)
- [79] C. Bindel, P. Pfeifer: **Sachstruktur zum Thema Glas**, *Naturwissenschaft im Unterricht. Chemie* 44 (1996), No. 35, pp. 4-8
- [80] DIN Deutsches Institut für Normung e.V.: **DIN ISO 7884-1 - Viskosität und viskosimetrische Festpunkte, Teil 1: Grundlagen für die Bestimmung der Viskosität und der viskosimetrischen Festpunkte (ISO 7884-1 : 1987)**, Beuth Verlag, Berlin, (1998)
- [81] DIN Deutsches Institut für Normung e.V.: **DIN ISO 7884-2 - Viskosität und viskosimetrische Festpunkte, Teil 2: Bestimmung der Viskosität mit Rotationsviskosimetern (ISO 7884-2 : 1987)**, Beuth Verlag, Berlin, (1998)
- [82] DIN Deutsches Institut für Normung e.V.: **DIN ISO 7884-3 - Viskosität und viskosimetrische Festpunkte, Teil 3: Bestimmung der Viskosität mit dem Fadenzieh-Viskosimeter (ISO 7884-3 : 1987)**, Beuth Verlag, Berlin, (1998)
- [83] DIN Deutsches Institut für Normung e.V.: **DIN ISO 7884-4 - Viskosität und viskosimetrische Festpunkte, Teil 4: Bestimmung der Viskosität durch Balkenbiegen (ISO 7884-4 : 1987)**, Beuth Verlag, Berlin, (1998)
- [84] DIN Deutsches Institut für Normung e.V.: **DIN ISO 7884-6 - Viskosität und viskosimetrische Festpunkte, Teil 6: Bestimmung der Erweichungstemperatur (ISO 7884-6 : 1987)**, Beuth Verlag, Berlin, (1998)
- [85] DIN Deutsches Institut für Normung e.V.: **DIN ISO 7884-7 - Viskosität und viskosimetrische Festpunkte, Teil 7: Bestimmung der oberen Kühltemperatur und der unteren Kühltemperatur durch Balkenbiegen (ISO 7884-7 : 1987)**, Beuth Verlag, Berlin, (1998)

- 
- [86] DIN Deutsches Institut für Normung e.V.: ***DIN ISO 7884-8 - Viskosität und viskosimetrische Festpunkte, Teil 8: Bestimmung der (dilatometrischen) Transformationstemperatur (ISO 7884-8 : 1987)***, Beuth Verlag, Berlin, (1998)
- [87] DIN Deutsches Institut für Normung e.V.: ***DIN EN 1748-1 - Glas im Bauwesen - Spezielle Basiserzeugnisse - Borosilicatgläser - Teil 1-1: Definitionen und allgemeine physikalische und mechanische Eigenschaften***, Beuth Verlag, Berlin, (2004)
- [88] Saint-Gobain Vetrotex; "***E, R and D glass properties - Technical data sheet***"; product information, Saint-Gobain Vetrotex Deutschland GmbH, Herzogenrath, Germany, (2002)
- [89] I. Kitaigorodski: ***Technologie des Glases***, R. Oldenbourg Verlag, München, (1957)
- [90] E. Danner: ***Process of Drawing Molten Material In Cylindrical Form, US Patent 1,218,598***, patented Mar. 06, (1917)
- [91] E. Danner: ***Tubular Glass Manufacturing Apparatus, US Patent 2,502,312***, patented Mar. 28, (1950)
- [92] A.P. Sivko: ***The Production of Glass Tubes Using the Vello Method***, *Glass and Ceramics* 33 (1976), pp. 728-730, DOI: 10.1007/BF00700491
- [93] R. Hüther: ***Kleben von Glas***, in *HVG Fortbildungskurs 1995 - Fügen von Glas*, Verlag der Deutschen Glastechnischen Gesellschaft, (1995), pp. 93-143
- [94] E. Rädlein: ***Reale Glasoberflächen und deren Charakterisierung***, in *HVG-Fortbildungskurs 2003 - Oberflächenveredlung von Glas*; Verlag der Deutschen Glastechnischen Gesellschaft, (2003), pp. 1-36
- [95] A. Peters: ***Reaktionen wässriger Lösungen mit Glasoberflächen***, in *HVG-Fortbildungskurs 1989 - Veränderung und Veredelung der Glasoberflächen*; 2. Auflage; Verlag der Deutschen Glastechnischen Gesellschaft (1989), pp. I/1-I/38
- [96] C. Scheffler, T. Förster, E. Mäder: ***Beschleunigte Alterung von Glasfasern in alkalischen Lösungen: Einflüsse auf die mechanische Eigenschaften***; in *Proceedings of the 4th Colloquium on Textile Reinforced Structures (CTRS4)*, (2009), pp. 63-74

- [97] H. Müller-Simon: **Transport und Lagerung in der Behälterglasindustrie**, in *HVG Fortbildungskurs 2006 - Transport und Lagerung in der Glasindustrie*; Verlag der Deutschen Glastechnischen Gesellschaft, (2006), pp. 83-94
- [98] H. Salmang: **Die Glasfabrikation - Physikalische und chemische Grundlagen**, Springer Verlag; Berlin, Göttingen, Heidelberg, (1957)
- [99] M. D. Lund: **Tensile Strength of Glass Fibers**, Aalborg University, Section of Chemistry, PhD Dissertation (2010)
- [100] DIN Deutsches Institut für Normung e.V.: **DIN EN ISO 1288-1 - Glas im Bauwesen - Bestimmung der Biegefestigkeit von Glas - Teil 1: Grundlagen der Glasprüfung (ISO/DIS 1288-1:2007) - Entwurf**, Beuth Verlag, Berlin, (2007)
- [101] G. Geiss: **Einfluss von Tieftemperatur und Wasserstoff auf das Versagensverhalten von Glasfaser-Verbundwerkstoffen unter statischer und zyklischer Belastung**, Forschungszentrum Karlsruhe GmbH, Karlsruhe, (2001)
- [102] DIN Deutsches Institut für Normung e.V.: **DIN ISO 3585 Borosilicatglas 3.3 Eigenschaften**, Beuth Verlag GmbH, Berlin, (1999)
- [103] AGY - strength in materials, Aiken, SC, USA: **Advanced Materials - Solution for Demanding Application (S-2 Glass Fiber - The high Performance System Solution)**, product information, (2004)
- [104] M. J. Matthewson, C.R. Kurkjian, S.T. Gulati: **Strength Measurement of Optical Fibers by Bending**, *Journal of the American Ceramic Society* 69 (1986), pp. 815-821, DOI: 10.1111/j.1151-2916.1986.tb07366.x
- [105] A. Smekal: **Bruchtheorie spröder Körper**, *Zeitschrift für Physik* 103 (1936), pp. 495-525, DOI: 10.1007/BF01333174
- [106] G.M. Bartenev: **The structure and strength of glass fibers**, *Journal of Non-Crystalline Solids* 1 (1968), pp. 69-90
- [107] A.F. Prebus, J.M. Michener: **Electron microscope investigation of glass**, *Industrial & Engineering Chemistry* 46 (1954), pp. 147-153, DOI: 10.1021/ie50529a046



- [108] M. Lund, Y. Yue: **Impact of Drawing Stress on the Tensile Strength of Oxide Glass Fibers**, *Journal of the American Ceramic Society* 93 (2010), pp. 3236-3243, DOI: 10.1111/j.1551-2916.2010.03879.x
- [109] W.H. Otto: **Relationship of tensile strength of glass fibers to diameter**, *Journal of the American Ceramic Society* 38 (1955), pp. 122-125, DOI: 10.1111/j.1151-2916.1955.tb14588.x
- [110] H. Stockhorst, R. Bruckner: **Structure sensitive measurements on E-glass fibers**, *Journal of Non-Crystalline Solids* 49 (1982), pp. 471-484
- [111] W.H. Otto, F.W. Preston: **Evidence against oriented structure in glass fibers**, *Journal of the Society of Glass Technology* 34 (1950), pp. 3-6
- [112] N. M. Cameron: **Relation between melt treatment and glass fiber strength**, *Journal of the American Ceramic Society* 49 (1966), pp. 144-148, DOI: 10.1111/j.1151-2916.1966.tb15392.x
- [113] L. Merker, H.P. Williams, W. Vogel, F. Krämer: **HVG Fortbildungskurs 1991 - Glastechnische Fabrikationsfehler**, Hüttentechnische Vereinigung der Deutschen Glasindustrie, 2.Auflage; (1992)
- [114] H. Jebesen-Marwedel: **Glastechnische Fabrikationsfehler**, 2nd Edition, Springer Verlag, Berlin, Göttingen, Heidelberg, (1959)
- [115] R.J. Hand: **Hidden Defects: Griffith's Flaws in Silicate Glasses**, in *Proceedings of the 12th Biennial Conference on Fracture - EFC 12*, Sheffield, U.K. (1998), pp. 461-466
- [116] H.H. Dunken: **Physikalische Chemie der Glasoberfläche**, VEB Deutscher Verlag für Grundstoffindustrie, Leipzig, (1981)
- [117] J. I. Goldstein, D.E. Newbury, P. Echlin, D.C. Joy, C. Fiori, E. Lifshin: **Scanning electron microscopy and X-ray microanalysis**, Plenum Press, 3<sup>rd</sup> edition, New York, (2003)
- [118] E. Heindl: **Rasterkraftmikroskopie (atomic force microscopy AFM)**, Universität Regensburg, (2003)
- [119] B. K. Agarwal: **X-ray spectroscopy**, 2<sup>nd</sup> edition, Springer Verlag, Berlin, (1991)

- [120] A. Ul-Hamid, H.M. Tawancy, A.I. Mohammed, S.S. Al-Jaroudi, N.M. Abbas: **Cyclic oxidation behavior of a Ni-Mo-Cr alloy at 800 °C**, *Anti-Corrosion Methods and Materials* 51 (2004), pp. 339-347, DOI: 10.1108/00035590410554900
- [121] P. Dobrinski, G. Krakau, A. Vogel: **Physik für Ingenieure**, 7<sup>th</sup> Edition; B. G. Teubner, Stuttgart, (1988)
- [122] E. Hornbogen, G. Eggerle, E. Werner: **Werkstoffe - Aufbau und Eigenschaften von Keramik-, Metall-, Polymer- und Verbundwerkstoffen**, 9<sup>th</sup> Edition, Springer Verlag, Berlin Heidelberg, (2008)
- [123] E. Hornbogen, H. Warlimont: **Metalle - Struktur und Eigenschaften der Metalle und Legierungen**, 5<sup>th</sup> Edition, Springer Verlag, Berlin Heidelberg, (2006)
- [124] L. Issler, H. Ruoß, P. Häfele: **Festigkeitslehre - Grundlagen**, 2<sup>nd</sup> Edition, Springer Verlag, Berlin Heidelberg, (2003)
- [125] D. Eliezer, Th. Böllinghaus, C.E. Cross: **The relation between microstructure, corrosion and hydrogen behavior of welded light alloys**, in: **4th International Workshop CRACKING PHENOMENA IN WELDS**, Berlin, Germany, (2014)
- [126] M. Winning: **Korngrenzen auf Wanderschaft**, *Physik Journal* 3 (2004), pp. 77-81
- [127] A. Barnoush: **Hydrogen embrittlement, revisited by in situ electrochemical nanoindentation**, Universität des Saarlandes, Saarbrücken, Germany, (2007)
- [128] Th. Böllinghaus: **Mechanisms of Stress Corrosion Cracking in Welds**, in: **4th International Workshop CRACKING PHENOMENA IN WELDS**, Berlin, Germany, (2014)
- [129] R.H. Doremus: **Glass Science**, 2<sup>nd</sup> Edition, John Willey & Sons Inc., New York, (1994)
- [130] W. Vogel: **Glass Chemistry**, 2<sup>nd</sup> revised Edition, Springer Verlag, Berlin Heidelberg, (1994)
- [131] [www.thiele-glas.de](http://www.thiele-glas.de); downloaded on 15-03-2013
- [132] DIN Deutsches Institut für Normung e.V.: **DIN ISO 7991 - Glas - Bestimmung des mittleren thermischen Längenausdehnungskoeffizienten (ISO 7991 : 1987)**, Beuth Verlag, Berlin, (1998)

- [133] H.G. Pfänder: **Schott guide to glass**, Chapman and Hall, London, (1996)
- [134] S.L. Gao, E. Mäder, R. Plonka: **Nanocomposite coatings for healing surface defects of glass fibers and improving interfacial adhesion**, *Composites Science and Technologies* 68 (2008), pp. 2892-2901, DOI: 10.1016/j.compscitech.2007.10.009
- [135] Sandia National Laboratories: **Coatings on Glass - Technology Roadmap Workshop**, Sandia National Laboratories, Livermore, California, USA, (2000)
- [136] O. Jylhä: **Atomic layer deposition to strengthen glass**, *GLASS WORLDWIDE* (2010), pp. 104-105
- [137] O. Jylhä: **Improved cracking resistance by thin film ALD coatings**, in *Proceedings of GLASS PERFORMANCE DAYS 2011*, (2011), pp. 144-146
- [138] DIN Deutsches Institut für Normung e.V.: **DIN EN 61649 - Weibull-Analyse (IEC 61649:2008)**, Beuth Verlag, Berlin, (2009)
- [139] H. Wilker: **Weibull-Statistik in der Praxis**, zweite, vollständig überarbeitete Auflage, Books on Demand GmbH, Norderstedt, (2010)
- [140] W. Weibull: **A statistical theory on the strength of materials**, Ingeniorsventenskapsakademiens Handlingar, (1939)
- [141] W. Weibull: **A statistical distribution function of wide applicability**; *Journal of Applied Mechanics* 18 (1951), pp. 293-297
- [142] B. Bergman: **On the estimation of the Weibull modulus**, *Journal of Material Science Letters* 3 (1984), pp. 689-692, DOI: 10.1007/BF00719924
- [143] DIN Deutsches Institut für Normung e.V.: **DIN-Taschenbuch 239: Verpackung - Terminologie, Prüfung, Maßordnung, Markierung, Kennzeichnung, Lieferbedingungen**, Beuth Verlag, Berlin, (1991)
- [144] DIN Deutsches Institut für Normung e.V.: **DIN EN ISO 7458 - Behältnisse aus Glas - Innendruckfestigkeit - Prüfverfahren (ISO 7458:2004)**, Beuth Verlag, Berlin, (2004)
- [145] UHU *data sheet*: **UHU PLUS ENDFEST 300**, Suter-Kunststoffe AG
- [146] Deutsche Edelstahlwerke: **data sheet stainless steel 1.4571 (X6CrNiMoTi17-12-2)**, Deutsche Edelstahlwerke GmbH, Witten, Germany, (2008)

- [147] Hilgenberg GmbH: **data sheet 0100, sodalime glass**, Hilgenberg GmbH, Malsfeld, (2009)
- [148] Hilgenberg GmbH: **data sheet 0500, borosilicate glass 3.3**, Hilgenberg GmbH, Malsfeld; (2009)
- [149] Hilgenberg GmbH: **data sheet 0620, quartz glass**, Hilgenberg GmbH, Malsfeld; (2009)
- [150] Hilgenberg GmbH: **data sheet 0812, aluminosilicate glass**, Hilgenberg GmbH, Malsfeld; (2009)
- [151] Incom: **data sheet, borosilicate glass C5**, Incom, Inc., (2011)
- [152] G. Holzmann, H. Meyer, G. Schumpich: **Technische Mechanik Festigkeitslehre**, 10<sup>th</sup> Edition, Vieweg & Teubner Verlag, Wiesbaden, (2012)
- [153] Schott AG: **technical data sheet Schott glass 8252**, Schott AG, Mainz, (2014)
- [154] Schott AG: **DURAN - technical data sheet**, Schott AG, Mainz, (2003)
- [155] I. Müller: **Grundzüge der Thermodynamik - mit historischen Anmerkungen**, 3<sup>rd</sup> Edition, Springer Verlag, Berlin Heidelberg, (2001)
- [156] H.D. Baehr, S. Kabelac: **Thermodynamik**, 13<sup>th</sup> Edition, Springer Verlag, Berlin Heidelberg, (2006)
- [157] CS Instruments: **Feuchtereferenzzellen, datasheet**, CS Instruments GmbH, Harrislee, Germany, (2004)
- [158] V.M. Sglavo, M. Gadotti, T. Micheletti: **Cyclic loading behavior of soda-lime silicate glass using indentation cracks**, *Fatigue and Fracture of Engineering Materials and Structures* 20 (1997), pp. 1225-1234, DOI: 10.1111/j.1460-2695.1997.tb00326.x
- [159] M. Ciccotti: **Stress corrosion mechanisms in silicate glasses**, *Journal of Physics D: Applied Physics* 42 (2009), pp. 1-18, DOI: 10.1088/0022-3727/42/21/214006
- [160] T.A. Michalske, S.W. Freiman: **A molecular mechanism for stress corrosion in vitreous silica**; *Journal of the American Ceramic Society* 66 (1983), pp. 284-288, DOI: 10.1111/j.1151-2916.1983.tb15715.x

- [161] E. Menthe, A. Bulak, J. Olfe, A. Zimmermann, K.-T. Rie: **Improvement of the mechanical properties of austenitic stainless steel after plasma nitriding**, *Surface and Coatings Technology* 133-134 (2000), pp. 259-263, DOI: 10.1016/S0257-8972(00)00930-0
- [162] B. Larisch, U. Brusky, H.-J. Spies: **Plasma nitriding of stainless steels at low temperatures**, *Surface and Coatings Technology* 116-119 (1999), pp. 205-211, DOI: 10.1016/S0257-8972(99)00084-5
- [163] K. Takeda, K. Mitsui, H. Tobushi, N. Levintant-Zayonts, S. Kucharski: **Influence of nitrogen ion implantation on deformation and fatigue of TiNi shape memory alloy wire**, *Archives of Mechanics* 65 (2013), pp. 391-405
- [164] Y. Tao, L. Lin, B. Wang: **Study of the surface hardening of photochromic glass by nitrogen ion implantation**, *Journal of Non-Crystalline Solids* 112 (1989), pp. 404-407
- [165] H. Würstner: **Über Diffusion und Absorption von Wasserstoff in Quarzglas**, *Annalen der Physik* 351 (1915), pp. 1095-1129, DOI: 10.1002/andp.19153510805
- [166] D. Eliezer, Y. Nissim, Th. Boellinghaus, Th. Kannengiesser: **Effects of shielding with various hydrogen-argon mixtures on supermartensitic stainless steel TIG welds**, *Materials Testing* 52 (2010), pp. 306-315, DOI: 10.3139/120.110135
- [167] J.E. Del Bene, K. Runge, R.J. Bartlett: **A quantum chemical mechanism for the water-initiated decomposition of silica**, *Computational Materials Science* 27 (2003), pp. 102-108, DOI: 10.1016/S0927-0256(02)00432-9
- [168] S.M. Wiederhorn: **Influence of water vapor on crack propagation in soda-lime glass**, *Journal of the American Ceramic Society* 50 (1967), pp. 407-414, DOI: 10.1111/j.1151-2916.1967.tb15145.x
- [169] S.M. Wiederhorn: **Moisture assisted crack growth in ceramics**, *The International Journal of Fracture Mechanics* 4 (1968), pp. 171-177, DOI: 10.1007/BF00188945
- [170] J. Yang, E.G. Wang: **Reaction of water on silica surfaces**, *Current Opinion in Solid State and Materials Science* 10 (2006), pp. 33-39, DOI: 10.1016/j.cossms.2006.02.001

- 
- [171] S.M. Wiederhorn, L. H. Bolz: ***Stress corrosion and static fatigue of glass***, *Journal of the American Ceramic Society* 53 (1970), pp. 543-548, DOI: 10.1111/j.1151-2916.1970.tb15962.x
- [172] DIN Deutsches Institut für Normung e.V.: ***DIN 2413 - Nahtlose Stahlrohre für öl- und wasserhydraulische Anlagen - Berechnungsgrundlage für Rohre und Rohrbögen bei schwellender Beanspruchung***, Beuth Verlag, Berlin, (2011)
- [173] S.M. Wiederhorn: ***Fracture surface energy of glass***, *Journal of the American Ceramic Society* 52 (1969), pp. 99-105, DOI: 10.1111/j.1151-2916.1969.tb13350.x
- [174] C. Gröschl: ***FEM simulation of stress and strain in glass structures at pressure treatment***, PhD Thesis, submitted (2015)
- [175] T. Rampe, A. Heinzl, B. Vogel: ***Hydrogen generation from biogenic and fossil fuels by autothermal reforming***, *Journal of Power Sources* 86 (2000), pp. 536-541, DOI: 10.1016/S0378-7753(99)00465-6
- [176] H. Richter, K. Blank, V. Caimann, R. Schmitt: ***HVG Fortbildungskurs 1987 - Festigkeit von Glas - Grundlagen und Prüfverfahren***, Hüttentechnische Vereinigung der Deutschen Glasindustrie, Frankfurt / Main, (1987)
- [177] Schott AG: ***Technical data sheet Schott glass 8242***, Schott AG, Mainz, (2014)
- [178] Schott AG: ***Technical data sheet Schott glass 8253***, Schott AG, Mainz, (2014)
- [179] L. Jäckel: ***Transiente Simulation zur Optimierung von ALD-Prozessen***, Bachelor Thesis, Technical University Freiberg, (2013)

---

**Curriculum Vitae****Personal details**

Name: Ronald Meyer-Scherf  
Born: 21st of October 1981 in Königs Wusterhausen  
Family status: married  
Nationality: German

**Education**

02/2010 – 12/2015 PhD-study at the Federal Institute for Materials Research and Testing (BAM) in Berlin, Germany  
10/2002 - 12/2009 Graduate Engineer (Dipl.-Ing.) in energy engineering and process engineering at Technical University in Berlin, Germany  
09/1994 - 06/2001 Gymnasium (academic high school) "Villa Elisabeth" in Eichwalde, Germany  
09/1988 – 07/1994 Grundschule (elementary school) in Königs Wusterhausen, Germany

**Career**

02/2010 – 12/2015 Research assistant at the Federal Institute for Materials Research and Testing (BAM) in Berlin, Germany  
10/2007 – 09/2009 Student assistant at the Federal Institute for Materials Research and Testing (BAM) in Berlin, Germany